



**HAL**  
open science

# Hydrogen production at low temperature by dry reforming and oxidative dry reforming of methane on various Ni-based catalysts

Yaqian Wei

► **To cite this version:**

Yaqian Wei. Hydrogen production at low temperature by dry reforming and oxidative dry reforming of methane on various Ni-based catalysts. Chemical engineering. Ecole Centrale de Lille, 2017. English. NNT : 2017ECLI0033 . tel-02422220

**HAL Id: tel-02422220**

**<https://theses.hal.science/tel-02422220>**

Submitted on 21 Dec 2019

**HAL** is a multi-disciplinary open access archive for the deposit and dissemination of scientific research documents, whether they are published or not. The documents may come from teaching and research institutions in France or abroad, or from public or private research centers.

L'archive ouverte pluridisciplinaire **HAL**, est destinée au dépôt et à la diffusion de documents scientifiques de niveau recherche, publiés ou non, émanant des établissements d'enseignement et de recherche français ou étrangers, des laboratoires publics ou privés.

N° d'ordre : 347

**CENTRALE LILLE**

**THÈSE**

Présentée en vue d'obtenir

le grade de

**DOCTEUR**

en

Spécialité: Molécules et Matière Condensée

par

**Yaqian WEI**

**DOCTORAT DELIVRE PAR CENTRALE LILLE**

Titre de la thèse:

**Production d'hydrogène à basse température par reformage à sec et reformage oxydant du méthane sur divers catalyseurs à base de nickel**

**Hydrogen production at low temperature by dry reforming and oxidative dry reforming of methane on various Ni-based catalysts**

Soutenue le 20/12/2017 devant le jury d'examen :

<b>Président</b>	Franck Dumeignil	Professeur	Université Lille
<b>Rapporteur</b>	Pascale Nolven Guilhaume	Chargé de Recherches CNRS, HDR	IRCELYON
<b>Rapporteur</b>	Fermin Cuevas	Directeur de Recherches CNRS	ICMPE Thiais
<b>Membre</b>	Mona Bahout	Maître de conférences, HDR	Université de Rennes
<b>Co-directeur</b>	Sébastien Paul	Professeur	Centrale Lille
<b>Directeur de thèse</b>	Louise Duhamel	Chargé de Recherches CNRS, HDR	Université Lille

Thèse préparée à l'Unité de Catalyse et Chimie du Solide (UCCS)

École Doctorale SMRE 104



## Acknowledgements

*First and foremost I would like to thank Pr. F. Dumeignil and Pr. L. Montagne very much for offering me this thesis and providing me all the necessary resources for my research. This work is performed in Unit é de Catalyse et Chimie du Solide – CNRS UMR8181, and Ecole Centrale de Lille. I would like to sincerely acknowledge China Scholarship Council (CSC) who financially supports my PhD studies in France.*

*I shall express my sincere and heartfelt gratitude to my supervisor, Dr. Louise Duhamel, who helps me quite a lot in every aspect. I would like to thank her for encouraging my research and for leading me to grow as an independent scientific researcher. The advice on both research as well as on my career have been priceless. I do appreciate her patience, encouragement and professional guidance during my three-year-long PhD studies.*

*I deeply thank Pr. Sbastien Paul for providing me valuable suggestions and the resources for my research. And also for his warm concern and kind help in both my study and life.*

*Last but not least, I also would like to dedicate my acknowledgements to all those who helped me during my PhD studies, our professional technicians: Mr. O. Gardoll, Ms. M. Trentesaux, Ms. P. Simon and Mr. S. Chambrey. As well as our nice secretaries and friendly colleagues: Mr. Y. Romani. Dr. C.pirez, Mr. H. Malbieres, Ms.H. Hu and Dr. C. Ciotonea. The times when we work together leave me very pleasant memories.*

*I finally would love to express my gratitude to my beloved wife and parents who have always been helping me out of difficulties and supporting me without a word of complaint. You are always there whenever I need you. I love you forever!*



Yaqian Wei

October, 2017



---

# Table of contents

<b>1</b>	<b>General introduction</b> .....	1
1.1	Hydrogen: energy for the future.....	2
1.2	Global manufacture of H <sub>2</sub> production .....	3
1.3	H <sub>2</sub> production from biomass .....	5
1.4	Biogas production .....	7
1.5	H <sub>2</sub> production from Catalytic Reforming of CH <sub>4</sub> .....	8
1.5.1	H <sub>2</sub> production from steam reforming of methane.....	9
1.5.2	Partial oxidation of methane.....	10
1.5.3	Dry reforming of methane .....	10
1.5.4	H <sub>2</sub> production from oxidative dry reforming of methane.....	12
1.5.5	H <sub>2</sub> production from other reforming processes of methane.....	14
1.6	Catalysts for reforming of methane.....	15
1.6.1	Catalysts for dry reforming .....	16
1.6.2	Catalysts for oxidative dry reforming of methane.....	19
1.7	Catalyst deactivation .....	21
1.7.1	Carbon formation.....	21
1.7.2	Sintering .....	25
1.8	Objective of the thesis.....	26
<b>2</b>	<b>Preparation and characterization of catalysts</b> .....	27
2.1	CeNi <sub>x</sub> (Al <sub>z</sub> )O <sub>y</sub> catalysts.....	29
2.2	Ni <sub>x</sub> Mg <sub>2</sub> AlO <sub>y</sub> catalysts.....	44
2.3	Ni <sub>x</sub> /SBA-15 .....	52
2.4	Conclusion .....	60
<b>3</b>	<b>Dry Reforming of Methane over Ni-based catalysts</b> .....	63
<b>3.1</b>	<b>Dry reforming over CeNi<sub>x</sub>(Al<sub>z</sub>)O<sub>y</sub> mixed oxides</b> .....	65
3.1.1	Influence of reaction temperature over CeNi <sub>x</sub> O <sub>y</sub> .....	65
3.1.2	Influence of pretreatment .....	67
3.1.3	Influence of Ni content.....	69
3.1.4	Influence of reactants concentration.....	72

---

3.1.5	Stability test.....	77
<b>3.2</b>	<b>Dry reforming over CeNi<sub>x</sub>Al<sub>0.5</sub>O<sub>y</sub> mixed oxides.....</b>	<b>80</b>
3.2.1	Influence of reaction temperature and pretreatments .....	81
3.2.2	Influence of Ni content.....	83
3.2.3	Performance in harsh condition.....	86
3.2.4	Stability test.....	89
3.2.5	The influence of Al in CeNi <sub>x</sub> (Al <sub>z</sub> )O <sub>y</sub> mixed oxides .....	91
3.2.6	Conclusion for CeNi <sub>x</sub> (Al <sub>z</sub> )O <sub>y</sub> in DRM .....	93
<b>3.3</b>	<b>Dry reforming over Ni<sub>x</sub>Mg<sub>2</sub>AlO<sub>y</sub> mixed oxides .....</b>	<b>94</b>
3.3.1	The influence of reaction temperature.....	94
3.3.2	Influence of pretreatment in H <sub>2</sub> .....	96
3.3.1	Catalytic performance in harsh conditions .....	99
3.3.2	Stability test.....	102
3.3.3	Conclusion for Ni <sub>x</sub> Mg <sub>2</sub> AlO <sub>y</sub> in DRM .....	104
<b>3.4</b>	<b>Dry reforming over Ni<sub>x</sub>/SBA-15 catalysts .....</b>	<b>105</b>
3.4.1	Influence of pretreatment .....	106
3.4.2	Influence of Ni loading.....	107
3.4.3	Catalytic performance in harsh condition.....	112
3.4.4	Conclusion for Ni <sub>x</sub> /SBA-15 in DRM.....	113
3.5	Conclusion for this chapter .....	114
<b>4</b>	<b>Oxidative dry reforming of methane over CeNi<sub>x</sub>(Al<sub>z</sub>)O<sub>y</sub> .....</b>	<b>117</b>
<b>4.1</b>	<b>Oxidative dry reforming over CeNi<sub>x</sub>O<sub>y</sub> mixed oxides.....</b>	<b>120</b>
4.1.1	Catalytic tests at low-temperature range .....	120
4.1.2	The effect of nickel content on CeNi <sub>x</sub> O <sub>y</sub> catalysts .....	121
4.1.3	Stability test.....	123
<b>4.2</b>	<b>Oxidative dry reforming over CeNi<sub>x</sub>Al<sub>0.5</sub>O<sub>y</sub> mixed oxides.....</b>	<b>124</b>
4.2.1	Temperature influence.....	125
4.2.2	Influence of Ni content.....	125
4.2.3	Influence of O <sub>2</sub> concentration.....	128
4.2.4	Stability test.....	130
4.2.5	The influence of Al in the catalysts.....	133
	Conclusions .....	134

---

<b>5</b>	<b>General discussion</b> .....	135
5.1	Comparison and discussion.....	137
5.2	Proposal of active site and possible mechanism .....	142
<b>6</b>	<b>General conclusion</b> .....	153
	<b>References</b> .....	159
	<i>Annex</i> .....	171
	Characterization method ..	172
	Experimental .....	176
	Thermodynamic study.....	178

# **Chapter 1**

## **General introduction**

## 1 General introduction

Access to clean, affordable and reliable energy has been a cornerstone of the world's increasing prosperity and economic growth since the beginning of the industrial revolution. Within 200 years, there is a wide scale of increase in the demand of energy and its resources, owing to a rapid increase in industrialization, urbanization, and population outgrowth [1]. Since then, various fossil fuels and their derivatives have remained the most favorite and widely exploited resource of energy for the world. The global use of petroleum and other liquid fossil fuels was 85.7 million barrels/day in 2008 with a projection for an increase to 97.6 million barrels/day in 2020 and 112.2 million barrels/day in 2035, respectively [2]. However, in the past several decades, with the continual growth of the exploitation and utilization of fossil fuels as well as the excessive greenhouse gas (GHG) emissions worldwide, exploiting renewable energy sources is a global strategy to meet the challenges of future sustainable development. Therefore, developing renewable and clean energy sources to substitute the conventional energy resources has become the mainstream development strategy in the present world.

Developing hydrogen as a promising future energy has drawn significant interest from both academy and industry fields [3,4]. It has a prominent role to play in the energy mix due to its high efficiency and nonpolluting. Hydrogen is the most potential source and also has been used in chemical industry as an indispensable raw material. However, today's capital costs for most of the hydrogen production methodologies are still higher than those for other kinds of fuels. Primary research needs are optimizing operations and developing low-cost, efficient catalysts to increase hydrogen yield to meet variable demand.

Up to date, hydrogen is mainly produced from fossil fuels by various reforming technologies of natural gas. In order to support a clean and sustainable hydrogen economy, it is urgently desirable to produce hydrogen from renewable energy sources, such as biomass-derived materials and/or biogas. Biogas is a mixture of gases mainly containing methane ( $\text{CH}_4$ ) and carbon dioxide ( $\text{CO}_2$ ), which is the result of the anaerobic digestion of various biomass, coming from different sources such as sewage, sludge, landfill or industry [5]. It has compatible properties of being clean and renewable for reforming process. Recently, the reforming process of biogas has received growing interest because of the

enhanced utilization of CO<sub>2</sub> and CH<sub>4</sub> (with greenhouse warming potential 21 times that of carbon dioxide) [6]. Approach for converting these GHG into highly valuable chemicals is desirable. In such a context, the crucial factor is developing highly active, selective, stable and low-cost catalysts that can efficiently break the C-C and C-H bonds and promote the subsequent production of H<sub>2</sub>.

After this general introduction, in Chapter 1, the bibliography on H<sub>2</sub> production from biomass, *e.g.*, biogas is reviewed. Many recent literatures on the catalytic systems of dry reforming of methane (DRM) and oxidative dry reforming of methane (ODRM) process are synthesized. Then Chapter 2 presents the methodology of preparation and the results of the different characterizations of the Ni-based catalysts studied in the present thesis. Chapter 3 and 4 synthesize the catalytic results in dry reforming and oxidative reforming of model biogas, many different reaction parameters are analyzed over different Ni-based catalysts. Finally, in chapter 5, general discussion based on catalysts characterizations and all the catalytic results is made. The features of different catalysts and the correlations between catalytic performances and catalyst properties are established and thoroughly discussed. Moreover, active site and reaction mechanism are proposed.

## **1.1 Hydrogen: energy for the future**

Hydrogen (H<sub>2</sub>) has the outstanding energy capacity than any other materials, with the amount of energy per mass unit as high as 121 kJ/kg. It is wildly used as raw material in the chemical industry, production of ammonia and methanol, Fischer-Tropsch synthesis and hydrogenation. In particular, It can store the energy from diverse domestic resources (including clean coal, nuclear, and intermittently available renewables) for use in mobile applications and more efficient [7]. The hydrogen economy is not a new idea. In 1874, Jules Verne recognized the finite supply of coal and the possibilities of hydrogen derived from water electrolysis, made the comment that “water will be the coal of the future” [8].

The production and utilization of hydrogen can not only provide a pathway for taking advantage of abundant renewable energy resources, but also can keep atmospheric CO<sub>2</sub> concentrations at levels that avoid irreversible climate changes. Hydrogen is regarded as the next generation energy carrier in the longer term. However, a lot of infrastructures and R&D work should be done in the short and medium

term. More attention focuses on hydrogen production activities such as H<sub>2</sub> from biomass, Photo-electrolysis (photolysis) and photo-biological hydrogen production (biophotolysis).

## 1.2 Global manufacture of H<sub>2</sub> production

Hydrogen can be produced from many different sources, several technologies are already available in the marketplace for the industrial production of hydrogen. Generally, on one aspect, Hydrogen could be produced from conventional sources such as steam reforming of natural gas, partial oxidation of hydrocarbons and coal gasification. It also could be produced from renewable energy sources (solar photovoltaic power for direct conversion, wind power and biomass).

The first commercial technology, dating from the late 1920s, was the electrolysis of water to produce pure hydrogen. In the 1960s, the industrial production of hydrogen shifted slowly towards a fossil-based feedstock, which is the main source for hydrogen production today [9]. As clearly demonstrated in **Fig. 1-1**, at present, globally 50 million tons of Hydrogen is produced each year, approximately 96% of the hydrogen is still produced from carbonaceous raw material, such as natural gas (48%), oil (30%) and coal (18%) [4,10].

Among all these routes, large-scale natural gas reforming is currently the lowest cost method for hydrogen production. However, reforming should not be seen as the single optimal route for the H<sub>2</sub> production in particular. Other processes like solar- or wind-driven electrolysis and photobiological water splitting hold great promise for clean hydrogen production [11]. For instance, water electrolysis is the process whereby water is split into hydrogen and oxygen through the application of electrical energy, as in **Eq.(1-1)**. Electrolysis is easily scalable; units with capacities from 1 kW (corresponding to a hydrogen production of about 250 Nm<sup>3</sup>/h) to 150 MWe (35 000 Nm<sup>3</sup>/h) are commercially available [12]. However, the main disadvantage of water electrolysis is that it requires large amounts of electricity. Efforts are being made to increase the efficiency and reduce electricity use. Advances must still be made before these technologies can be economically competitive.



It should be emphasized that, today's H<sub>2</sub> manufacture based mainly on fossil fuels cannot be considered as sustainable. Reducing the demand on fossil resources remains a significant concern for

many nations [13]. It is urgently desirable to produce  $H_2$  from renewable resources such as biomass or biomass-derived materials.

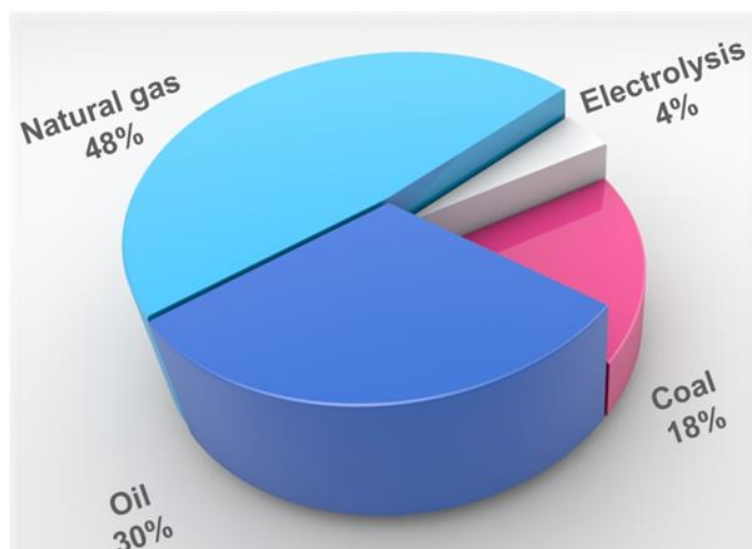


Fig. 1-1 Feedstock used in the present global hydrogen production.[4]

### Present status of utilization and demand of $H_2$

Up to date, the total annual worldwide hydrogen consumption is in the range of 400-500 billion  $Nm^3$ [14]. The demand for hydrogen ( $H_2$ ) is ever growing, with wide applications such as the refining of crude oil, production of ammonia and methanol, surface treatment in metallurgy process and other chemical uses. **Table 1-1** illustrates the global utilization of  $H_2$  production.

**Table 1-1** World hydrogen consumption by different uses.

Hydrogen uses	Consumption	Percentage
Ammonia production	250	50
Production of other chemical products	65	13
Petrochemistry	185	37
Total	500	100

A summary of chemical and physical properties of hydrogen, methane, and gasoline is given in **Table 1-2**, with the outstanding properties compared to other fuels. In the future, hydrogen is likely to be used as fuel in almost all applications where fossil fuels are used today. For example, fuel cell is an emerging technology concerning  $H_2$  utilization. It is a promising route for transportation, household

power generation and portable energy installations. Hydrogen's share in the energy market is increasing with the implementation of fuel cell systems and the growing demand for zero-emission fuels. By 2040, it is expected that the utilization of hydrogen in fuel cell-powered vehicles could replace consumption of 18.3 million barrels of petroleum per day. Up to date, a lot of the research on reforming process of  $\text{CH}_4$  are focused on producing hydrogen for fuel cell applications [15,16,17].

**Table 1-2** Physical and chemical properties of three fuel options (hydrogen, methane, and gasoline) [3]

	Hydrogen	Methane (H/C = 4)	Gasoline (H/C = 1.87)
Molecular weight (g/mol)	2.016	16.04	~ 110
Mass density ( $\text{kg}/\text{N}_\text{A}\text{m}^3$ ) at $P = 1 \text{ atm} = 0.101 \text{ MPa}$ , $T = 0 \text{ }^\circ\text{C}$	0.09	0.72	720–780 (liquid)
Mass density of liquid $\text{H}_2$ at 20 K ( $\text{kg}/\text{N}_\text{A}\text{m}^3$ )	70.9	–	–
Boiling point (K)	20.2	111.6	310–478
Higher heating value (MJ/kg) (assumes water is produced)	142.0	55.5	47.3
Lower heating value (MJ/kg) (assumes steam is produced)	120.0	50.0	44.0
Flammability limits (% volume)	4.0–75.0	5.3–15.0	1.0–7.6
Detonability limits (% volume)	18.3–59.0	6.3–13.5	1.1–3.3
Diffusion velocity in air (m/s)	2.0	0.51	0.17
Ignition energy (mJ)			
– At stoichiometric mixture	0.02	0.29	0.24
– At lower flammability limit	10	20	n/a
Flame velocity in air (cm/s)	265–325	37–45	37–43
Toxicity	Nontoxic	Nontoxic	Toxic above 50 ppm

### 1.3 $\text{H}_2$ production from biomass

With the increasing global concern about the climate change and  $\text{CO}_2$  emissions, it is urgent to produce  $\text{H}_2$  in a  $\text{CO}_2$  neutral route. Renewable resources offer a long-term potential for sustainable hydrogen production with low environmental impact. It is worth mentioning that biomass has the potential to accelerate the realization of hydrogen as a major fuel of the future. In general, Hydrogen can be produced from biomass by pyrolysis, gasification, and enzymatic decomposition of sugars [15,16]. There are two types of biomass feedstock available to produce hydrogen [20], specific bioenergy crops, and less expensive biomass residues, such as organic waste from regular agricultural processing. Though  $\text{CO}_2$  is produced as a by-product in the process using biomass as a raw material, it can be fixed by the growing plants during photosynthesis to produce new biomass, which brings a small net  $\text{CO}_2$

impact compared to fossil fuels.

Biomass has tremendous potential to accelerate the realization and utilization of H<sub>2</sub> as a primary fuel of the future, as biomass is the fourth largest source of energy in the global context. It accounts for 15% of world's primary energy consumption and about 38% of the primary energy consumption in developing countries such as India, China, and Brazil [1].

The worldwide biomass energy potential in 2050 has been estimated to reach to 150–450 exajoule/year with an energy equivalence of  $\sim 76 \times 10^9$  barrels of oil energy equivalent [21]. As clearly shown in **Fig. 1-2**, renewables are the world's fastest-growing energy source in the coming decades. Renewable energy consumption increases by an average 2.6%/year between 2012 and 2040 [4]. In this scenario, renewable energy sources such as biomass could provide hydrogen locally, and will play a significant role to match the volumes of global hydrogen requirement.

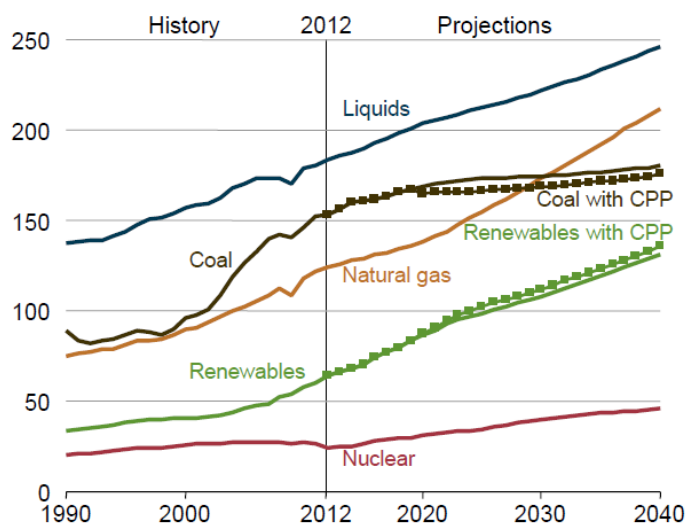


**Fig. 1-2** Total world energy consumption by energy source, 1990–2040 (quadrillion Btu) [22]

However, hydrogen from biomass has some challenges. The major technical barriers facing biomass thermochemical conversion include the effect of variable feedstock composition on downstream processing, efficient and durable catalysts for gas conditioning, and efficient heat integration [23].

## 1.4 Biogas production

Renewables are the world's fastest-growing energy source over the projection period. Renewable energy consumption increases by an average 2.6%/year between 2012 and 2040 [2]. As a high-potential raw material for hydrogen production, Biogas can be used as an alternative CH<sub>4</sub> source in the reforming process. Biogas is a mixture of gases mainly containing methane (CH<sub>4</sub>) and carbon dioxide (CO<sub>2</sub>), associated with the small amount of some other impurities such as hydrogen sulfide (H<sub>2</sub>S) and ammonia (NH<sub>3</sub>). Although amounts of residual compounds are quite lower compared with methane, they can still have environmental influences such as the toxicity hazard, the greenhouse effect and/or deleterious to the quality of local air [24].

Normally, Biogas is produced by the anaerobic digestion of various biomass, coming from different sources such as sewage, sludge, landfill or industry [5]. The typical chemical composition of biogas is summarized in **Table 1-3** [25, 26], but it could alter related to the starting substrate. Biogas is used as energy purposes have been through a two-class development. The first class is the direct heat utilization of CH<sub>4</sub> in the biogas, for power generation or as an urban gas source for cooking or heating. However, the direct use of biogas has two main drawbacks due to the relatively high content of CO<sub>2</sub>, which both lowers the heating value of biogas and contributes to greater emissions of CO<sub>2</sub> into the atmosphere [27]; The second class of biogas utilization is upgrading to other energy sources, such as H<sub>2</sub> or syngas for the synthesis of other liquid fuels. Every organic material can be degraded to generate biogas, which has compatible properties of being clean and renewable for reforming process. Hydrogen production from biogas can promote the hydrogen economy in industrial and domestic sectors, particularly in rural areas [28]. It should be concerned as a potential route especially in developing countries, due to lack of resources and ability to invest in sewage systems, solid and liquid wastes are difficult to manage[29].

**Table 1-3** Chemical composition of biogas[17]

Composite	Percentage
CH <sub>4</sub>	55-70 (vol%)
CO <sub>2</sub>	30-45 (vol%)
H <sub>2</sub> S	500-4000 (ppm)
NH <sub>3</sub>	100-800 (ppm)
H <sub>2</sub>	<1 (vol%)

---

N <sub>2</sub>	<1 (vol%)
O <sub>2</sub>	<1 (vol%)
H <sub>2</sub> O	<1 (vol%)

---

Recently, the reforming process of biogas has received growing interest because of the enhanced utilization of CO<sub>2</sub> and CH<sub>4</sub>. By the way, CH<sub>4</sub> is a gas with greenhouse warming potential 21 times that of carbon dioxide [6]. Atmospheric methane, the fraction of which has risen from 1 in 1920 to 1.7 ppm in 1990 [30]. Approach for converting these GHG into highly valuable chemicals is desirable. In various reforming processes, biogas with appropriate composition is available to be used as a methane source. Thus, most of the research on methane reforming can also be adapted to biogas reforming. Furthermore, there are more and more researches focus on performing biogas reforming using different strategies, such as solar energy [31] and plasma [32]. More and more researchers [33,34,35] also investigated the effect of a major impurity (i.e., H<sub>2</sub>S) on the reforming process of biogas.

## 1.5 H<sub>2</sub> production from Catalytic Reforming of CH<sub>4</sub>

As introduced above, the reforming of biogas is in the same principle of methane reforming, which is widely studied worldwide. Methane is a well-developed energy source in our daily life, it can be directly used for combustion thus generating heat and/or power [36]. The attention on catalytic conversion and sequestration of methane is increasing rapidly in recent years with receiving growing attention from the view point of global-warming issue as well as the development of shale gas and methane clathrate [37,38].

Many strategies are developed for the conversion of methane to more valuable chemicals and fuels. There are two strategies for conversion of methane, which are described as an indirect and direct method. In the direct processes, methane may be converted to methanol, formaldehyde, ethylene, aromatics or acetic-acid [39]. The indirect method is based on the formation of synthesis gas (CO and H<sub>2</sub>). Particularly, the steam reforming of methane source such as natural gas and byproduct of petroleum refining, which is the most commonly used method for hydrogen production.

As we know, the average bond energy of methane is 414 kJ/mol, and 435 kJ/mol for CH<sub>3</sub>-H bond, it is difficult to break this stable structure. Therefore, achieving effective activation and conversion of

methane molecules are crucial topic worldwide. In current studies, There are mainly three mainstream reactions to convert methane to produce H<sub>2</sub>, namely Steam Reforming (SRM), Dry Reforming (DRM) and Partial Oxidation of methane (POM). Moreover, combining two or three reforming processes mentioned above, people proposed many new concepts as bi-reforming or tri-reforming of methane.

### 1.5.1 H<sub>2</sub> production from steam reforming of methane

Steam reforming of methane (SRM) is the most widespread method of producing hydrogen, with an energy consumption rate of about 1.23–1.35 GJ-NG/GJ-H<sub>2</sub> [43]. In the steam reforming of methane, the natural gas or other methane streams, such as biogas or landfill gas reacts with water vapor in the presence of catalyst under 3–25 atm pressure to produce H<sub>2</sub>, CO and a small amount of CO<sub>2</sub> (Eq.1-2). According to DOE of USA (2010), SMR is approximately 72% efficient in hydrogen generation when starting with natural gas. It is worth mentioning that, natural gas reforming produces about half of the global supply of hydrogen and remains the most commonly used method for hydrogen production. However, as an endothermic process, SRM is still not a flawless route with defects in the attempts of high energy consumption and carbon formation. Also, side reactions need to be inhibited. Recently, many new catalysts and strategies are studied by researchers as follow.

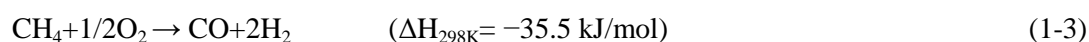


Antzara et al. [44] evaluated the SMR performance of NiO-based oxygen carriers supported on ZrO<sub>2</sub>, TiO<sub>2</sub>, SiO<sub>2</sub>, Al<sub>2</sub>O<sub>3</sub> and NiAl<sub>2</sub>O<sub>4</sub> as conventional reforming catalysts at low temperature (650 °C). NiO/SiO<sub>2</sub> and NiO/TiO<sub>2</sub> were found to have low activity (<50% initial CH<sub>4</sub> conversion) and deactivated rapidly, eventually dropping to less than 10% CH<sub>4</sub> conversion after 2 h on stream. NiO/ZrO<sub>2</sub> exhibited good activity with initial CH<sub>4</sub> conversion higher than 80% and had excellent stability.

Min-Ho et al. [45] investigated the methane steam in microchannel reformers by using porous-membrane-type catalysts and shifting a combustion point onto the top of the catalysts. Improved heat transfer efficiency has been obtained and methane conversion has increased by 14.7% at the same supply rate of fuel. In addition, the long-term stability of the microchannel reformers was verified by methane reforming tests for 500 h.

### 1.5.2 Partial oxidation of methane

Partial oxidation of methane (POM) is an alternative method to produce H<sub>2</sub> with reduced energy costs, since the reaction is moderately exothermic (Eq. (1-3)), contrary to SRM which is highly endothermic. Methane is partially oxidized to CO and H<sub>2</sub> (H<sub>2</sub>/CO ratio close to 2) and reduce carbon formation. However, a slight decrease in CO selectivity causes the methane to react with oxygen to form CO<sub>2</sub> (Eq. 1-4), leading to combustion (strong exothermic reaction), which results in high reaction temperature increase. It can form hot-spots in the reactor bed and carbon occurs simultaneously on the catalyst surface. According to the literature [46], the CH<sub>4</sub> conversion increases with increasing space velocity because of the presence of hot spots.

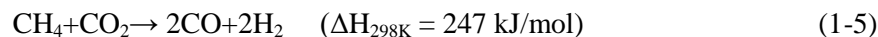


Several studies [27, 49] have shown that in most cases, the POM reaction follows the combustion-reforming mechanism, in which the total combustion of methane (TCM) produces CO<sub>2</sub> and H<sub>2</sub>O as primary products, and is followed by dry reforming of methane (DRM) and steam reforming of methane (SRM), to produce syngas. On the other hand, the direct oxidation mechanism was proposed by Schmidt and Hickman [31,32] they evidenced that the methane is decomposed into H<sub>2</sub> and carbon species on the surface. Then carbon species react with oxygen on the surface, to form carbon monoxide. The reaction rate of POM is much faster than the SMR, and it could be conducted at atmospheric pressure and high space velocity.

### 1.5.3 Dry reforming of methane

The production of hydrogen by dry reforming of methane (DRM) followed by water-gas shift reaction have received much attention due to the environmental concerns [50]. The carbon dioxide reforming reaction is a highly endothermic process which favors the production of syngas with H<sub>2</sub>/CO ratio of 1. This reaction is attractive from an environmental point of view since it consumes two major greenhouse gases (CH<sub>4</sub> and CO<sub>2</sub>), seen in (Eq.1-5). This reaction requires higher temperatures being

equally favored by low pressure. According to the literature [36,51], it can be accompanied by several side reactions such as reverse water-gas shift (RWGS) (Eq. 1-6), which is the main water formation route.



The generalized reaction sequence corresponds to the following overall reaction stoichiometry [52]:



Thus, the amount of CO always exceeds that of hydrogen, which means that  $\text{H}_2/\text{CO}$  ratios are below unity. However, upon carbon formation in the methane dry reforming, the  $\text{H}_2/\text{CO}$  ratio is enhanced [52]. It is generally agreed that a heavy carbon deposition can be occurred during the reaction leading to instability in catalytic activity [53, 55]. Moreover, it is the most endothermic reforming reaction due to the fact that  $\text{CO}_2$  is very stable and most oxidized. Therefore, dry reforming has become a good option for biogas renewable, although several obstacles might prevent its further industrial application. It requires a significant amount of energy to activate it as an oxidant. Furthermore, the endothermicity of the reaction necessitates high rates of energy input, high operating temperatures and harsh reaction conditions. Another concern is the fast catalyst deactivation, mainly caused by the carbon deposition and active metal sintering. Under this scenario, effective process integration is required to obtain practicable efficiencies: these present considerable challenges for catalyst development as well as reactor design and engineering, etc.

Paksoy et al. [56] prepared 5% Co–2% Ce/ $\text{ZrO}_2$  catalyst for the dry reforming test. The experiments were performed at the temperature range of 873–973K with  $\text{CH}_4/\text{CO}_2$  feed ratios of 1/1, 2/1, 1/2 and space velocities of 30,000, 20,000 and 10,000 mL/h/ $\text{g}_{\text{cat}}$ . The comparative analysis of Co and Ce site concentrations measured on the freshly reduced and confirmed that methane dehydrogenation is the primary function of Co sites. Co–Ce/ $\text{ZrO}_2$  catalyst has a stable activity for  $\text{CH}_4/\text{CO}_2$  feed ratio of 1. Carbon accumulation was mostly observed when temperature and  $\text{CH}_4/\text{CO}_2$  feed ratio were both high. Decreasing space velocity is beneficial for high and stable activities and high  $\text{H}_2/\text{CO}$  product ratio.

Benrabaa et al. [57] used nickel ferrite spinel as catalyst precursor in the dry reforming of methane.

Three samples of NiFe<sub>2</sub>O<sub>4</sub> nickel ferrite are obtained by varying the preparation method. The catalytic performance of methane reforming with CO<sub>2</sub> was measured with and without the pre-treatment of catalysts under H<sub>2</sub> in 650–800 °C range of temperature. The catalytic conversions of methane and CO<sub>2</sub> were quite low without pretreatment, but improved results are obtained when the catalysts were reduced. A significant contribution of reverse water gas shift reaction accounted for the low values of H<sub>2</sub>/CO ratio, but minimal quantity of carbon formation can be observed. The presence of Ni-Fe alloy seems to play an important role in inhibiting the carbon deposition through a dilution effect of Ni active sites.

#### 1.5.4 H<sub>2</sub> production from oxidative dry reforming of methane

A comprehensive strategy to evade the aforementioned defects and improve the conversion at a lower temperature is combining the DRM and POM in a single reactor (Eq.1-8). It has been reported to be effective in compensating energy consumption of dry reforming and adjusting the H<sub>2</sub>/CO ratio of syngas. Co-feeding O<sub>2</sub> with CH<sub>4</sub> and CO<sub>2</sub> provides additional advantages such as: reducing the global energy requirement, enhanced catalyst stability, increased deactivation resistance [4] and inhibit the carbon deposition rate by gasifying carbon species, as demonstrated by Lucredio et al. [58]. Furthermore, the H<sub>2</sub>/CO ratio could be manipulable for downstream. Another advantage is compensating the energy of endothermic reforming reactions, significantly reducing the global requirements of energy.



Typically, the exothermic nature in oxidative biogas reforming increases for a given temperature as the O<sub>2</sub> concentration in the feed increased. This is due to the fact that the addition of O<sub>2</sub> determines the oxidation process. It was reported in the literature [59,60] that this process was emerged in two separate reaction periods — in the first period, a part of methane is combusted into CO<sub>2</sub> and steam to ensure the complete conversion of oxygen in the feed. Subsequently, in the second period, the remained methane is reformed to H<sub>2</sub> and CO by CO<sub>2</sub> and steam reforming. As the combustion reaction is much faster than the reforming reaction, it usually proceeds on the catalyst near the bed inlet, while the reforming reaction takes place over the catalyst bed after oxygen is consumed [59].

In the aspect of combination of two reforming techniques involving exothermal reaction, several studies pursue the so-called auto-thermal process [61,62] from a point of view for energy saving, when a net  $\Delta H=0$  is obtained by manipulating the feed gases, which means no or very few external energy supply is required for maintaining the reaction. Moreover, some researchers [41,63] showed that  $H_2/CO$  molar ratio in product gas could be controlled by controlling the relative concentrations of  $CO_2$  and  $O_2$  in the feed gases.

According to the study [61] on supported noble metal catalyst ( $Rh/Al_2O_3$ ) at low GHSV( $5000-8000h^{-1}$ ), it was found that the oxidative reforming of landfill gas produces more syngas compared to dry reforming due to the combustion and partial oxidation of  $CH_4$  providing  $CO_2$  and  $H_2O$  and energy which is favored to a greater reforming process. Van Herle et al. [30] investigated the minimum quantity of oxygen (air) required to avoid carbon formation above  $800\text{ }^\circ C$  for a methane-rich biogas composition ( $CH_4/CO_2 = 2/1$ ). The results were determined by thermodynamic calculation and were plotted in Fig. 1-3.

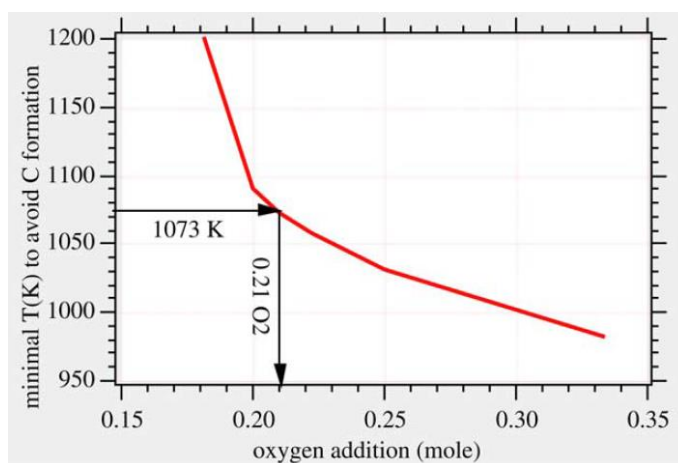


Fig. 1-3 Minimal  $O_2$  addition (in mole) required to the biogas feed  $0.67CH_4 + 0.33 CO_2$ , so as to avoid carbon formation [30].

Lau and Tsolakis [64] studied the oxidative reforming of biogas at different temperatures and they inferred that at low temperatures, oxidative reforming is the dominant process. Increasing the  $O_2/CH_4$  ratio at low temperature promotes hydrogen production. On the other hand, dry reforming of biogas is dominant, and the overall reaction is net endothermic at high exhaust temperatures ( $> 600\text{ }^\circ C$ ). As demonstrated by Lucrecio et al. [58] the addition of oxygen in the dry reforming of biogas ( $1.5CH_4:1CO_2$ ) could improve the  $CH_4$  conversion, decrease the carbon deposition rates by gasifying

carbon species. Akri and Chafik et al. [65] reported the effect oxygen in the reforming process of methane at 800 °C with a series of Nickel–cerium catalysts, they found that the addition of oxygen plays a crucial role since the carbon balance is significantly higher as compared to CH<sub>4</sub>/CO<sub>2</sub> mixture. The addition of oxygen into the feed strongly increases the methane conversion, while CO<sub>2</sub> conversion remains unaffected since complete oxidation of CH<sub>4</sub> into CO<sub>2</sub> probably occurs.

### 1.5.5 H<sub>2</sub> production from other reforming processes of methane

There are other similar processes reported in the literature for the production of H<sub>2</sub> from methane, such as: auto-thermal reforming (ATR), bi-reforming [66], oxidative bi-reforming [67] and tri-reforming [68]. In all cases the process uses an oxidizing agent that will oxidize CH<sub>4</sub> to CO while producing H<sub>2</sub> in a ratio depending on the oxidant used [69].

Optimum conditions were established in the literature [70] for the tri-reforming process with a nickel-silica core@shell catalyst. Syngas with different H<sub>2</sub>/CO molar ratios was obtained by varying the feedstock gas composition. Increasing oxygen partial pressure improved methane conversion to 90% but did not improve the H<sub>2</sub>:CO ratio in produced syngas at 750 °C. Moreover, Solov'ev et al. [71] observed that not all catalysts applicable for methane steam reforming could be used for tri-reforming. For example, the NiO/Al<sub>2</sub>O<sub>3</sub> catalyst employed in their work which had almost 100% of methane conversion during steam reforming, gave a methane conversion of only 15% during tri-reforming.

In Pino's work [72], a series of Ni catalysts supported on La-Ce-O mixed oxides with different Ni content was tested in tri-reforming reaction of simulated biogas at 800 °C (GHSV = 31,000 h<sup>-1</sup>). It should be highlighted that Ni and La ions were partially incorporated into CeO<sub>2</sub> framework, cubic fluorite structure of CeO<sub>2</sub> support was also retained at high level of doping. Ce<sub>0.7</sub>OLa<sub>0.2</sub>Ni<sub>0.1</sub>O<sub>2</sub> sample showed high stability (CH<sub>4</sub>, CO<sub>2</sub> conversion rates and the H<sub>2</sub>/CO molar ratio in the reformed gas were 1.56 mmol/s gNi, 0.56 mmol/s gNi and 1.57, respectively).

Italiano, et al. [5] worked with nanocrystalline Ni/CeO<sub>2</sub> catalysts in the biogas oxy-steam-reforming (OSR) process. Catalytic tests under biogas oxy-steam reforming reaction were carried out at fixed GHSV=30000 h<sup>-1</sup> (CH<sub>4</sub>:CO<sub>2</sub>H<sub>2</sub>O:O<sub>2</sub>:N<sub>2</sub> = 1.0:0.67:0.3:0.1:0.1). At high temperature (800°C), the experimental results are very close to the equilibrium values. The use of urea allows obtaining powders with higher surface area, higher dispersion and lower particle size in comparison with those obtained

using the other fuels. Velu et al. [73] investigated the oxidative steam reforming over a series of multi-component (Cu, Co, Zn, Al) mixed oxide catalysts. It was revealed that the Co free catalyst offered high H<sub>2</sub> production rates because of the presence of Co favors the CO hydrogenation reaction.

## 1.6 Catalysts for reforming of methane

The conversion of methane and the selectivity of the reactions to hydrogen or synthesis gas depend on several variables such as temperature, pressure, reagents feed ratio, and the most important one: the catalyst used. Numerous studies have conducted on understanding the active phase, the structure, and morphology of catalysts, influence of support and the effect of different promoters. Further interpretation of the effect in the change of structural properties, the reduction behavior, and the catalytic performance is also motivating to learn.

Although noble metals such as Pt [46], Pd [74], Rh [75] and Ru are reported with compatible activity in reforming processes. Generally, noble metal-based catalysts require a lower loading amount (1-5%), due to higher activity. Even though, they are still not used in industrial applications due to the high costs. On the other hand, among non-noble metals catalysts, most of the group VIII metal-based catalysts are in some extent presenting activity toward methane reforming reactions. Such as Ni or Co, normally requires a higher loading amount to ensure an efficient performance in reforming process.

In particular, the nickel-based catalysts have been proved to be superior one showing comparable activities for methane reforming to those reported for noble based catalysts. Researchers have proposed a multitude of methods to improve the performances of Ni-based catalysts. Studies on catalysts for reforming reactions are usually directed to support development or the insertion of a second and/or third metal associated with Ni to achieve enhanced activity and reduced carbon deposits, thereby, to enhance its stability [76, 77]. In addition, the activity is affected by various factors, such as the loading amount [78] and the type of precursor [79]. The presented studies of nickel-based catalysts showed that the catalytic performance of materials in methane reforming reaction is dependent on various factors. It is difficult to select the best support and promoter, as reported materials were tested under different conditions, with different loadings of metals and were prepared by different methods. Recent studies in literature are focusing on the addition of promoters for changing catalytic properties of a material or

preparing materials with high dispersion and small size nickel particles, which can be achieved by increasing interactions between nickel species and support [80,81,82].

### 1.6.1 Catalysts for dry reforming

Catalysts for DRM are studied during a long time, comprehensive review on noble metal catalysts are conducted by Pakhare and Spivey [51] as well as the strategies for improving the performance and stability of Ni-based catalysts are reviewed by Shuirong and Jinlong [83]. Other aspects of dry reforming are also reviewed by Usman [84], and by Abdullah et al. [85]. Thus, the present section will mainly focus on synthesizing recent literature on Ni-based catalysts with the relevant or similar parameters regarding this thesis.

Vasiliades et al. [81] studied dry reforming over 5 wt. % Ni/CeO<sub>2</sub> and Ni/Ce<sub>1-x</sub>Pr<sub>x</sub>O<sub>2-δ</sub> catalyst at 750 °C, (20% CH<sub>4</sub>; CH<sub>4</sub>/CO<sub>2</sub> = 1) with GHSV = 30,000 h<sup>-1</sup>. After 25h of test, the CH<sub>4</sub> and CO<sub>2</sub> conversions are 76 % and 83%, respectively, and the H<sub>2</sub>/CO ratio is 1.0. However, inactive carbon in filamentous and graphitic structure is largely formed after test. It was also found that the relative amount of inactive carbon formed via the CH<sub>4</sub> and CO<sub>2</sub> activation routes was strongly depending on reaction temperature and Pr-dopant support composition. Introduction of Pr-dopant into the ceria support matrix at the level of 20 atom% drastically reduces the rate of carbon deposition compared to the Ni/CeO<sub>2</sub>, while keeping high activity and products selectivity a little bit lower than those obtained by Ni/CeO<sub>2</sub>.

Joung and co-workers developed highly coke-resistant Ni catalysts by immobilizing premade Ni nanoparticles of 5.2 nm in size onto functionalized silica supports [86]. They tested 300 mg of catalyst for DRM at 800 °C in total flow of 20 mL reactants (CH<sub>4</sub>:CO<sub>2</sub>=45%:45%). The silica-coated Ni catalysts giving CH<sub>4</sub> conversion at 42% and CO<sub>2</sub> conversion at 64%, the H<sub>2</sub>/CO ratio is 0.7. It operated stably for 170 h without any degradation in activity. No carbon deposition was observed by temperature programmed oxidation (TPO).

Recently, the Ce-Ni-(Al) based mixed oxides have been extensively studied because of the strong interactions between nickel and cerium species leading to interesting properties of the materials [87]. Han et al. [88] studied DRM at 700 °C on a series of Ni-Ce-Al composite oxides with various Ni molar contents prepared by co-precipitation method. 50mg of catalyst was tested in

CH<sub>4</sub>:CO<sub>2</sub>=45%:45% condition, with a GHSV=40,000 mL g<sup>-1</sup> h<sup>-1</sup>. The catalysts with 10% Ni is giving 67% and 77% of conversions for CH<sub>4</sub> and CO<sub>2</sub> respectively. The H<sub>2</sub>/CO ratio obtained is quite high at 0.95. The Ni10CeAl catalyst was selected to undergo 30 h stability test and the conversion of CH<sub>4</sub> and CO<sub>2</sub> decreased by 2.8% and 2.6%, respectively.

Odedairo et al. [89] investigated dry reforming on Ni/CeO<sub>2</sub> catalyst in the continuous fixed-bed flow reactor (GHSV=38400 mL/(hg<sub>cat</sub>), CO<sub>2</sub>/CH<sub>4</sub>=1:1, T=700 °C). They treated the catalyst with microwave plasma, the higher activity and stability are obtained compared with conventional thermal calcination: 34% of CH<sub>4</sub> conversion and 67% of CO<sub>2</sub> conversion are obtained after 8h of test. This can be attributed to the clean metal– support interface generated by the novel synthesis route.

As we know, the nature of the support strongly affects the catalytic behavior. Compounds with strong interacting with the support possess high resistance to sintering and higher metallic dispersion [90]. Xinyu et al. [91] synthesized a Ni/La<sub>2</sub>O<sub>3</sub> catalyst using La<sub>2</sub>O<sub>2</sub>CO<sub>3</sub> nanorod as a support precursor for dry reforming of methane. Highly dispersed Ni particles were obtained and the increased exposed Ni active sites can significantly enhance DRM activity compared to conventional routes. More medium-strength basic sites which could facilitate CO<sub>2</sub> adsorption and activation on the surface are obtained. The stability test was performed at 700 °C in condition of CH<sub>4</sub>/CO<sub>2</sub>/N<sub>2</sub> =15/15/70 and GHSV=60,000 mLg<sup>-1</sup>h<sup>-1</sup>. The Ni/La<sub>2</sub>O<sub>3</sub>-LOC catalyst reached 70% of CH<sub>4</sub> conversion and 75% of CO<sub>2</sub> conversion at 700°C after 50 h DRM reaction with a H<sub>2</sub>/CO ratio of 0.87.

Omogbe et al. [92] studied the effect of operating parameters on DRM reaction in a fixed-bed reactor using 10%Ni/SBA-15 catalyst prepared by incipient wetness impregnation method. A decrease in both CH<sub>4</sub> and CO<sub>2</sub> conversion of about 15% and 10%, respectively were experienced at 650 °C because of carbonaceous deposition from CH<sub>4</sub> decomposition reaction. Finally, the conversions are 50% and 61% for CH<sub>4</sub> and CO<sub>2</sub>.

In the literature, the combination of Ni, Mg and Al in catalyst has shown interesting results towards the DRM [93,94,95]. In this kind of catalysts, the basic properties of MgO promote the activation of CO<sub>2</sub> helping the Boudouard reaction towards CO kinetically. On the other hand, increasing the basicity of the catalysts enhances the rate of activation of mildly acidic CO<sub>2</sub>, which assists in the oxidation of surface carbon and increases the catalyst resistance to deactivation [51]. The beneficial basicity effect can also

be understood by considering some mechanistic aspects already established for Ni-based catalysts supported on Mg. For example, the high melting point of MgO (2850 °C) would enhance the property of resistance to thermal sintering.

Miletić's group [96] indicated that the deactivation of Ni/Al<sub>2</sub>O<sub>3</sub>-La<sub>2</sub>O<sub>3</sub> might occur due to the high concentration of La. High La<sub>2</sub>O<sub>3</sub> concentration may increase strong metal-support interactions and prompt a decrease in the catalyst activity due to the reduced exposure of Ni to the gaseous reactants. Bimetallic catalysts (CoO-NiO-Al<sub>2</sub>O<sub>3</sub>) were prepared by Huang et al. [97], the formation of Ni-Co nano-alloy supported in the ordered mesoporous skeleton led to the enhancement of stability of active sites and thus suppressed carbon deposition during reforming reaction. The thermal sintering was avoided owing to the dual confinement effects stemmed from the formation of Ni-Co alloy and the rigid mesoporous skeleton.

Solid solutions can play an important role in the catalysts for reforming reactions. The effect of solid solutions on methane reforming process is also largely studied in the literature [98,99]. Hu et al. [100] indicated that the solid solution structure formed between MgO and NiO exhibits good resistance to carbon deposition and high catalytic activity and selectivity in dry reforming. For example, under the condition of 790 °C, GHSV = 60 L/g/h, 20 wt% NiO-MgO catalyst exhibits a complete CO<sub>2</sub> conversion and the methane conversion rate > 91%. It summarized that this excellent catalytic activity is attributed to the ultrafine Ni particles formed from the reduction of NiO-MgO solid solution.

In recent research, Li et al. [101] introduced defects by doping a small amount of Ni atoms (~1.8 at. %) into ceria lattice at the atomic level. A homogeneous solid solution with uniform lotus-like morphology was obtained. Reduced formation energy of oxygen vacancy originated from local chemical effect caused by local distortion after Ni doping is observed. This leads to an increased oxygen storage capacity and the associated catalytic reactivity.

Moreover, increased Ni dispersion is generally obtained by adding promoter into the system. Generally, the promoters can be divided into three groups: (I) alkali or alkaline earth metals, (II) rare earth metals and (III) other metals, such as Au, Ag, Sn, and Bi. It was also found in Hongjing's study that [102] the small amount of Au and Pt addition plays a vital role on the catalytic performance of bi-/trimetallic catalysts and preventing it from carbon poisoning. The improvement of catalytic activity

and stability obtained for the trimetallic Ni-Au-Pt /Al<sub>2</sub>O<sub>3</sub> catalyst was attributed to the formation of high active Ni-Au-Pt nanoparticles.

For example, the performance of modified Ni/Mg-Al (mixed oxides, MO) by different Ce weight percentage (X = 0, 1, 3, 5, and 10 wt%) is investigated in the literature [103]. They found that the catalyst (Ni/Mg-Al) modified by 3 wt% of Ce showed higher CH<sub>4</sub> (99%) and CO<sub>2</sub> (95%) conversions without any decrease in stability up to 100 h of reforming reaction (CH<sub>4</sub>/CO<sub>2</sub>/He:10/10/80). Filamentous type carbon deposition was present in the catalyst promoted by 1 wt% Ce, but it was absent in the catalyst promoted with 3wt% Ce.

Chen et al. [104] studied the effect of Cu on Ni catalyst for methane dry reforming. Copper may stabilize the structure of the active site on Ni surface for methane cracking reaction, preventing the deactivation of the Ni catalyst caused by sintering or by the loss of nickel crystallites. The addition of Cu into Ni catalyst system can fine-tune the catalytic activity so that the CH<sub>4</sub> cracking and removal of carbon by CO<sub>2</sub> is balanced and prevent inactive carbon accumulation on Ni particle. Thus encapsulated carbon layer does not form on supported Cu/Ni giving the catalyst a stable activity.

### 1.6.2 Catalysts for oxidative dry reforming of methane

Normally the catalysts for dry reforming are also effective in oxidative dry reforming of methane. Even better performance could be obtained for some catalysts in presence of O<sub>2</sub>. For example, In Moral's study, [105] various Rh-based catalysts prepared using different supports:  $\gamma$ -Al<sub>2</sub>O<sub>3</sub>, SiO<sub>2</sub> and CeO<sub>2</sub>. Different O<sub>2</sub>/CH<sub>4</sub> ratios were studied: 0 (dry reforming), 0.10, 0.20 and 0.45. They got the order of performance as Rh/Al<sub>2</sub>O<sub>3</sub> > Rh/ SiO<sub>2</sub> > Rh/CeO<sub>2</sub> in dry reforming. The benefits of enhanced initial and overall CH<sub>4</sub> conversions as well as hydrogen yields are obtained by adding O<sub>2</sub> to the reactor feed, which followed an increasing trend with increasing O<sub>2</sub>/CH<sub>4</sub> ratios in all cases. For the condition of O<sub>2</sub>/CH<sub>4</sub> = 0.2, GHSV was augmented to 150 N L CH<sub>4</sub>/(g<sub>cat</sub> h), the CH<sub>4</sub> conversion value measured is 44% after 2h.

Lucr dio et al. [106] studied the reforming of a model sulfur-free biogas on Ni catalysts supported on Mg(Al)O derived from hydrotalcite precursors. The addition of synthetic air into the system was proven to be efficient for improving the CH<sub>4</sub> conversion and mitigating carbon deposition. The NiMgAl catalyst presented the best performance: In a CH<sub>4</sub>/CO<sub>2</sub>/O<sub>2</sub> ratio of 1:0.67:0.165, 100 mg

of NiMgAl catalyst exhibited 90% and 83% for CH<sub>4</sub> and CO<sub>2</sub> conversion at 750°C. The H<sub>2</sub>/CO ratio was 1.1. This probably due to these strong interactions yielding to a catalyst with more stable active phase at the reactions conditions and avoiding the carbon deposition. Moreover, it has been interestingly found that the addition of Rh and La increased the amount of reducible Ni species and facilitated the reduction of the species interacting strongly with the support which could lead to more carbon deposition.

In Xuejing's study [107] the effects of various O<sub>2</sub> concentrations in biogas on initial conversions and stability at various temperatures on a Ni/SiO<sub>2</sub> catalyst were investigated. They used O<sub>2</sub> co-feeding with model biogas mixture (CH<sub>4</sub>/CO<sub>2</sub>/N<sub>2</sub> = 0.4:0.4:0.2) over 100 mg of catalysts with GHSV of 30,000 mL /h/g<sub>cat</sub>. In the CH<sub>4</sub>/CO<sub>2</sub>/O<sub>2</sub> = 1:1:0.3 condition, the catalyst provided 73% of CH<sub>4</sub> conversion and 45% of CO<sub>2</sub> conversion, and the H<sub>2</sub>/CO ratio was 1.0. They showed that lower percentage of O<sub>2</sub> in biogas improved the activity and stability of the catalysts which was attributed to the inhibited sintering. Higher O<sub>2</sub> concentrations (P10%) in biogas resulted in severe decrease in CO<sub>2</sub> conversion and greater H<sub>2</sub>O productivity.

Asencios et al.[27] tested the catalysts composed of NiO/Y<sub>2</sub>O<sub>3</sub>/ZrO<sub>2</sub> mixtures in the oxidative reforming of a model biogas (1.5CH<sub>4</sub>:1CO<sub>2</sub>) at 750°C for 6h. The formation of Y<sub>2</sub>O<sub>3</sub>-ZrO<sub>2</sub> and NiO-Y<sub>2</sub>O<sub>3</sub> solid solutions increased the rates of conversion of the reactants also promoted the removal of the carbon deposited. The catalyst with 20% of Ni showed the highest conversion and a relatively low amount of carbon during the oxidative reforming of biogas The obtained conversions of CH<sub>4</sub> and CO<sub>2</sub> are 65% and 70%, respectively in presence of oxygen (1.5CH<sub>4</sub> + 1CO<sub>2</sub> + 0.25O<sub>2</sub>) at 750°C, with a H<sub>2</sub>/CO ratio of around 1.

In another example, Gao et al. [108] prepared Ni/5ZrO<sub>2</sub>-SiO<sub>2</sub> catalyst with large Ni-ZrO<sub>2</sub> boundary and tested it in the conditions of CH<sub>4</sub>/CO<sub>2</sub>/O<sub>2</sub> = 1:0.4:0.3 at 700 °C. With a GHSV = 90,000h<sup>-1</sup>, the result after 8 h is obtained as CH<sub>4</sub> Conv. ≈ 68% and CO<sub>2</sub> Conv. ≈ 52% with very slight deactivation. Akri [109] investigated oxidative reforming of methane at 800 °C using a GHSV = 60,000 mL/g/h in CH<sub>4</sub>/CO<sub>2</sub>/O<sub>2</sub> = 1:0.8:0.2. The best result over 10Ni15Ce/illite catalyst after 5h are as follow: CH<sub>4</sub> Conv. ≈ 84%; CO<sub>2</sub> Conv. ≈ 78% and H<sub>2</sub>/CO ratio ≈ 0.9.

Meshkani et al. [110] studied dry reforming, partial oxidation and oxidative reforming of

methane over Ni/MgO catalyst at different temperatures ranging from 500 °C to 700 °C. In the condition of  $\text{CH}_4/\text{CO}_2/\text{O}_2 = 1:1:0.5$  and  $\text{GHSV} = 18000 \text{ mL/h/g}_{\text{cat}}$ . At 700 °C, 200 mg of catalyst containing 15 wt.% nickel revealed the most active catalytic performance: conversion of  $\text{CH}_4$  is 93 % and the  $\text{H}_2/\text{CO}$  ratio is 1.2. Moreover, the obtained results showed that Ni/MgO catalyst with lower Ni content (5%) showed high stability without any decrease in activity during 50 h time on stream.

Gao and Hou et al. [108] investigated the oxidative  $\text{CO}_2$  reforming of methane with different  $\text{ZrO}_2$ -promoted  $\text{SiO}_2$  supported Ni catalysts in a fluidized bed reactor. They found that Ni/5 $\text{ZrO}_2$ - $\text{SiO}_2$  catalyst exhibited the best activity and stability due to the larger Ni- $\text{ZrO}_2$  boundary. A stable result for  $\text{CH}_4$  (70%) and  $\text{CO}_2$  (60%) conversions was obtained at 700 °C at a quite high space velocity  $90,000 \text{ h}^{-1}$ . They also investigated the different-sized Ni catalysts (4.5–45.0 nm) in oxidative dry reforming in another study [111], it was found that both the activity and stability depend strongly on the particles size of Ni catalysts and the space velocity. Small sized Ni is more active and stable at space velocity  $<54,000 \text{ h}^{-1}$ . On larger Ni particles and/or at higher space velocity conditions, surface Ni was oxidized gradually to NiO by remaining  $\text{O}_2$ , causing further Ni catalyst deactivation.

Deng et al. [112] developed a  $\text{LaPrFeNiO}_3$  nano-catalyst for oxidative methane reforming. They found that the Ni particles on the surface could reversibly diffuse back into the perovskite structure by introducing an oxidative atmosphere into the reduced catalyst system. A dynamic separation–embedment cycle could be obtained and precisely adjusted by using promoters under this oxidative  $\text{CO}_2$  reforming condition. The anti-sintering and coking effect of Ni and the catalytic performance are significantly improved in this approach.

## 1.7 Catalyst deactivation

### 1.7.1 Carbon formation

It is well-known that the deactivation of Ni-based catalysts for the methane reforming reaction mainly results from the carbon deposition and the sintering of active Ni particles [113]. Despite high conversion rates observed for many nickel catalysts, the major problem is carbon deposition, which most probably leads to a deactivation during the time on stream. The calculation of the thermodynamics tendency of dry reforming and oxidative dry reforming indicates that carbon formation is favored at a

temperature below 800 °C. In this reaction condition, the carbon formation on the surface of catalysts is unavoidable due to the thermodynamic and kinetic mechanisms. It is usually desired for the carbon to be on the catalyst surface in the form of nanotubes, which causes lower carbon dispersion over the surface, thus preserving its activity for a longer period of time. Moreover, the carbon formation is difficult to eliminate because Ni promotes three reactions leading to carbon deposition: CO disproportionation (Eq. 1-9), CO reduction (Eq.1-10), and CH<sub>4</sub> decomposition (Eq.1-11) [114]. Since pure dry reforming does not involve water, the water-gas shift reaction does not occur significantly, and the loss of CO is essentially due to the formation of carbon. According to Nikoo and Amin [115], from 650 °C up to 1000 °C, the CH<sub>4</sub> decomposition reaction is favored over the CO disproportionation. And they could be mitigated by adding oxygenated species in the gas feed.

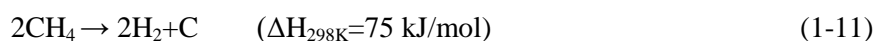
CO disproportionation:



CO reduction:



CH<sub>4</sub> decomposition:



CH<sub>4</sub> decomposition is an endothermic reaction, increase of temperature satisfies this reaction. However, CO disproportionation reaction is an exothermic one, it would be inhibited when temperature increased. Thermodynamic calculations show that the reaction temperature above 582 °C is promoting the occurrence of CH<sub>4</sub> decomposition reaction, while the reaction temperature below 674 °C is beneficial to CO disproportionation. By doing a kinetic calculation, Shamsi, et al. [116] also found that carbon deposition is favored at high-temperature and low-pressure conditions. As shown in **Fig.1-4**, while a low-temperature, high-pressure condition promotes CO disproportionation to form carbon. Usually, CH<sub>4</sub> dry reforming reaction thermodynamically requires temperatures higher than 650 °C, in this range of temperature, the formation of carbon mainly comes from CH<sub>4</sub> decomposition.

At higher temperatures, carbon can be easily oxidized by CO<sub>2</sub>, therefore, when the rate of gasification is equivalent or greater than the rate of carbon formation, there is no carbon deposition in

the reaction.

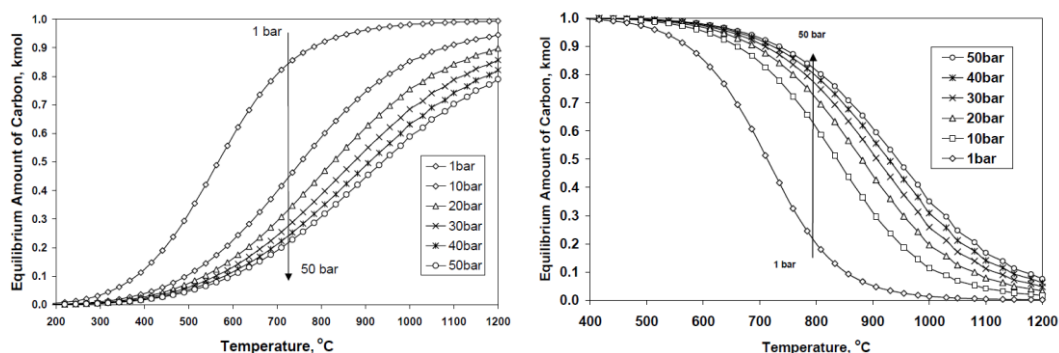


**Fig. 1-4** Left) Effects of temperature and pressure on equilibrium amount of carbon for methane decomposition reaction; Right) Effects of temperature and pressure on equilibrium amount of carbon for CO disproportionation reaction. [116]

In most cases, the  $H_2/CO$  ratio lower than 1 would show that there is more carbon monoxide produced with regards to the hydrogen. Such observation could as well be related to carbon formation via  $CO_2$  direct reduction with hydrogen ( $CO_2 + 2H_2 \rightarrow C + 2H_2O$ ). Occurrence of this reaction could be confirmed by the formation of water at the output of the catalytic system [69].

Depending on the results of characterization study [117], the vast amount of bigger Ni crystallites exist on the catalysts with the highest Ni content promoted direct  $CH_4$  decomposition, resulting in faster catalyst deactivation. Laosiripojana et al. [118] tested  $CeO_2$  doped  $Ni/Al_2O_3$  catalyst in dry reforming of methane. According to the range of temperature in this study, 800–900 °C, carbon formation would be formed via the decomposition of methane and Boudouard reactions. The amount of carbon formation decreased with increasing Ce content. Finally, no carbon species was observed when the Ce doping content was higher than 8%.

Kohn and co-researchers [61] indicated that both the thermodynamic and kinetic mechanisms for dry reforming result in surface carbon that must be removed using oxygenated species either in the catalyst support or in the gas feed to maintain the activity of the catalyst.  $O_2$  has a higher oxidation potential than  $CO_2$  or  $H_2O$ , so it is ideal for removing surface carbon. This is shown in **Fig. 1-5**, where at least 1.5 mol of  $CO_2$  is needed per mole of  $CH_4$  to be outside of the carbon formation regime, but only 0.03 mol of  $O_2$  is needed per mole of  $CH_4$ .

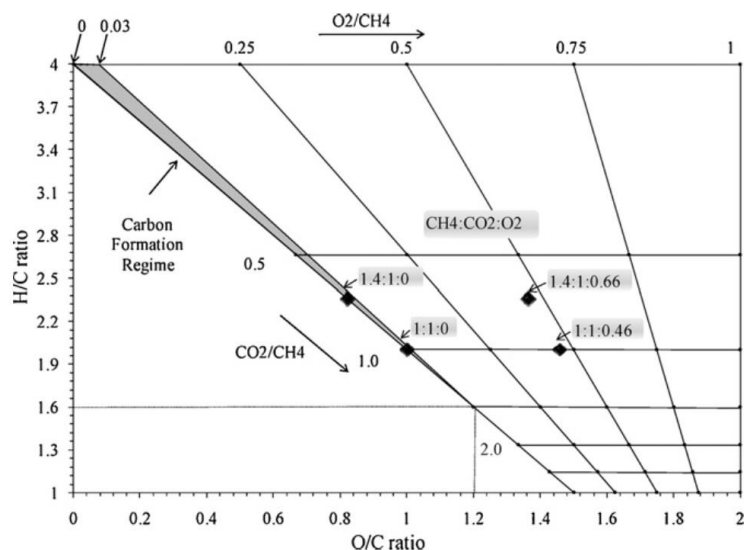


Fig. 1-5 Thermodynamic carbon formation regime at 450 °C and 1 atm.[61]

Zhang and Muratsugu [119] evaluated carbonaceous deposits on the spent Ni catalysts by Raman spectra after dry reforming. And they observed the relatively strong intensity of the D band to the G band, which suggests the presence of more disordered carbonaceous species than graphitic carbon on all the used Ni catalysts since the intensity of the D band increases with the increasing structural imperfections of graphite. The active  $C_a$  species is presumed to result from the thermal decomposition of methane, and considered as important intermediates for the formation of CO. In addition, the reactivity of the deposited carbon on Ni metal in dry reforming was improved by the accompanied Ce promoters in NiCe/SBA-16.

Coking phenomenon was found to be limited in case of highly dispersed metal species at the surface of the support.  $CeO_2$  is widely known as an effective support and the effect is ascribed to its excellent oxygen storage capacity, which might be favoring the oxidation of the carbon deposits formed upon direct methane decomposition [96]. Metallic catalysts promoted with cerium are interesting due to the improved mechanic, thermal resistance and higher Ni dispersion of the catalyst. In general better catalytic performance and lower carbon content are obtained [120]. In Albarazi's study [121], they found that ceria and zirconia as promoters have significant influence on the stability of catalysts. The results indicated that the unmodified Ni/SBA-15 showed clear deactivation especially in the first period of the stability test and between 600 °C and 630 °C during the activity test whereas the ceria-zirconia doped samples had better stability.

Akri and Chafik et al. [65] compared carbon balance value obtained with 10Ni15Ce and 10Ni catalysts with 10% of Ni in the methane reforming process, they confirmed that the presence of cerium in the catalyst reduces carbon deposition efficiently. The better catalytic activity of the Ce-promoted catalyst was attributed to the presence of oxygen vacancies in fluorite structure facilitating CO<sub>2</sub> adsorption and gasification of the CH<sub>x</sub> species according to Eqs. (1-12) and (1-13) [122]:



### 1.7.2 Sintering

The sintering and agglomeration of metal particles are leading to a loss of stability or severe deactivation. Generally, the growth of component size could lead to the aggregation of active particles, which is reported as one of the main reason of the deactivation. The limited surface areas or the high temperature (>800 °C) is adopted to both damage for active particles subjected to sintering. Many studies have been focused on avoiding sintering during reforming process. Generally, at high temperature, one can expect to enhance the stability of Ni based catalysts by adding a third metal, such as Si [123] or Al [124] to improve different properties like obtaining higher surface area or a better dispersion of the active sites. The strong metal-support interaction and fine dispersion could suppress sintering according to the literature [125]. It has been evidenced that the addition of aluminum into Ce-Ni-O systems has advantages on both the catalytic and mechanical properties. The addition of aluminum leads to disorganization of the structure with favored interactions between Al<sup>3+</sup> cations and Ni<sup>2+</sup> cations [87]. In Zuo's study [126], the catalyst performance of dual support Mg-Al mixed oxides and SBA-15 catalysts were prepared and tested in DRM. For metals well-dispersed over SBA-15 support, the Ni<sup>0</sup> particles were isolated from one another so that the clustering of Ni was prevented. As a result, Ni sintering was suppressed, which can be attributed to the strong metal-support interaction and the channel local effect of SBA-15.

Another example is that Joung et al. [86] invested the Ni-based catalysts resistant to sintering in DRM. They deposited Ni nanoparticles with a small size of 5.2 ± 0.4 nm onto functionalized SiO<sub>2</sub> nanospheres (Ni/SiO<sub>2</sub>), presenting a fine dispersion, the Ni/SiO<sub>2</sub> was coated with a silica overlayer which prevents the small Ni nanoparticles from sintering, and no carbon formation is observed after 170

h of the reaction.

## 1.8 Objective of the thesis

In summary, catalytic transformation of methane in the presence of carbon dioxide and oxygen is a very desirable route to produce H<sub>2</sub>. In the literature, Ni-based catalysts have been widely reported for H<sub>2</sub> production from the catalytic transformation of methane based on its excellent activity to break the C-C and C-H bonds. However, Ni-based catalysts easily suffer deactivation caused by metal sintering and carbon formation with the time on stream. Very few systems have been reported as good candidates for efficient conversion rates and H<sub>2</sub> production from dry reforming or oxidative biogas reforming at low temperatures ( $\leq 700$  °C).

The aim of the present work is to develop stable Ni-based catalysts for H<sub>2</sub> production via DRM and ODRM at low temperatures. Ni-based mixed oxide and SBA-15 supported catalyst are systematically studied in detail by investigating the compositional properties and influence of different parameters. Furthermore, comprehensive structural characterizations of the obtained compounds are performed.

Herein in the present thesis, catalytic DRM and ODRM tests are carried out at different conditions and particular interest is devoted to the understanding of the correlation between structure and catalytic performance, as well as carbon deposition. Many different parameters are comprehensively analyzed. Specifically, testing is also performed with pure reactants at a low temperature of 600 °C, to gain further knowledge about the catalyst in severe conditions. Another objective is dedicated to studying on parameters optimization for ODRM, to obtain an energy efficiency benefits and carbon-free process. Finally, the active phase, active sites and possible mechanism are discussed.

## **Chapter 2**

# **Preparation and characterization of catalysts**



## 2 Preparation and characterization of catalysts

In the present thesis, different types of Ni-based catalysts are synthesized.  $\text{CeNi}_x(\text{Al}_z)\text{O}_y$  and  $\text{Ni}_x\text{Mg}_2\text{AlO}_y$  catalysts are prepared by co-precipitation method (CP), while  $\text{Ni}_x\%$ /SBA-15 catalysts are prepared by deposition precipitation procedure (DP). Various physicochemical techniques, such as  $\text{N}_2$  physisorption, XRD, Raman,  $\text{H}_2$ -TPR, XPS, *etc.* are employed to systematically characterize the properties of the catalysts. The characterization methods are detailed in *Annex I*.

### 2.1 $\text{CeNi}_x(\text{Al}_z)\text{O}_y$ catalysts

#### Preparation of $\text{CeNi}_x(\text{Al}_z)\text{O}_y$ mixed oxides ( $0.1 \leq x \leq 5$ , $z = 0$ or $0.5$ ) by co-precipitation method

The material was prepared by co-precipitation method of the corresponding hydroxides from mixtures of nickel and cerium nitrates. Triethylamine (TEA) ( $\text{C}_2\text{H}_5)_3\text{N}$ , (Sigma-Aldrich,  $\geq 99.5\%$  assay) is used as the precipitant agent in the presence of methanol (Sigma-Aldrich,  $\geq 99.8\%$  assay). The co-precipitation technique has been widely used to promote strong interactions retarding the sintering of the active phase during the catalytic processes and maintaining the desired small particle size. Compared with impregnation method, the catalyst prepared following the co-precipitation synthesis route does not favor methane decomposition, and thus minimizes carbon formation and deposition, which results in the deactivation of the catalyst [127].

At first, salt precursors (nickel nitrate hexahydrate 99%)  $\text{Ni}(\text{NO}_3)_2 \cdot 6\text{H}_2\text{O}$ ,  $\text{Ce}(\text{NO}_3)_3 \cdot 6\text{H}_2\text{O}$ , and/or  $\text{Al}(\text{NO}_3)_3 \cdot 6\text{H}_2\text{O}$  were dissolved in an appropriate volume of distilled water, respectively. Then the mixture was continuously added dropwise into a mixed solution of trimethylamine (TEA) and methanol under stirring. After filtration, the solids were dried at  $100\text{ }^\circ\text{C}$ , subsequently calcined in air at  $500\text{ }^\circ\text{C}$  for 4h. The  $\text{Ni}/\text{M}_T$  molar ratio is according to the nickel molar proportion in all the metals. Binary catalysts prepared in this study were designated as  $\text{CeNi}_{0.1}\text{O}_y$ ,  $\text{CeNi}_{0.3}\text{O}_y$ ,  $\text{CeNi}_{0.5}\text{O}_y$ ,  $\text{CeNi}_1\text{O}_y$  and  $\text{CeNi}_2\text{O}_y$ . While ternary catalysts were designated as  $\text{CeNi}_{0.5}\text{Al}_{0.5}\text{O}_y$ ,  $\text{CeNi}_1\text{Al}_{0.5}\text{O}_y$ ,  $\text{CeNi}_2\text{Al}_{0.5}\text{O}_y$  and  $\text{CeNi}_5\text{Al}_{0.5}\text{O}_y$ .

#### Elemental analysis and textural properties

The precise Ni contents and the specific surface areas of  $\text{CeNi}_x\text{O}_Y$  and  $\text{CeNi}_x\text{Al}_{0.5}\text{O}_Y$  catalysts are analyzed and summarized in **Table 2-1**. The elemental chemical analysis confirms that Ni compositions of the catalysts are very similar to the nominal values. All the binary catalysts exhibit surface area higher than  $95 \text{ m}^2 \text{ g}^{-1}$ . Specifically, the  $\text{CeNi}_{0.3}\text{O}_Y$  and  $\text{CeNi}_{0.5}\text{O}_Y$  catalysts present specific areas in the range of about  $117\text{-}127 \text{ m}^2 \text{ g}^{-1}$ . Whereas ternary  $\text{CeNi}_x\text{Al}_{0.5}\text{O}_Y$  compounds have larger surface areas ranging from  $73$  to  $141 \text{ m}^2 \text{ g}^{-1}$  depending on different Ni content.

**Table 2-1** Ni content, specific surface area and average crystallites size of Ce-Ni-(Al) catalysts

Sample	Ni(wt.%)	Ni/ $M_T$	Surface BET ( $\text{m}^2/\text{g}$ )	$d_{\text{CeO}_2}(\text{nm})^s$	$d_{\text{NiO}}(\text{nm})^s$
NiO	—	—	—	—	>20
CeO <sub>2</sub>	—	—	53	7	—
CeNi <sub>0.1</sub> O <sub>Y</sub>	2.8	0.09	95	4.7	—
CeNi <sub>0.3</sub> O <sub>Y</sub>	6.5	0.23	117	4.6	—
CeNi <sub>0.5</sub> O <sub>Y</sub>	11.7	0.33	127	4.3	10.1
CeNi <sub>1</sub> O <sub>Y</sub>	22.6	0.50	111	4.3	8.3
CeNi <sub>2</sub> O <sub>Y</sub>	35.8	0.67	109	3.8	10.2
CeNi <sub>0.5</sub> Al <sub>0.5</sub> O <sub>Y</sub>	12.0	0.25	141	3.9	—
CeNi <sub>1</sub> Al <sub>0.5</sub> O <sub>Y</sub>	19.5	0.4	115	4.1	7.2
CeNi <sub>2</sub> Al <sub>0.5</sub> O <sub>Y</sub>	30.8	0.57	73	3.8	5.9
CeNi <sub>5</sub> Al <sub>0.5</sub> O <sub>Y</sub>	49.2	0.77	106	4.4	5.5

<sup>s</sup> Measured by XRD.  $\text{Ni}/M_T = x/(x + 1)$  for  $\text{CeNi}_x\text{O}_Y$  and  $\text{Ni}/M_T = x/(x + 1.5)$  for  $\text{CeNi}_x\text{Al}_{0.5}\text{O}_Y$ . (—) = not observed.

## XRD studies

### CeNi<sub>x</sub>O<sub>Y</sub> catalysts

The structure and crystalline phase of  $\text{CeNi}_x(\text{Al}_z)\text{O}_Y$  catalysts are investigated by XRD analysis. **Fig. 2-1** shows the XRD patterns of the  $\text{CeNi}_x\text{O}_Y$  nano-compounds with various Ni contents. Only a ceria like phase (34-0394 JCPDS file) which has a fluorite structure is clearly apparent in each sample, while the NiO crystalline phase (4-0835 JCPDS file) could be detected when a specific value of  $X \geq 0.5$  (corresponding to the Ni wt%  $\geq 11.7$  wt%). Furthermore, the diffraction peaks of crystallized NiO become gradually more intense with higher Ni content. On the other hand, there is no peak related to NiO that could be observed with lower Ni content ( $X < 0.5$ ). This suggests that Ni species is probably incorporated into the  $\text{CeO}_2$  lattice and that a solid solution of cerium and nickel is formed. As reported

in previous studies, the addition of nickel has an effect both on the broadness and their positions of  $\text{CeO}_2$  peaks. This phenomenon is attributed to the substitution of  $\text{Ce}^{4+}$  cations by  $\text{Ni}^{2+}$  cations inside the  $\text{CeO}_2$  lattice and was interpreted by the formation of the cerium-nickel solid solution [128][129]. Noting that the  $\text{Ni}^{2+}$  cation ionic radius (0.7 Å) is smaller than that of  $\text{Ce}^{4+}$  cation (0.9 Å).[87] Therefore, the  $\text{CeNi}_x\text{O}_y$  compounds were able to be divided into two categories depending on the nickel content: the first category with  $x \leq 0.5$  corresponds to a solid solution with the substitution of  $\text{Ni}^{2+}$  ions in the  $\text{CeO}_2$  lattice and the second category with  $x > 0.5$  concerns compounds in which crystallized NiO and solid solution coexist [130,131]. Moreover, it has been also proposed that small NiO nano-crystallites (non visible by XRD) can be always present whatever the Ni content. It also has been reported that the highest proportion of solid solution is obtained for the  $\text{CeNi}_{0.5}\text{O}_y$  compound ( $\text{Ni}/\text{M}_T = 0.3$ ) [87]. The average sizes of the NiO particles are measured using the Scherrer Equation from the XRD results. The NiO average crystallites sizes are found between 8 and 10 nm (Table 2-1). While the size of  $\text{CeO}_2$  particles maintain between 4 and 5 nm which are slightly increased when the content of Ce increases.

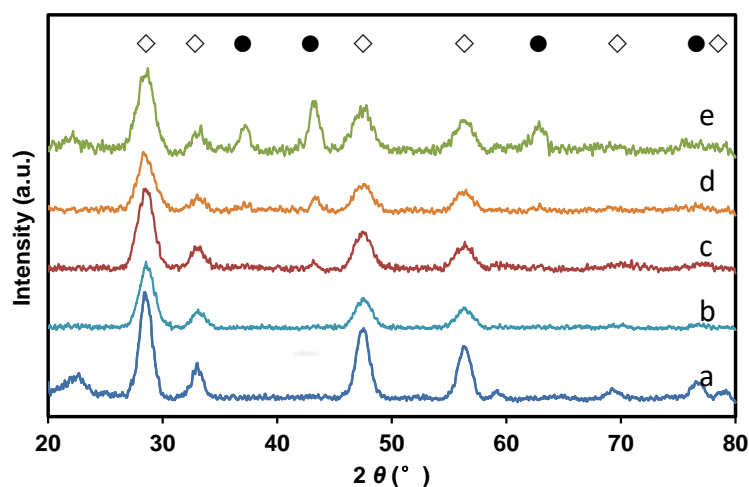


**Fig. 2-1** XRD patterns of  $\text{CeNi}_x\text{O}_y$  catalysts: a )  $x = 0.1$  , b)  $x = 0.3$ , c)  $x = 0.5$ , d)  $x = 1$ , e)  $x = 2$ .  $\text{CeO}_2$   $\diamond$ , NiO  $\bullet$ .

### $\text{CeNi}_x\text{Al}_{0.5}\text{O}_y$ catalysts

**Fig. 2-2** shows the diffraction patterns obtained on  $\text{CeNi}_x\text{AlO}_y$  catalysts, ( $x=0.5, 1, 2$  and  $5$ ). Similar as binary compound, only the  $\text{CeO}_2$  like phase could be detected in all samples analyzed. When the  $x$  value is  $0.5$ , there is no NiO crystallites are able to be observed by XRD. This phenomenon can be attributed to the substitution of  $\text{Ce}^{4+}$  cations by  $\text{Ni}^{2+}$  cations inside the  $\text{CeO}_2$  lattice and, as previously explained on binary compounds, can be interpreted by the formation of the cerium-nickel solid solution.

However, the presence of very small NiO nano-crystallites (not visible by XRD) cannot be discarded. No peak related to Al could be detected in any compounds, which can be due to the same reasons, with the insertion of aluminum species into Ni–Ce–O phase to form Ni–Ce–Al–O solid solution. However, the presence of an amorphous phase cannot be discarded also. With higher Ni content, crystallized NiO phase appears for a value of x above 0.5, and the NiO peak intensity increases with the nickel content as expected. An estimation of the average crystallites size at about 4 nm for CeO<sub>2</sub> phase and at about 7nm for NiO phase is obtained (**Table 2-1**). Therefore, the nickel species would be in close interaction with the cerium and also aluminum species. Compared with binary catalysts, the introduction of aluminum in these systems allows the nickel oxide crystallization to be diminished [87], in good agreement with known dispersing effect of Al.

For higher nickel contents, small crystallites can be still present, but the solid solution formation could be limited to the benefit of the growth of larger crystallites. Other authors [132] have observed similar features that nickel content beyond a limit would prevent further formation of solid solution. Consequently, the results obtained are in agreement with some favored interactions between aluminum and nickel and cerium. Under this scenario, as for the binary compounds, different types of systems can be conceived, and Ni species can be found i) in solid solution of cerium nickel and aluminum, ii) in small NiO nano-crystallites (not visible by XRD) and iii) in larger nano-crystallites (7 nm) when detected by XRD. Besides, the presence of amorphous phases cannot be discarded. Moreover, the average dimensions obtained for each ternary oxide are summarized in **Table 2-1**, evidencing that the size of the crystallites of the mixed oxides is always smaller than the size measured for the pure oxides. Moreover, the presence of Al seems to delay the crystallization of NiO, shifting the NiO average crystallites size to smaller values (6-7 nm) compared to binary compounds (8-10 nm).

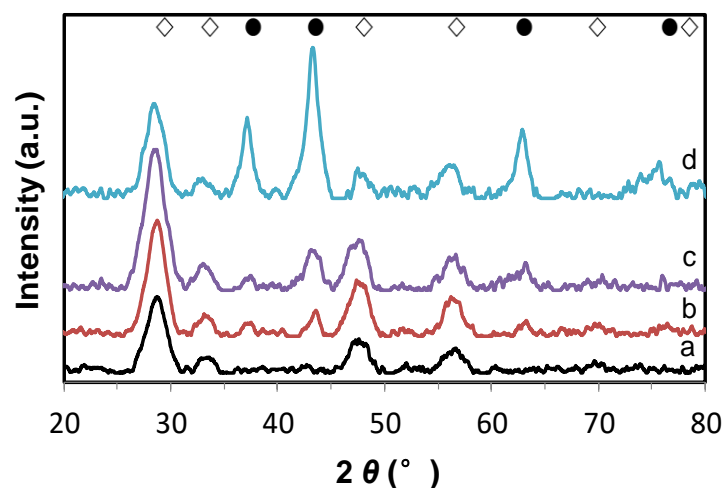


**Fig. 2-2** XRD patterns of  $\text{CeNi}_x\text{Al}_{0.5}\text{O}_y$  catalysts: a )  $x = 0.5$ , b)  $x = 1$ , c)  $x = 2$ , d)  $x = 5$ .  $\text{CeO}_2$   $\diamond$ ,  $\text{NiO}$   $\bullet$

### Raman studies

In general, Raman characterization is an effective technique to gain insight into the structure and formation of oxygen vacancy defects. The catalysts are characterized by Raman spectroscopy and the results of  $\text{CeNi}_x\text{O}_y$  and  $\text{CeNi}_x\text{Al}_{0.5}\text{O}_y$  are shown in **Fig. 2-3** and **Fig. 2-4**, respectively. In both cases, there is a strong frequency shift and broadening for the first-order  $F_{2g}$  ceria peak located near  $460\text{ cm}^{-1}$  related to fluorite nano-crystalline  $\text{CeO}_2$  [133], [134]. For  $\text{CeNi}_x\text{O}_y$ , shifts to lower frequencies could be seen for several compounds. Similarly, For  $\text{CeNi}_x\text{Al}_{0.5}\text{O}_y$  catalysts it shifts to  $449\text{ cm}^{-1}$ . The same trend was reported in the literature on the cerium-nickel mixed oxides (shift to  $443\text{ cm}^{-1}$ ) [135]. This behavior can be interpreted as an occurrence of the nickel species dissolved into the ceria phase, which is in agreement with the presence of a solid solution [136]. The shift forwards to lower energies and the lines shape of this feature gets broader as the particle size get smaller. Moreover, according to the literature [82], the shoulder and asymmetry towards lower wave numbers can be interpreted as the presence of particles below 10 nm, thus in better accordance with XRD crystallites size.

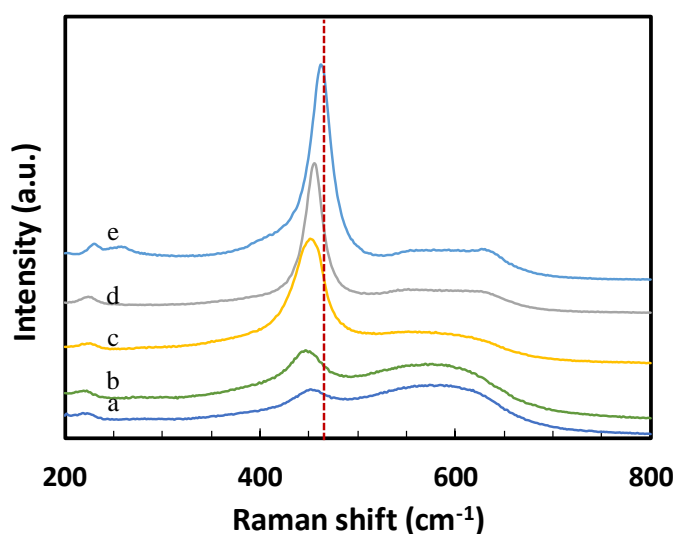


Fig. 2-3 Raman spectra of CeNi<sub>x</sub>O<sub>y</sub> catalysts: x = 2 (a), x = 1 (b), x = 0.5 (c), 0.3 (d) and 0.1 (e).

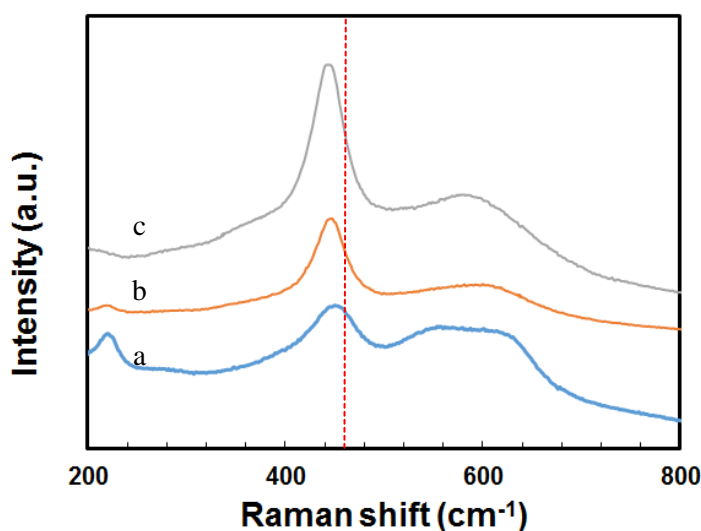


Fig. 2-4 Raman spectra of CeNi<sub>x</sub>Al<sub>0.5</sub>O<sub>y</sub> catalysts: x = 5 (a), 2 (b) and 0.5 (c).

Secondary peak at about 230 cm<sup>-1</sup> assigned to ceria nanostructures are also observed in all cases [135]. The band at 600 cm<sup>-1</sup> is characteristic of oxygen vacancies in the ceria lattice [137] or to defects in nanoparticles [82]. In all cases, it is difficult to detect the signal at approximately 520 cm<sup>-1</sup> related to NiO because of a shadowing effect by the long tail of the first-order CeO<sub>2</sub> peak [138]. As a matter of fact, weak shoulders between 500 cm<sup>-1</sup> and 650 cm<sup>-1</sup> were observed for all samples, this phenomenon has already been observed on doped cerium oxides and attributed to oxygen vacancies created by the incorporation of the dopant [139]. It can be decomposed in two contributions at 547 cm<sup>-1</sup> and 615 cm<sup>-1</sup>. The component at 547 cm<sup>-1</sup> was assigned to an extrinsic defect mode induced by oxygen vacancies that

can be increased in case of the substitution of  $\text{Ce}^{4+}$  by lower valence cations in a solid solution [82]. A similar explanation is: two modes positioned at  $540\text{ cm}^{-1}$  and  $600\text{ cm}^{-1}$  were related to the local vibrations of different oxygen vacancy ( $\text{V}_\text{O}$ ) complexes. It has been reported that the mode at  $600\text{ cm}^{-1}$  originates from the existence of  $\text{Ce}^{3+}\text{-V}_\text{O}$  complexes in the ceria lattice [140]. Therefore, the Raman analysis shows the presence of a solid solution of cerium and nickel (and aluminum) and validated the XRD results, indicating strong interactions between Ni, Ce and/or Al species.

## XPS studies

### $\text{CeNi}_x\text{O}_y$

Herein, a careful examination of the  $\text{Ni}2p_{3/2}$  band shapes of the mixed oxides is illustrated in **Fig. 2-5**. It has to be noted that for the very low Ni content the uncertainty is high. When for the  $\text{Ni}/M_\text{T} \leq 0.3$  ( $\text{CeNi}_{0.5}\text{O}_y$ ), only one main peak can be identified. And the binding energy found at about 855.2-855.4 eV shows the presence of  $\text{Ni}^{2+}$  species in strong interaction with other species, in agreement with the formation of a solid solution [141]. There is an intensity increasing effect and multiplet splitting with the nickel content increases. And two peaks are observed for  $\text{Ni}2p_{3/2}$  [142] when the  $\text{Ni}/M_\text{T}$  increased to 0.5. on Ni-CeO<sub>2</sub> systems, such peak at 855.4 eV has also been attributed to  $\text{Ni}^{2+}$  species in strong interaction with Ce species [82]. The  $\text{Ni}2p_{3/2}$  core-level satellite lines are also seen at around 861 eV, about 6 eV up to the main peak confirming the presence of  $\text{Ni}^{2+}$  species. For high Ni/Ce ratios several types of surface nickel seem to coexist, in complement to the previous  $\text{Ni}^{2+}$  species with a BE at 855.2-855.4 eV there are also  $\text{Ni}^{2+}$  with a BE at about 853.5 eV which is in agreement with the presence of NiO observed by XRD results. Therefore, all the results show the presence of  $\text{Ni}^{2+}$  cations in strong interaction with other cations. The relevant atomic ratios as well as the binding energies (BE), from fitting of the main peaks related to Ni2p and O1s are summarized in **Table 2-2**. As shown in **Fig. 2-6**, O1s lines of the compounds have all binding energies of 529.3-529.7 eV, showing unambiguously that the oxygen element is characteristic of some typical  $\text{O}^{2-}$  lattice oxygen species in agreement with the presence of oxides. Depending on literature [143], while the higher energy band at 531.3-531.4 eV can be ascribed to oxygen species related to the presence of hydroxyl groups ( $\text{OH}^-$ ) at the surface of the compounds.

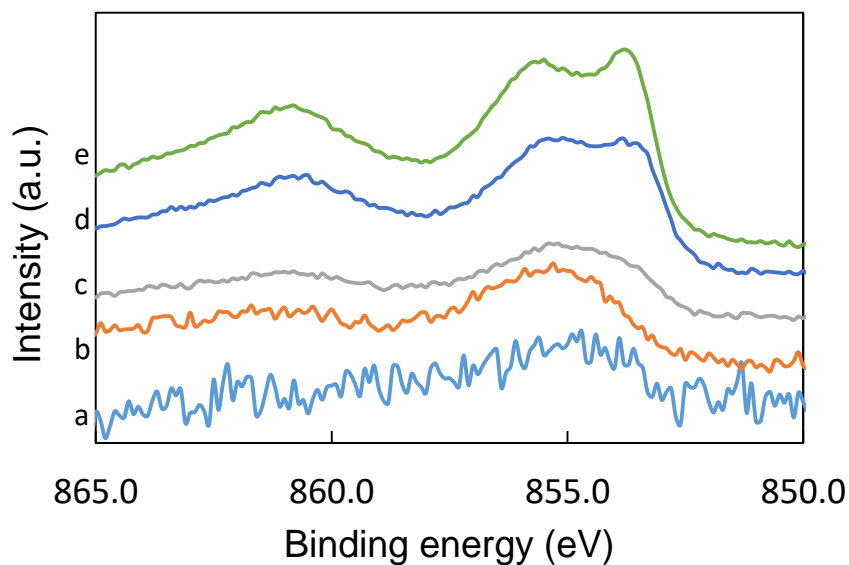


Fig. 2-5 Ni  $2p_{3/2}$  XPS spectra of (a)  $\text{CeNi}_{0.1}\text{O}_y$  (b)  $\text{CeNi}_{0.3}\text{O}_y$  (c)  $\text{CeNi}_{0.5}\text{O}_y$  (d)  $\text{CeNi}_1\text{O}_y$  and (e)  $\text{CeNi}_2\text{O}_y$

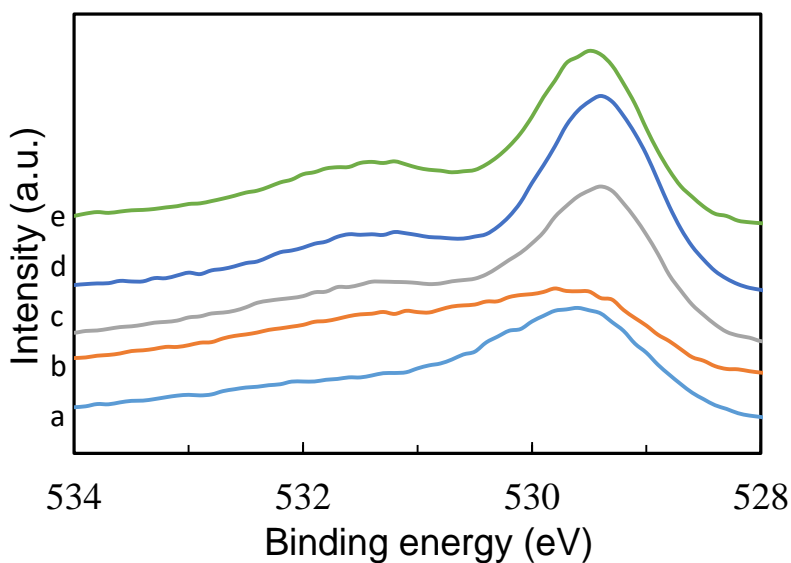


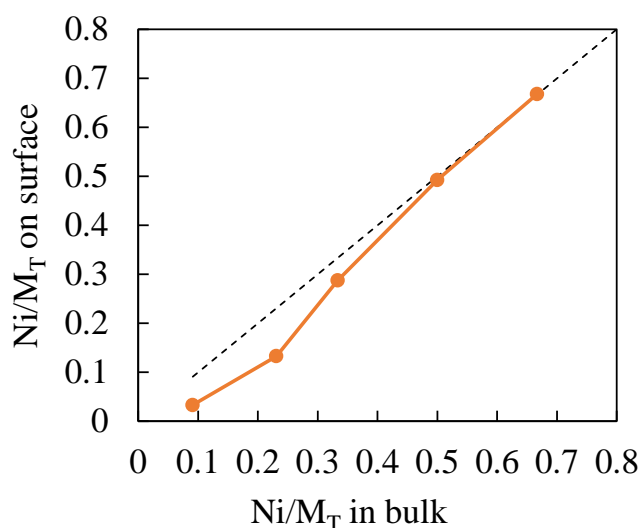
Fig. 2-6 O1s, XPS spectra of  $\text{CeNi}_x\text{O}_y$  catalysts (a)  $\text{CeNi}_{0.1}\text{O}_y$  (b)  $\text{CeNi}_{0.3}\text{O}_y$  (c)  $\text{CeNi}_{0.5}\text{O}_y$  (d)  $\text{CeNi}_1\text{O}_y$  and (e)  $\text{CeNi}_2\text{O}_y$

Table 2-2 Binding energies and surface Ni molar ratio of the  $\text{CeNi}_x\text{O}_y$  catalysts

Catalyst	Ni $2p_{3/2}$ / eV	Ni $2p_{1/2}$ / eV	O1s/ eV	Ni/ $M_T$	Ni/ $M_T$ On surface
$\text{CeNi}_{0.1}\text{O}_y$	854.7	861.8	529.7	0.09	0.03
$\text{CeNi}_{0.3}\text{O}_y$	855.2	861.7	529.7	0.23	0.13

CeNi <sub>0.5</sub> O <sub>Y</sub>	853.4/ 855.2	860.8	529.4/ 531.3	0.33	0.29
CeNi <sub>1</sub> O <sub>Y</sub>	853.8/ 855.3	860.6	529.4/ 531.3	0.50	0.49
CeNi <sub>2</sub> O <sub>Y</sub>	853.7/ 855.4	860..8	529.3/ 531.4	0.67	0.67

However, some quantitative XPS features provide additional information. Superficial nickel compositions of the mixed oxides determined from XPS atomic ratios are compared to bulk nickel content in **Fig. 2-7**. It is clear that the evolution of superficial nickel composition versus bulk nickel content is close to the case of a homogeneous distribution of nickel inside the solid (45° diagonal line). Only CeNi<sub>0.3</sub>O<sub>Y</sub> appears slightly lower. It can be seen that, globally, the Ni/M<sub>T</sub> ratios on surface are close to those in bulk, showing relatively well homogeneous distribution of nickel species in this series of catalysts.



**Fig. 2-7** Variation of Ni/M<sub>T</sub> surface ratio (XPS) as a function of Ni/M<sub>T</sub> bulk ratio in CeNi<sub>x</sub>O<sub>Y</sub> compounds.

### CeNi<sub>x</sub>Al<sub>0.5</sub>O<sub>Y</sub>

The ternary mixed oxides were also studied by XPS. In the literature, a binding energy of 74.5 eV has been reported for the Al 2p photopeak in an Al matrix. The binding energy of Al 2p is very close to the satellite line of Ni 3p. Nevertheless, the uncertainty of the Al 2p photopeak positions in the CeNi<sub>x</sub>Al<sub>0.5</sub>O<sub>Y</sub> compounds does not allow an interpretation of the environment of the Al species. It could be only found and inferred by showing the spectra of Ni 3p, as presented in **Fig. 2-8**. The spectra obtained for the ternary catalysts at Ni 3p level could be considered incorporating Ni 3p and an Al 2p

simultaneously. Therefore, it is possible to infer the Ni/Al ratio. The result is summarized in **Fig. 2-9**. It shows that the Ni/Al ratio on the surface is getting lower compared with that in bulk with the Ni content increase. However, when aluminum is present, the Ni 2p<sub>3/2</sub> and O 1s binding energies are higher than those measured for the binary oxides, showing that the introduction of aluminum influences the top-surface nickel species. A Ni2p<sub>3/2</sub> binding energy of 855.5-855.7 eV is obtained showing the presence of Ni<sup>2+</sup> species in strong interaction with other cations. The value is even higher than the one obtained on the binary oxides showing higher interactions. The value is intermediate between binding energies due to nickel in a spinel structure and nickel in the binary oxide.

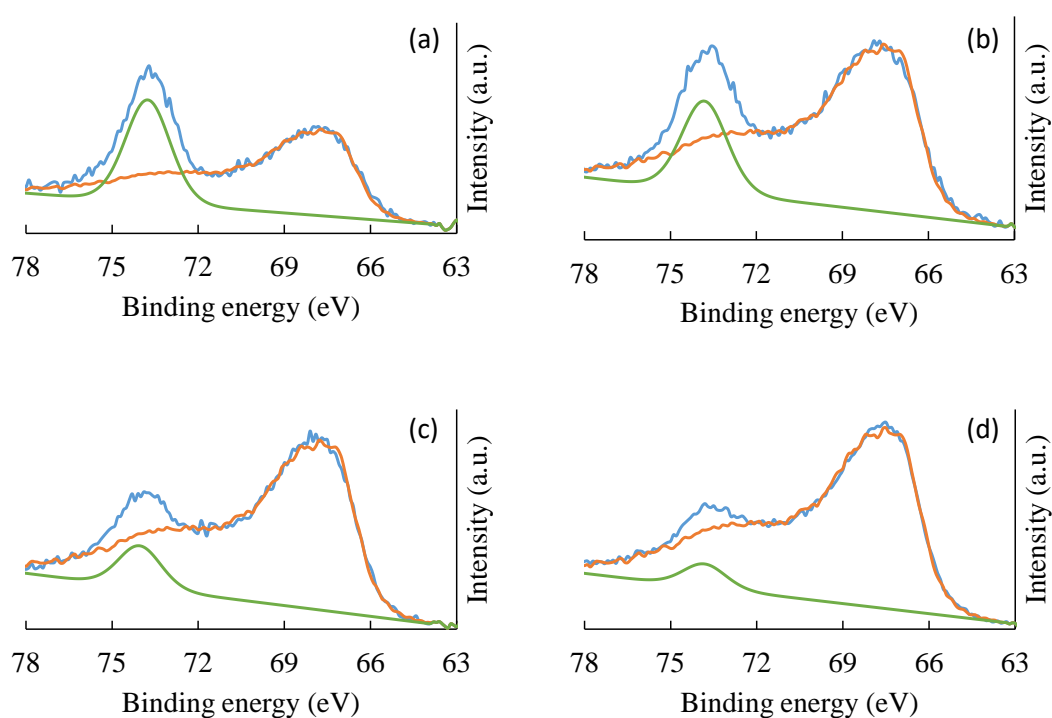


**Fig. 2-8** XPS spectra of Al 2p and Ni 3p of CeNi<sub>5</sub>Al<sub>0.5</sub>O<sub>γ</sub> (a) CeNi<sub>2</sub>Al<sub>0.5</sub>O<sub>γ</sub> (b), CeNi<sub>1</sub>Al<sub>0.5</sub>O<sub>γ</sub> (c) and CeNi<sub>0.5</sub>Al<sub>0.5</sub>O<sub>γ</sub> (d). blue: global spectra; orange: component Ni 3p; green: component Al 2p

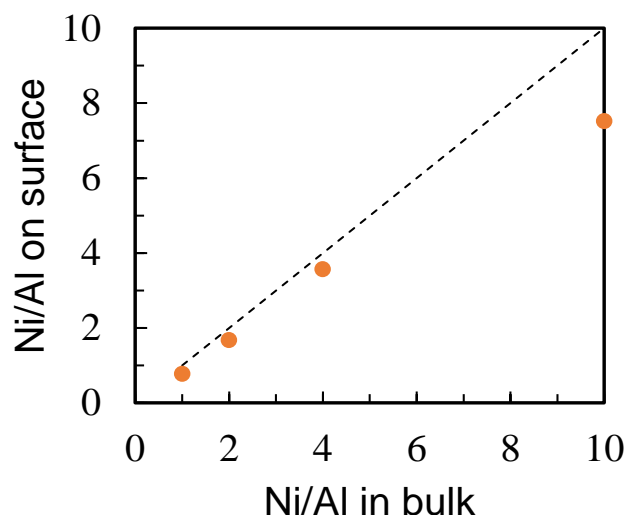


**Fig. 2-9** Variation of Ni/Al surface ratio (XPS) as a function of Ni/Al bulk ratio (microanalysis) in  $\text{CeNi}_x\text{Al}_{0.5}\text{O}_y$  compounds.

For all the  $\text{CeNi}_x\text{Al}_{0.5}\text{O}_y$  catalyst analyzed, a main emission peak in  $\text{Ni}2p_{3/2}$  region is observed (**Fig. 2-10** and **Table 2-3**). There are also  $\text{Ni}^{2+}$  species with a BE at about 853.8-854.6 eV showing the presence of other  $\text{Ni}^{2+}$  species which is in agreement with the presence of NiO observed by XRD results. The O1s spectra are also reported in **Fig. 2-11**. Whereas two peaks with BE at 529.4-529.8 eV and 531.3-532.0 eV are observed, showing that there are two types of oxygen states in these catalysts. As reported for binary catalysts, the peak at about 531.3 eV is assigned to the oxygen species in hydroxyl groups while the peak at about 529.8 eV corresponds to the typical  $\text{O}^{2-}$  lattice oxygen species in oxides.

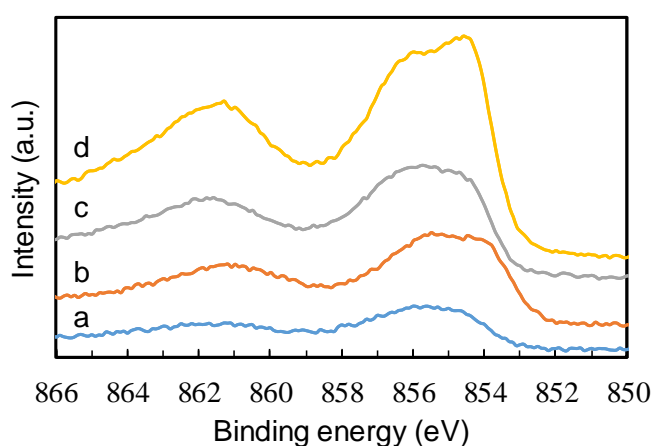


**Fig. 2-10** Ni  $2p_{3/2}$  XPS spectra of (a)  $\text{CeNi}_{0.5}\text{Al}_{0.5}\text{O}_y$  (b)  $\text{CeNi}_1\text{Al}_{0.5}\text{O}_y$  (c)  $\text{CeNi}_2\text{Al}_{0.5}\text{O}_y$  and (d)  $\text{CeNi}_5\text{Al}_{0.5}\text{O}_y$

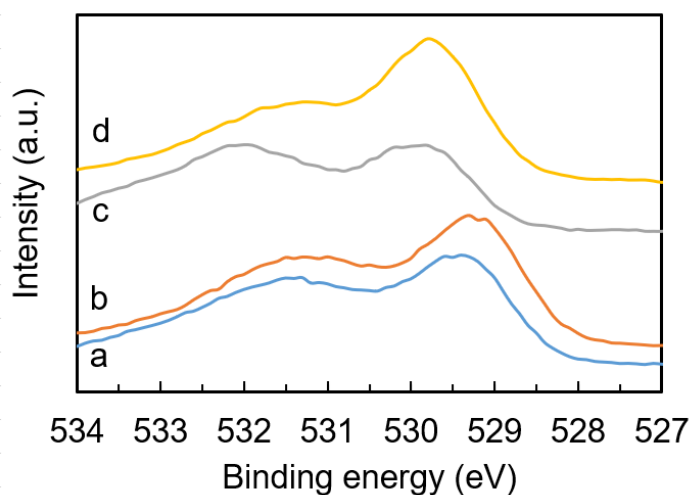


**Fig. 2-11** O1s, XPS spectra of  $\text{CeNi}_x\text{Al}_{0.5}\text{O}_y$  catalysts (a)  $\text{CeNi}_{0.5}\text{Al}_{0.5}\text{O}_y$  (b)  $\text{CeNi}_1\text{Al}_{0.5}\text{O}_y$  (c)  $\text{CeNi}_2\text{Al}_{0.5}\text{O}_y$  and (d)  $\text{CeNi}_5\text{Al}_{0.5}\text{O}_y$

**Table 2-3** Binding energies and surface Ni molar ratio of the  $\text{CeNi}_x\text{Al}_{0.5}\text{O}_y$  catalysts

Catalyst	Ni2p <sub>3/2</sub> / eV	Ni2p <sub>3/2</sub> / eV	O1s/ eV
$\text{CeNi}_{0.5}\text{Al}_{0.5}\text{O}_y$	855.6	860.8	529.4/ 531.3
$\text{CeNi}_1\text{Al}_{0.5}\text{O}_y$	853.8/ 855.5	861.0	529.3/ 531.3
$\text{CeNi}_2\text{Al}_{0.5}\text{O}_y$	854.3/ 855.7	861.7	529.8/ 532.0
$\text{CeNi}_5\text{Al}_{0.5}\text{O}_y$	854.6/ 855.5	861.3	529.8/ 531.3

**Fig. 2-12** illustrates the  $\text{Ni}/\text{M}_T$  surface ratio obtained by XPS versus the bulk  $\text{Ni}/\text{M}_T$  molar ratio. The evolution of nickel composition on the surface versus bulk nickel content is well close to the case of a homogeneous distribution of nickel inside the solid (45 diagonal line). There is a well-fitted curve precision for the surface and bulk  $\text{Ni}/\text{M}_T$  ratio among all the  $\text{CeNi}_x\text{Al}_{0.5}\text{O}_y$  catalysts tested.

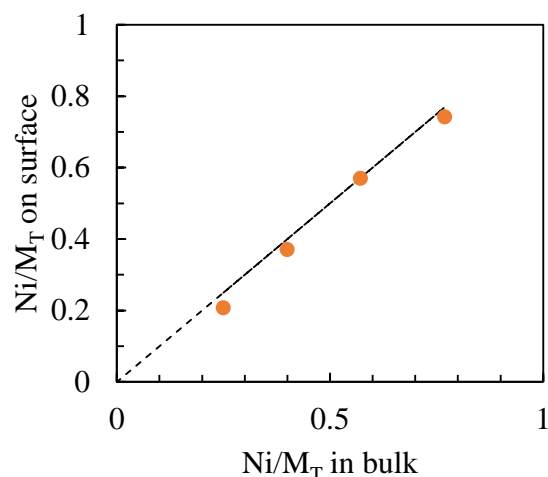


**Fig. 2-12** Variation of surface Ni molar ratios as a function of bulk Ni molar ratios in  $\text{CeNi}_x\text{Al}_{0.5}\text{O}_y$ .

### TPR studies

#### $\text{CeNi}_x\text{O}_y$ catalysts

The temperature-programmed reduction (TPR) profiles in  $\text{H}_2$  of the catalysts are shown in **Fig. 2-13**. For a low Ni content when  $x=0.3$ , one reduction peak is obtained at low temperature at about  $250\text{ }^\circ\text{C}$ . When the  $x$  value increases from 0.3 up to 2, a second reduction peak at about  $330\text{ }^\circ\text{C}$  is observed, and the intensity of this peak increases and shift towards higher temperature of  $380\text{ }^\circ\text{C}$  with Ni content. Furthermore, it is commonly accepted that the TPR analysis of  $\text{CeO}_2$  presents two peaks at approximately  $500\text{ }^\circ\text{C}$  and  $820\text{ }^\circ\text{C}$ , hence the reduction peak obtained at around  $820\text{ }^\circ\text{C}$  is assigned to the reduction of bulk  $\text{Ce}^{4+}$  to  $\text{Ce}^{3+}$ . Furthermore, **Fig. 2-13 b)** shows that linear relationship is obtained between total  $\text{H}_2$  consumption and Ni content (represented as  $\text{Ni}/M_T$  ratio). Meaning  $\text{H}_2$  is consumed in completely priority to reduce nickel species in this range of temperatures (below  $600\text{ }^\circ\text{C}$ ). It is also worth to mention that, the quantity of  $\text{H}_2$  consumed in TPR analysis is in good agreement with the Ni content of the solids. Therefore, it can be proposed that TPR peaks correspond to the reduction of nickel species in various environments. The low temperature peak can be attributed to nickel species: (i) belonging to the solid solution and/ or to (ii) small NiO crystallites (not visible by XRD), easily reducible, (but with the simultaneous reoxidation of a part of these species by reduction of some  $\text{Ce}^{4+}$  ions in strong interaction, as shown in (**Eqs. 2-1** and **2-2**) [144,145]. Then the larger NiO crystallites are reduced when increasing the reduction temperature.





(Eq. 2-2)

(□ represents an anionic vacancy)

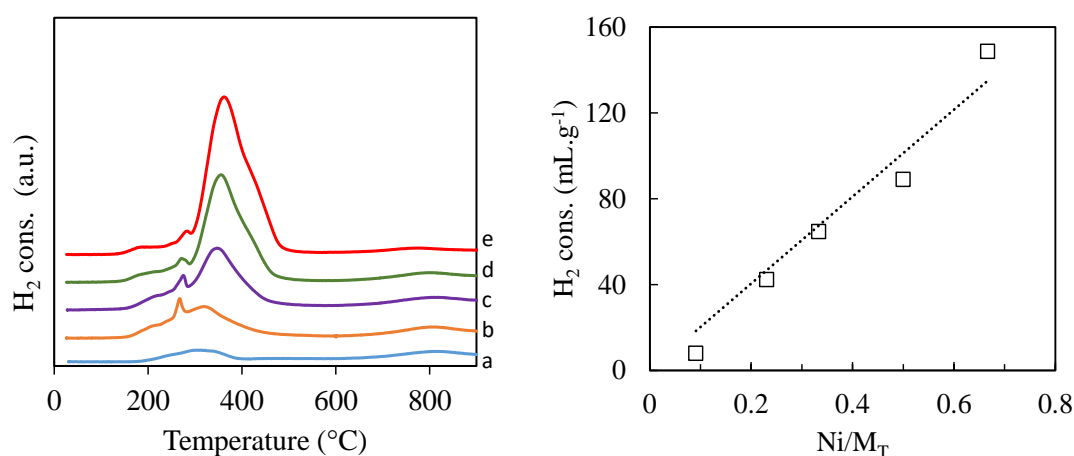


**Fig. 2-13** a) TPR profiles of  $\text{CeNi}_x\text{O}_y$  catalysts. Left)  $x = 0.1$ , b)  $x = 0.3$ , c)  $x = 0.5$ , d)  $x = 1$ , e)  $x = 2$ . Right)  $\text{H}_2$  consumption in TPR as a function of the Ni content of  $\text{CeNi}_x\text{O}_y$  catalysts.  $\text{Ni}/M_T = x/(1+x)$

### $\text{CeNi}_x\text{Al}_{0.5}$ catalysts

The reductive properties of Ce-Ni-Al catalysts are analyzed by  $\text{H}_2$ -TPR technique (**Fig. 2-14**). Similar as the results of binary catalysts, it can be proposed that TPR peaks correspond to the reduction of nickel species in various environments. Concretely, the reduction peak at low temperature (between 200  $^\circ\text{C}$  and 300  $^\circ\text{C}$ ) is attributed to the nickel species: in strong interaction with other cations like in solid solution and/or in small NiO nanoparticles (not visible by XRD) [146]. A series of reactions have been proposed accounting for the reduction mechanism that takes place in the solid solution. Redox processes between  $\text{Ce}^{4+}$ ,  $\text{Ce}^{3+}$ ,  $\text{Ni}^0$  and  $\text{Ni}^{2+}$  have been demonstrated [130]. The presence of strong interacting  $\text{Ni}^{2+}$  species may be related to the ability of Ni and Ce species (and Al species) to form a solid solution. Then, larger NiO nanoparticles (visible by XRD) are reduced when increasing the temperature to about 500  $^\circ\text{C}$ . Moreover, with the Ni content raised, the intensity of this main reduction peak around 300-550  $^\circ\text{C}$  increases and it shifts towards higher temperature. According to the literature [15], this increase in reduction temperature could be contributed to the strong interaction among all the species involved. Thus, the catalysts with a large amount of small-sized NiO and  $\text{CeO}_2$  nanoparticles can improve the strong interactions between the Ni and Ce species, which enables the mixed oxides to be easily and reversibly reduced and re-oxidized. At last, the peak at 900  $^\circ\text{C}$  associated to the reduction of

$\text{Ce}^{4+}$  cations to  $\text{Ce}^{3+}$ . The promoting effect of Ce species for NiO reduction can be attributed to the existence of  $\text{Ce}^{3+}/\text{Ce}^{4+}$  redox pairs, which enable the electron transfer favoring the reduction of NiO species in the adjacent sites [120]. As shown in **Fig. 2-14** (right), the reduction temperatures lower than 700 °C, a linear relationship can be found between the total hydrogen consumption and the Ni content of  $\text{CeNi}_x\text{Al}_{0.5}\text{O}_y$  nano compounds, which indicates that  $\text{H}_2$  is completely consumed to reduce the Ni species.

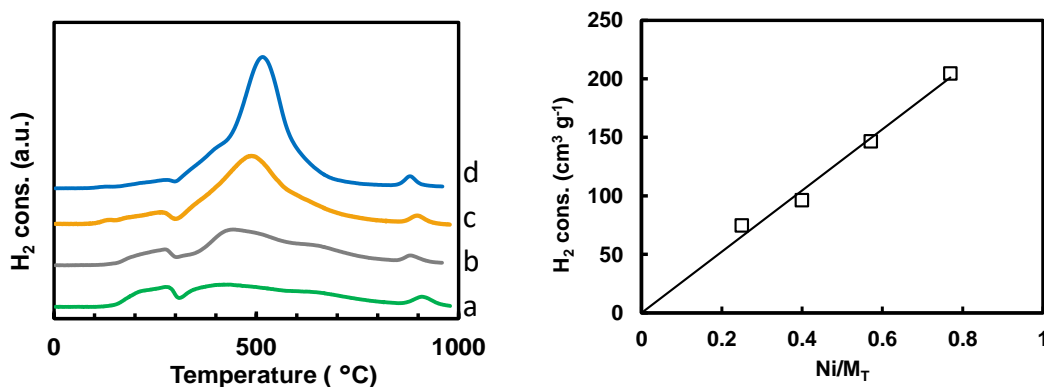


**Fig. 2-14** Left: TPR profiles of the  $\text{CeNi}_x\text{Al}_{0.5}\text{O}_y$  catalysts:  $x=0.5$  (a), 1 (b), 2 (c) and 5 (d). Right:  $\text{H}_2$  consumed during TPR versus Ni content of  $\text{CeNi}_x\text{Al}_{0.5}\text{O}_y$  catalysts  $\text{Ni}/\text{M}_T=x/(1+x+0.5)$

## Conclusion

The surface areas for  $\text{CeNi}_x\text{O}_y$  compounds are ranging between 95-127  $\text{m}^2 \text{g}^{-1}$  with different  $\text{Ni}/\text{M}_T$  ratios ( $x=0.1, 0.3, 0.5, 1$  and 2). Whereas ternary  $\text{CeNi}_x\text{Al}_{0.5}\text{O}_y$  compounds have larger surface areas ranging from 73 to 141  $\text{m}^2 \text{g}^{-1}$  for varying  $\text{Ni}/\text{M}_T$  ratios ( $x=0.5, 1, 2,$  and 5 corresponding to Ni wt.% ranging from 12% to 50%). In  $\text{CeNi}_x\text{Al}_{0.5}\text{O}_y$  catalysts, only a ceria like phase is clearly apparent in each sample, The NiO crystalline phase only could be detected in high Ni content conditions, ( $x \geq 0.5$ ) for binary compounds and  $x$  above 0.5 for the ternary compounds. No crystallographic structure involving aluminum has ever been detected in these catalysts. However, adding aluminum into Ce-Ni-O system leads to a delay of the appearance of NiO crystalline phase with Ni content. For the binary  $\text{CeNi}_x\text{O}_y$  catalysts, the average crystallites size is distributed in the range of 4-5 nm for  $\text{CeO}_2$  and 8-10 nm NiO when visible by XRD. However, for  $\text{CeNi}_x\text{Al}_{0.5}\text{O}_y$  catalysts, the presence of aluminum allows decreasing the average crystallites size of NiO to 5-7 nm, while the average crystallites size maintains at

around 4 nm for CeO<sub>2</sub>. Raman and XPS results evidence the existence of strong interactions between nickel and cerium (and aluminum) species. Therefore, the CeNi<sub>x</sub>O<sub>y</sub> and CeNi<sub>x</sub>Al<sub>0.5</sub>O<sub>y</sub> compounds are able to be ascribed as a mixture of NiO and CeO<sub>2</sub> nanoparticles, coexisting with a cerium-nickel (and aluminum) solid solution depending on Ni content.

The reduction of Ni<sup>2+</sup> species in different environments can be observed in CeNi<sub>x</sub>O<sub>y</sub> and CeNi<sub>x</sub>Al<sub>0.5</sub>O<sub>y</sub> compounds. Concretely, the Ce-Ni-(Al)-O based mixed oxides show two peaks at low temperature (280 °C for binary and 250 °C for ternary catalysts) and higher temperatures (350 °C for binary and 500 °C for ternary catalysts). This phenomenon is assigned to reduction of Ni<sup>2+</sup> species in 1) solid solution and/or small NiO nano-crystallites (not visible by XRD) at low temperature, and 2) larger NiO nano-crystallites (visible by XRD) at higher temperature. On the other hand, the addition of Al significantly influences the reducibility of the catalysts. Moreover, Ni<sup>2+</sup> species present the characteristic of being able to be reduced and reoxidized easily and reversibly allowed by their close interaction with other cations, in particular Ce species.

## 2.2 Ni<sub>x</sub>Mg<sub>2</sub>AlO<sub>y</sub> catalysts

### Preparation of Ni<sub>x</sub>Mg<sub>2</sub>AlO<sub>y</sub> (1 ≤ x ≤ 12) catalysts by co-precipitation method

The Ni<sub>x</sub>Mg<sub>2</sub>AlO<sub>y</sub> catalysts are obtained by the calcination of the hydrotalcites (HT) precursors. They were prepared by the co-precipitation method by using NaOH/Na<sub>2</sub>CO<sub>3</sub> as the precipitant. An aqueous mixed solution (1 M) of nitrate metal with a proper molar ratio of Ni/Mg/Al = X/2/1 was added drop-wise into NaOH (1 M) and Na<sub>2</sub>CO<sub>3</sub> (0.5M) mixed solution at room temperature. Then the slurry was kept stirring at 80 °C for 18 h. The solids were recovered by filtration, followed by thorough washing to obtain the pH value = 7. Then the solids were dried at 120 °C overnight. Finally, the resulting powders were obtained after calcination in air at 500 °C for 4 h. The catalysts with different Ni content obtained are designated as Ni<sub>1</sub>Mg<sub>2</sub>AlO<sub>y</sub>, Ni<sub>3</sub>Mg<sub>2</sub>AlO<sub>y</sub> and Ni<sub>12</sub>Mg<sub>2</sub>AlO<sub>y</sub>.

### Catalyst characterizations

The molar compositions and specific surface areas of these compounds are listed in **Table 2-4**. The real Ni/Mg/Al molar ratios are precisely measured and are proved to be very close to the theoretical values, which confirmed that there is no significant loss of components during the co-precipitation

procedure. There is a global increase in the surface area with the increased Ni content ranging between 106 and 196 m<sup>2</sup> g<sup>-1</sup>.

**Table 2-4** Ni/Mg/Al molar ratio, specific surface area and crystalline parameters of Ni<sub>x</sub>Mg<sub>2</sub>AlO<sub>y</sub>

Catalyst	Ni content/ wt% <sup>a</sup>	Ni/Mg/Al molar ratio <sup>a</sup>	Ni/M <sub>T</sub>	S <sub>BET</sub> / m <sup>2</sup> g <sup>-1</sup>	Lattice parameter <i>a</i> / nm <sup>b</sup>	Oxide crystal <i>d</i> / nm <sup>b</sup>
Mg <sub>2</sub> AlO <sub>y</sub>	0	0/2.1/1	0	106	0.42	3.2
Ni <sub>1</sub> Mg <sub>2</sub> AlO <sub>y</sub>	21.9	1/2.1/1	0.24	127	0.41	3.6
Ni <sub>3</sub> Mg <sub>2</sub> AlO <sub>y</sub>	43.7	3/2.0/1	0.50	168	0.38	3.9
Ni <sub>12</sub> Mg <sub>2</sub> AlO <sub>y</sub>	61.4	12/2/1	0.80	196	0.26	5.9

<sup>a</sup> Measured by ICP technique. <sup>b</sup> Calculated from the (200) plane.

### XRD studies

The Ni<sub>x</sub>Mg<sub>2</sub>AlO<sub>y</sub> catalysts are studied by XRD analysis after calcination at 500 °C, as presented in **Fig. 2-15**. Main reflections are exhibited at around 37, 43 and 63 ° for 2θ values, which may be assigned to the periclase (rock salt) crystal structure of MgO, or NaCl (rock salt) structure of NiO with octahedral Ni<sup>2+</sup> and O<sup>2-</sup> sites, or solid solution of Mg(Ni,Al)O mixed oxides [147]. Therefore, the diffraction patterns of Ni<sub>x</sub>Mg<sub>2</sub>AlO<sub>y</sub> catalysts can be attributed either to MgO (65-0476 JCPDS file), Ni-Mg-O solid solution (24-0712 JCPDS file) and NiO (47-1049 JCPDS file). In fact, the diffraction patterns of MgO, Ni-Mg-O and NiO almost overlap each other, and not able to distinguished. Otherwise, no diffraction patterns related to the presence of Al is observed probably due to three possible causes: (i) high dispersion, (ii) an amorphous state or/and (iii) the insertion of Al species in the Ni-Mg-O phase forming the Ni-Mg-Al-O solid solution.

The addition of nickel affects not only the intensity of the peaks but also their broadness. It can be attributed to the incorporating Ni species into solid solution even doped with Al<sup>3+</sup> cations. The diffraction patterns become more intense and thinner by increasing the Ni content, which is in good agreement with the growing average crystallites size of oxide, NiO, MgO and/or Ni-Mg-O solid solution (**Table 2-4**). In some literature it has been observed that [110], with higher nickel content, part of Ni species could incorporate in to the lattice of the MgO and the other part could exist in the form of free NiO.

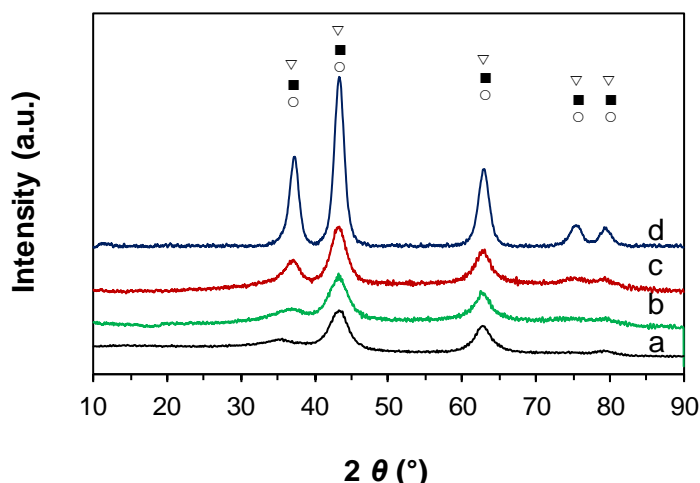


**Fig. 2-15** XRD patterns of  $\text{Ni}_x\text{Mg}_2\text{AlO}_y$  mixed oxides.  $x = a) 0, b) 1, c) 3, d) 12$ .  $\text{MgO}$  (○),  $\text{Ni-Mg-O}$  (■),  $\text{NiO}$  (▽).

As shown in **Table 2-4**, a lattice parameter  $a$  of 0.41 nm is calculated for the  $\text{Ni}_1\text{Mg}_2\text{AlO}_y$  catalyst. Nevertheless, it decreases to 0.26 nm for the  $\text{Ni}_{12}\text{Mg}_2\text{AlO}_y$  catalyst. It may be owing to the substitution of  $\text{Mg}^{2+}$  cations by  $\text{Ni}^{2+}$  cations, which leads to the reduction of the average distance of metal ions within the oxides, as a result, the lattice parameter  $a$  decreases. Noting that the  $\text{Ni}^{2+}$  radius (0.69 Å) is smaller than that of  $\text{Mg}^{2+}$  (0.72 Å).

### XPS studies

The surface information of  $\text{Ni}_x\text{Mg}_2\text{AlO}_y$  catalysts is studied by XPS analysis. The  $\text{Ni}2p$  core-level spectra are presented in **Fig. 2-16**, and the binding energies obtained from the XPS spectra are listed in **Table 2-5**. The  $\text{Ni}_1\text{Mg}_2\text{AlO}_y$ ,  $\text{Ni}_3\text{Mg}_2\text{AlO}_y$  and  $\text{Ni}_{12}\text{Mg}_2\text{AlO}_y$  catalysts exhibit a main emission peak in the  $\text{Ni}2p_{3/2}$  region. For the  $\text{Ni}_3\text{Mg}_2\text{AlO}_y$  and  $\text{Ni}_{12}\text{Mg}_2\text{AlO}_y$  catalysts, the related BE peak is at 855.6-856.1 eV, which is very similar to that reported for the  $\text{Ni-Mg-Al-O}$  mixed oxides (855.5 eV), with the  $\text{Ni}_1\text{Mg}_2\text{AlO}_y$  catalyst presenting a slightly higher BE at 856.1 eV. This value is higher than the BE of pure  $\text{NiO}$  (853.7-854.6 eV) in the literature, but very close to those observed for  $\text{NiAl}_2\text{O}_4$  (856 eV) [148]. These peaks are shifting to higher BE values which indicate the strong interactions between  $\text{Ni}^{2+}$  species with  $\text{Al}^{3+}$  and/or  $\text{Mg}^{2+}$  species due to the different electron-transfer effects. Moreover, the trend of interactions seems associated with Ni molar ratio.

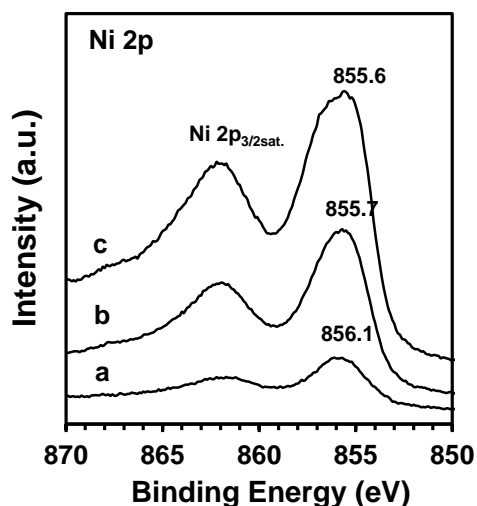


Fig. 2-16 Ni 2p<sub>3/2</sub> XPS spectra of Mg<sub>2</sub>AlNi<sub>x</sub>O<sub>y</sub> compounds. x = a) 1, b) 3, and c) 12.

Besides, for this Ni2p<sub>3/2</sub> core-level, satellite lines are observed at around 862.1 eV, about 6 eV up to the main peak. This 6 eV satellite is associated with a predominant surface plasmon loss due to a two hole c3d<sup>9</sup>4s<sup>2</sup> (c is a core hole) final state effect [148]. All the results show the presence of Ni<sup>2+</sup> species. Moreover, a careful examination of the Ni2p<sub>3/2</sub> band shapes of the Ni<sub>x</sub>Mg<sub>2</sub>AlO<sub>y</sub> mixed oxides present a line broadening effect with higher Ni content (**Table 2-5**).

Table 2-5 XPS parameters of Ni2p, Mg1s, Al2s, and O1s lines.

Catalyst	Ni2p <sub>3/2</sub>	FWHM	Ni2p <sub>3/2</sub> satellite	Mg1s	Al2s	O1s/ eV	FWHM
	eV	(Ni2p <sub>3/2</sub> )/ eV	eV	eV	eV		(O1s)/ eV
Mg <sub>2</sub> AlO <sub>y</sub>	—	—	—	1303.6	119.4	531.7	2.48
Ni <sub>1</sub> Mg <sub>2</sub> AlO <sub>y</sub>	856.1	3.34	862.2	1303.6	119.1	531.7	2.93
Ni <sub>3</sub> Mg <sub>2</sub> AlO <sub>y</sub>	855.7	3.62	861.9	1303.6	119.4	530.6/531.7	3.08
Ni <sub>12</sub> Mg <sub>2</sub> AlO <sub>y</sub>	855.6	4.10	862.2	1303.6	119.5	530.6/531.7	3.42

The O1s, Mg1s and Al2s spectra are similarly analyzed and illustrated in **Fig. 2-17**. The O1s core level presents one peak at BE of 531.7 eV for the Mg<sub>2</sub>AlO<sub>y</sub> and Ni<sub>1</sub>Mg<sub>2</sub>AlO<sub>y</sub> compounds, whereas two peaks at BE values of 530.6 eV and 531.7 eV are observed for the Ni<sub>3</sub>Mg<sub>2</sub>AlO<sub>y</sub> and Ni<sub>12</sub>Mg<sub>2</sub>AlO<sub>y</sub> compounds, respectively. The peak at BE of 530.6 eV can be attributed to the typical O<sup>2-</sup> lattice oxygen

species in oxides of NiO and/or MgO and/or in the Ni-Mg-(Al)-O solid solution [149,143], while the peak at 531.7 eV can be attributed to oxygen species related to the presence of hydroxyl groups (OH<sup>-</sup>).

The Mg1s line (1303.6 eV) and Al2s line (119.4 eV) present almost no variation with the different Ni content. The value of 119.4 eV in this study is higher than the value reported on CeNi-Mg/AlO compounds in literature (118.1 eV) [150], showing higher interactions in the present catalyst. It should be recalled that no relevant diffraction patterns related to Al phase was identified by XRD, and all the results obtained are in agreement with the formation of a Ni-Mg-(Al)-O solid solution.

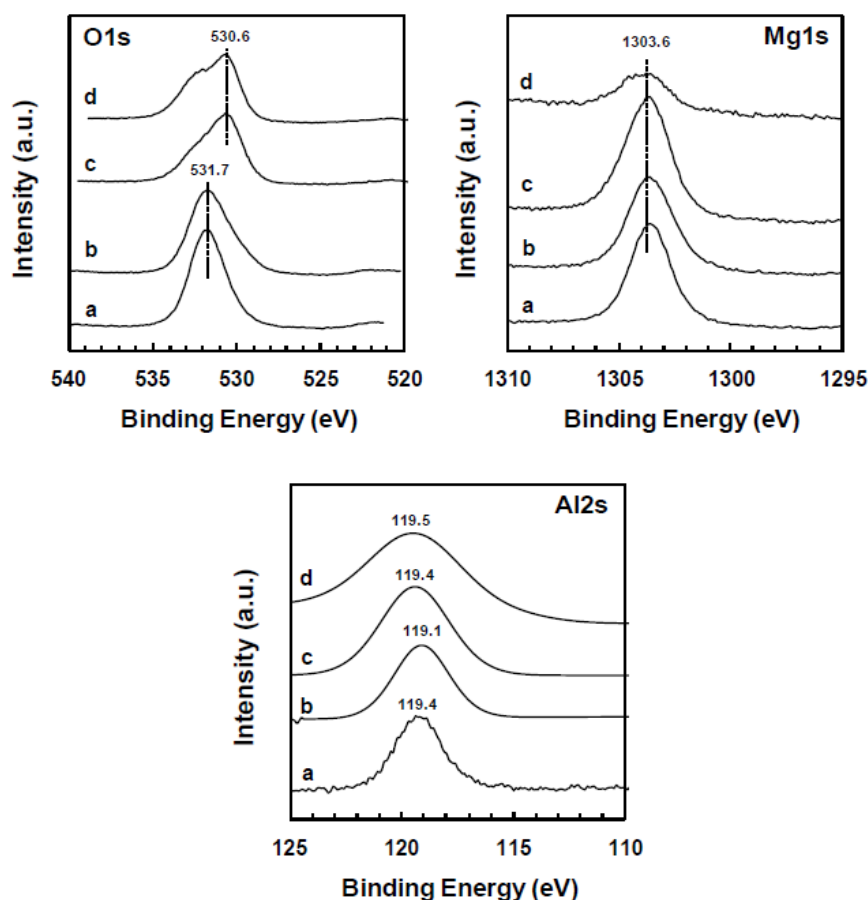


**Fig. 2-17** O1s, Mg1s and Al2s XPS spectra of Ni<sub>X</sub>Mg<sub>2</sub>AlO<sub>Y</sub> catalysts. a) Mg<sub>2</sub>AlO<sub>Y</sub>, b) Ni<sub>1</sub>Mg<sub>2</sub>AlO<sub>Y</sub>, c) Ni<sub>3</sub>Mg<sub>2</sub>AlO<sub>Y</sub>, d) Ni<sub>12</sub>Mg<sub>2</sub>AlO<sub>Y</sub>.

However, some quantitative XPS features can provide additional information. The comparison between the surface Ni/M<sub>T</sub> molar ratio determined by XPS and the bulk Ni/M<sub>T</sub> molar ratio measured by ICP-MS are summarized in **Fig. 2-18**. The variation of Ni concentration with depth in the Ni<sub>X</sub>Mg<sub>2</sub>AlO<sub>Y</sub> catalysts may be observed. The 45 ° diagonal line corresponds to the ideal case of a homogeneous distribution of nickel in the catalysts. It is clear that the Ni/M<sub>T</sub> ratio on the surface is relatively lower

than that in bulk, showing a relative segregation on the surface. On the other hand, the surface Ni/M<sub>T</sub> and Ni/Mg ratios are still in a positive linear relationship with the Ni content. However, the Ni/Al ratio on surface appears significantly lower than the value in bulk, it becomes more noticeable for higher Ni content. This is maybe interpreted as the increase in particles sizes with the higher Ni content (seen in **Table 2-4**), in agreement with the XRD results showing a variation of the average crystallites size between about 4 and 6 nm when increasing Ni content.

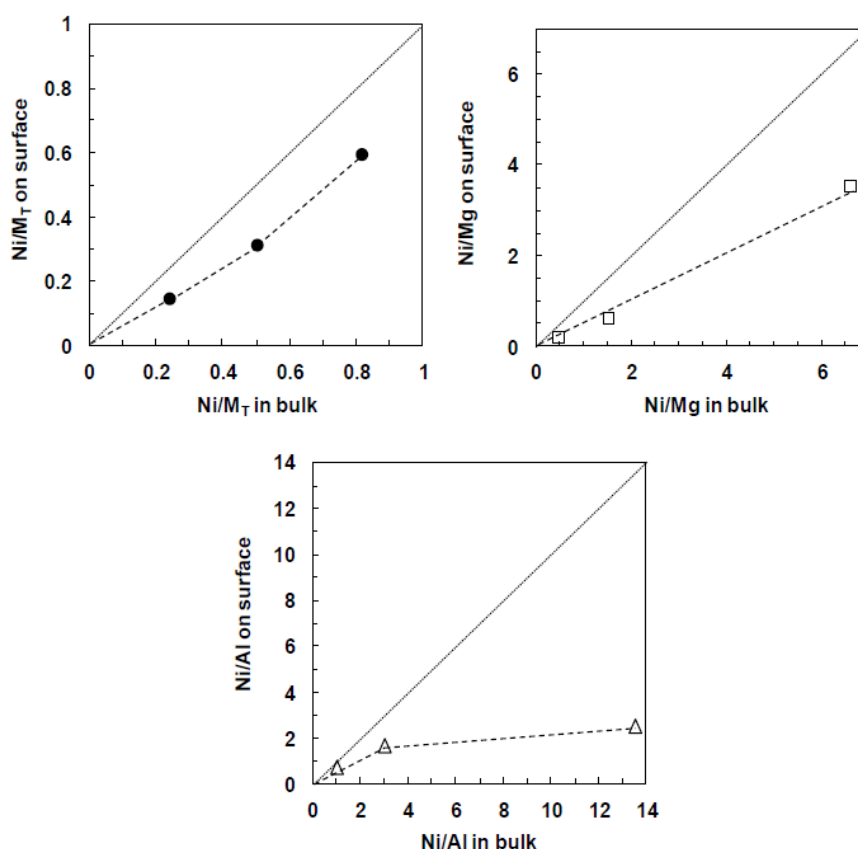


**Fig. 2-18** Variation of surface Ni molar ratios as a function of bulk Ni molar ratios in Ni<sub>x</sub>Mg<sub>2</sub>AlO<sub>y</sub> catalysts.

### TPR studies

The reducibility of the catalysts was studied by TPR and the profiles are presented in **Fig. 2-19**. One main single broad reduction peaks attributed to the Ni species are obtained for each sample regardless to the Ni content. This peak is located in the temperature range of 560-755 °C. The reduction temperature and the peak shifts towards lower temperatures are clearly associated with the Ni content of the catalyst. Obviously, the elemental composition (Ni/Mg/Al molar ratio) has an effect on the

reducibility of nickel species. The interactions between Ni species and Mg or/and Al species can be significantly modified by tuning the Ni content.

The  $\text{Ni}_1\text{Mg}_2\text{AlO}_Y$  catalyst presents the reduction peak at 755 °C, whereas that of the  $\text{Ni}_{12}\text{Mg}_2\text{AlO}_Y$  catalyst appears at a much lower temperature of 560 °C. In other words, the catalyst with high amounts of Ni is easier to be reduced. The high temperature of reduction with low Ni content could be assigned to the reduction of thermal stable phases involving strong interactions between the cations of the solid solution Ni-Mg-Al-O. Dahdah et.al. [151] reported that in nickel and magnesium based catalysts, an electron transfer occurs from Ni species to Mg species, which generates strong interactions between the cations, therefore, accounts for the higher reduction temperature with high magnesium content and the presence of aluminum in the solid. Moreover, it is known that the bulk NiO presents a single broad reduction peak located at around 370 °C. Therefore, there are still strong interactions existing between Ni cations and some other cations, as aforementioned the reduction temperature of Ni species is much higher than the one necessary to reduce bulk NiO, i.e. 560°C for the  $\text{Ni}_{12}\text{Mg}_2\text{AlO}_Y$  catalyst compared to 370°C for NiO.

It can be remarked that the obtained atomic H/Ni ratios reach to ca. 2.4 during TPR, which are higher than the stoichiometric value of 2.0. Meaning that some more hydrogen species are consumed than the amount required to reduce  $\text{Ni}^{2+}$  species completely to  $\text{Ni}^0$  (**Fig. 2-20**). This phenomenon is in agreement with a hydrogen “spillover” process as followed.



Further analysis discloses that a linear relationship can be established between the total hydrogen consumption during TPR and the Ni content of  $\text{Ni}_x\text{Mg}_2\text{AlO}_Y$  catalysts (**Fig. 2-20**), showing that hydrogen is nearly completely consumed so as to reduce the nickel species in this range of temperatures.

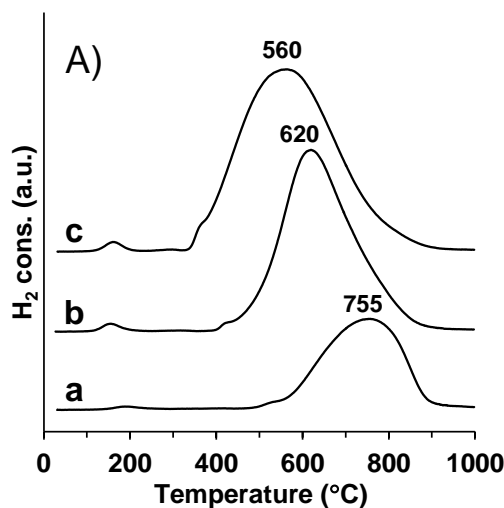


Fig. 2-19 TPR profiles of  $\text{Ni}_x\text{Mg}_2\text{AlO}_y$  catalysts. a)  $\text{Ni}_1\text{Mg}_2\text{AlO}_y$ , b)  $\text{Ni}_3\text{Mg}_2\text{AlO}_y$ , c)  $\text{Ni}_{12}\text{Mg}_2\text{AlO}_y$ .

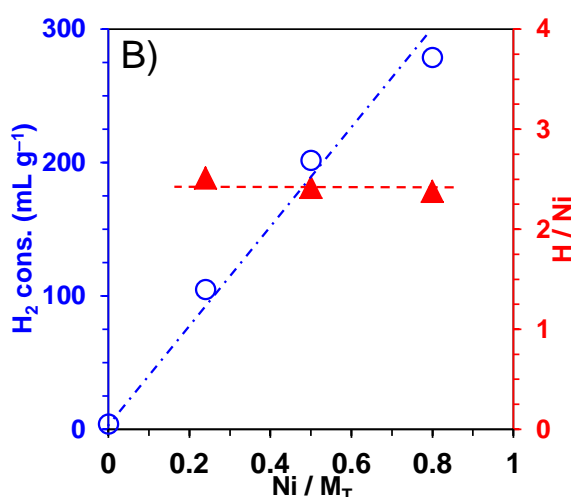


Fig. 2-20  $\text{H}_2$  consumption (○) and H/Ni atomic ratio (▲) of  $\text{Ni}_x\text{Mg}_2\text{AlO}_y$  during TPR in  $\text{H}_2$ .

## Conclusion

$\text{Ni}_x\text{Mg}_2\text{AlO}_y$  catalysts ( $x=1, 3$  and  $12$ ) with different Ni contents (wt%=21.9%, 43.7%, and 61.4%) are carefully studied. The  $\text{Ni}_x\text{Mg}_2\text{AlO}_y$  catalysts are assigned to a mixture of nanoparticles of NiO, MgO and/or solid solution of Ni-Mg-(Al)-O. Very small and uniform nano-crystallites ranging between 3-6 nm are obtained depending on the Ni content. The surface areas of these compounds are ranging between 100 and 200  $\text{m}^2 \text{g}^{-1}$ . The XPS, XRD and TPR results have shown the existence of strong interactions between Ni species and Mg and/or Al species in agreement with the formation of Ni-Mg-O and/or Ni-Mg-Al-O solid solution.  $\text{Ni}_x\text{Mg}_2\text{AlO}_y$  mixed oxides show a single broad TPR peak at between 560 and 844 °C which is assigned to the reduction of Ni species. Moreover, the increase of Ni

content makes the solid more easily to be reduced.

## 2.3 Ni<sub>x</sub>/SBA-15

### Synthesis of Ni<sub>x</sub>/SBA-15 by Deposition Precipitation

All chemicals required to prepare the mesoporous SBA-15 silica support and the transition metal-containing materials were used as purchased: tetraethylorthosilicate ( $\text{Si}(\text{OC}_2\text{H}_5)_4$ , TEOS, 98%, Sigma-Aldrich), non-ionic triblock copolymer Pluronic P123,  $\text{PEO}_{20}\text{PPO}_{70}\text{PEO}_{20}$ , molecular weight of 5800, (BASF Corp.), hydrochloric acid (HCl, 37%, Sigma-Aldrich), nickel nitrate ( $\text{Ni}(\text{NO}_3)_2 \cdot 6\text{H}_2\text{O}$ , 98%, Sigma-Aldrich) and urea  $\text{CO}(\text{NH}_2)_2$ , 99.0-100%, (Sigma-Aldrich, ACS reagent).

**Support synthesis:** SBA-15 support was synthesized according to the procedure used by Zhao et al [152]. In a typical procedure is used 4 g of Pluronic P123 ( $\text{PEO}_{20}\text{PPO}_{70}\text{PEO}_{20}$ ) with  $M_n=5800$  g and 1.6 M solution of HCl were stirred at 40 °C until the complete dissolution of surfactant. Then the silica source, 8.5g of TEOS tetraethyl ortho-silicate was added drop wise, followed by magnetic stirring for 24 h. The resulting gel was submitted to hydrothermal treatments for 48h at 100 °C. The SBA-15 pore structure was obtained by calcination at 550 °C for 6h in a muffle oven (heating ramp 1.5 °C  $\text{min}^{-1}$ ).

**Deposition Precipitation (DP)** route to the phyllosilicate-mediated stabilization: The Ni-containing material was prepared from a suspension of calcined SBA-15 support in an aqueous solution of 0.14 mol  $\text{L}^{-1}$  metal nitrate to obtain a final Ni loading of 5 to 40 wt.%. The reaction was performed in a double wall thermostat reactor, at a temperature of 90 °C. Initially, the pH of the suspension was adjusted to 2 by using nitric acid as pH-adjustor and then urea solution (3 mol  $\text{L}^{-1}$ ) was added dropwise. To ensure a complete and stable precipitation, the solution was stirred for 24 h. At the end of the reaction, and under the conditions selected, the pH obtained was  $7.4 \pm 0.1$ . pH evolution with time was monitored during all the reaction. The obtained solid was separated by filtration, followed by washing with distilled water and drying at 40 °C for 12 h before being calcined in a muffle oven at 500 °C for 6 h (heating ramp 1.5 °C  $\text{min}^{-1}$ ). Materials prepared by DP are denoted in the text Ni<sub>x</sub>%/SBA-15, where x is the Ni loading (x= 5, 10, 20, 40 wt%).

### Physico-chemical characterization of Ni<sub>x</sub>/SBA-15

Textural properties of the samples prepared by DP method have been analyzed by nitrogen physisorption at -196 °C. The results are presented in **Table 2-6**. The adsorption/desorption isotherms obtained for DP mediated materials ( **Fig. 2-21**) are type IV, specific for mesoporous materials having cylindrical pores, the hysteresis obtained is of type H<sub>3</sub>, typical of materials with a wide pore distribution. The displacement of the hysteresis at relatively high pressures, P/P<sub>0</sub> values between 0.65-0.92 indicates the presence of wide large pores for the samples, compared to the SBA-15 support, whose hysteresis is located at P/P<sub>0</sub> between 0.65 and 0.80. The alteration of the support, which initially has a very ordered structure, is due to the alkaline conditions created by the synthesis medium necessary to precipitate the metal precursor, which causes partial dissolution of the SBA-15 support with the formation of silicic acid, this one will may later participate in the formation of lamellar structure of the phyllosilicate.

**Table 2-6** Textural properties for Nickel phyllosilicates

Compounds	S <sub>BET</sub> m <sup>2</sup> /g	S <sub>μ</sub> m <sup>2</sup> /g	V <sub>pores</sub> cm <sup>3</sup> /g	V <sub>μ</sub> cm <sup>3</sup> /g	D <sub>pores</sub> nm
SBA-15	735	119	1.02	0.05	6.7
Ni <sub>5%</sub> /SBA-15	353	65	0.82	0.02	8.3
Ni <sub>10%</sub> /SBA-15	306	64	0.89	0.02	11.1
Ni <sub>20%</sub> /SBA-15	346	66	0.86	0.03	8.7
Ni <sub>40%</sub> /SBA-15	363	61	0.6	0.02	8.3

S<sub>BET</sub>, specific surface area; S<sub>μ</sub>, microporous surface area; V<sub>pore</sub>, total pores volume; V<sub>μ</sub>, micropores volume; -

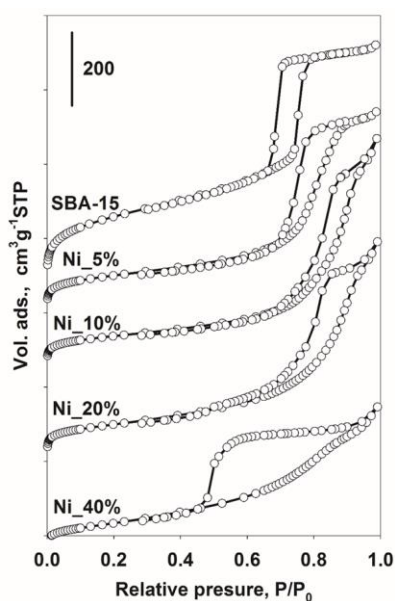


**Fig. 2-21.** N<sub>2</sub>-adsorption/desorption isotherms

The solubilization of silicic acid by the alkaline medium, besides the positive effect of the formation of the phyllosilicates, which have the principle role in stabilizing the species derived from the metal precursor used for the preparation of the catalyst, also have a negative effect by dissolving the walls leading to the formation of larger non-uniform pores and even the partial collapse of the ordered SBA-15 type structure as it can be observed for Ni\_40% which has a different porosity with smaller pores (i.e. 4.1 nm) (also can be seen later on from TEM images at higher metal loading). Therefore, by analyzing the values corresponding to the textural properties presented in **Table 2-6**, it can be seen that due to the alkaline reaction conditions the specific surface of the new materials drastically decreases with almost 50 % compared to the original SBA-15 support. Specifically, incorporation of Ni into SBA-15 led to a decrease of the specific surface area from 735 to 306 m<sup>2</sup>/g. Also, as mentioned above, an increase in the pore size can be noticed due to the digestion of the silica walls affected by the alkaline urea solution. Under these slightly alkaline conditions, a significant reduction of the microporous surface is observed (~ 60 m<sup>2</sup>/g) and occurs over the microporous surface of the support used (119 m<sup>2</sup>/g). For the sample Ni\_40% the porosity of the silica is entirely destroyed and replaced by a porosity formed between the layers of phyllosilicates.

The wide-angle XRD patterns of Ni phyllosilicates with different contents of Ni are exposed in **Fig. 2-22**. A broad diffraction peak at  $2\theta \approx 22.5^\circ$  was assigned to the amorphous SiO<sub>2</sub> wall of SBA-15 [153]. All the samples are showing the reflexions corresponding to 1:1 PS type kerolite (ICDD No: 43-0664) having the chemical structure: Ni<sub>3</sub>Si<sub>4</sub>O<sub>10</sub>(OH)<sub>2</sub> · 5H<sub>2</sub>O. The phyllosilicates present large peaks at  $2\theta$  of 35° and 60° [154], [155].

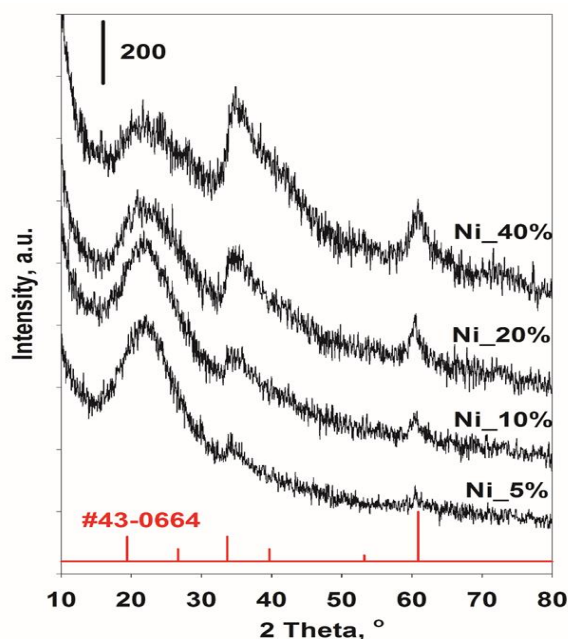


**Fig. 2-22.** XRD patterns for nickel phyllosilicates with different metal loadings; bottom: reference ICDD 43-0664;

The representative TEM images (**Fig. 2-23**) were recorded for samples prepared by the DP method and are showing an alteration of the ordered structure of the SBA-15 support due to the alkaline conditions imposed by the DP method and the appearance of the fibrous particles with the phyllosilicate structure [156], [157]. The included TEM images are recorded after calcination at 500 °C. As can be seen, several changes are evaluated with Ni loading: *i*) the porosity alteration is noticeable when the Ni loading is increased; *ii*) the filaments are formed preferentially outside the silica grain, then with high metal loading the phyllosilicates are growing also inside the silica grain; *iii*) the number of filaments contained by an aggregate of phyllosilicates is increasing with the metal loading; *iv*) the length of the filaments is increasing with the Ni loading, 40-50 nm for Ni\_5%, ~100 nm for Ni\_10%, ~150 nm for Ni\_20% and > 200 nm for Ni\_40%.

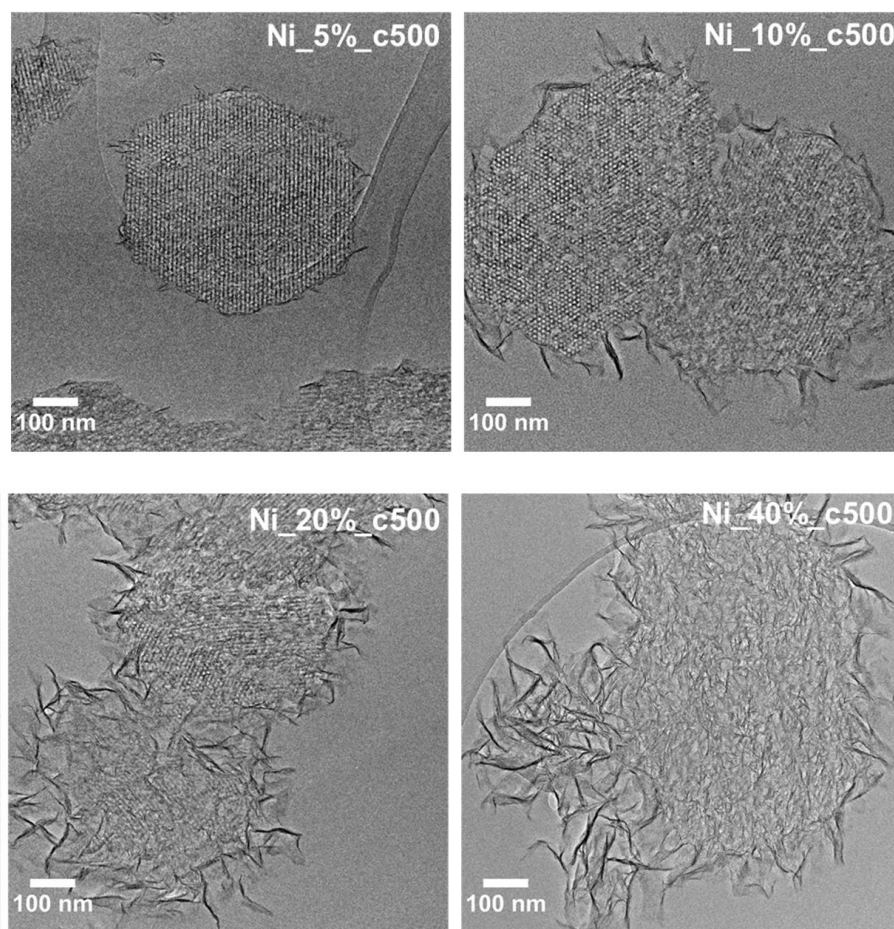


**Fig. 2-23.** TEM images collected for calcined nickel phyllosilicates with different Ni loadings

The reducibility of the calcined samples was investigated by using the hydrogen reduction method under programmed temperature conditions, the TPR profiles being recorded up to a reduction temperature of 900 °C (seen in **Fig. 2-24**). The reduction profile provides information about the nature of the reducing phases, the particles size which contain the reducible cations and the interactions metal-support. It is well known that phyllosilicates are metal precursors in which the metal interaction with the support is very strong. For this reason, unlike the oxidic forms, it requires a high temperature to reduce it. Thus, the reduction temperature for these materials was observed at 620 °C, the quantity of H<sub>2</sub> consumed is in relation with the metal loading from each sample. A slight increase of temperature of 640 °C is observed for Ni<sub>40%</sub>, this can be related to the reduction of layers containing a significant number of filaments (10-20 filaments).

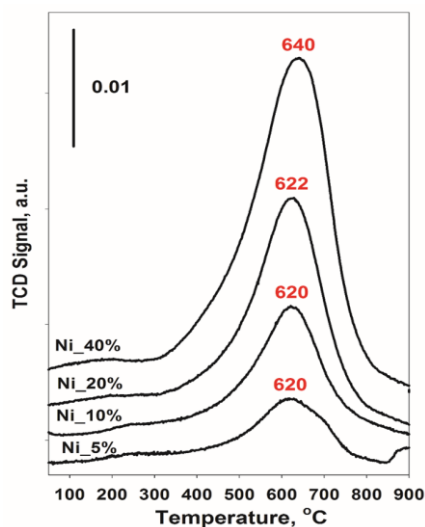


**Fig. 2-24.** TPR profiles for calcined nickel phyllosilicates with different Ni loadings

In order to monitor the evolution of the crystalline phases during the reduction at different temperatures, as well for the identification of the Ni species, *in situ* XRD analyses were performed in hydrogen atmosphere. The recorded diffractograms are shown in **Fig. 2-25**. It can be seen that for all the materials containing nickel phyllosilicate phase can be identified in the recorded diffractograms and after treatment under hydrogen at high reduction temperatures (i.e. 600 °C), thus confirming their thermal stability. Their intensity decreases slightly with the increase in the reduction temperature due to a partial reduction of the corresponding cations of  $\text{Ni}^{2+}$  into the metallic phase. This metallic phase is, however, very well dispersed and therefore difficult to be identified by XRD at temperatures up to 800 °C for Ni\_5% and Ni\_10%. For higher metal loadings, the  $\text{Ni}^0$  is revealed by large peaks indicating a very narrow distribution of small metallic crystallites, presenting an average crystallites size of 4.4 nm for Ni\_20% and 5.2 nm for Ni\_40%, respectively.

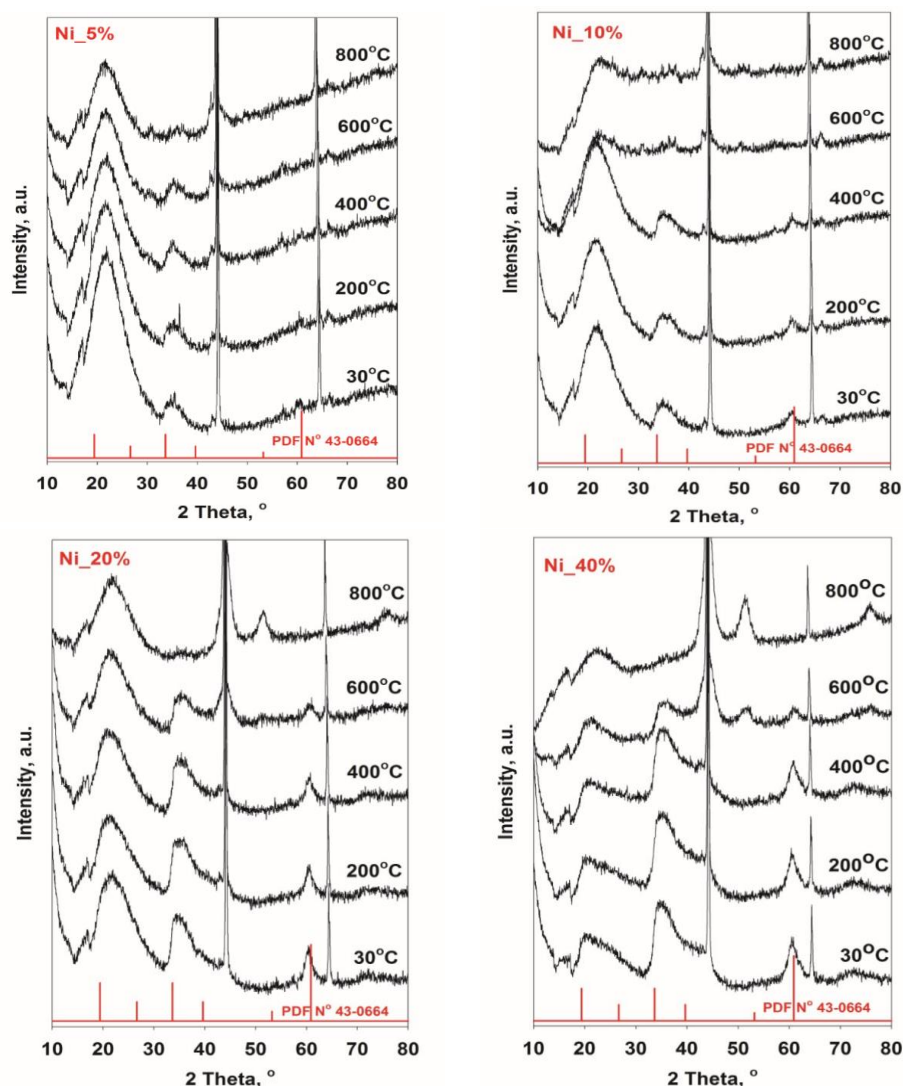


**Fig. 2-25.** *In situ* XRD of reduction in  $H_2$  for calcined nickel phyllosilicates with different Ni loadings

After reduction up to 600 °C, TEM images were recorded for all the samples in order to observe the morphology of metal nanoparticles (**Fig. 2-26**). It can be observed the homogeneously dispersed NiO particles and the non-rigorous phyllosilicate filaments, thus confirming the results from *in situ* XRD indicating the partial reduction of Ni phyllosilicates when the reduction temperature is increased. The Ni particles size was essentially in the 2.5 – 4.5 nm range, with some larger particles around 6–7 nm. The remained unsupported phyllosilicates are located both inside the support and on the external surface, but there are also areas where the filaments are completely detachable from the support. The presence of these separate support filaments (which is more evident for samples with high metal loading ie Ni\_40%) which leads to the conclusion that their reduction is related to the accessibility of  $H_2$  through layers with more filaments, requires reduction temperatures higher than 600 °C [156], [158].

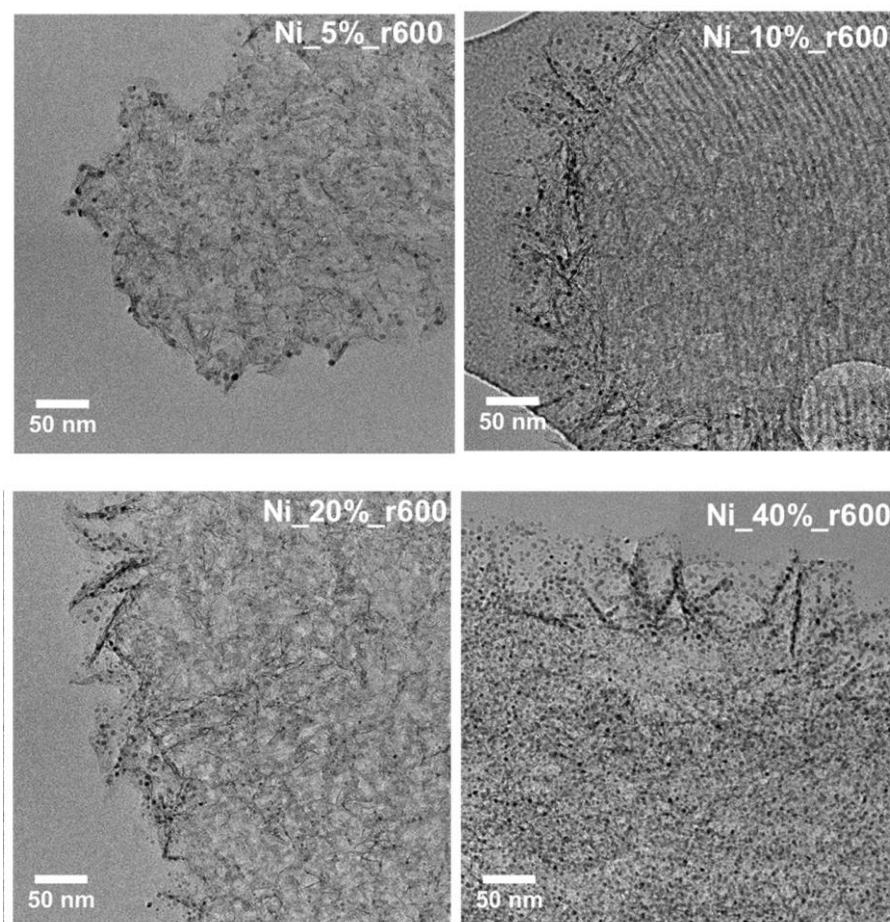


**Fig. 2-26** TEM images collected for samples in-situ reduced in H<sub>2</sub> at 600 °C with different Ni loadings

A series of TEM images were collected after reduction up to 800 °C, in order to observe if the reduction of phyllosilicate phase is complete but also to confirm the high stability of Ni<sup>0</sup> nanoparticles in extreme temperature conditions (**Fig. 2-27**). First of all, it can be observed only the Ni<sup>0</sup> phases after a total reduction for all the samples. Also the NPs are not sintering even for high metal loading, thus confirming the results from *in situ* XRD. However, larger Ni particles could be seen from TEM images, i.e. for Ni<sub>10%</sub>.

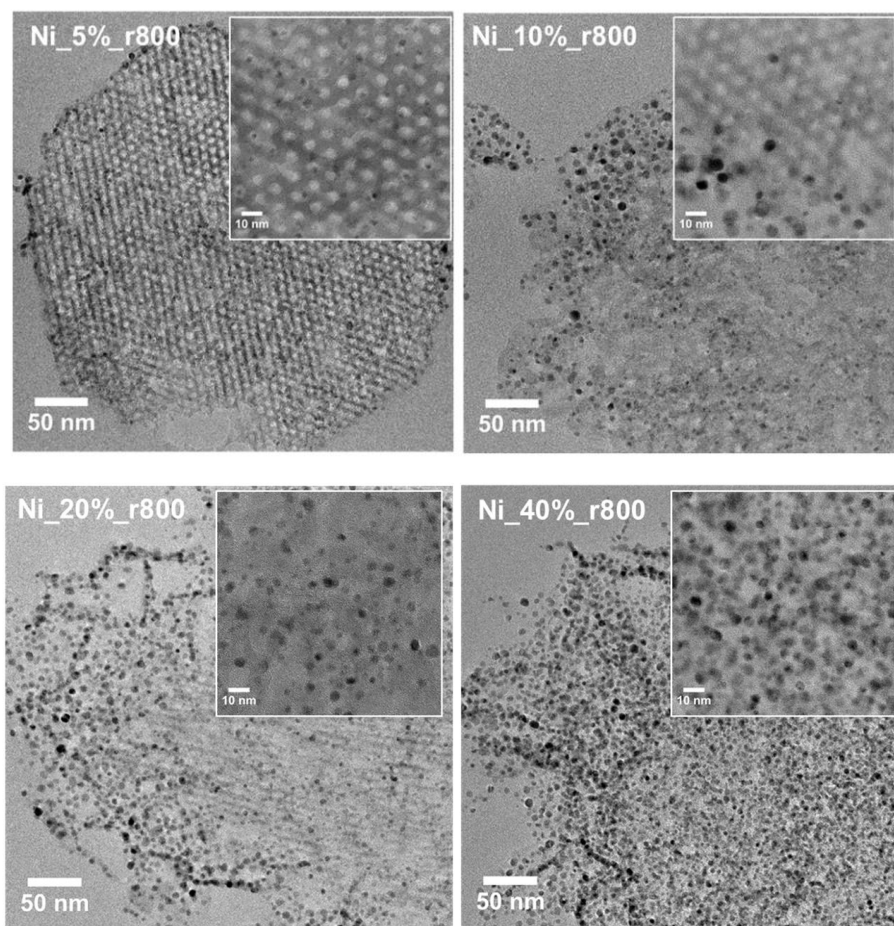


Fig. 2-27. TEM images collected for samples *in situ* reduced in H<sub>2</sub> at 800 °C with different metal loadings

## 2.4 Conclusion

In this study, different series of Ni-based catalysts are prepared by different methods. CeNi<sub>x</sub>(Al<sub>z</sub>)O<sub>y</sub> (z=0 and 0.5) and Ni<sub>x</sub>Mg<sub>2</sub>AlO<sub>y</sub> mixed oxides are prepared by the co-precipitation method (CP), while the SBA-15 supported Ni catalysts (Ni<sub>x</sub>%/SBA-15) are prepared by the deposition-precipitation (DP) method, respectively.

The surface areas for CeNi<sub>x</sub>O<sub>y</sub> compounds are ranging between 95-127 m<sup>2</sup> g<sup>-1</sup> (with x= 0.1, 0.3, 0.5, 1 and 2 corresponding to Ni wt.% ranging from 5% to 40% ). Whereas ternary CeNi<sub>x</sub>Al<sub>0.5</sub>O<sub>y</sub> compounds have larger surface areas ranging from 73 to 141 m<sup>2</sup> g<sup>-1</sup> (with x= 0.5, 1, 2, and 5 corresponding to Ni wt.% ranging from 12% to 50%). In CeNi<sub>x</sub>(Al<sub>z</sub>)O<sub>y</sub> catalysts, only a ceria like phase is clearly apparent in all samples, while the NiO crystalline phase only could be detected in high Ni content conditions, (x ≥ 0.5) for binary compounds and x above 0.5 for the ternary compounds. No crystallographic structure involving aluminum has ever been detected in these catalysts. However,

adding aluminum into Ce-Ni system leads to a delay of the appearance of NiO crystalline phase with Ni content. For  $\text{CeNi}_x\text{O}_y$ , the average crystallites size is distributed in the range of 4-5 nm for  $\text{CeO}_2$  and 8-10 nm for NiO when observed by XRD. However, for  $\text{CeNi}_x\text{Al}_{0.5}\text{O}_y$ , the presence of aluminum allows better dispersion with the average crystallites size of NiO to 5-7 nm. Therefore, the  $\text{CeNi}_x\text{O}_y$  and  $\text{CeNi}_x\text{Al}_{0.5}\text{O}_y$  compounds are able to be ascribed as a mixture of NiO and  $\text{CeO}_2$  nanoparticles, coexisting with a cerium nickel and aluminum solid solution. Raman and XPS results evidence the existence of strong interactions between nickel and cerium (and aluminum) species.

The reduction of  $\text{Ni}^{2+}$  species in different environments can be observed in  $\text{CeNi}_x\text{O}_y$  and  $\text{CeNi}_x\text{Al}_{0.5}\text{O}_y$  compounds.  $\text{CeNi}_x\text{O}_y$  solids possess Ni species which present a reduction peak at about 270 °C, allowing to be reduced and reoxidized easily and reversibly by their close interaction with Ce species. On the other hand, the  $\text{CeNi}_x\text{Al}_{0.5}\text{O}_y$  mixed oxides show two peaks at low temperature (around 250 °C) and higher temperatures (450-500 °C) regardless of the Ni content. This phenomenon is assigned to the reduction of  $\text{Ni}^{2+}$  species in different environments: 1) in solid solution and/or small NiO oxides at low temperature; and 2) in larger NiO nano-crystallites at higher temperature. The addition of Al significantly influences the reducibility of the catalysts.

$\text{Ni}_x\text{Mg}_2\text{AlO}_y$  catalysts ( $x= 1, 3$  and  $12$ ) with different Ni contents (Ni wt%=21.9%, 43.7%, and 61.4%, respectively) are also carefully studied. The  $\text{Ni}_x\text{Mg}_2\text{AlO}_y$  catalysts are assigned to a mixture of nanoparticles of NiO, MgO and/or to the Ni-Mg-(Al)-O solid solution. Very small and uniform nano-crystallites ranging between 3-6 nm are obtained depending on the Ni content. The surface areas of these compounds are ranging between 100 and 200  $\text{m}^2 \text{g}^{-1}$ . The XPS, XRD and TPR results show the existence of strong interactions between Ni species and Mg and/or Al species due to the formation of Ni-Mg-O and/or Ni-Mg-Al-O solid solution.  $\text{Ni}_x\text{Mg}_2\text{AlO}_y$  mixed oxides show a single broad TPR peak between 560 and 844 °C which is assigned to the reduction of Ni species. For low Ni content the strong interactions between nickel species and other cations either in Ni-Mg-(Al)-O solid solution and/or at the interfaces between small nanoparticles of NiO, MgO and/or Ni-Mg-(Al)-O make the solid difficult to reduce. Then, the increase of Ni content makes the solid becomes closer to that of bulk NiO, which is easier to be reduced. However, there are still strong interactions existing between Ni cations and some other cations, because the required temperature for reduction of Ni species is still much higher than the

one necessary to reduce bulk NiO.

Ni<sub>x</sub>/SBA-15 catalysts with 4 different Ni loadings (Ni wt%= 5%, 10%, 20% and 40%) are prepared by a different method of deposition precipitation (DP). After calcination, the samples remained at quite high surface area values between 306-363 m<sup>2</sup>g<sup>-1</sup>, which are the highest values for the catalysts in this thesis. High thermal stability of Ni<sub>x</sub>/SBA-15 catalysts is revealed by *in situ* XRD and confirmed by TEM. For low Ni content, the Ni species are well dispersed on the surface of SBA-15. For higher Ni loading condition, more Ni species are loaded and extended surround the edges instead of inside the silica grains. The alteration of the ordered structure is confirmed by TEM, which also reveals that filaments are formed preferentially outside the silica grain. Moreover, with increasing metal loading, both of the number and length of phyllosilicates are growing, regardless of out and inside the silica grain. The catalysts with highest Ni loading present a higher reduction temperature than the low Ni loaded samples. Thus, for higher reduction temperature at 800 °C, the total reduction of Ni phyllosilicate leads to very well dispersed Ni metal particles and the non-rigorous phyllosilicate filaments. The remained unsupported phyllosilicates are located both inside the support and on the external surface. For all the samples, the totally reduced Ni<sup>0</sup> phase can be observed alone only after a total reduction at 800 °C. Also the nanoparticles are not sintering even for high metal loading, thus confirming the results from *in situ* XRD.

## **Chapter 3**

# **Dry Reforming of Methane over Ni-based catalysts**



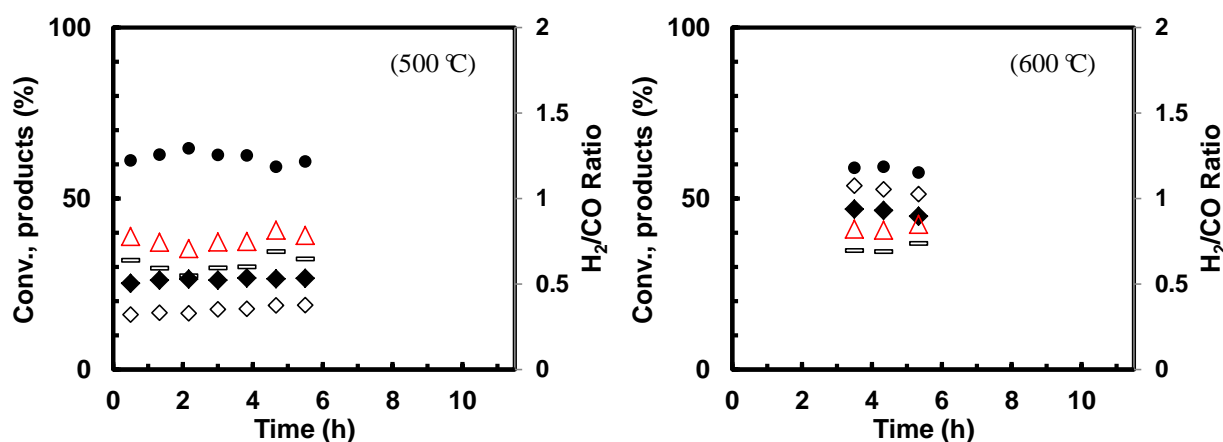
### 3 Dry Reforming of Methane over Ni-based catalysts

#### 3.1 Dry reforming over CeNi<sub>x</sub>O<sub>y</sub> mixed oxides

##### 3.1.1 Influence of reaction temperature over CeNi<sub>x</sub>O<sub>y</sub>

The dry reforming reaction (DRM) in CH<sub>4</sub>/CO<sub>2</sub>/ N<sub>2</sub>= 20:20:60% conditions was studied in the temperature range of 500-800 °C on CeNi<sub>x</sub>O<sub>y</sub> catalysts. (Experiment process detailed in *Annex 2*) The influence of reaction temperature was studied and, as an example, the results are presented on CeNi<sub>0.5</sub>O<sub>y</sub> catalyst (50mg) in-situ pretreated in H<sub>2</sub> at 250 °C for 12 h. As illustrated in **Fig. 3-2**, an increase in temperature leads to an increase in both CH<sub>4</sub> and CO<sub>2</sub> conversions, which is due to the endothermic nature of DRM reaction. The conversions of CH<sub>4</sub> and CO<sub>2</sub> increase from 19.0% and 27.2% at 500 °C to 83.8% and 91.4% at 800 °C, respectively. The CO<sub>2</sub> conversion is always higher than CH<sub>4</sub> conversion in all the tested temperatures. It is generally agreed that this is due to the RWGS reaction. Moreover, the experimental data is in good agreement with the result of thermodynamic equilibrium calculation in this condition, although stoichiometric equilibrium is not totally reached in all range of tested temperatures. Specifically, very interesting results are obtained with conversions of 43% for CH<sub>4</sub>, and 51% for CO<sub>2</sub> at the low temperature of 600 °C.

This is a strong indication that this CeNi<sub>0.5</sub>O<sub>y</sub> catalyst exhibits high activity for CH<sub>4</sub>-CO<sub>2</sub> reforming, and it is worth to mention that, in contrast to most of counterparts [159][160][161], this catalyst has a distinct advantage on the aspect of conversions at the low-temperature range.



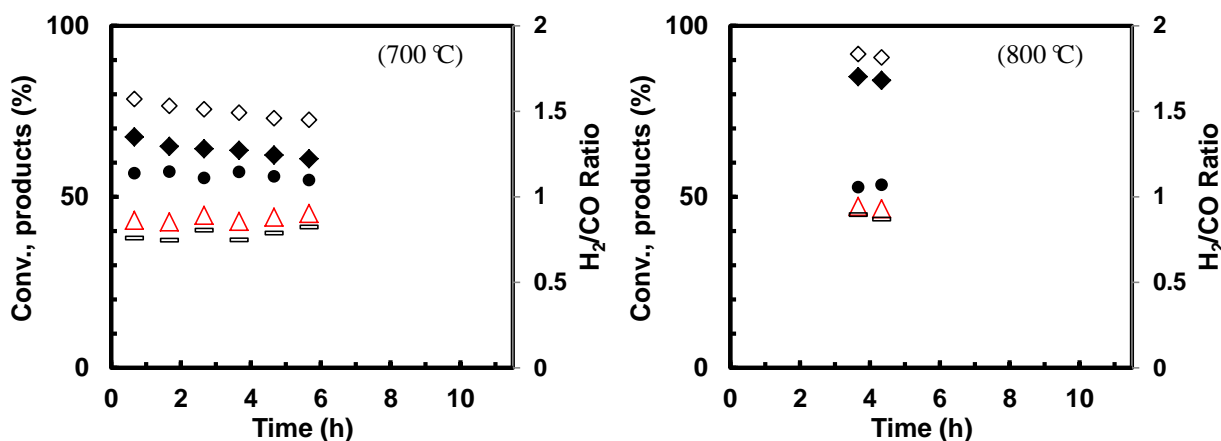


**Fig. 3-1** Catalytic activity of DRM on  $\text{CeNi}_{0.5}\text{O}_Y$  (50 mg) pretreated in  $\text{H}_2$  at 250 °C at different reaction temperatures.  $\text{CH}_4$  ( $\blacklozenge$ ),  $\text{CO}_2$  ( $\diamond$ ) conversions,  $\text{H}_2$  ( $\triangle$ ),  $\text{CO}$  ( $\bullet$ ), in mol % and the  $\text{H}_2/\text{CO}$  ratio ( $\square$ ).  $\text{CH}_4/\text{CO}_2/\text{N}_2 = 20:20:60\%$ .

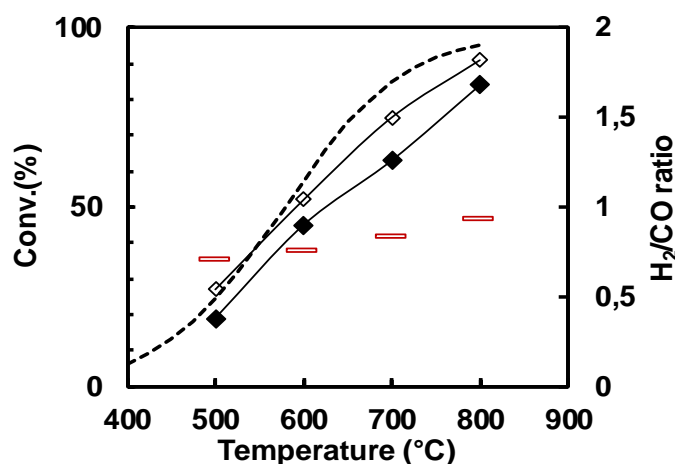


**Fig. 3-2.** DRM over the  $\text{CeNi}_{0.5}\text{O}_Y$  catalyst (50 mg) pretreated in  $\text{H}_2$  at 250 °C as a function of reaction temperature.  $\text{CH}_4$  ( $\blacklozenge$ ),  $\text{CO}_2$  ( $\diamond$ ) conversions and  $\text{H}_2/\text{CO}$  ratio ( $\square$ ). Reaction conditions:  $\text{CH}_4/\text{CO}_2/\text{N}_2 = 20:20:60\%$ ; time reported: 5 h for each temperature.

The selectivity expressed as  $\text{H}_2/\text{CO}$  value is quite helpful in understanding the behavior of the catalysts and their difference. In this study, the  $\text{H}_2/\text{CO}$  ratio is varying between 0.7 and 0.9 for all temperature ranges. It increases with increasing reaction temperature, which is very close to the stoichiometric value (0.98) for the reaction at a high temperature of 800 °C, but slightly lower. The occurrence of side reactions is probably obtained, mainly RWGS reaction and  $\text{CH}_4$  decomposition. The latter is favored at high temperatures, which could lead to the enrichment of  $\text{H}_2$  in the mixture. At high temperature, the DRM is more favored, and the  $\text{CH}_4$  and  $\text{CO}_2$  reactants are converted efficiently.

Therefore, the smaller amount of CO<sub>2</sub> available for the RWGS gives H<sub>2</sub>/CO ratio closer to unity as expected when only the DRM reaction occurs. Besides, it is known that high temperature also facilitates steam reforming of methane (SRM), which could be another possible reason for the increased H<sub>2</sub>/CO ratio at a high temperature. Globally, the same evolution of catalytic behaviors can be obtained on other catalysts with different Ni contents. This is also explained in Serrano-Lotina's work [162], methane conversion approached CO<sub>2</sub> conversion because steam reforming of methane and carbon gasification were favored at high temperatures. This would explain the increase of H<sub>2</sub>/CO ratio and the decrease in water concentration in the outlet stream at temperatures higher than 600 °C. The maximum conversions and selectivity towards H<sub>2</sub>/CO are achieved for the reaction condition at high temperature, evidencing the high efficiency of the catalyst.

### 3.1.2 Influence of pretreatment

In this study, the effect of pretreatment temperature ( $T_T$ ) at 250 °C, 450 °C and 600 °C, as well as without pretreatment is studied on CeNi<sub>0.5</sub>O<sub>Y</sub> catalyst. As shown in **Fig. 3-3**, both CH<sub>4</sub> and CO<sub>2</sub> conversions (31% for CH<sub>4</sub> and 45% for CO<sub>2</sub>) are quite high under the conditions i) without catalyst pretreatment and ii) with in-situ pretreatment in H<sub>2</sub> ( $T_T$ ) at 250 °C of the catalyst. Nevertheless, another interesting effect is increasing the pretreatment temperature  $T_T$  higher than 450 °C leads to lower conversions for both CH<sub>4</sub> and CO<sub>2</sub>. This means that an over-reduced catalyst has less activity than a partially reduced one. Depending on the TPR result, hydrogen starts to be consumed at low temperature on this catalyst, which could show the ability of this solid to be activated at low pretreatment temperatures. Catalytic activity results in combination with carbon deposition data (**Table 3-1**) indicate that for optimal performance with low carbon generated in the products, it is preferable that the catalyst is previously in-situ pretreated in H<sub>2</sub> at 250 °C. As a matter of fact, on CeNi<sub>0.5</sub>O<sub>Y</sub> catalyst a pretreatment in H<sub>2</sub> at 250 °C leads to a carbon formation of 0.19 g g<sub>cat</sub><sup>-1</sup> h<sup>-1</sup> while much higher carbon formation of 0.32 g g<sub>cat</sub><sup>-1</sup> h<sup>-1</sup> is obtained once the catalyst is pretreated in H<sub>2</sub> at 600 °C.

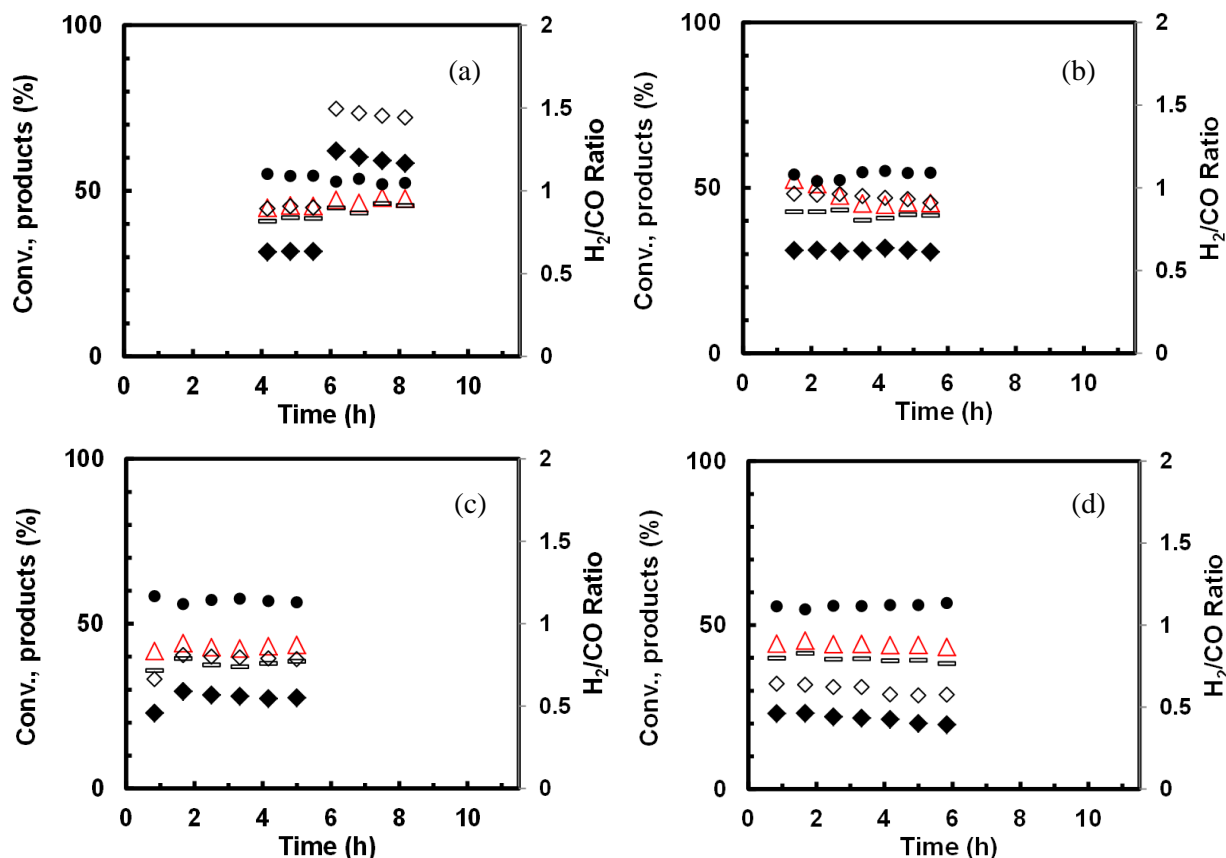


**Fig. 3-4.** Catalytic activity at 600 °C on 10 mg of CeNi<sub>0.5</sub>O<sub>y</sub>, using different treatment temperatures under H<sub>2</sub>/CH<sub>4</sub> (◆), CO<sub>2</sub> (◇) conversions, H<sub>2</sub> (△), CO (●), in mol % and the H<sub>2</sub>/CO ratio (◻). (a) without pretreatment; and pretreated in-situ in H<sub>2</sub> at T<sub>T</sub> (b) 250 °C; (c) 450 °C; and (d) 600 °C. T<sub>exp.</sub>=5h,

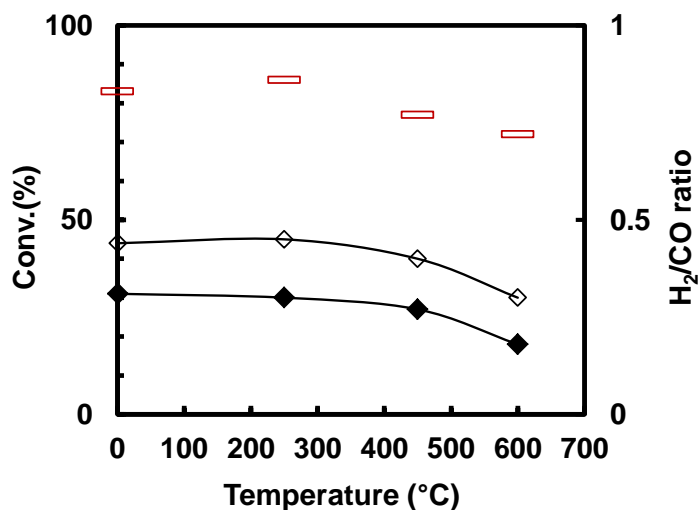


**Fig. 3-5** Catalytic activity at 600 °C on 10 mg of CeNi<sub>0.5</sub>O<sub>y</sub> using different treatment temperatures T<sub>T</sub> in H<sub>2</sub> (the point at zero is without pretreatment). CH<sub>4</sub> (◆), CO<sub>2</sub> (◇) conversions and H<sub>2</sub>/CO ratio (◻); CH<sub>4</sub>/CO<sub>2</sub>/ N<sub>2</sub>= 20:20:60%. t<sub>exp.</sub>=5h.

However, a remarkable characteristic is that the catalyst is already activated even without the

pretreatment under H<sub>2</sub>. Therefore, plenty of energy could be saved by avoiding the high-temperature treatment procedure. This catalyst is capable of being active towards DRM starting directly on the oxide phase. Hence, deletion of the pretreatment step is a fascinating attempt from technical and economical points of view. Maybe the higher reaction temperature of 600 °C at the beginning of the experiment or even the 20% concentration of the reactants makes easier/faster the activation. Similar phenomenon has been found in the literature [99], which reported on the 20% Ni-CeO<sub>2</sub> mixed metal oxide catalyst in DRM, a rapid reduction of the surface of the catalyst by methane at 700K. In another study of the reduction effect on the Ni-based catalyst, nickel particles are found to be larger in the case of a pre-reduced catalyst than in that of the non-pre-reduced catalyst [163]. It has been also reported that [164], high reduction temperatures ( $\geq 450^{\circ}\text{C}$ ) could simultaneously exhibit high activity toward producing carbon deposition which usually makes troubles to the catalytic stability.

**Table 3-1** Carbon formation rate on CeNi<sub>0.5</sub>O<sub>Y</sub> under different pretreatment conditions (zero is corresponding to without pretreatment). Results are reported after 5h of test.

Pretreatment temperature in H <sub>2</sub> ( °C)	0	250	450	600
Carbon formation rate (g g <sub>cat</sub> <sup>-1</sup> h <sup>-1</sup> )	0.28	0.19	0.25	0.32

In the literature, there are some controversial points of view on this subject. the pre-treatment of Ni–Ce catalysts were almost performed at high temperatures ( $\geq 500^{\circ}\text{C}$ ), and the metallic nickel species is often believed to be the active sites [54]. High temperatures are indispensable to have Ni<sup>2+</sup> species reduced. Therefore, the reduction step for obtaining the catalytic active species is generally an important process. In Emma’s work [165], Ni-SiO<sub>2</sub> catalysts were reduced, oxidized and subsequently re-reduced before the test. It was demonstrated that ROR treatment at low temperature decreased the average Ni deposit size and altered the interaction between the Ni and SiO<sub>2</sub>, which significantly enhanced catalytic performance.

### 3.1.3 Influence of Ni content

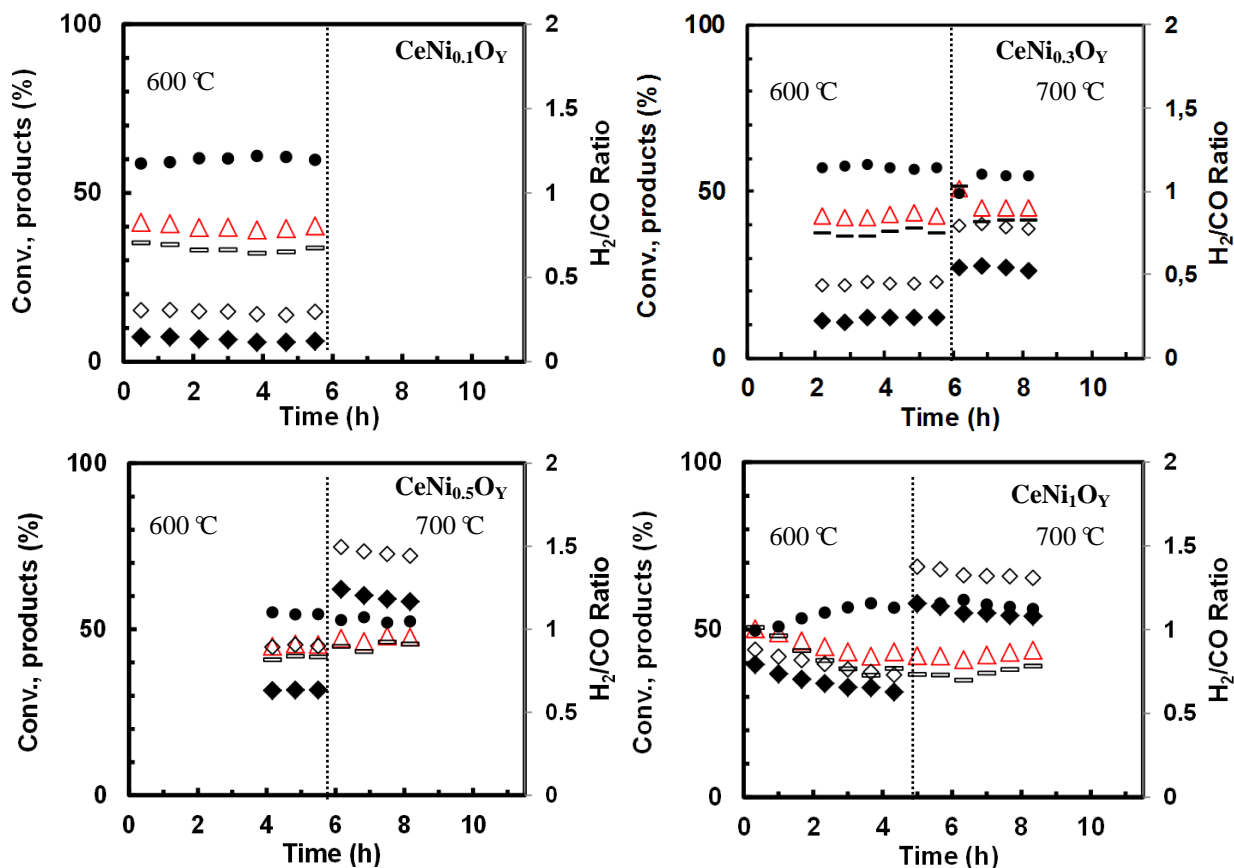
Dry reforming of methane is studied in the present work over the CeNi<sub>x</sub>O<sub>Y</sub> catalysts with different Ni contents, in a first approach without pretreatment. Due to the difficulty to compare the catalytic

results of catalysts with CH<sub>4</sub> conversion close to equilibrium values at 600 °C (57.8% for CH<sub>4</sub> and 67.9% for CO<sub>2</sub>), the CeNi<sub>x</sub>O<sub>y</sub> catalysts are analyzed by using a low mass of catalyst of 10 mg. The CH<sub>4</sub> and CO<sub>2</sub> conversions and H<sub>2</sub>/CO ratio in the products as a function of the Ni content (Ni/M<sub>T</sub>) are shown in **Fig. 3-6** and **Fig. 3-7**.

The 5h of catalytic test indicates that the conversion rates of CH<sub>4</sub> keep constant over CeNi<sub>0.1</sub>O<sub>y</sub> and CeNi<sub>0.3</sub>O<sub>y</sub> catalysts, while the decline is noticeable in the CeNi<sub>1</sub>O<sub>y</sub> and CeNi<sub>2</sub>O<sub>y</sub> catalysts, owing to the high Ni content that leads to a strong trend of carbon formation. Literature [117] showed that a large amount of bigger Ni crystallites exists on the catalysts with the highest Ni content promoting direct CH<sub>4</sub> decomposition, resulting in faster catalyst deactivation. Some differences were also observed in H<sub>2</sub>/CO ratio. In all cases, H<sub>2</sub>/CO ratios were always less than unity, CH<sub>4</sub> conversions are less than the values of CO<sub>2</sub> conversion, which means that the reaction is affected by the simultaneous occurrence of RWGS reaction. Furthermore, the H<sub>2</sub>/CO ratio is increased at 700 °C due to the participation of steam reforming of methane and methane decomposition which is favored at high temperatures. Concretely, the H<sub>2</sub>/CO ratio maintains in a range of 0.6-0.8, it does not show monotonic change with the Ni content at the same temperature.

In this series, the reactivity order globally follows the Ni content. However, for catalysts with higher Ni content, the catalytic activity is not directly proportional to Ni content, particularly for the test at higher temperature of 700 °C. One reason could be that all the data are obtained after 5h of test (stable state), and there is always a decrease of both CH<sub>4</sub> and CO<sub>2</sub> conversions in different extent and in particular in the test with high Ni content. Among all the catalysts tested, CeNi<sub>0.5</sub>O<sub>y</sub> (11.7 wt% of Ni) appears to be the most competitive one as it shows a similar conversion as using higher content of nickel and exhibits less carbon deposition. Concretely, at 600 °C, CH<sub>4</sub> and CO<sub>2</sub> conversions are about 32% and 44% respectively for CeNi<sub>0.5</sub>O<sub>y</sub> after 5 h of test, with a H<sub>2</sub>/CO ratio of around 0.83 (**Fig. 3-7**). It was reported previously that the highest proportion of solid solution is obtained for the CeNi<sub>0.5</sub>O<sub>y</sub> compound (Ni/M<sub>T</sub> = 0.3) [145]. It can be seen that, for CeNi<sub>1</sub>O<sub>y</sub> and CeNi<sub>2</sub>O<sub>y</sub> catalysts, higher Ni content leads to a higher deactivation may be due to the higher potential carbon deposited (0.48 g g<sub>cat</sub><sup>-1</sup> h<sup>-1</sup> for CeNi<sub>1</sub>O<sub>y</sub> and 1.9 g g<sub>cat</sub><sup>-1</sup> h<sup>-1</sup> for CeNi<sub>2</sub>O<sub>y</sub>) on the catalysts. Regardless of the carbon formation and catalytic stability, the H<sub>2</sub> production obtained on the present CeNi<sub>x</sub>O<sub>y</sub> catalysts are comparable to the values

reported in the recent literature [89], in which the authors reported the dry reforming over 50 mg of Ni/CeO<sub>2</sub> catalyst at 700 °C, with a sample reduced in H<sub>2</sub> at 350 °C. Their best result, 34% of CH<sub>4</sub> conversion and 67% of CO<sub>2</sub> conversion were obtained after 8h of test. The H<sub>2</sub>/CO ratio was 0.57. As a result, CeNi<sub>x</sub>O<sub>y</sub> is a highly efficient, stable catalyst for methane dry reforming at relatively low temperatures. Furthermore, the CeNi<sub>x</sub>O<sub>y</sub> will be tested in severe conditions due to the high activity potential of this series of catalysts at low operating temperature.



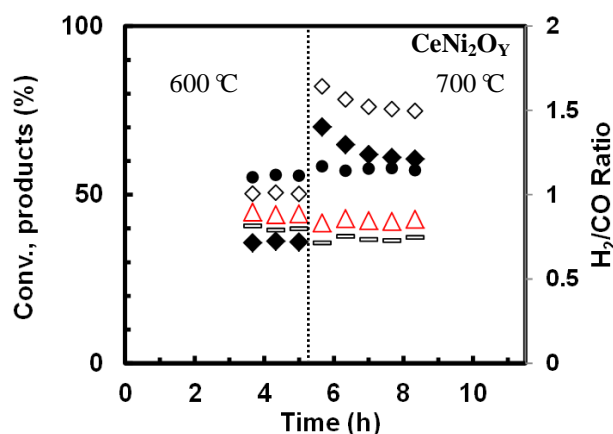


**Fig. 3-6** Catalytic activity in DRM at 600-700 °C on  $\text{CeNi}_x\text{O}_y$  (10 mg) without pretreatment.  $\text{CH}_4$  (◆),  $\text{CO}_2$  (◇) conversions,  $\text{H}_2$  (Δ),  $\text{CO}$  (●), in mol % and the  $\text{H}_2/\text{CO}$  ratio (◻).  $\text{CH}_4/\text{CO}_2/\text{N}_2=20:20:60\%$ .

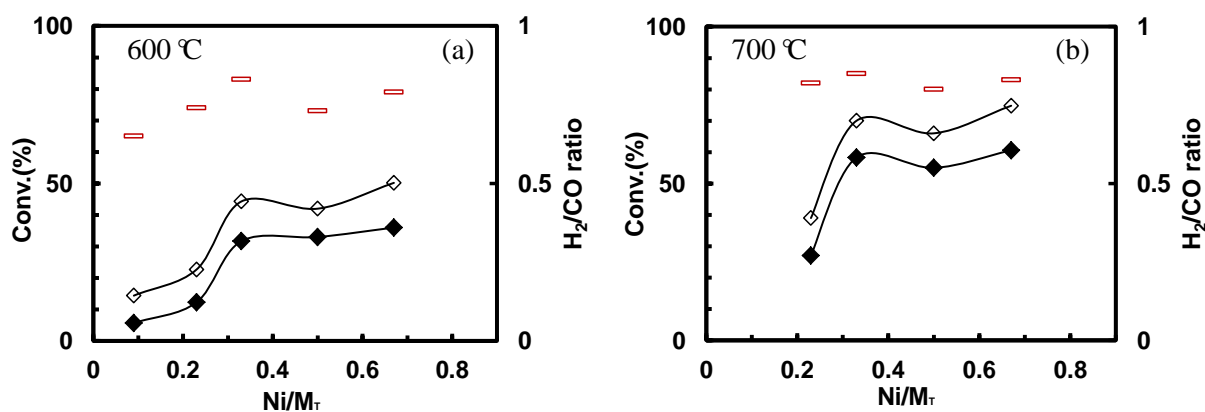


**Fig. 3-7**  $\text{CH}_4$  conversion (◆),  $\text{CO}_2$  conversion (◇)  $\text{H}_2/\text{CO}$  ratio (◻) obtained at a) 600 °C and b) 700 °C. over  $\text{CeNi}_x\text{O}_y$  catalyst (10 mg) Without pretreatment. The feed gas mixture containing  $\text{CH}_4:\text{CO}_2:\text{N}_2$  is 20:20:60%.  $\text{Ni}/\text{M}_T$  molar ratio=  $x/(x+1)$

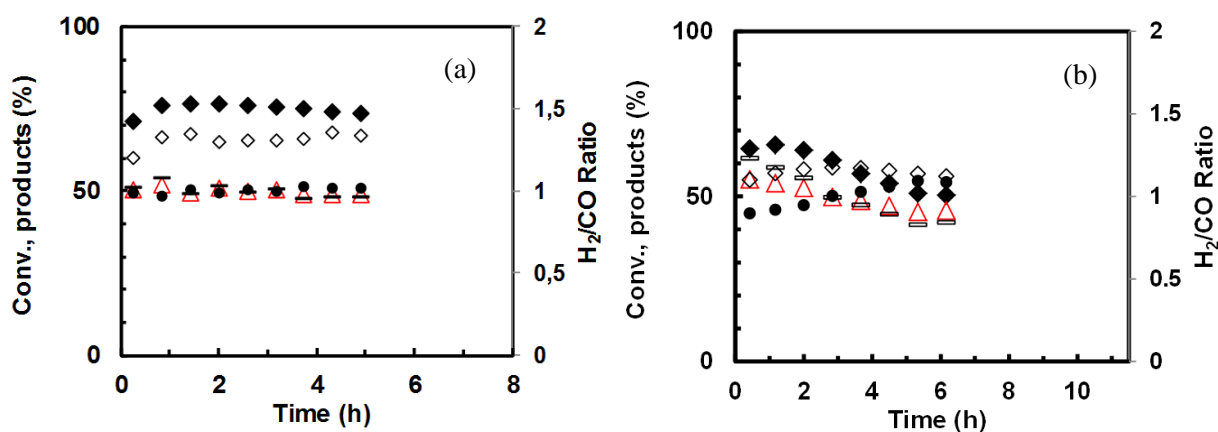
### 3.1.4 Influence of reactants concentration

In order to analyze the resistance of the  $\text{CeNi}_x\text{O}_y$  catalysts to harsh conditions, the influence of reactants concentration, are tested at 600 °C in DRM reaction with different feed gas compositions (**Fig. 3-8**). Firstly, the  $\text{CeNi}_1\text{O}_y$  catalyst is subjected to testing with 3 different conditions in  $\text{CH}_4$  and  $\text{CO}_2$  concentrations (5%, 20% (diluted in  $\text{N}_2$ ), and 50%). Prior to the test, the catalysts are pretreated in pure  $\text{H}_2$  for 12h at 250 °C. Note that there is an increase in methane conversion observed in **Fig. 3-8** (a) during the first 1 hour of reaction. This could be due to fast methane decomposition on the catalytic surface [166]. Although the tests in 20% and 50% conditions demonstrate relatively similar evolution for  $\text{CH}_4$ ,  $\text{CO}_2$  conversions and products distribution after 5h time on stream. However, the initial conversions (**Fig. 3-8**) and carbon formation rate (**Fig. 3-9**) are quite different. For the 20% of reactant concentration

condition, the conversion of  $\text{CH}_4$  decreased from 63.4 % to 55.2% over 5 h on stream while  $\text{CO}_2$  remains at 60%. On the other hand, it is clear that higher conversion of about 75% and 69% can be obtained with a more diluted feed ( $\text{CH}_4:\text{CO}_2:\text{N}_2 = 5:5:90\%$ ). The methane reaction rate is higher than that of carbon dioxide for this experiment, this could be due to a lower rate of RWGS and greater rate of methane cracking than carbon removal by  $\text{CO}_2$  activation and therefore carbon deposition. The  $\text{H}_2/\text{CO}$  ratio higher than unity at 600 °C could be explained by the dominance of the  $\text{CH}_4$  cracking reaction producing  $\text{H}_2$  and carbon.

Gennequin et al. [167] reported a maximum of  $\text{H}_2/\text{CO}$  ratio which they ascribed to the  $\text{H}_2$  formation by the steam reforming reaction and methane decomposition on  $\text{Co}_4\text{Mg}_2\text{Al}_2$ . When the reaction temperature was increased higher than 600 °C,  $\text{CH}_4$  conversion was higher than  $\text{CO}_2$  conversion, which may be ascribed to methane decomposition and methane steam reforming participation.

**Fig. 3-9** shows the activity and selectivity after 5h of test on the  $\text{CeNi}_1\text{O}_Y$  catalyst pretreated in  $\text{H}_2$  at 250 °C. A small amount of carbon formation ( $0.46 \text{ g}\cdot\text{g}_{\text{cat}}^{-1}\text{h}^{-1}$ ) is obtained in most diluted conditions (5%), while the conversions values are quite stable in 5 h test. However, in 20% conditions, a higher amount of carbon ( $1.6 \text{ g}\cdot\text{g}_{\text{cat}}^{-1}\text{h}^{-1}$ ) is measured after the test, indicating that carbon formation could be one reason for the slight deactivation. As seen in **Fig. 3-8 (c)**, when increasing the concentrations of  $\text{CH}_4$  and  $\text{CO}_2$  to 50% (without dilution), 48.3% of  $\text{CH}_4$  conversion and 55.2% of  $\text{CO}_2$  conversion are obtained after 5h of test. More interestingly, increasing the concentration of the reactants from 20% to 50% in the mixture does not lead to an apparent decrease in the activity, the catalyst allows obtaining a stable activity even in the most severe conditions ( $\text{CH}_4\text{-CO}_2=50\%\text{-}50\%$ ) within such a case a carbon formation that increases up to  $2.3 \text{ g}\cdot\text{g}_{\text{cat}}^{-1}\text{h}^{-1}$ .



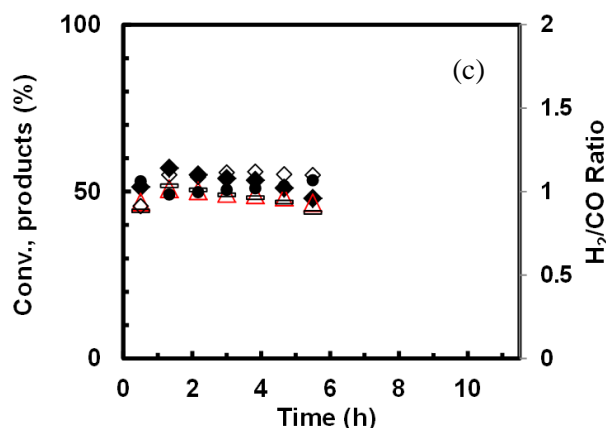


**Fig. 3-8** Catalytic results obtained in DRM at 600 °C on the CeNi<sub>1</sub>O<sub>Y</sub> catalyst (50 mg) pretreated in H<sub>2</sub> at 250 °C by feeding different concentrations of CH<sub>4</sub> and CO<sub>2</sub> in a ratio at 1:1. (a) 5%, (b) 20% (diluted in N<sub>2</sub>) and (c) 50%. CH<sub>4</sub> (◆), CO<sub>2</sub> (◇) conversions, H<sub>2</sub> (△), CO (●), in mol % and the H<sub>2</sub>/CO ratio (□).

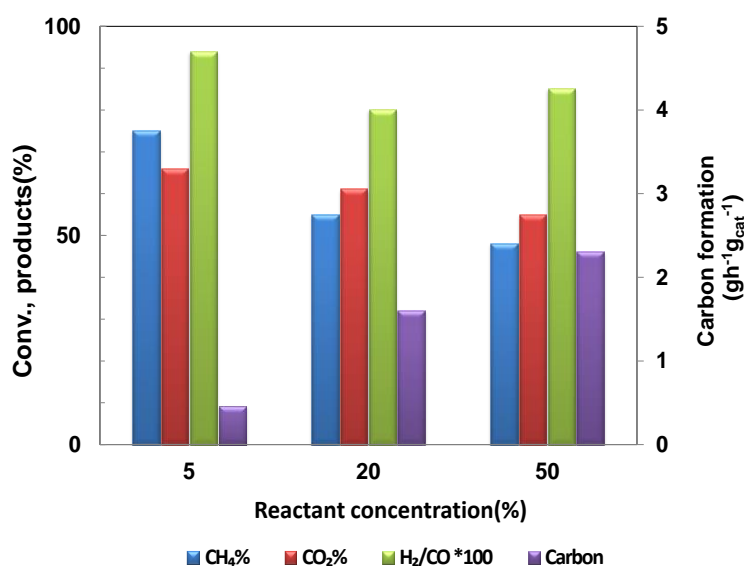


**Fig. 3-9** Catalytic results in DRM obtained at 600 °C on the CeNi<sub>1</sub>O<sub>Y</sub> catalyst (50 mg) pretreated in H<sub>2</sub> at 250 °C by feeding different concentrations of CH<sub>4</sub> and CO<sub>2</sub> in a ratio at 1:1.

The CeNi<sub>0.5</sub>O<sub>Y</sub> catalyst was tested at 600 °C in DRM reaction under the severe conditions (CH<sub>4</sub>:CO<sub>2</sub> = 50:50%) as a comparison. The result of the test was presented in **Fig. 3-10**, the result for CeNi<sub>1</sub>O<sub>Y</sub> is impressive due to higher conversion of CH<sub>4</sub> than CO<sub>2</sub> in the initial period of time, then it decreases to a lower value than CO<sub>2</sub> conversion. Compared with CeNi<sub>0.5</sub>O<sub>Y</sub>, which provides CH<sub>4</sub> and CO<sub>2</sub> conversions at 37.2% and 49.5%, respectively, this shift on the CH<sub>4</sub> conversion of CeNi<sub>1</sub>O<sub>Y</sub> could be related to carbon deposition, probably the methane cracking reaction is facilitated at such high Ni content. As a matter of fact, higher carbon formation rate and H<sub>2</sub>/CO ratio are obtained on CeNi<sub>1</sub>O<sub>Y</sub> catalyst in such conditions. Similarly, Luo et al. [168] also reported that CH<sub>4</sub> conversion was higher than CO<sub>2</sub>

conversion at 700 and 800 °C over Ni–La<sub>2</sub>O<sub>3</sub> supported on 5A molecular sieve in DRM, which was attributed to the presence of both CH<sub>4</sub> decomposition and CO<sub>2</sub> complete dissociation (i.e., CO<sub>2</sub> → CO + O and then CO → C + O; the surface oxygen species adsorbed could enhance CH<sub>4</sub> decomposition).

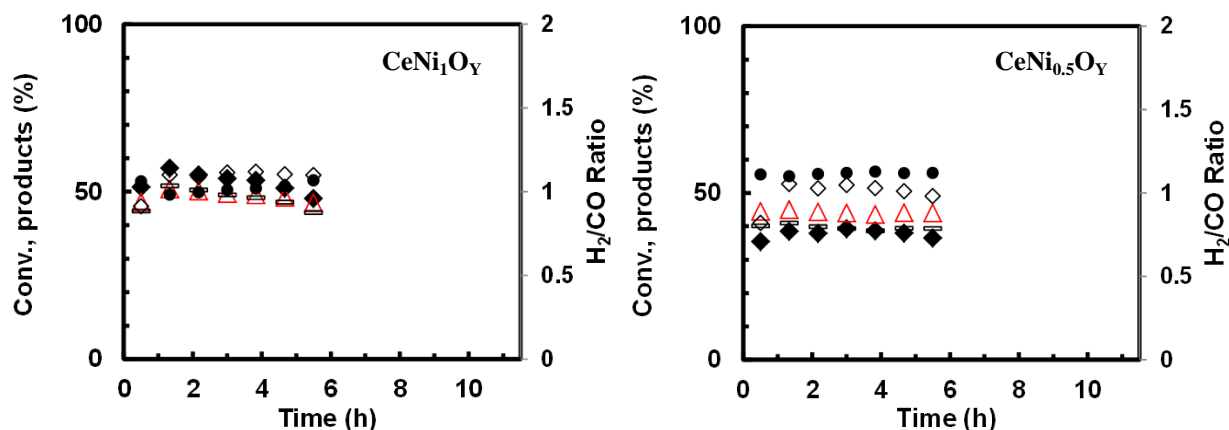


**Fig. 3-10.** Comparison of activity for CeNi<sub>1</sub>O<sub>Y</sub> and CeNi<sub>0.5</sub>O<sub>Y</sub> at 600 °C . CH<sub>4</sub> (◆), CO<sub>2</sub> (◇) conversions, H<sub>2</sub> (△), CO (●), in mol % and the H<sub>2</sub>/CO ratio (◻) obtained versus time over catalyst (50mg) with pretreatment at 250 °C., CH<sub>4</sub>:CO<sub>2</sub> = 50:50%.

The methane and carbon dioxide conversions, as well as the H<sub>2</sub>/CO ratio, are measured in DRM at 700 °C, which are shown in **Fig. 3-11**. At initial period, CeNi<sub>1</sub>O<sub>Y</sub> gives higher conversion rates than CeNi<sub>0.5</sub>O<sub>Y</sub>. However, the decrease in CH<sub>4</sub> and CO<sub>2</sub> conversions values for CeNi<sub>1</sub>O<sub>Y</sub> catalyst is higher compared to CeNi<sub>0.5</sub>O<sub>Y</sub>, which reaches about 62% conversion of CH<sub>4</sub> and 73% conversion of CO<sub>2</sub> after 5h on stream. While 58% and 71% of conversions for CH<sub>4</sub> and CO<sub>2</sub> are obtained after 5h of test for CeNi<sub>0.5</sub>O<sub>Y</sub>. It is seen that two catalysts with different Ni content show similar conversions while H<sub>2</sub>/CO ratio of CeNi<sub>0.5</sub>O<sub>Y</sub> is about 0.78, which is lower than the value obtained on CeNi<sub>1</sub>O<sub>Y</sub> (0.85).

As expected, carbon formation at 700 °C is largely decreased to 0.34 g g<sub>cat</sub><sup>-1</sup> h<sup>-1</sup> and 0.90 g g<sub>cat</sub><sup>-1</sup> h<sup>-1</sup> for CeNi<sub>0.5</sub>O<sub>Y</sub> and CeNi<sub>1</sub>O<sub>Y</sub>. In such a case, reaction temperature clearly influences the carbon formation rate. For CeNi<sub>1</sub>O<sub>Y</sub> catalyst, in contrast with the results obtained at 600 °C, methane conversion is always lower than CO<sub>2</sub> conversion, H<sub>2</sub>/CO ratio is stable in 5h of test, meaning that besides RWGS, other side reactions are less favored at 700 °C. This also depends on the reactants concentrations. On the other hand, carbonaceous species can exist in different forms. If the carbon formed is kind of carbon nano-materials [169], which does not lead to a deactivation, it can be regarded as an added value accompanied by H<sub>2</sub> production.

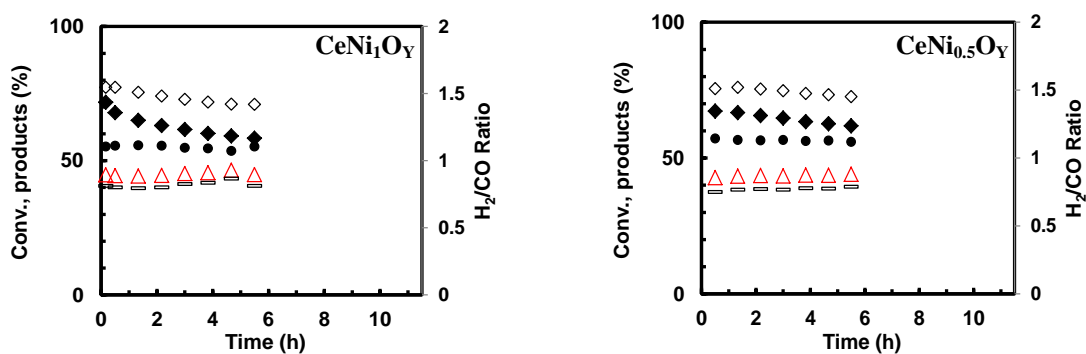


**Fig. 3-11** Comparison of activity for  $\text{CeNi}_1\text{O}_Y$  and  $\text{CeNi}_{0.5}\text{O}_Y$  at 700 °C.  $\text{CH}_4$  ( $\blacklozenge$ ),  $\text{CO}_2$  ( $\diamond$ ) conversions,  $\text{H}_2$  ( $\triangle$ ),  $\text{CO}$  ( $\bullet$ ), in mol % and the  $\text{H}_2/\text{CO}$  ratio ( $\square$ ) obtained versus time over catalyst (50mg) with pretreatment at 250 °C.  $\text{CH}_4:\text{CO}_2 = 50:50\%$ .

Well dispersed and low Ni content catalyst for mitigating the carbon deposition has been widely recognized. The test of 50 mg of  $\text{CeNi}_{0.3}\text{O}_Y$  in harsh conditions in range of 600-700 °C is performed and the result is illustrated in **Fig. 3-12**. Low Ni content results in lower  $\text{CH}_4$  and  $\text{CO}_2$  conversions. In spite of this, it seems interesting that the conversions are quite constant and carbon formation is well suppressed.

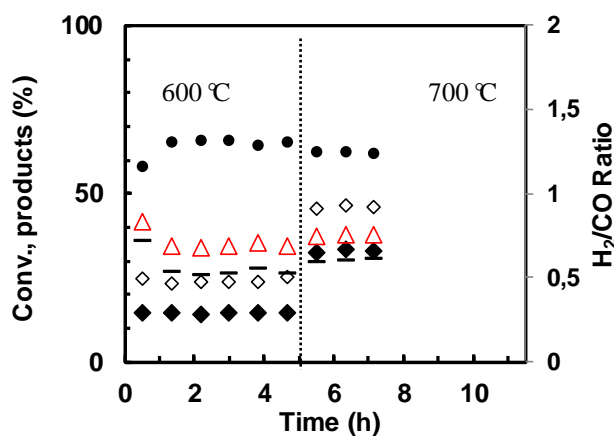


**Fig. 3-12**  $\text{CH}_4$  ( $\blacklozenge$ ),  $\text{CO}_2$  ( $\diamond$ ) conversions,  $\text{H}_2$  ( $\triangle$ ),  $\text{CO}$  ( $\bullet$ ), in mol % and the  $\text{H}_2/\text{CO}$  ratio ( $\square$ ) obtained at 600 °C and 700 °C versus time over  $\text{CeNi}_{0.3}\text{O}_Y$  catalyst (50mg) with pretreatment at 250 °C.  $\text{CH}_4:\text{CO}_2$  in a ratio of 50%:50%.

The  $\text{CeNi}_{0.3}\text{O}_Y$  catalyst shows good stability but lower activity due to the low Ni content (6.7 w.t%). It could be interesting to see how it works with a higher amount of catalyst. In order to investigate that how the mass of catalyst influences the activity, tests were carried out in the condition of  $\text{CH}_4:\text{CO}_2 =$

50%:50% on  $\text{CeNi}_{0.3}\text{O}_Y$  with different mass from 10-300 mg. As shown in **Fig. 3-13**,  $\text{CH}_4$  and  $\text{CO}_2$  conversions become more efficient as the mass increases. Globally, relatively stable conversions in 5h of time on stream with carbon formation lower than  $0.05 \text{ g g}_{\text{cat}}^{-1} \text{ h}^{-1}$  (seen in **Table 3-2**) are obtained. Furthermore, the  $\text{H}_2/\text{CO}$  ratio slightly increases with the increase of the mass, while carbon formation rate also decreases. The conversion of  $\text{CH}_4$  and  $\text{CO}_2$  are about 40% and 50%, respectively, which are very close to the thermodynamic equilibrium values of 41% and 54%. Meaning that even with a low Ni content in this series of compounds, high activity can be reached by increasing the catalyst mass. Most prominently, carbon formation is diminished under this scenario.

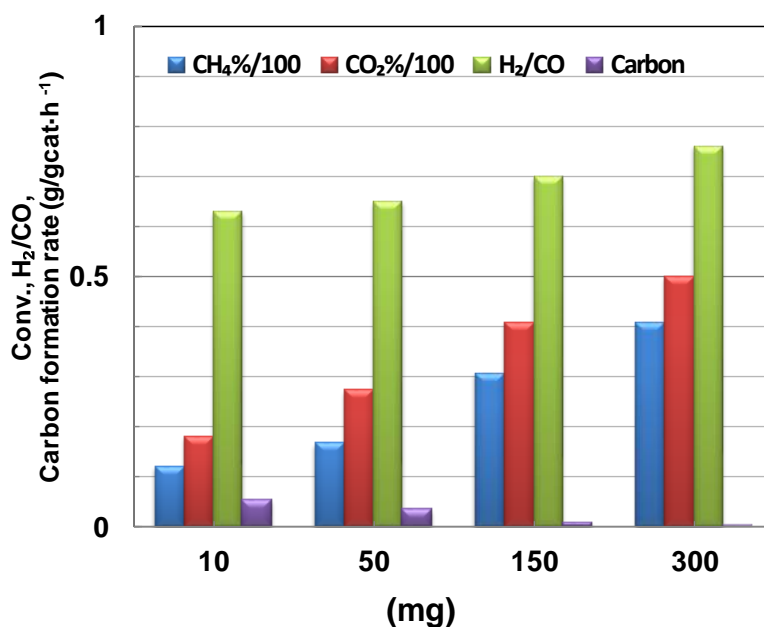


**Fig. 3-13**  $\text{CH}_4$  and  $\text{CO}_2$  conversions and  $\text{H}_2/\text{CO}$  ratio obtained at 600 °C versus the mass of the  $\text{CeNi}_{0.3}\text{O}_Y$  catalyst (10-300 mg) pretreated in  $\text{H}_2$  at 250 °C.  $\text{CH}_4:\text{CO}_2 = 50\%:50\%$

**Table 3-2**  $\text{H}_2/\text{CO}$  ratio and carbon formation rate in different mass of  $\text{CeNi}_{0.3}\text{O}_Y$  catalyst  $\text{CH}_4:\text{CO}_2 = 50\%:50\%$

Mass (mg)	10	50	150	300
$\text{H}_2/\text{CO}$ ratio	0.63	0.65	0.69	0.75
Carbon formation rate ( $\text{g g}_{\text{cat}}^{-1} \text{ h}^{-1}$ )	0.05	0.04	0.01	0.003

### 3.1.5 Stability test

In order to clarify the stability and eventual causes of deactivation, the catalyst with the best

performance is subjected to long-term testing. The experiment is carried out to investigate the performance of the  $\text{CeNi}_{0.5}\text{O}_Y$  catalyst over a long time of 50h time-on-stream at 700 °C in a reactants mixture of  $\text{CH}_4:\text{CO}_2:\text{N}_2 = 20\%:20\%:60\%$ .

The obtained conversion values ( $\text{CH}_4$  and  $\text{CO}_2$ ) and products ratio ( $\text{H}_2/\text{CO}$ ) are plotted as a function of time on stream in **Fig. 3-14**. A mild but steady decay in  $\text{CH}_4$  and  $\text{CO}_2$  conversions is observed. The decrease of conversion of  $\text{CH}_4$  is slightly greater than the drop of conversion of  $\text{CO}_2$  in the initial period. After 50 h of reaction at 700 °C, the methane conversion decreases down to values around 60% (from 77%), while  $\text{CO}_2$  conversion decreases from 83% to 72%. Moreover, the initial  $\text{H}_2/\text{CO}$  molar ratio is 0.78 and the value increases to 0.83 in 5h of time on stream.

The obtained results are interesting when compared to literature. Vasiliades et al. [81] studied dry reforming over 5 wt. % Ni/ $\text{CeO}_2$  catalyst at a higher temperature of 750 °C, (with 20%  $\text{CH}_4$ ;  $\text{CH}_4/\text{CO}_2 = 1$  and a total flow of 150 mL/min with 150 mg of catalysts,  $\text{GHSV} = 30,000 \text{ h}^{-1}$ ). The  $\text{CH}_4$  and  $\text{CO}_2$  conversions were 76 % and 83%, respectively, and the  $\text{H}_2/\text{CO}$  ratio was 1.0. Besides, carbon in filamentous and graphitic structure was largely formed after test. In the present study, very similar results are obtained at lower temperature and lower mass of catalysts.

Since the  $\text{CH}_4$  dissociation and carbon formation take place on surfaces of the catalyst, distinct deactivation did not occur even if carbon species are formed with a rate of  $0.03 \text{ g g}_{\text{cat}}^{-1} \text{ h}^{-1}$ . The carbon species are analyzed by  $\text{O}_2$ -TPO after test. In the literature, the types of carbonaceous species can be identified by the numbers and position of TPO peaks associated with different reactivity towards oxidation [170][149]. Firstly, there is no peak observed at the temperatures lower than 400 °C, which is assigned to the amorphous carbon that is highly reactive and easily oxidized from the catalyst surface. Temperatures around 510 °C were assigned to the single walled carbon nanotubes (SWCNTs), while temperatures around 610 °C could be attributed to the multiwalled carbon nanotubes (MWCNTs). Carbon nanofibers (CNFs) were supposed to burn off in lower temperature range than MWCNTs [171]. As shown in **Fig. 3-15**, an almost single and asymmetric peak is presented at around 580 °C for the carbon species formed, which can be generally due to a mixture of CNFs possibly with some CNTs. It has been reported that the single broad peak at around 600 °C is ascribed to more graphitic carbon that is more stable and oxidizes at higher temperatures [149]. It has been reported previously this type of carbon

filaments related to CNFs and/or CNTs can allow a catalytic stability [169][149].

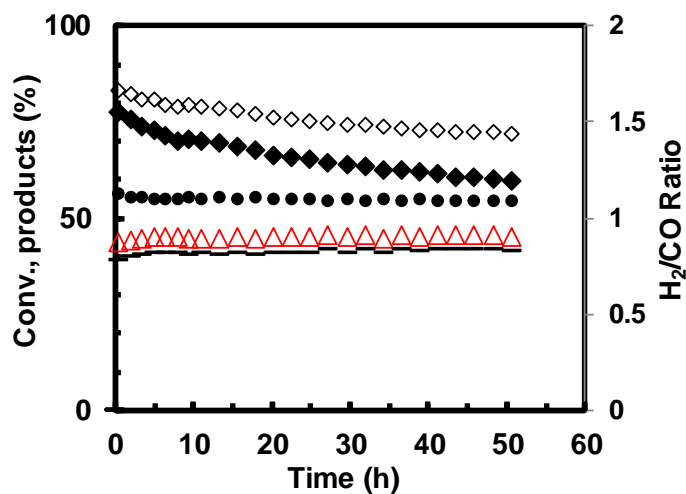


**Fig. 3-14** Catalytic stability of  $\text{CeNi}_{0.5}\text{O}_Y$  catalyst (50 mg without pretreatment) at 700 °C for 50 h.  $\text{CH}_4$  (◆),  $\text{CO}_2$  (◇) conversions,  $\text{H}_2$  (△),  $\text{CO}$  (●), in mol % and the  $\text{H}_2/\text{CO}$  ratio (□).  $\text{CH}_4:\text{CO}_2:\text{N}_2=20\%:20\%:60\%$ .

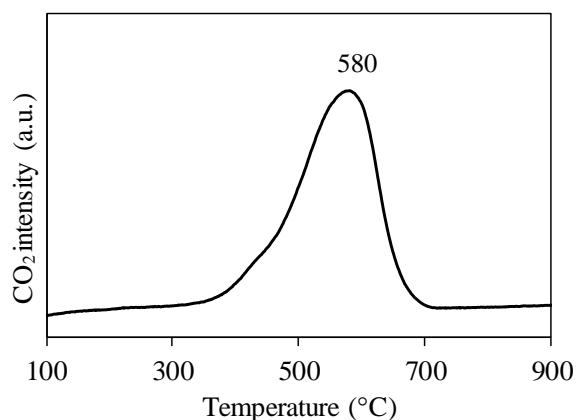


**Fig. 3-15** TPO profiles of the  $\text{CeNi}_{0.5}\text{O}_Y$  catalyst after 50h of test in condition ( $\text{CH}_4:\text{CO}_2=20\%:20\%$ ) at 700 °C.

Another objective is to explore the catalyst stability and process sustainability issues in the conditions favorable for carbon deposition at 600 °C (via decomposition of methane). On this purpose,  $\text{CeNi}_{0.3}\text{O}_Y$  which contains less of nickel (6.5 wt.%) is chosen for this experiment. Higher amount of catalyst (300 mg) is carried in the reactor to balance the low content of nickel. The temperature of the experiment is set at 600 °C for studying DRM in harsh conditions. Long-term stability test were carried out for 72 h of test in gas mixture of  $\text{CH}_4$  and  $\text{CO}_2$  without dilution on  $\text{CeNi}_{0.3}\text{O}_Y$ , directly after *in situ*  $\text{H}_2$ -reduction at 250 °C (best conditions, as discussed above).

It can be seen from **Fig. 3-16** that, for  $\text{CeNi}_{0.3}\text{O}_Y$ , the  $\text{CH}_4$  conversion,  $\text{CO}_2$  conversion and  $\text{H}_2/\text{CO}$  molar ratios are found extremely stable with 72h of time-on-stream. The catalytic activity towards  $\text{CH}_4$  and  $\text{CO}_2$  at this temperature is high but below the equilibrium values. The conversions of methane and carbon dioxide reach 41% and 49%, respectively. Moreover, the  $\text{H}_2/\text{CO}$  molar ratio obtained is about 0.76. All these results show that  $\text{CeNi}_{0.3}\text{O}_Y$  is highly active for DRM reaction and does not suffer from activity loss during the reaction under severe conditions (low temperature, pure  $\text{CO}_2\text{-CH}_4$  feed). The carbon formation rate is  $0.003 \text{ g g}_{\text{cat}}^{-1} \text{ h}^{-1}$  (by weighting the spent catalyst).

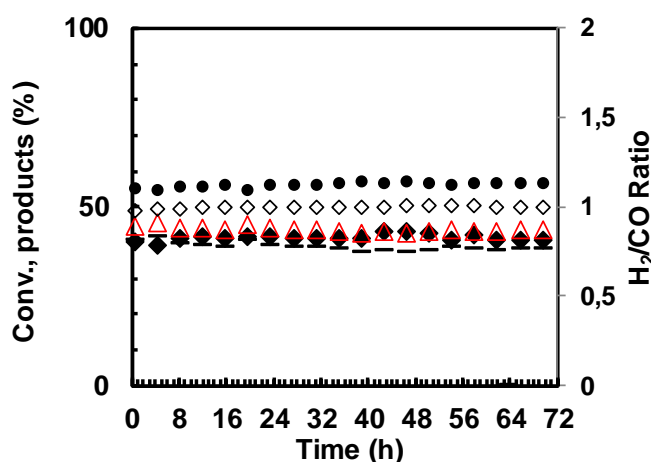


**Fig. 3-16** Catalytic stability of  $\text{CeNi}_{0.3}\text{O}_Y$  catalyst at 600 °C. (300 mg) with pretreatment at 250 °C.  $\text{CH}_4$  ( $\blacklozenge$ ),  $\text{CO}_2$  ( $\diamond$ ) conversions,  $\text{H}_2$  ( $\triangle$ ),  $\text{CO}$  ( $\bullet$ ), in mol % and the  $\text{H}_2/\text{CO}$  ratio ( $\square$ ) obtained versus time over catalyst.  $\text{CH}_4:\text{CO}_2=50\%:50\%$ .

### 3.2 Dry reforming over $\text{CeNi}_x\text{Al}_{0.5}\text{O}_Y$ mixed oxides

It is often reported that Al provides unique properties such as a high metallic dispersion and high particle stability against sintering. The role of Al in the catalysts is getting greater dispersion of active metal on the surface which reduces the ensemble size and generally limits carbon deposition [51]. However, the correlation between addition of Al and the catalytic performance needs investigation. Therefore, the effect on DRM of Al addition in the catalyst with different Ni contents, and the influence of the pretreatment temperature are presented in this section

### 3.2.1 Influence of reaction temperature and pretreatments

At first, the influence of pretreatment is investigated over  $\text{CeNi}_2\text{Al}_{0.5}\text{O}_Y$  catalyst. Comparison study results are shown in **Fig. 3-17**. As already reported the DRM reaction is thermodynamically favored at high temperatures, therefore, the conversions increase with the increase of temperature in the studied temperature range of 600-700 °C. Both methane and  $\text{CO}_2$  conversions slightly decrease during tests.

**Fig. 3-17** (a) and (b) show that the pretreatment at 250 °C in  $\text{H}_2$  has no apparent influence on the  $\text{CH}_4$  and  $\text{CO}_2$  conversions at stabilization state. But there is a different evolution for  $\text{CH}_4$  and  $\text{CO}_2$  conversions at the initial period at 600 °C, meaning that there is an activation process under reaction conditions. At high temperature of 700 °C, the deactivation is milder than that at 600 °C. Moreover, the conversions obtained with and without catalyst pretreatment are close to each other. The  $\text{CH}_4$  and  $\text{CO}_2$  conversions are 62% and 72% for the test without pretreatment and 60% and 71% with catalyst pretreated at 250 °C.

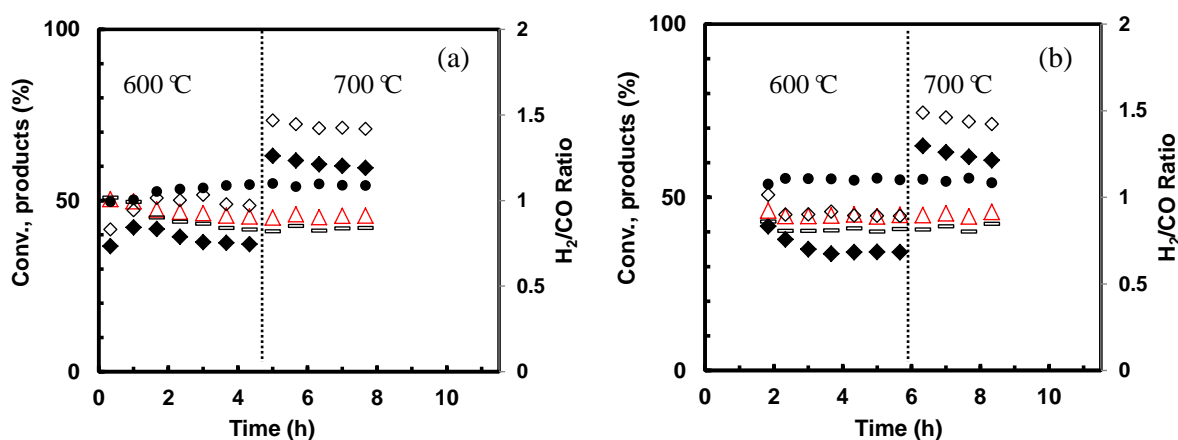
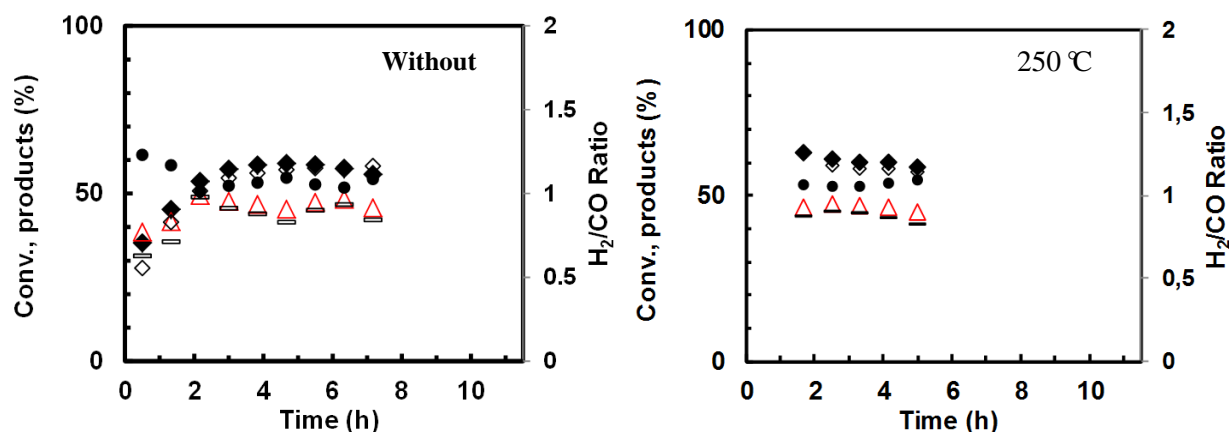


**Fig. 3-17**  $\text{CH}_4$  ( $\blacklozenge$ ),  $\text{CO}_2$  ( $\diamond$ ) conversions,  $\text{H}_2$  ( $\triangle$ ),  $\text{CO}$  ( $\bullet$ ), in mol % and the  $\text{H}_2/\text{CO}$  ratio ( $\square$ ) obtained at 600-700 °C versus time over the  $\text{CeNi}_2\text{Al}_{0.5}\text{O}_Y$  catalyst (10mg) without pretreatment (a), and (b) pretreated in  $\text{H}_2$  at 250 °C.  $\text{CH}_4:\text{CO}_2=20:20\%$  in  $\text{N}_2$ .

It can be also observed that in spite of the similar conversions obtained, the amount of carbon formation in the catalysts is different, sample without pretreatment leads to a higher carbon deposition rate  $0.64 \text{ g g}_{\text{cat}}^{-1} \text{ h}^{-1}$  compared to  $0.28 \text{ g g}_{\text{cat}}^{-1} \text{ h}^{-1}$  obtained on the pretreated in  $\text{H}_2$  sample. Depending on literature [164], for the catalyst without pretreatment, a certain structure or distribution of Ni is developed which is more selective for the decomposition of  $\text{CH}_4$  or  $\text{CO}$  disproportionation. This could

be one explanation for the different amount of carbon formed.

**Fig. 3-18** and **Table 3-3** show the different experimental conditions of the pretreatments and the catalytic activity expressed as  $\text{CO}_2$  and  $\text{CH}_4$  conversions as well as the  $\text{H}_2/\text{CO}$  ratio, also for the values of the amount of carbon accumulated on the  $\text{CeNi}_2\text{Al}_{0.5}\text{O}_Y$  catalyst in severe conditions. The results show that relatively similar conversion for both  $\text{CH}_4$  and  $\text{CO}_2$  is obtained after 5h of test for different pretreatment temperatures ( $T_T$ ) in  $\text{H}_2$ . However, **Fig. 3-18** clearly shows that the conversions are continually decreasing after 5h for test with pretreatment in  $\text{H}_2$  at  $600\text{ }^\circ\text{C}$ . The amount of carbon after the test is entirely different, catalyst pretreated in  $\text{H}_2$  at  $250\text{ }^\circ\text{C}$  leads to the lowest carbon formation ( $1.3\text{ g g}_{\text{cat}}^{-1}\text{ h}^{-1}$ ) while the pretreatment in  $\text{H}_2$  at  $600\text{ }^\circ\text{C}$  leads to the highest carbon formation ( $2.42\text{ g g}_{\text{cat}}^{-1}\text{ h}^{-1}$ ). These findings are similar to that obtained on  $\text{CeNi}_{10.5}\text{O}_Y$  catalyst (section 3.1.2), for which lower performances have been obtained for higher pretreatment temperature of  $600\text{ }^\circ\text{C}$ . This phenomenon has been also analyzed in literature, Horváth et al. [172] investigated dry reforming over 10%  $\text{Co}/\text{Al}_2\text{O}_3$  reduced at different temperatures up to 1173 K, they proposed that the different structures of the catalysts formed at different reduction temperatures resulted in the different catalytic behavior. The pretreatment temperature of  $\text{Co}/\text{Al}_2\text{O}_3$  catalysts influenced the type of the surface carbon which was determined by XPS. On the catalysts reduced at low temperature, the amount of the amorphous carbon increased. Juan-juan et al. investigated the influence of pretreatment method on  $\text{Ni}/\text{Al}_2\text{O}_3$  catalyst in DRM [170]. They indicated that activity is not affected by the pretreatment carried out but a noticeable amount of deposited carbon has been observed on catalyst without pretreatment, the similar active state is obtained with or without pretreatment at  $700\text{ }^\circ\text{C}$  over Ni-Al based catalyst. This probably related to an influence of the pretreatment on the size and structure of the nickel particles.



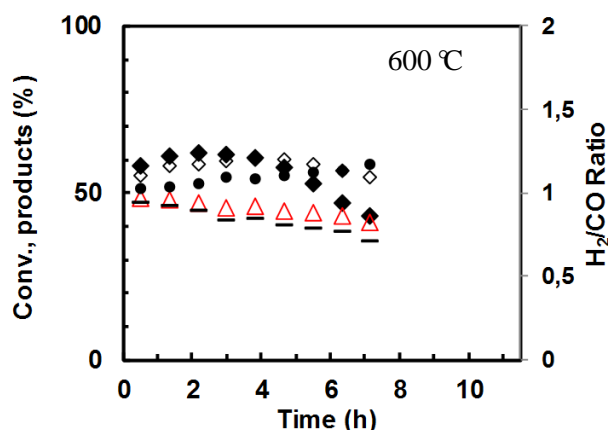


**Fig. 3-18.** Catalytic activity at 600 °C on 50 mg of CeNi<sub>2</sub>Al<sub>0.5</sub>O<sub>Y</sub> without and with pretreatment in H<sub>2</sub> at different T<sub>T</sub> CH<sub>4</sub> (◆), CO<sub>2</sub> (◇) conversions, H<sub>2</sub> (Δ), CO (●), in mol % and the H<sub>2</sub>/CO ratio (□) CH<sub>4</sub>:CO<sub>2</sub> = 50:50%

**Table 3-3** Catalytic activity (5 h, CH<sub>4</sub>:CO<sub>2</sub> = 50:50%) on CeNi<sub>2</sub>Al<sub>0.5</sub>O<sub>Y</sub> catalyst (50mg) submitted to different pretreatments.

Treatment in H <sub>2</sub> at different T <sub>T</sub> (°C)	Reaction (°C)	CH <sub>4</sub> conv. (%)	CO <sub>2</sub> conv. (%)	H <sub>2</sub> /CO ratio	Carbon formation rate (g g <sub>cat</sub> <sup>-1</sup> h <sup>-1</sup> )
without	600	56	58	0.84	1.76
250	600	61	58	0.80	1.3
600	600	56	60	0.80	2.42

### 3.2.2 Influence of Ni content

Several papers in the existing literature report on the activity, selectivity and stability of Ce-Ni-Al based catalysts in DRM. The influence of the preparation method [173], in terms of Ce introduction [118] has been described. However, to the best of our knowledge, the effect of a wide range of nickel content in CeNi<sub>X</sub>Al<sub>0.5</sub>O<sub>Y</sub> compounds has not been reported yet. Depending on the previous test showing the pretreatment has low influence on catalytic activity of CeNi<sub>X</sub>O<sub>Y</sub> catalysts, the study of Ni content in the ternary CeNi<sub>X</sub>Al<sub>0.5</sub>O<sub>Y</sub> catalysts is carried out at 600 °C and 700 °C avoiding the pretreatment in H<sub>2</sub>, using 10 mg of catalyst. The reaction conditions used are CH<sub>4</sub>/CO<sub>2</sub>/ N<sub>2</sub>= 20:20:60%. The result of methane and CO<sub>2</sub> conversions measured during the reaction and the H<sub>2</sub>/CO ratio vs. Ni content at 600 and 700 °C are shown in **Fig. 3-19** and **Fig. 3-20**. It is clear that the CH<sub>4</sub> and CO<sub>2</sub> conversions globally increase with increasing Ni-content. At 600 °C, on the catalyst containing a high amount of Ni (CeNi<sub>5</sub>Al<sub>0.5</sub>O<sub>Y</sub>), the initial CH<sub>4</sub> and CO<sub>2</sub> conversions are quite high. Afterward, the conversions continuously decrease during the first 3 hours of reaction. Finally, the steady-state values around 33%

and 49% for CH<sub>4</sub> and CO<sub>2</sub> conversions are obtained. This is possibly due to the occurring of methane decomposition, in particular on the catalyst that contains a high amount of Ni species. According to thermodynamics, carbon-forming reactions, such as direct methane decomposition, CH<sub>4</sub> = C + 2H<sub>2</sub>, are favored at such low temperatures around 600 °C. As shown in **Fig. 3-21**, among the different catalysts tested, the catalyst with low Ni content shows the lowest amount of carbon produced. CeNi<sub>2</sub>Al<sub>0.5</sub>O<sub>Y</sub> seems to be the most competitive one as it shows similar high activity and potentially less carbon deposition compared to higher Ni content catalyst. However, the relationship between carbon formation and Ni content is not linear as the amount of carbon deposited on catalyst CeNi<sub>5</sub>Al<sub>0.5</sub>O<sub>Y</sub> is quite high, which indicates that probably not only the Ni content determines the carbon deposit, but other factors also, as particle morphology or structure could affect carbon deposition. Moreover, the activity is ameliorated compared with the values reported on binary Ni-Ce based catalysts, where the CeNi<sub>10.5</sub>O<sub>Y</sub> catalyst with low Ni content gives similar methane conversion compared to CeNi<sub>2</sub>Al<sub>0.5</sub>O<sub>Y</sub> at 700 °C. This will be further more deeply discussed later on in comparison part. The result is competitive compared to the literature [88] which presented the dry reforming over 50 mg of Ni-Ce-Al catalyst with different Ni content at 650 °C, approximately 55% of methane and CO<sub>2</sub> conversions are obtained with 20wt% of Ni. Also in Luisetto's work [174], similar compound Ni/CeO<sub>2</sub>-Al<sub>2</sub>O<sub>3</sub> was prepared by co-precipitation method. It has been found that this catalyst (50 mg) gave 54% of CH<sub>4</sub> conversion and 68% of CO<sub>2</sub> conversion in dry reforming at 700 °C with 40% reactant concentration condition.

In the studied series, the H<sub>2</sub>/CO values are not obviously influenced by Ni content or the variation of temperature from 600 °C to 700 °C (**Fig. 3-20**), ranging from 0.75-0.85. There are some different findings in the literature, for example, Lee et al. [175] observed in their study that a higher nickel content provides an increased H<sub>2</sub>/CO ratio. This suggests the role of additional bulk-like nickel species could facilitate WGS activity, subsequently leading to greater amounts of hydrogen yielded per mole of methane converted. However, in the present study, the H<sub>2</sub>/CO ratio is similar in different catalysts that could be related to the average crystallize sizes which is very close between 5-7 nm in the different catalysts. On the other hand, it is also possible that parts of the carbon formed at 600 °C could be oxidized by CO<sub>2</sub> or H<sub>2</sub>O to produce more CO in the products when increasing the temperature to 700 °C, explaining why the H<sub>2</sub>/CO ratios could be kept at same value when increasing the reaction temperature.

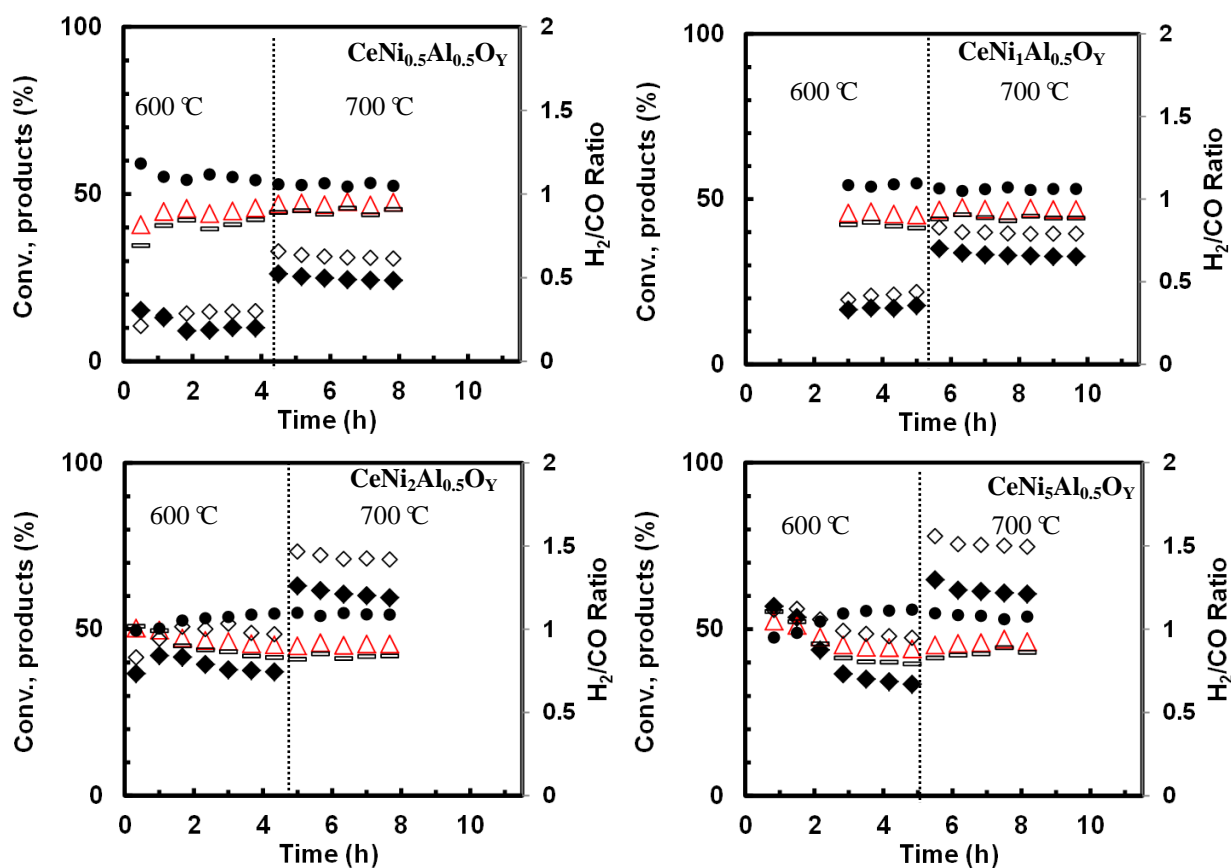


Fig. 3-19 Catalytic activity of DRM at 600-700 °C on  $\text{CeNi}_x\text{Al}_{0.5}\text{O}_Y$  (10 mg) without pretreatment.  $\text{CH}_4$  ( $\blacklozenge$ ),  $\text{CO}_2$  ( $\diamond$ ) conversions,  $\text{H}_2$  ( $\triangle$ ),  $\text{CO}$  ( $\bullet$ ), in mol % and the  $\text{H}_2/\text{CO}$  ratio ( $\square$ ).  $\text{CH}_4/\text{CO}_2/\text{N}_2 = 20:20:60\%$ .

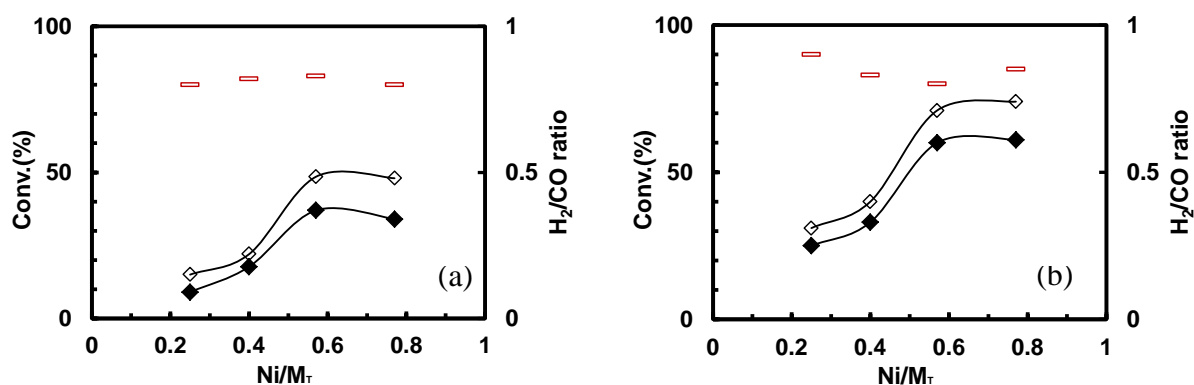
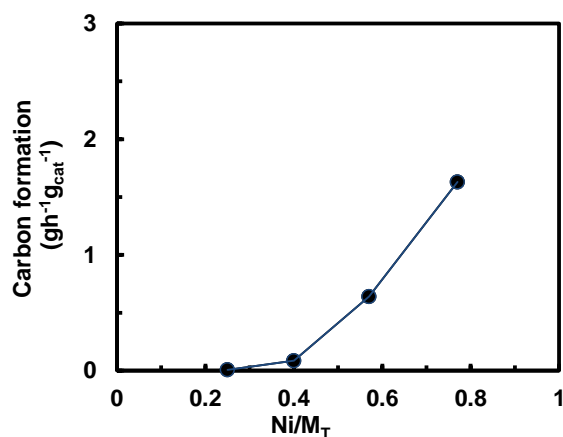


Fig. 3-20  $\text{CH}_4$  conversion  $\blacklozenge$ ,  $\text{CO}_2$  conversion  $\diamond$  and  $\text{H}_2/\text{CO}$  ratio  $\square$  obtained at a) 600 °C and b) 700 °C versus  $\text{Ni}/\text{M}_T$  ratio over the  $\text{CeNi}_x\text{Al}_{0.5}\text{O}_Y$  catalyst (10 mg) without pretreatment.  $\text{CH}_4:\text{CO}_2 = 20\%:20\%$ .  $\text{Ni}/\text{M}_T = X/(X + 0.5 + 1)$ .



**Fig. 3-21** Carbon formation rate ● at 600 °C to 700 °C versus Ni/M<sub>T</sub> ratio over the CeNi<sub>x</sub>Al<sub>0.5</sub>O<sub>y</sub> catalyst (10mg) CH<sub>4</sub>:CO<sub>2</sub>= 20%:20%. (from the test in **Fig. 3-19**).

### 3.2.3 Performance in harsh condition

To analyze the behavior of the catalysts in harsh condition, dry reforming is firstly studied over CeNi<sub>2</sub>Al<sub>0.5</sub>O<sub>y</sub> at two different reaction temperatures 600 °C and 700 °C as a function of the reaction time in concentrated conditions of CH<sub>4</sub>/CO<sub>2</sub>= 50%:50%. **Fig. 3-22** reports the results obtained in the steady state after 7h of reaction at 600 °C. The initial conversions of CH<sub>4</sub> and CO<sub>2</sub> are 35% and 28%, respectively. Then they increase gradually to 58% within about 4h on stream. Finally, the CH<sub>4</sub> conversion decreases to 56% after 7h of test. Furthermore, the H<sub>2</sub>/CO ratio also increases from 0.62 with time on stream then maintains at around 0.80. The carbon formation rate is about 1.76 g g<sub>cat</sub><sup>-1</sup> h<sup>-1</sup>. Quiroga et al. [160] also found a kind of similar evolution in dry reforming of methane on Ni-Ce based catalysts at 550 °C. In their study, the catalyst reached a maximum in both reactant conversions during the first hour on stream; afterward, a deactivation process begun.

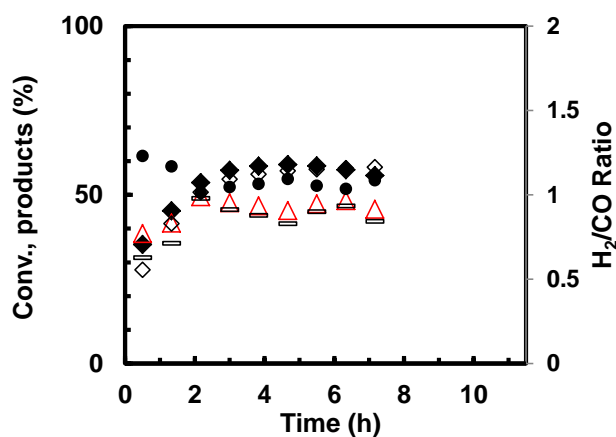


**Fig. 3-22** CH<sub>4</sub> (◆), CO<sub>2</sub> (◇) conversions, H<sub>2</sub> (△), CO (●), in mol % and the H<sub>2</sub>/CO ratio (◻) obtained at 600 °C versus time over the CeNi<sub>2</sub>Al<sub>0.5</sub>O<sub>Y</sub> catalyst (50mg) without pretreatment. CH<sub>4</sub>:CO<sub>2</sub> =50:50%.

The results obtained at 700 °C are shown in **Fig. 3-23**. The CeNi<sub>2</sub>Al<sub>0.5</sub>O<sub>Y</sub> catalyst presents a high activity with 74% of CH<sub>4</sub> conversion and 82% of CO<sub>2</sub> conversion, while the H<sub>2</sub>/CO ratio is about 0.88. The CH<sub>4</sub> and CO<sub>2</sub> equilibrium conversions under the studied operational conditions are 72% and 82%, evidencing that the experimental values obtained are almost identical to the limits. To the best of our knowledge, this value is one of the best reported for the Ni-based catalysts. At 600 °C, an initial increase of conversions is not observed in this case. However, a slight deactivation is observed in methane conversion but not notable in CO<sub>2</sub> conversion. The reason why CO<sub>2</sub> is not simultaneously affected could be linked to the high surface area of the catalysts containing slightly basic sites where CO<sub>2</sub> adsorption (then activation) could continue.[176] From another point of view, it could be described as the initial conversion of CH<sub>4</sub> is higher than the value of its stable state, maybe due to the carbon deposition period in the first several hours caused by CH<sub>4</sub> decomposition. This is in agreement with a slight increase of H<sub>2</sub>/CO ratio during the test. Similar study are reported by Jun Han et al. [88], they performed DRM at 700 °C on a series of Ni-Ce-Al composite oxides with various Ni molar contents prepared by co-precipitation method. 50 mg of catalyst was tested in CH<sub>4</sub>:CO<sub>2</sub>=45%:45% condition, with a GHSV= 40,000 mLg<sup>-1</sup>h<sup>-1</sup>. The best catalyst with 10wt% Ni was giving 67% and 77% of conversions for CH<sub>4</sub> and CO<sub>2</sub> respectively. The H<sub>2</sub>/CO ratio obtained in their study was quite high at 0.95.

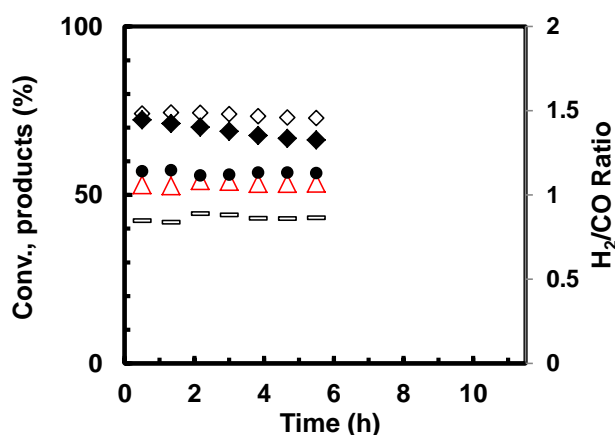


**Fig. 3-23** CH<sub>4</sub> (◆), CO<sub>2</sub> (◇) conversions, H<sub>2</sub> (△), CO (●), in mol % and the H<sub>2</sub>/CO ratio (◻) obtained at 700 °C versus time over the CeNi<sub>2</sub>Al<sub>0.5</sub>O<sub>Y</sub> catalyst (50 mg) without pretreatment. CH<sub>4</sub>:CO<sub>2</sub> =50:50%.

On Ce-Ni based binary catalyst, the correlation of stability, carbon formation rate, reactant concentration and Ni content were discussed. It was easy to obtain a more stable result on the catalyst with low Ni content. The test of DRM in harsh condition on the ternary catalyst with low Ni contents (CeNi<sub>0.5</sub>Al<sub>0.5</sub>O<sub>Y</sub>) is carried out at 700 °C for 5 h. **Fig. 3-24** illustrates the conversions of CH<sub>4</sub> and CO<sub>2</sub> and H<sub>2</sub>/CO ratio versus time on stream. The activity is quite stable after 1h of stabilization. Concretely, after the 5h test, conversions of CH<sub>4</sub> and CO<sub>2</sub> are 57% and 66%, respectively. The H<sub>2</sub>/CO ratio is about 0.84 and the carbon formation rate is only of 0.01g g<sub>cat</sub><sup>-1</sup> h<sup>-1</sup>. It is clear that this catalyst shows more stable activity due to the low Ni content. Finally, the CeNi<sub>X</sub>Al<sub>0.5</sub>O<sub>Y</sub> catalysts are very active at low temperature as shown by the high H<sub>2</sub>/CO ratio obtained and they are able to sustain harsh conditions as presented before. Odedairo et al. [89] investigated dry reforming on Ni/CeO<sub>2</sub> catalyst in the continuous fixed-bed flow reactor (GHSV=38400 mL/(hg<sub>cat</sub>), CO<sub>2</sub>/CH<sub>4</sub>=1:1, T=700 °C). They treated the catalyst with microwave plasma to mitigate the carbon deposition. Higher activity and stability were obtained compared with conventional thermal calcination: 34% of CH<sub>4</sub> conversion and 67% of CO<sub>2</sub> conversion were obtained after 8h of test. And the H<sub>2</sub>/CO ratio was ~0.58. We get higher conversions values in this study even in harsher conditions with a simple preparation method.

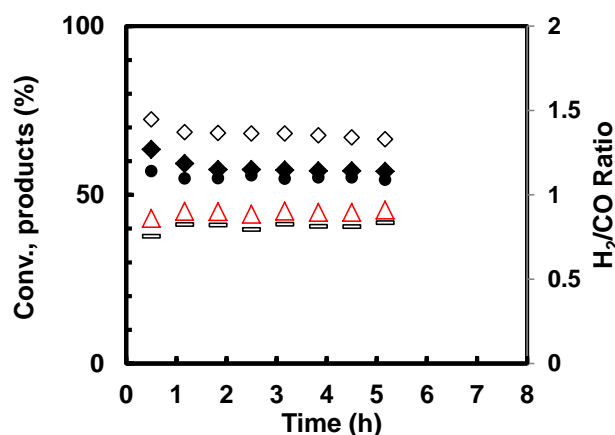


**Fig. 3-24** CH<sub>4</sub> (◆), CO<sub>2</sub> (◇) conversions, H<sub>2</sub> (△), CO (●), in mol % and the H<sub>2</sub>/CO ratio (□) obtained at 700 °C versus time over the CeNi<sub>0.5</sub>Al<sub>0.5</sub>O<sub>γ</sub> catalyst (300mg) pretreated in H<sub>2</sub> at 250 °C. CH<sub>4</sub>:CO<sub>2</sub> =50:50%.

### 3.2.4 Stability test

In order to examine catalysts application in the DRM reaction in harsh condition, stability tests of 60 h of time on stream are conducted over CeNi<sub>0.5</sub>Al<sub>0.5</sub>O<sub>γ</sub> with low Ni content. **Fig. 3-25** illustrates methane and CO<sub>2</sub> conversions and H<sub>2</sub>/CO ratio as a function of time during the long-term test at 600 °C. The catalytic conversions towards CH<sub>4</sub> and CO<sub>2</sub> reach 38% and 49%, respectively. The H<sub>2</sub>/CO molar ratio obtained is about 0.77. The carbon formation rate is 0.003 g g<sub>cat</sub><sup>-1</sup> h<sup>-1</sup>. Moreover, the catalyst maintains stable activity without deactivation during 60 h on stream. This could be attributed to the small crystallites size on the surface, resulting in greater carbon resistance.

Generally, the Ni-based catalyst could be less active in longer reaction time or lower reaction temperatures [159]. In spite of this, all these results show that CeNi<sub>0.5</sub>Al<sub>0.5</sub>O<sub>γ</sub> is highly active for DRM reaction and does not suffer from activity loss after 60 h of reaction under severe conditions. This improved behavior with respect to the good dispersion of Ni species and strong interaction between Ce, Ni as well as Al cations. This is also in agreement with the study of Wenjia et al. [177], they reported that in dry reforming reaction, the enhancement of the catalytic stability of Ni-based catalyst was closely associated with the stabilization of the active nickel particles by alumina support. In the test condition of CH<sub>4</sub>:CO<sub>2</sub> = 40%:40%, GHSV=90,000 cm<sup>3</sup>g<sup>-1</sup>h<sup>-1</sup>, the result obtained on 10 wt.% Ni-CeO<sub>2</sub>-γ-Al<sub>2</sub>O<sub>3</sub> at 600 °C was 33% and 44% for CH<sub>4</sub> and CO<sub>2</sub>, respectively. And the H<sub>2</sub>/CO ratio was 0.125 g g<sub>cat</sub><sup>-1</sup> h<sup>-1</sup>.

In the present study, higher conversions and lower carbon formation rate are obtained on  $\text{CeNi}_{0.5}\text{Al}_{0.5}\text{O}_Y$  in relatively similar conditions.

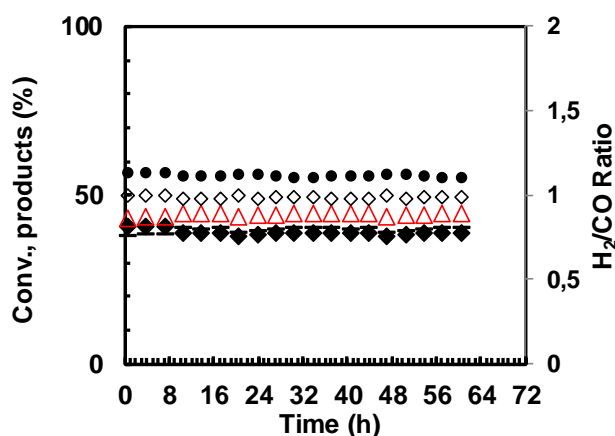


**Fig. 3-25** Catalytic stability at 600 °C on  $\text{CeNi}_{0.5}\text{Al}_{0.5}\text{O}_Y$  catalyst (300mg) pretreated in  $\text{H}_2$  at 250 °C.  $\text{CH}_4$  (◆),  $\text{CO}_2$  (◇) conversions,  $\text{H}_2$  (△),  $\text{CO}$  (●), in mol % and the  $\text{H}_2/\text{CO}$  ratio (◻) obtained versus time on stream.  $\text{CH}_4:\text{CO}_2=50\%:50\%$ .

Temperature programmed oxidation (TPO) of the spent sample has been applied in order to identify the carbon deposition. The profile is shown in **Fig. 3-26**, unlike the spectra of binary catalysts, there are 2 main peaks emerging at around 400 °C and 580 °C, respectively. As discussed in **section 3.1.5**, the first peak at low temperature could be probably assigned to amorphous carbon that is highly reactive and easily oxidized from the nickel surface. The second peak located at 580 °C could be ascribed to mixture of CNFs possibly with some CNTs. It is in agreement with the catalyst stability certainly due to the low amount of carbon formation and mainly in amorphous form.

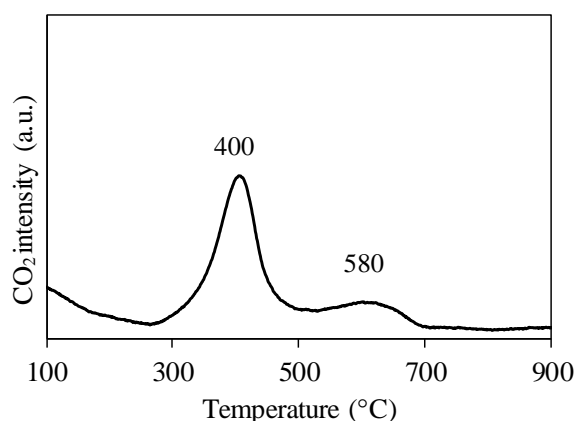


**Fig. 3-26** TPO profile of the used  $\text{CeNi}_{0.5}\text{Al}_{0.5}\text{O}_Y$  catalysts after running 60h,  $\text{CH}_4:\text{CO}_2=50\%:50\%$ .

### 3.2.5 The influence of Al in $\text{CeNi}_x(\text{Al}_z)\text{O}_y$ mixed oxides

The influence of Al in  $\text{CeNi}_x(\text{Al}_z)\text{O}_y$  mixed oxides can be observed by the comparison study shown in **Fig. 3-27** (a) and (b), at 600 and 700 °C, respectively. Both the Ce-Ni and Ce-Ni-Al system exhibit high activity at low temperatures even with 10mg of catalyst. The ternary catalysts with low Ni content are found to have lower activities but be more resistance to carbon deposition than binary catalysts (**Fig. 3-28**). When increasing the Ni/ $M_T$  ratio to above 0.57, the binary and ternary catalysts show the similar activity and selectivity, the  $\text{H}_2/\text{CO}$  ratio is around 0.80 at 600 °C. It seems that all the catalysts activities obey linear relationship with increase of Ni content, up to a Ni/ $M_T$  ratio of about 0.3 on binary catalysts and up to a Ni/ $M_T$  ratio of about 0.6 on ternary catalysts whatever at 600 °C and 700 °C. The slope of the curve is different on binary and ternary catalysts: the increase is much faster on binary catalysts. Therefore, the  $\text{CeNi}_{0.5}\text{O}_y$  catalyst presents similar activity results compared to higher Ni content ternary catalysts. Therefore, the beneficial effect of nickel and ceria ratio on catalysts activity is maximized on  $\text{CeNi}_{0.5}\text{O}_y$  catalyst, which combined strong Ni-Ce interactions whatever in solid solution and/or at the interface of small crystallites. Another possible explanation could be diffusional limitations or, most probably, a number of active sites not proportional to the metal amount in this kind of catalyst, suggesting in turn either a higher accessibility hindrance to the active sites with nickel enrichment or a decrease of metal dispersion [176].

On the ternary compounds, it is clear that the addition of Al directly or indirectly influences the catalytic activity and carbon formation. Many studies have shown that the redox properties can be considerably enhanced if additional elements are introduced into the  $\text{CeO}_y$  lattice by forming a solid solution [178][80]. It is known that  $\text{CeO}_2\text{-MO}_x$  solid solution has good thermal stability and better oxygen storage capacity than  $\text{CeO}_2$  alone [179]. Moreover, our previous study also showed that, compared to the binary mixed oxides  $\text{CeNi}_x\text{O}_y$ , the presence of other cations allows increasing the hydrogen storage and gives a better stability to the system [131].

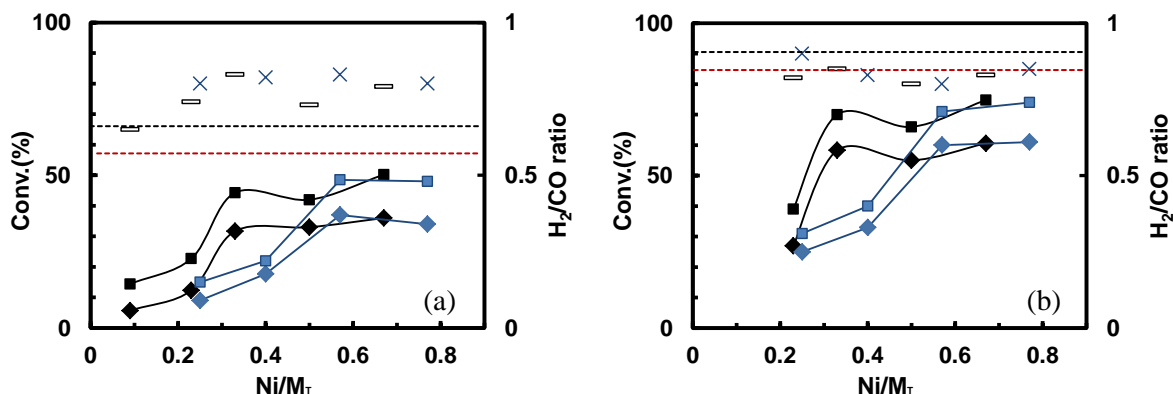


**Fig. 3-27** CH<sub>4</sub> (◆) and CO<sub>2</sub> (■) conversions and the H<sub>2</sub>/CO ratio (□) over CeNi<sub>x</sub>O<sub>y</sub> (black) and CeNi<sub>x</sub>Al<sub>0.5</sub>O<sub>y</sub> (blue) H<sub>2</sub>/CO ratio (×) versus Ni content. (a) at 600 °C, (b) at 700 °C. Thermodynamic limit for CH<sub>4</sub> (---) and CO<sub>2</sub> (---). 10 mg of catalyst without pretreatment. CH<sub>4</sub>/CO<sub>2</sub> = 20%:20%.

The carbon formation rate is also estimated and compared in **Fig. 3-28** among different catalysts. Ternary catalysts with Al still have better ability for mitigating the carbon deposition. According to literature, the ensemble size necessary for carbon formation is larger than that for methane reforming [180]. XRD results reveal that the average dimension of NiO crystallites size is also minimized by the presence of Al in the system. In the literature, Chen et al. [181] studied the Ni/Ce-Al catalyst in dry reforming of methane. They suggested that the presence of CeAlO<sub>3</sub> in the catalyst can inhibit the growth of graphitic carbon on nickel surface while the formation of amorphous carbon is independent of the CeAlO<sub>3</sub>. The CeAlO<sub>3</sub> species showed the ability for decomposing CO<sub>2</sub> to form active surface oxygen and therefore the carbon resistance promotion by nature was suggested to be contributed to an oxidative environment around Ni particles.

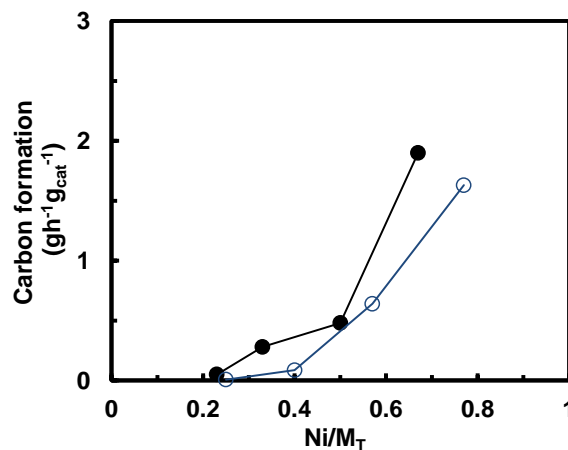


**Fig. 3-28** carbon formation rate over Ni/M<sub>T</sub> ratio on CeNi<sub>x</sub>O<sub>y</sub> ● and CeNi<sub>x</sub>Al<sub>0.5</sub>O<sub>y</sub> ○

### 3.2.6 Conclusion for $\text{CeNi}_x(\text{Al}_z)\text{O}_y$ in DRM

Dry reforming of  $\text{CH}_4$  (DRM) has been studied on  $\text{CeNi}_x(\text{Al}_z)\text{O}_y$  ( $z = 0$  or  $0.5$ ) catalysts with different nickel contents obtained using co-precipitation method. The influence of different parameters is examined, such as the reaction temperature, pretreatment in  $\text{H}_2$ , Ni content, reactants concentrations and the mass of catalyst.

Raising reaction temperature pronouncedly increases conversions of  $\text{CH}_4$  and  $\text{CO}_2$  and  $\text{H}_2/\text{CO}$  ratio. For  $\text{CeNi}_{0.5}\text{O}_y$ , it allows obtaining high conversions of methane (85%), carbon dioxide (93%) and a high selectivity ( $\text{H}_2/\text{CO} = 0.93$ ) at the temperature of  $800\text{ }^\circ\text{C}$  under 20% initial concentration of the reactants.

Three different pretreatment temperatures as well as without pretreatment have been studied, indicating that changing pretreatment temperatures has no significant influence on steady-state conversion results, but leads to different conversion evolutions and carbon formation rate. The optimum treatment temperature can be proposed at  $250\text{ }^\circ\text{C}$  taking promoting conversions, products distribution, and the carbon formation into account. It is attributed to the presence of very active Ni species being able to be reduced and reoxidized readily and reversibly in  $\text{CeNi}_x(\text{Al}_z)\text{O}_y$  compounds.

Conversions globally increase with Ni content while  $\text{H}_2/\text{CO}$  ratio maintained around 0.7-0.8. The gas product distribution seems not be influenced by Ni content. There is a decline of conversion over catalysts with high Ni content. Moreover, solid carbon is formed and it also increases with Ni content.  $\text{CeNi}_{0.5}\text{O}_y$  and  $\text{CeNi}_2\text{Al}_{0.5}\text{O}_y$  compounds appear as the best catalysts in binary and ternary series, respectively, due to the high activity in  $\text{CH}_4$  and  $\text{CO}_2$  conversions, and resistance to carbon formation.

The studied catalysts allow obtaining a good activity even in the severe conditions ( $\text{CH}_4/\text{CO}_2 = 50/50\%$ ). Higher amount of catalyst with low Ni content provides a more stable result. For low Ni content  $\text{CeNi}_{0.3}\text{O}_y$  catalyst, conversions are quite constant, and carbon formation is well suppressed. On the other hand, on high Ni content catalysts,  $\text{CeNi}_1\text{O}_y$  and  $\text{CeNi}_2\text{O}_y$  show higher activity in 50%:50% concentration condition, although the carbon formation leads to a decrease of conversions at the initial period of time.

The long-term stability test in DRM has been studied on  $\text{CeNi}_{0.5}\text{O}_y$  and  $\text{CeNi}_{0.3}\text{O}_y$  catalysts under different conditions. The  $\text{CH}_4$  and  $\text{CO}_2$  conversions reach 60% and 72%, respectively, after 50 h of reaction on  $\text{CeNi}_{0.5}\text{O}_y$ , showing good stability towards carbon deposition. In stability test under harsh

condition, the catalytic activity of  $\text{CeNi}_{0.3}\text{O}_Y$  catalyst towards  $\text{CH}_4$  and  $\text{CO}_2$  transformations leads to 41 and 49%, respectively. Moreover, the  $\text{H}_2/\text{CO}$  molar ratio obtained is about 0.76. Similarly, it is shown that stable results are also obtained on  $\text{CeNi}_{0.5}\text{Al}_{0.5}\text{O}_Y$  catalyst in DRM reaction without activity loss after 60 h of reaction under severe conditions.

Finally, the addition of Al into the Ce-Ni system decreases the conversions for both  $\text{CH}_4$  and  $\text{CO}_2$  in low Ni content condition, but maintains high activity in catalysts with high Ni content. Anyway, it significantly modifies the catalytic nature and decreases the amount of carbon deposits.

### 3.3 Dry reforming over $\text{Ni}_X\text{Mg}_2\text{AlO}_Y$ mixed oxides

The HT-like compounds can incorporate various metal cations such as  $\text{Ni}^{2+}$ ,  $\text{Co}^{2+}$  and  $\text{Cu}^{2+}$ . Many researchers have taken them as the catalyst precursor or as the catalyst support [149]. Different authors have employed the co-precipitation technique to obtain hydrotalcite-type precursors of Ni, Mg and Al, obtaining materials with excellent catalytic behavior in methane dry reforming reaction [182][183]. After thermal treatment, the mixed oxides obtained show several unique properties such as high thermal stability, surface area and metal dispersion. It has been reported that the synergetic effect between the metal cations in ex-hydrotalcite catalysts can lead to the resistance to carbon formation and/or the sintering of Ni particles[149]. Under this scenario, Ni-based ex-hydrotalcite catalysts are able to bring benefit to the dry reforming process and it also could be comparable to other Ni-based catalysts in the previous study.

In the present section, the influences of different parameters have been investigated on  $\text{Ni}_X\text{Mg}_2\text{AlO}_Y$  catalysts such as the Ni content, *in situ* pretreatment in  $\text{H}_2$  and concentration of the reactants. Catalyst performances are investigated in the reaction of dry reforming of methane. Based on the previous study with  $\text{CeNi}_X\text{O}_Y$  catalysts, the working conditions applied to the ternary  $\text{Ni}_X\text{Mg}_2\text{AlO}_Y$  compounds are directly on 10mg of catalyst and 600 °C of reaction temperature.

#### 3.3.1 The influence of reaction temperature

The values of  $\text{CH}_4$  and  $\text{CO}_2$  conversions and  $\text{H}_2/\text{CO}$  molar ratio registered during 5h DRM tests carried out at 600 and 700 °C are depicted in **Fig. 3-29**. In each test, 10 mg of  $\text{Ni}_1\text{Mg}_2\text{AlO}_Y$  catalyst is *in situ* pretreated in  $\text{H}_2$  at 450 °C. It shows that the conversion of  $\text{CH}_4$  and  $\text{CO}_2$  and the selectivity obtained

during 5h of reaction are stable at 600 °C while there was a decline of related values at 700 °C.

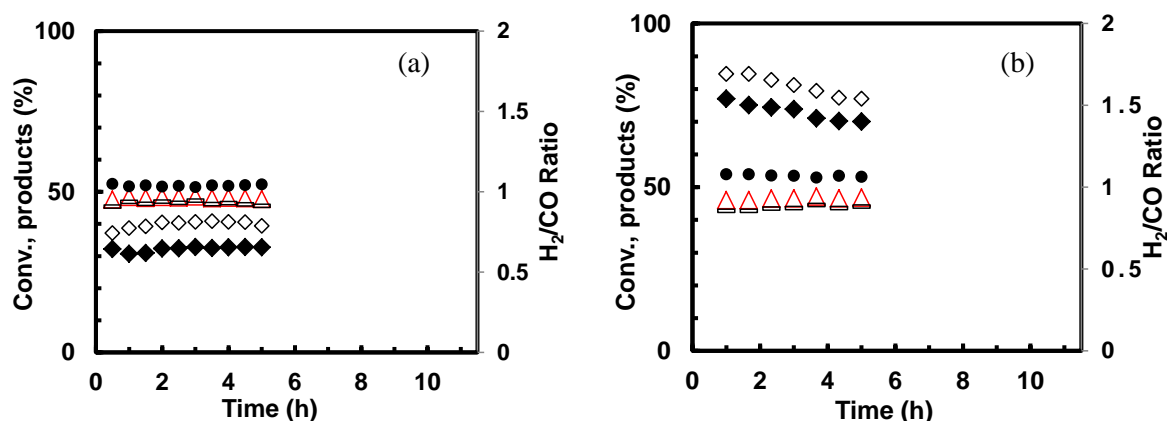


**Fig. 3-29** CH<sub>4</sub> (◆), CO<sub>2</sub> (◇) conversions, H<sub>2</sub> (△), CO (●), in mol % and the H<sub>2</sub>/CO ratio (◻) obtained versus time at 600 °C (a) and 700 °C (b) over the Ni<sub>1</sub>Mg<sub>2</sub>AlO<sub>Y</sub> catalyst (10mg) with pretreatment at 450 °C. CH<sub>4</sub>:CO<sub>2</sub> = 20%:20%.

The most interesting fact at low reaction temperature of 600 °C is that 33% and 39% conversions of CH<sub>4</sub> and CO<sub>2</sub> are obtained with a high selectivity with a H<sub>2</sub>/CO ratio of 0.9, which indicates that the catalysts are notably active towards dry methane reforming at low temperature.

In Dębek's study of Ni-Mg-Al mixed oxides in DRM [93], the measured H<sub>2</sub>/CO ratio values, was well above 1, pointing an excess of H<sub>2</sub> production, and thus, to direct methane decomposition taking place to a significant extent, especially for the catalysts containing the highest amounts of Ni. Similar result was found in study [120] in DRM of Ni-Mg-Al and Ni-Mg-Ce catalysts, with a H<sub>2</sub>/CO ratio between 0.9-1.

Specifically, in the test at 700 °C, the conversions for CH<sub>4</sub> and CO<sub>2</sub> decrease from 78% and 84% to 70% and 77% after 5h of reaction, respectively. And the H<sub>2</sub>/CO molar ratio is 0.88, which is slightly lower than the value obtained at 600 °C, that can be attributed to the simultaneous presence of the reverse water gas shift reaction. This performance can be compared to the one with CeNi<sub>1</sub>O<sub>Y</sub> as both of them have approximately identical content of nickel (22.6 wt.% for CeNi<sub>1</sub>O<sub>Y</sub> and 21.9 wt.% for Ni<sub>1</sub>Mg<sub>2</sub>AlO<sub>Y</sub>). The CH<sub>4</sub> and CO<sub>2</sub> conversions for the former are 56% and 67%, respectively, which are lower than the values obtained for Ni<sub>1</sub>Mg<sub>2</sub>AlO<sub>Y</sub>. Carbon deposition is observed after the test, and it is measured as the carbon formation rate of 0.20 g g<sub>cat</sub><sup>-1</sup> h<sup>-1</sup> at 600 °C and 0.13 g g<sub>cat</sub><sup>-1</sup> h<sup>-1</sup> at 700 °C. This

value is lower than that obtained on  $\text{CeNi}_x\text{O}_y$  catalysts. Depending on literature [106][184], Ni-Mg-Al catalysts were efficient in reducing carbon deposition which could be related to the basic environment.

As the thermodynamic equilibrium is not reached in such conditions,  $\text{CH}_4$  and  $\text{CO}_2$  conversions can be improved by increasing Ni content. Therefore,  $\text{Ni}_3\text{Mg}_2\text{AlO}_y$  catalyst, which corresponds to 44 wt.% of nickel, is applied to the same tests. As shown in **Fig. 3-30**, compared with the results for  $\text{Ni}_1\text{Mg}_2\text{AlO}_y$ , higher conversion is obtained at a low temperature of 600 °C in this case. However, conversions are not stable due to higher amount of carbon formed. The details are assessed in

Table 3-4. At 700 °C, the two catalysts show similar conversions. It seems that adding higher amount of Ni has no significant influence on the activity toward DRM, but leads to much higher carbon formation.

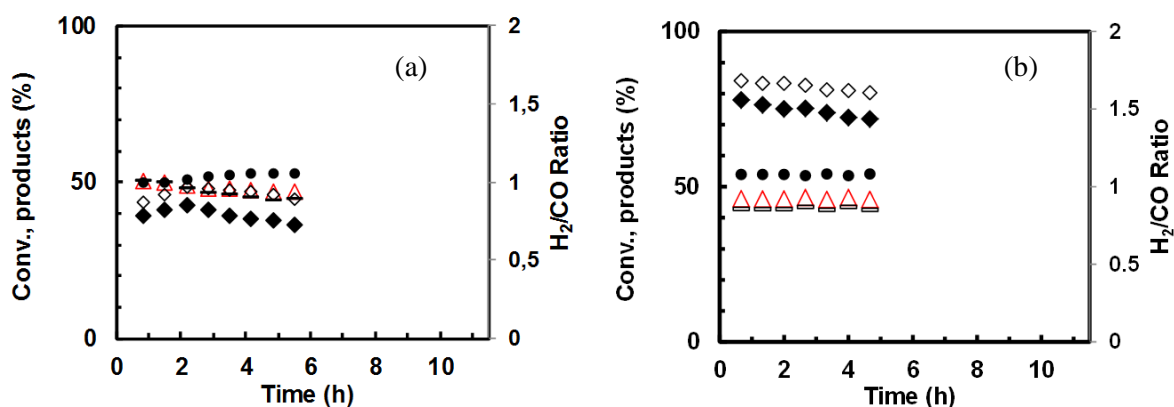


**Fig. 3-30**  $\text{CH}_4$  ( $\blacklozenge$ ),  $\text{CO}_2$  ( $\diamond$ ) conversions,  $\text{H}_2$  ( $\triangle$ ),  $\text{CO}$  ( $\bullet$ ), in mol % and the  $\text{H}_2/\text{CO}$  ratio ( $\square$ ) obtained versus time at 600 °C (a) and 700 °C (b) over the  $\text{Ni}_3\text{Mg}_2\text{AlO}_y$  catalyst (10 mg) with pretreatment in  $\text{H}_2$  at 450 °C,  $\text{CH}_4:\text{CO}_2 = 20:20\%$ .

**Table 3-4** DRM on  $\text{Ni}_x\text{Mg}_2\text{AlO}_y$  catalysts pretreated in  $\text{H}_2$  at 450 °C (5 h,  $\text{CH}_4:\text{CO}_2 = 20:20\%$ )

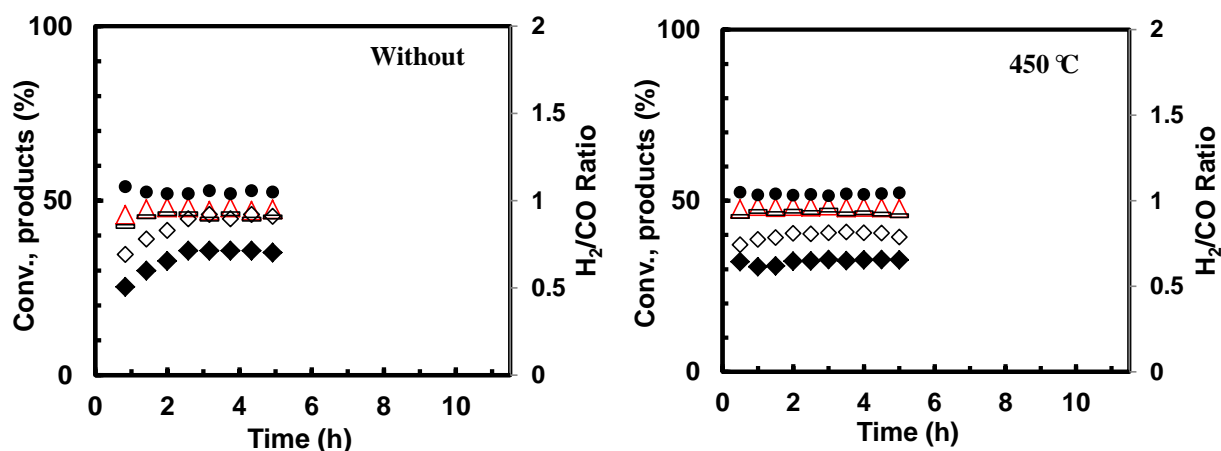
Catalysts	Reaction (°C)	$\text{CH}_4$ conv. (%)	$\text{CO}_2$ conv. (%)	$\text{H}_2/\text{CO}$ ratio	Carbon formation rate ( $\text{g g}_{\text{cat}}^{-1} \text{h}^{-1}$ )
$\text{Ni}_1\text{Mg}_2\text{AlO}_y$	600	33	39	0.90	0.20
$\text{Ni}_3\text{Mg}_2\text{AlO}_y$	600	40	46	0.95	2.25
$\text{Ni}_1\text{Mg}_2\text{AlO}_y$	700	70	77	0.88	0.13
$\text{Ni}_3\text{Mg}_2\text{AlO}_y$	700	72	80	0.82	1.72

### 3.3.2 Influence of pretreatment in $\text{H}_2$

Influence of pretreatment of Ni-Mg-Al catalysts was widely studied in the literature, a higher pretreatment temperature between 700-800 °C is commonly employed to reduce these compounds

[120][84]. Some catalyst was even pretreated at 900 °C to get high performance [185]. However, in our previous study of DRM on Ce-Ni-(Al) based catalysts, higher pretreatment temperature leads to bigger amount of solid carbon. The pretreatment temperature in H<sub>2</sub> ( $T_T$ ) of Ni<sub>x</sub>Mg<sub>2</sub>AlO<sub>y</sub> catalysts in steam reforming of ethanol has been studied in the laboratory [143]. It has been shown that when increasing  $T_T$  an increase of the conversion can be obtained up to an optimum. However, carbon formation increases also, therefore, a good compromise could be obtained for a  $T_T$  in H<sub>2</sub> at 450 °C. As shown by H<sub>2</sub>-TPR, the reductive properties of the Ni<sub>x</sub>Mg<sub>2</sub>AlO<sub>y</sub> mixed oxides can be modified by the Ni content. On the other hand, the catalyst could be activated at the beginning of the experiment under the 20% concentration of the reactants at 600 °C (Fig. 3-31). In order to achieve acceptable catalytic activities and stabilities, it is important to employ a beneficial pretreatment method depending on different catalysts.

In this part, three different tests including without pretreatment in H<sub>2</sub> and the treatment temperatures of 450 °C and 550 °C, respectively, are studied on Ni<sub>1</sub>Mg<sub>2</sub>AlO<sub>y</sub> in DRM at 600 °C. The activity and H<sub>2</sub>/CO ratio versus time on stream are shown in Fig. 3-31. In the test without pretreatment, conversions for methane and CO<sub>2</sub> are increased by 10% in the first 3h on stream, then reach 35% and 46%, respectively after 5h. Besides, the carbon formation rate of 0.32 g g<sub>cat</sub><sup>-1</sup> h<sup>-1</sup> is highest compared with other pretreatment temperatures (450 °C, 0.19 g g<sub>cat</sub><sup>-1</sup> h<sup>-1</sup>). On the other hand, by using high treatment temperature, even 2% lower conversions is obtained at  $T_T = 550$  °C. Also the H<sub>2</sub>/CO ratio declines to 0.82 from 0.90. Clearly, on this compound the pretreatment in H<sub>2</sub> has a beneficial effect, and in particular for a  $T_T$  at 450 °C allows high stable conversion with limited carbon formation.



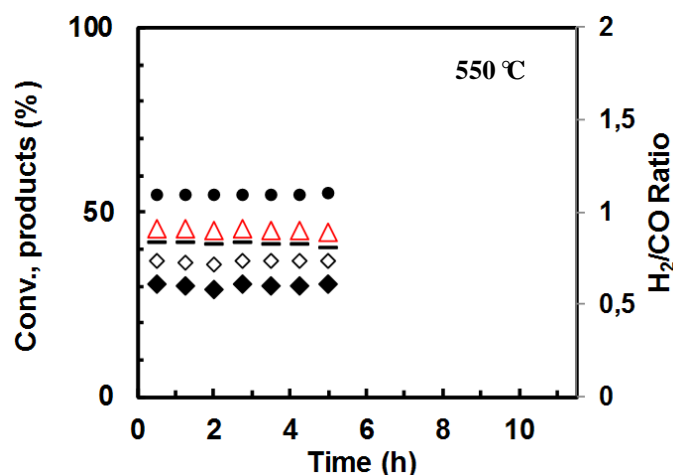


**Fig. 3-31** DRM on Ni<sub>1</sub>Mg<sub>2</sub>AlO<sub>Y</sub> catalyst (10 mg) a) without pretreatment and with pretreatment in H<sub>2</sub> at b) 450 °C and c) 550 °C. CH<sub>4</sub> (◆), CO<sub>2</sub> (◇) conversions, H<sub>2</sub> (△), CO (●), in mol % and the H<sub>2</sub>/CO ratio (□) obtained versus time at 600 °C. CH<sub>4</sub>:CO<sub>2</sub> = 20:20%.

**Fig. 3-32** (a) and (b) show the methane and CO<sub>2</sub> conversions, together with the H<sub>2</sub>/CO ratio measured during the DRM experiments over Ni<sub>3</sub>Mg<sub>2</sub>AlO<sub>Y</sub> catalyst at 600 °C. From the TPR results, the reduction temperature is clearly associated with the Ni content of the catalyst, the peaks shift toward lower temperatures with increasing Ni content, meaning that the catalyst with higher Ni content is easier to reduce. Nevertheless, the Ni<sub>3</sub>Mg<sub>2</sub>AlO<sub>Y</sub> catalyst pretreated in H<sub>2</sub> at 450 °C behaves similarly to the catalyst without pretreatment. Both CH<sub>4</sub> and CO<sub>2</sub> conversions reach similar values, 36%-38% for CH<sub>4</sub> conversion and 44-46% for CO<sub>2</sub> conversion. However, there is a different evolution of H<sub>2</sub>/CO ratio during the first 3h. The higher fluctuation of conversions and H<sub>2</sub>/CO ratios in the condition of non-pretreated catalyst could be attributed to the activation period in stream of reactants. A high H<sub>2</sub>/CO ratio value of 0.90 is obtained after 5h of stabilization in both tests. This high H<sub>2</sub>/CO ratio (close to 1) shows a notable selectivity of the Ni<sub>3</sub>Mg<sub>2</sub>AlO<sub>Y</sub> catalyst towards dry methane reforming at low temperature. In Radosław's study [185], they also found the similar behavior of the hydrotalcite catalyst with 25% of Ni content in DRM at 550 °C : the H<sub>2</sub>/CO ratio was maintaining around 1.

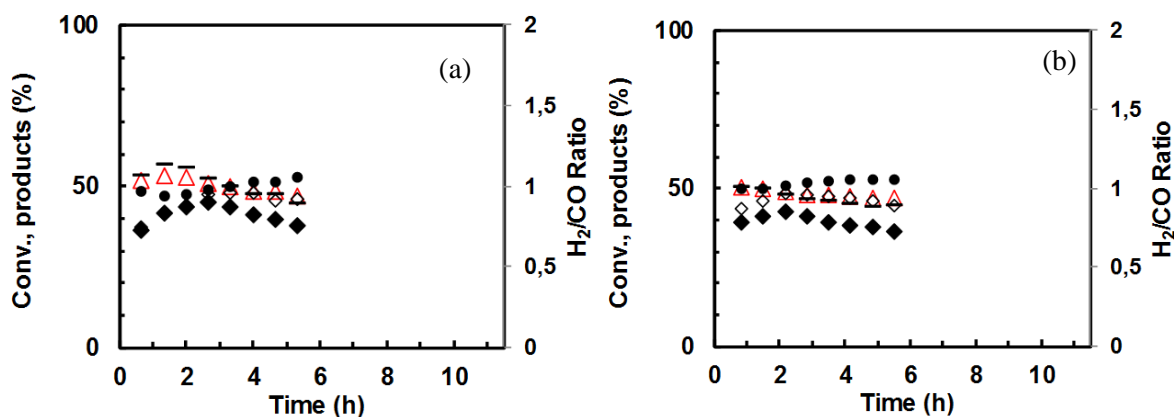


**Fig. 3-32** Catalytic test results over the  $\text{Ni}_3\text{Mg}_2\text{AlO}_Y$  catalyst (10mg) (a) without pretreatment (b) pretreated at 450 °C.  $\text{CH}_4$  (◆),  $\text{CO}_2$  (◇) conversions,  $\text{H}_2$  (△),  $\text{CO}$  (●), in mol % and the  $\text{H}_2/\text{CO}$  ratio (◻) obtained at 600 °C.  $\text{CH}_4:\text{CO}_2 = 20:20\%$ .

Fixing the pretreatment temperature in  $\text{H}_2$  at 450 °C leads to that the compounds are only partially reduced. For all the nano-oxides a  $T_T$  at 450 °C corresponds to a temperature before the TPR peak, avoiding too deep reduction of the solids. Besides, as the TPR peak presents a shift, the compounds are not reduced to the same extent. Ultimately, pretreatment at 450 °C could provide the best performance to  $\text{Ni}_X\text{Mg}_2\text{AlO}_Y$  catalysts due to the comprehensive consideration of activity to  $\text{CH}_4$  and  $\text{CO}_2$ , as well as the carbon formation rate.

### 3.3.1 Catalytic performance in harsh conditions

In this first approach, this series of catalyst indicates a remarkable activity and high selectivity. It is also important to identify the catalytic performance under a harsh condition of  $\text{CH}_4:\text{CO}_2$  ratio of (50%:50%). In order to avoid the thermodynamic limit influence at this condition, 10mg of catalyst was employed in each test.

**Fig. 3-33** shows the results obtained over  $\text{Ni}_X\text{Mg}_2\text{AlO}_Y$  catalysts in harsh conditions after a pretreatment in  $\text{H}_2$  at 450 °C. At 600 °C, 30% and 41% conversions of  $\text{CH}_4$  and  $\text{CO}_2$  respectively are observed on  $\text{Ni}_1\text{Mg}_2\text{AlO}_Y$  catalyst with a  $\text{H}_2/\text{CO}$  ratio of 0.76. Besides, the result evidences the stability of the test along the 5h experiment without showing any kind of deactivation during this period. For such conditions, the products distribution and the conversions of  $\text{CH}_4$  and  $\text{CO}_2$  along the 5h of experiment are shown in **Table 3-5**.

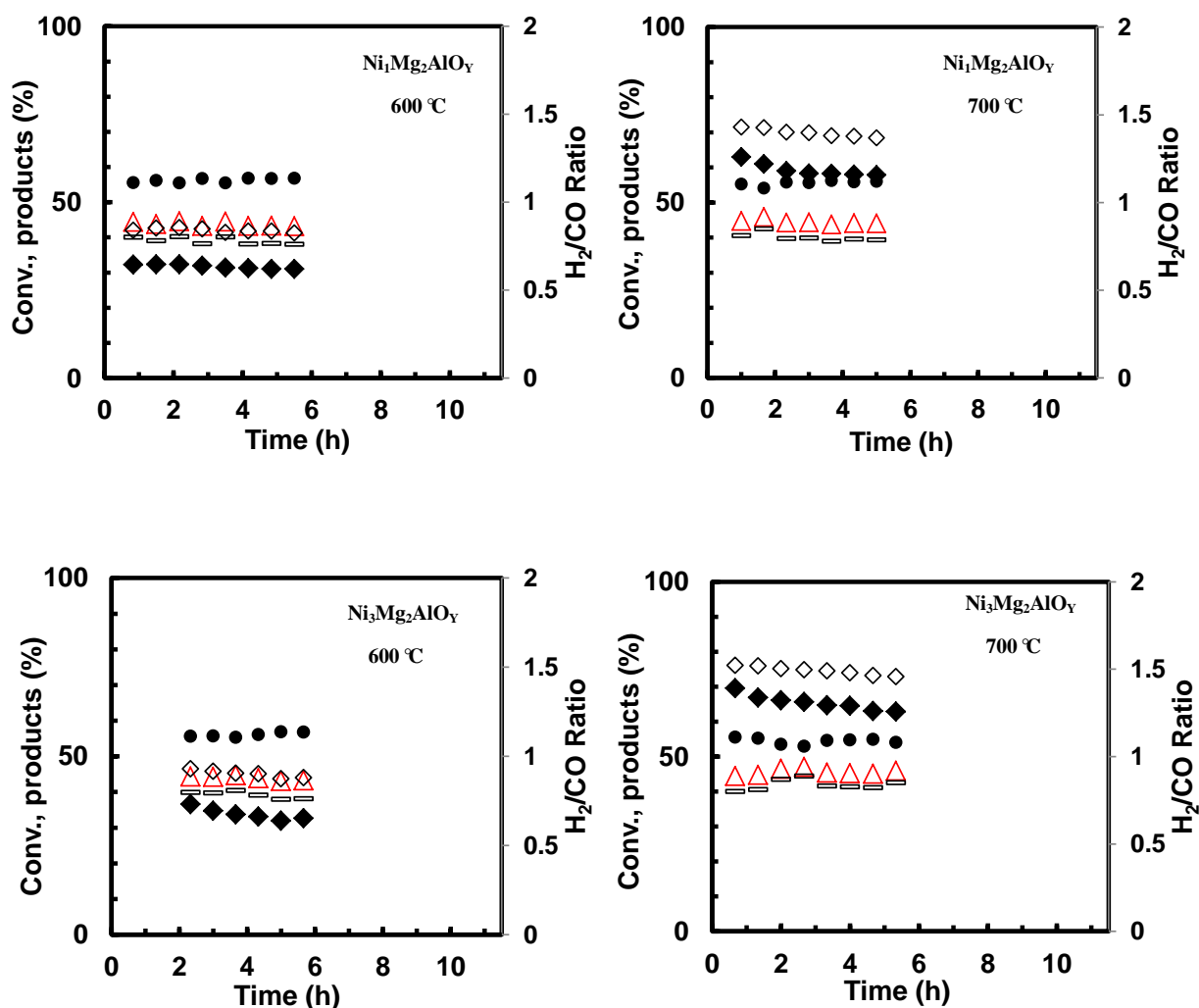


**Fig. 3-33** CH<sub>4</sub> (◆), CO<sub>2</sub> (◇) conversions, H<sub>2</sub> (Δ), CO (●), in mol % and the H<sub>2</sub>/CO ratio (◻) obtained versus time over the Ni<sub>x</sub>Mg<sub>2</sub>AlO<sub>Y</sub> catalyst (10 mg) pretreated in H<sub>2</sub> at 450 °C, CH<sub>4</sub>:CO<sub>2</sub> = 50:50%.

**Table 3-5** Catalytic activity (5 h, CH<sub>4</sub>:CO<sub>2</sub> = 50:50%) of catalysts submitted to different conditions.

Catalysts	Reaction (°C)	CH <sub>4</sub> conv. (%)	CO <sub>2</sub> conv. (%)	H <sub>2</sub> /CO ratio	Carbon formation rate (g g <sub>cat</sub> <sup>-1</sup> h <sup>-1</sup> )
Ni <sub>1</sub> Mg <sub>2</sub> AlO <sub>Y</sub>	600	30	41	0.76	0.25
Ni <sub>3</sub> Mg <sub>2</sub> AlO <sub>Y</sub>	600	32	44	0.78	2.51
Ni <sub>1</sub> Mg <sub>2</sub> AlO <sub>Y</sub>	700	58	68	0.85	0.18
Ni <sub>3</sub> Mg <sub>2</sub> AlO <sub>Y</sub>	700	63	73	0.80	1.37

Besides, as shown in **Fig. 3-34**, another test is carried out at 600 °C over Ni<sub>12</sub>Mg<sub>2</sub>AlO<sub>Y</sub> catalyst in CH<sub>4</sub>:CO<sub>2</sub> = 50%:50% reaction mixture. The CH<sub>4</sub> conversion quickly declines from 48% to 42% in 2h and this value is higher than the equilibrium limits (41% for CH<sub>4</sub> conversion), meaning there are other

side reactions occurring. While the  $\text{CO}_2$  conversion curve almost overlapped with that of  $\text{CH}_4$  at  $\sim 42\%$  during 2h of the test. Therefore, the results demonstrate that higher Ni content promotes the decomposition of  $\text{CH}_4$ . In addition, the conversions and  $\text{H}_2/\text{CO}$  ratios versus  $\text{Ni}/\text{M}_T$  is summarized in **Fig. 3-35**.  $\text{CH}_4$  conversion globally increases with Ni content, as well as the  $\text{H}_2/\text{CO}$  ratio, while the  $\text{CO}_2$  conversion declines when increasing the  $\text{Ni}/\text{M}_T$  ratio to 0.80. Moreover, the carbon formation rate on different catalysts is shown in **Fig. 3-36**. For  $\text{Ni}_1\text{Mg}_2\text{AlO}_Y$ , the carbon production rate is estimated at  $0.25 \text{ g g}_{\text{cat}}^{-1} \text{ h}^{-1}$ . However, the carbon formation at  $600 \text{ }^\circ\text{C}$  is largely increased to  $2.5 \text{ g g}_{\text{cat}}^{-1} \text{ h}^{-1}$  for  $\text{Ni}_3\text{Mg}_2\text{AlO}_Y$  and  $4.88 \text{ g g}_{\text{cat}}^{-1} \text{ h}^{-1}$  for  $\text{Ni}_{12}\text{Mg}_2\text{AlO}_Y$ . The carbon starts to grow fast on  $\text{Ni}_3\text{Mg}_2\text{AlO}_Y$  catalyst, which contains 43.7% wt% of Ni. Excessive carbon accumulation on  $\text{Ni}_{12}\text{Mg}_2\text{AlO}_Y$  results in the pressure increase and the reactor blockage. So the test is not able to continue after 2h time on stream. In such a case, Ni content clearly influences the carbon formation rate and the type of carbon formed, and it also depends on the reactant concentrations. Consequently,  $\text{H}_2/\text{CO}$  ratio as well as carbon formation could be considered as optimum on  $\text{Ni}_1\text{Mg}_2\text{AlO}_Y$  catalyst.

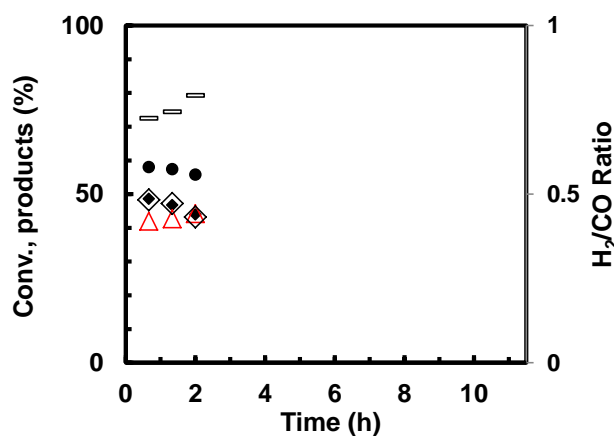


**Fig. 3-34**  $\text{CH}_4$  (◆),  $\text{CO}_2$  (◇) conversions,  $\text{H}_2$  (△),  $\text{CO}$  (●), in mol % and the  $\text{H}_2/\text{CO}$  ratio (□) obtained versus time at  $600 \text{ }^\circ\text{C}$  over the  $\text{Ni}_{12}\text{Mg}_2\text{AlO}_Y$  catalyst (10 mg) pretreated in  $\text{H}_2$  at  $450 \text{ }^\circ\text{C}$ .  $\text{CH}_4:\text{CO}_2 = 50:50\%$ .

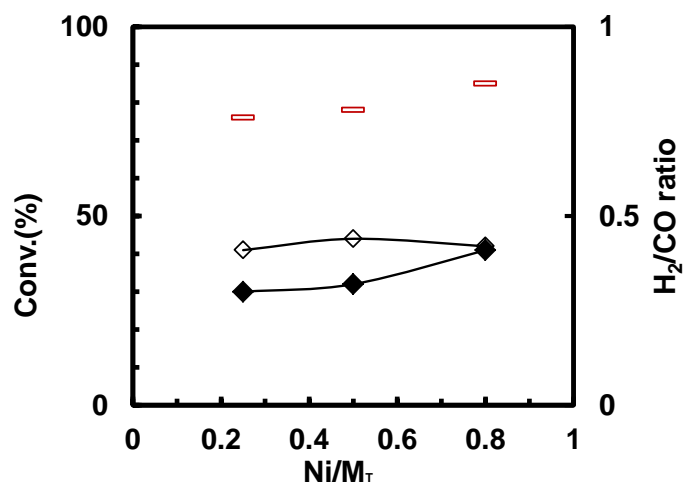


Fig. 3-35 CH<sub>4</sub> (◆), CO<sub>2</sub> (◇) conversions and the H<sub>2</sub>/CO ratio (◻) obtained versus Ni/M<sub>T</sub> ratio at 600 °C over the Ni<sub>x</sub>Mg<sub>2</sub>AlO<sub>y</sub> catalyst (10 mg) with pretreatment at 450 °C. CH<sub>4</sub>:CO<sub>2</sub> = 50%:50%.

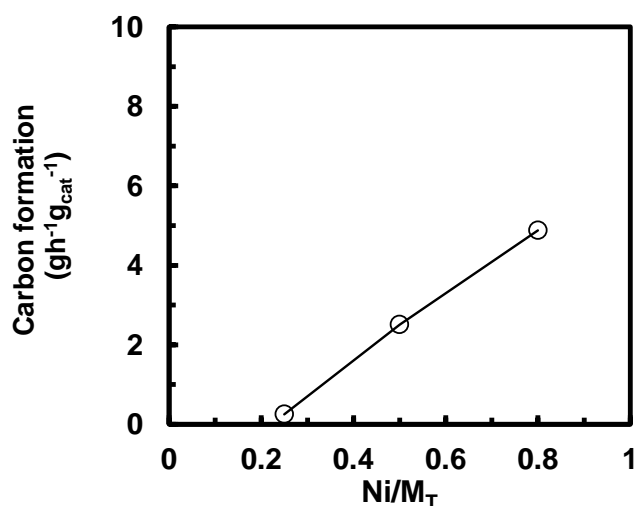


Fig. 3-36 The carbon formation rate versus Ni/M<sub>T</sub> ratio at 600 °C over the Ni<sub>x</sub>Mg<sub>2</sub>AlO<sub>y</sub> catalyst (10 mg) with pretreatment at 450 °C. CH<sub>4</sub>:CO<sub>2</sub> = 50%:50%.

### 3.3.2 Stability test

The objective of the stability tests is to explore the catalyst stability and process sustainability issues at the conditions favorable to avoid carbon formation. The Ni<sub>1</sub>Mg<sub>2</sub>AlO<sub>y</sub> sample, which shows the lowest amount of carbon deposits after 5h DRM catalytic test is chosen for stability tests carried out at 700 °C. The results obtained over 50 mg of catalyst are gathered in Fig. 3-37. The activity and stability of the Ni<sub>1</sub>Mg<sub>2</sub>AlO<sub>y</sub> catalyst is examined for a period of about 50h on stream. Stable conversions of 67%

and 76% for CH<sub>4</sub> and CO<sub>2</sub> are achieved after 50h of test. Furthermore, the conversions of methane and carbon dioxide are high and close to the equilibrium values in this condition (72% and 82% for CH<sub>4</sub> and CO<sub>2</sub> conversions). It can also be seen that there is a slight deactivation in about first 10h on stream and visible carbon deposition was formed after test. The H<sub>2</sub>/CO ratio is around 0.84 and carbon formation rate is of 0.04 g g<sub>cat</sub><sup>-1</sup> h<sup>-1</sup>.

In a recent literature, Xingyi et al. [186] studied Ni–Mg–Al with 18 wt.% of Ni in DRM at 700 °C. 50 mg of catalyst were tested in condition of 25% of CH<sub>4</sub> and CO<sub>2</sub> in a ratio of 1, GHSV= 60,000 mL g<sup>-1</sup> h<sup>-1</sup>. 86% and 91 % of conversion for CH<sub>4</sub> and CO<sub>2</sub> were obtained after 30h of test, the H<sub>2</sub>/CO ratio was 0.85. Although the values are higher than that in this study, the condition employed in our test is much more severe (pure reactants and higher flow value of 96,000 mL g<sup>-1</sup> h<sup>-1</sup>).

A continuous decline is found in both CH<sub>4</sub> and CO<sub>2</sub> conversion with time, the possible reason for such deactivation could be the loss of active phase area due to sintering of metal particles or carbonaceous deposits leading to a blocking of the surface sites. In fact, very less loss of activity is observed after 40 h on stream indicating that stabilization is obtained after a long time on stream and part of this carbon is not poisonous. Literature indicating that carbon can play a role as a reaction intermediate and favour close contact, and acts as CH<sub>x</sub> collector and prevents carbon species residence on the surface, what can limit deactivation process despite the significant amount of carbon deposit [167].

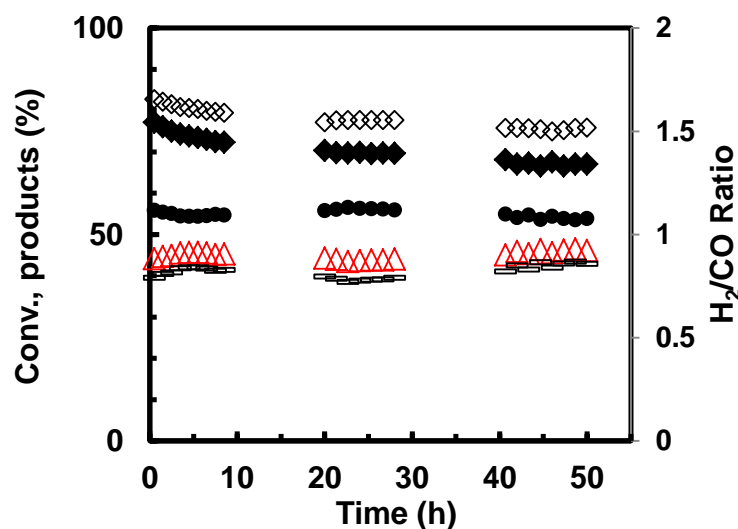


**Fig. 3-37** Catalytic stability at 700 °C for 50 h on Ni<sub>1</sub>Mg<sub>2</sub>AlO<sub>y</sub> catalyst (50 mg) pretreated in H<sub>2</sub> at 450 °C. CH<sub>4</sub> (◆), CO<sub>2</sub> (◇) conversions, H<sub>2</sub> (△), CO (●), in mol % and the H<sub>2</sub>/CO ratio (□), CH<sub>4</sub>:CO<sub>2</sub>=50%:50%.

In order to investigate the characteristic of the carbon species, O<sub>2</sub>-TPO test was performed on the spent Ni<sub>1</sub>Mg<sub>2</sub>AlO<sub>Y</sub> catalyst. In the literature, the types of carbonaceous species can be identified by the numbers and position of TPO peaks related to different reactivity towards oxidation. **Fig. 3-38** shows only one main peak located at 665 °C. This peak is probably associated with the oxidation of the filamentous carbon [48]. It is widely reported that the single broad peak at around 600 °C is ascribed to more graphitic carbon that is more stable and oxidizes at higher temperatures. Usually, the temperature of oxidation of graphitic carbon is about 725 °C in the condition without Ni. It has been suggested that Ni-based catalysts are active for the oxidation of carbon species, and the oxidation temperature of the carbon species can be affected by the nature of both carbon and catalyst, as well as the interaction between the carbon and the Ni particles.

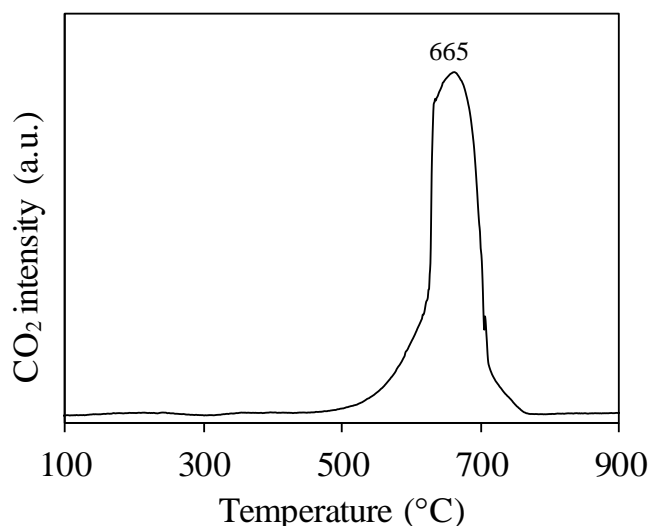


**Fig. 3-38** TPO profiles of the Ni<sub>1</sub>Mg<sub>2</sub>AlO<sub>Y</sub> catalyst after long test at 700 °C in harsh conditions (CH<sub>4</sub>:CO<sub>2</sub>=50%:50%).

### 3.3.3 Conclusion for Ni<sub>x</sub>Mg<sub>2</sub>AlO<sub>Y</sub> in DRM

The well dispersed Ni<sub>x</sub>Mg<sub>2</sub>AlO<sub>Y</sub> catalysts demonstrate high efficiency toward DRM at 600 °C and 700 °C, the influence of pretreatment temperature and reactant concentrations have been studied.

Treatment temperature in H<sub>2</sub> at 450 °C or 550 °C has a slight influence on activity results in stabilized state. However, there is a different evolution of conversions and H<sub>2</sub>/CO ratio at first period of

time on stream. Moreover, absence of pretreatment leads to an increase of the carbon formation.  $\text{Ni}_1\text{Mg}_2\text{AlO}_Y$  allows the best catalytic results for the dry reforming of methane at the low temperature of 600 °C with 10mg of catalyst, 33% and 39% conversions of  $\text{CH}_4$  and  $\text{CO}_2$  are obtained with a high selectivity with a  $\text{H}_2/\text{CO}$  ratio of 0.9. The carbon formation rate is  $0.2 \text{ g g}_{\text{cat}}^{-1} \text{ h}^{-1}$ .

In harsh conditions (50%-50%), the catalyst still have the best performance with low carbon formation as 30% of  $\text{CH}_4$  conversion and 41% of  $\text{CO}_2$  conversion are obtained. However, the  $\text{H}_2/\text{CO}$  ratio value of 0.76 is lower than that in diluted conditions (0.90). In addition,  $\text{Ni}_1\text{Mg}_2\text{AlO}_Y$  allows the 50h test at 700 °C working with pure  $\text{CH}_4$  and  $\text{CO}_2$  and shows a remarkable stability along the whole experiment. The  $\text{Ni}_{12}\text{Mg}_2\text{AlO}_Y$  catalyst allows higher catalytic activity at initial period, but strong carbon formation leads to a deactivation and a blockage in only 2h of test. The improvement of catalytic activity and stability of the  $\text{Ni}_x\text{Mg}_2\text{AlO}_Y$  ex-hydrotalcite catalysts is attributed to the presence in these compounds of very strong interactions between Ni species and Mg and/or Al cations either in Ni-Mg-(Al)-O solid solution and/or at the interfaces between small nanoparticles of NiO, MgO and/or Ni-Mg-(Al)-O.

### 3.4 Dry reforming over $\text{Ni}_x/\text{SBA-15}$ catalysts

Considering that maintaining a small nickel particle size is a major determining factor for the activity and stability of a catalyst, a good strategy for synthesis is to largely disperse small amounts of nickel over a high surface area support to produce nanoparticles which are stable against sintering. In methane reforming studies, SBA-15 displays relevant textural properties as a host support. Thus, the high specific surface area, uniform two-dimensional hexagonal pore arrangements and narrow pore size distribution with large pore size (typically in the range of 5-30 nm) and thick walls (in the range of 3.1-6.4 nm) [187] make SBA-15 a promising support to obtain catalyst with high metal dispersion and uniform particles diameter.

However, to the best of our knowledge, research on the effect of different operating conditions such as wide Ni content on Ni/SBA-15 catalyst for DRM reaction is very limited in the literature. In this part of work, the reaction was carried out under atmospheric pressure at varying  $\text{CH}_4\text{-CO}_2$  volume ratios of 20%:20% to 50:50%. The influence of Ni content and pretreatment approach on catalytic performances

and stability at low temperature (600-700°C) are studied on Ni-based SBA-15 catalysts.

### 3.4.1 Influence of pretreatment

The effect of pretreatment in H<sub>2</sub> at different temperatures is studied over Ni<sub>20%</sub>/SBA-15 and Ni<sub>40%</sub>/SBA-15. Pretreatment is generally conducted at a high temperature around 700 °C in the literature [121] on this type of catalysts. The catalytic performance toward DRM is investigated under stream (CH<sub>4</sub>:CO<sub>2</sub>= 20%:20%) over 5 h at 600 °C and 700 °C. The CH<sub>4</sub> and CO<sub>2</sub> conversions curves, as well as the values of H<sub>2</sub>/CO ratio as a function of pretreatment temperature during the methane dry reforming experiments, is shown in **Fig. 3-39**. The pretreatment temperature of zero corresponds to without reduction prior to the test. In this study, depending on the TPR result for each catalyst, the pretreatment temperatures of 600 °C and 650 °C are studied on Ni<sub>20%</sub>/SBA-15, while Ni<sub>40%</sub>/SBA-15 is studied at pretreatment temperature of 600 °C and 700 °C. For the Ni<sub>20%</sub>/SBA-15, increase of pretreatment temperature to 650 °C leads to a slight increase in activity. However, for Ni<sub>40%</sub>/SBA-15, the growth of the pretreatment temperature leads to a small decrease on both of CH<sub>4</sub> and CO<sub>2</sub> conversions in the test at 600 °C. Minimal amount of carbon seems to be formed in all cases (observed from the darkness of the spent catalysts). A mass of carbon formed could only be measured in the case of Ni<sub>40%</sub>/SBA-15 without pretreatment. This is in agreement with the previous study on Ce-Ni based catalysts, showing that direct reduction of the catalyst under reaction reactants probably promotes a structure of the nickel particles that increase the carbon deposition rate [164]. In another words, increased pretreatment temperature leads benefit to Ni<sub>20%</sub>/SBA-15 while it has a negative effect on Ni<sub>40%</sub>/SBA-15. For higher Ni content catalyst, this is mainly due to the agglomeration of a large amount of Ni particles (larger Ni particles) during the reducing process [188]. Another possible reason is that the dispersion of Ni is not homogeneous which results in blockage of the pores on the support.

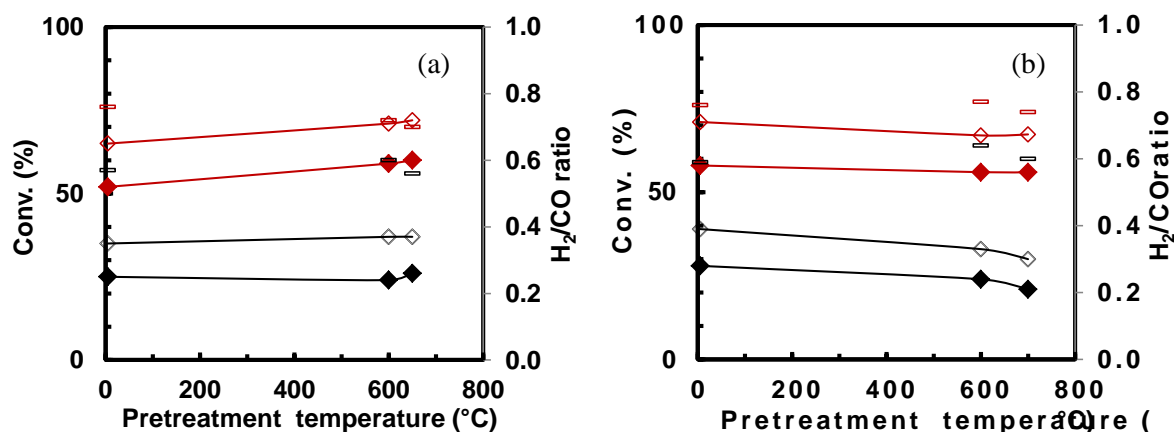


**Fig. 3-39** CH<sub>4</sub> (◆), CO<sub>2</sub> (◇) conversions and the H<sub>2</sub>/CO ratio (◻) at 700 °C (red) and at 600 °C (black) obtained as a function of pretreatment temperature. (a) Ni<sub>20</sub>%/SBA-15, (b) Ni<sub>40</sub>%/SBA-15. (10mg). CH<sub>4</sub>:CO<sub>2</sub> = 20%:20%.

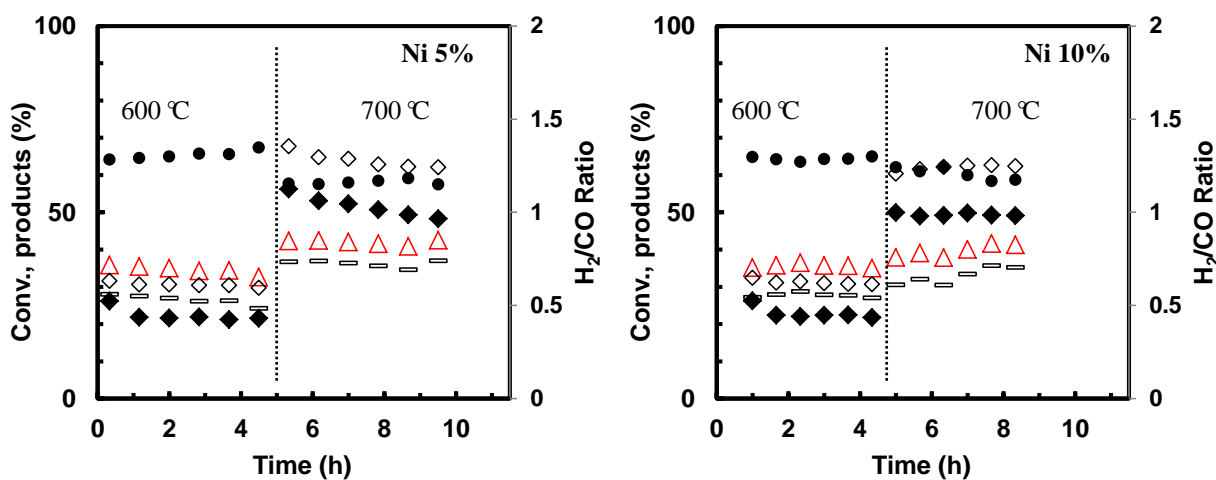
### 3.4.2 Influence of Ni content

The influence of Ni content is studied at 600 and 700 °C in dry reforming reaction. In each test, 10 mg of catalyst without pretreatment is used under flow condition of CH<sub>4</sub>:CO<sub>2</sub> = 20%:20%. The catalytic performances of various Ni content catalysts are shown in **Fig. 3-41**. Both CH<sub>4</sub> and CO<sub>2</sub> conversions slightly increase with increasing Ni content. The catalyst with lower Ni content results in slightly lower catalytic activity compared to the catalyst with higher Ni content, however, improved stability is obtained and better resistance towards deactivation. Therefore, the Ni<sub>40</sub>%/SBA-15 is the most active for CH<sub>4</sub> and CO<sub>2</sub> since 27% and 37% of CH<sub>4</sub> and CO<sub>2</sub> conversions are reached at 600 °C, while 57% and 68% of conversions are obtained at 700 °C.

Compared to literature, Linping et al. [189] studied 6%Ni/SBA-15 catalyst in dry reforming at 600°C, 45 mg of catalyst were used in the test and total flow rate was 15 mL/min, CH<sub>4</sub> and CO<sub>2</sub> cofed in a ratio of 20%: 20%. The catalyst with large surface area and promoted dispersion showed conversion for CH<sub>4</sub> and CO<sub>2</sub> at 28% and 34%, respectively, at 600 °C after 1 h reaction. While 53% of CH<sub>4</sub> conversion and 58% of CO<sub>2</sub> conversion were obtained at 700 °C. The H<sub>2</sub>/CO ratio was about 0.73 at 600 °C and 0.81 at 700 °C. In the present study, similar results are achieved by using harsher conditions (lower mass and higher flow rate). However, the H<sub>2</sub>/CO ratio in our work is lower (~0.6 at 600 °C and ~0.8 at 700 °C), less than unity over the whole catalysts and temperature range tested, especially much lower at low temperatures. It seems that the H<sub>2</sub>/CO ratio is slightly increased with Ni

content, indicating that there is some difference in the selectivity and activity toward RWGS reaction for different Ni content catalysts. In particular, at 600 °C, the correlation between Ni content and H<sub>2</sub>/CO ratio becomes more notable. Consistent with the literature[121] indicating that the low ratio of Ni/CZ in 5% Ni/CZ/SBA-15 led to low H<sub>2</sub>/CO ratio compared with higher Ni content.

The active site number can depend on the amount of Ni in the catalyst and conversions could be notably increased with Ni content. However, the activity is not significantly influenced by the Ni content and is not proportional to it. This may indicate diffusional limitations or, most probably, a number of active sites not proportional to the metal amount, suggesting in turn either a higher accessibility hindrance to the active nanoparticles with nickel enrichment or a decrease of metal dispersion [176]. Similar results were observed by Abdulkader Albarazi et al. [121], who presented the DRM catalytic performances over 5, 10 and 15 wt.% Ni/CZ/SBA-15 samples respectively, with temperature. Among these catalysts, the one with 5 wt.% Ni loading showed a stable increase of CH<sub>4</sub> conversion with temperature without any deactivation. On the contrary, 10 wt.% and 15 wt.% Ni samples had almost identical behavior for CH<sub>4</sub> conversion and they showed, between 600 °C and 630 °C, a constant methane conversion of 60%.



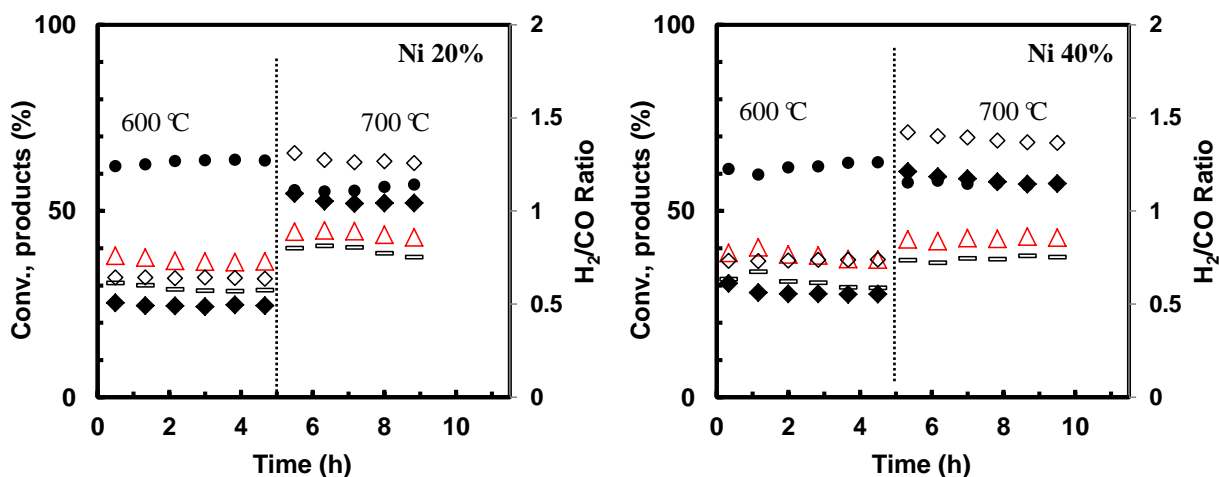


**Fig. 3-40** Catalytic activity in DRM at 600-700 °C on Ni<sub>x</sub>/SBA-15 (10 mg) without pretreatment. CH<sub>4</sub> (◆), CO<sub>2</sub> (◇) conversions, H<sub>2</sub> (△), CO (●), in mol % and the H<sub>2</sub>/CO ratio (◻). CH<sub>4</sub>/CO<sub>2</sub>/N<sub>2</sub> = 20:20:60%.

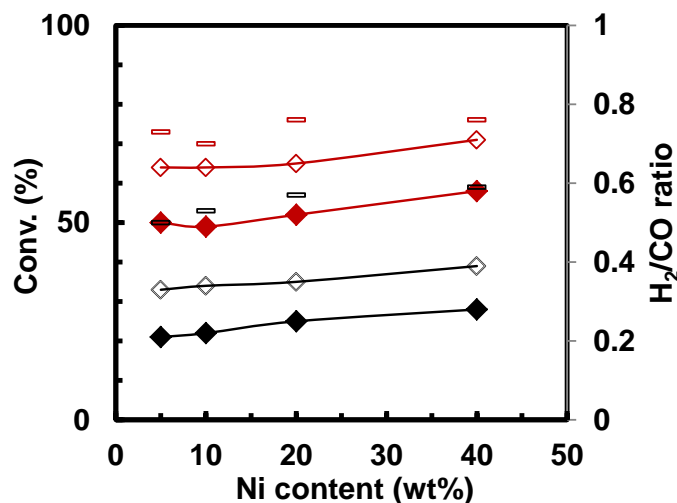


**Fig. 3-41** CH<sub>4</sub> (◆), CO<sub>2</sub> (◇) conversions and the H<sub>2</sub>/CO ratio (◻) at 600 °C (black) and at 700 °C (red) obtained versus Ni loading over the Ni<sub>x</sub>/SBA-15 catalyst (10 mg) without pretreatment. CH<sub>4</sub>:CO<sub>2</sub> = 20%:20%.

During all of the tests, it seems that carbon is formed on the surface of the catalysts, (carbon balance calculated value is over 90%) but for low Ni loading catalyst, the mass of carbon is undetectable by weighing. Only 0.6 mg of carbon production is measured for Ni<sub>40</sub>/SBA-15 after test, the carbon formation rate is of 0.006 g g<sub>cat</sub><sup>-1</sup> h<sup>-1</sup>.

Arcotumapathy et al.[190] found that Ni supported on SBA-15 catalyst exhibited the great resistance towards carbon deposition compared with that on SiO<sub>2</sub> and Al<sub>2</sub>O<sub>3</sub> during methane steam reforming reaction.

As illustrated in **Fig. 3-42**, in the condition of doing the pretreatment at 600 °C, the growth of Ni

loading shows no significant influence on the activity. In fact, it has been shown in **section 3.4.1** that pretreatment at 600 °C has a different effect on the different catalysts. However, the differences of activity among catalysts are quite small. Therefore, it is hard to define the influence of pretreatment. But it is clear from the results that the carbon formation is mitigated by doing a pretreatment. In particular, increasing Ni loading from 20% to 40% has no benefit on activity. This could be due to the agglomeration of Ni particles leading to larger Ni particles during the reducing process [188]. Another possible reason is the dispersion of Ni is not homogeneous which leads to a blockage of the pores of the support. Active component should be kept in an appropriate range, the lower the loading amount, the less active site involved, leading to a low catalytic activity. On the contrary, excess amount of active metal loading facilitate carbon deposition and cause active phase sintering.

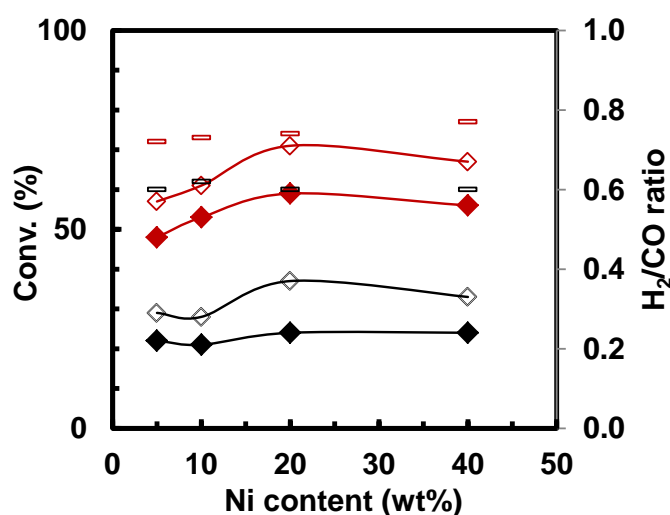


**Fig. 3-42** CH<sub>4</sub> (◆), CO<sub>2</sub> (◇) conversions and the H<sub>2</sub>/CO ratio (◻) at 600 °C (black) and at 700 °C (red) obtained versus Ni loading over the Ni<sub>x</sub>/SBA-15 catalyst (10mg) pretreated in H<sub>2</sub> at 600 °C. CH<sub>4</sub>:CO<sub>2</sub> = 20%:20%.

TEM images were registered for the spent catalyst and representative images are shown in **Fig. 3-44**. It unambiguously confirms the integrity of well-ordered hexagonal mesostructure of SBA-15 for 5% Ni condition. And the Ni species are well dispersed on the surface and the edges. This may be a direct evidence for the existence of the confinement effect of SBA-15, and can also indirectly demonstrate that majorities of Ni particles are distributed inside the pores of SBA-15 [153]. On the other hand, the micrographs outline a clear formation of carbon (nanotubes) for Ni<sub>40</sub>/SBA-15 which can explain the decrease in the stability of the catalyst. For samples at loading lower than 20%, it is

observed that the nano-particles size is not dramatically affected, moreover no carbon can be detected. It should be noticed that the Ni particles still have a good dispersion in the SBA-15 supported structure after the catalytic test. Partial reduction of Ni species in thermally stable PS phases results in well dispersed nanometric Ni particles. Moreover, the remaining unreduced PS structure with surface OH groups serves as better support for Ni<sup>0</sup> nanoparticles and is shown to inhibit the carbon formation, thereby enhancing the catalytic stability [158].

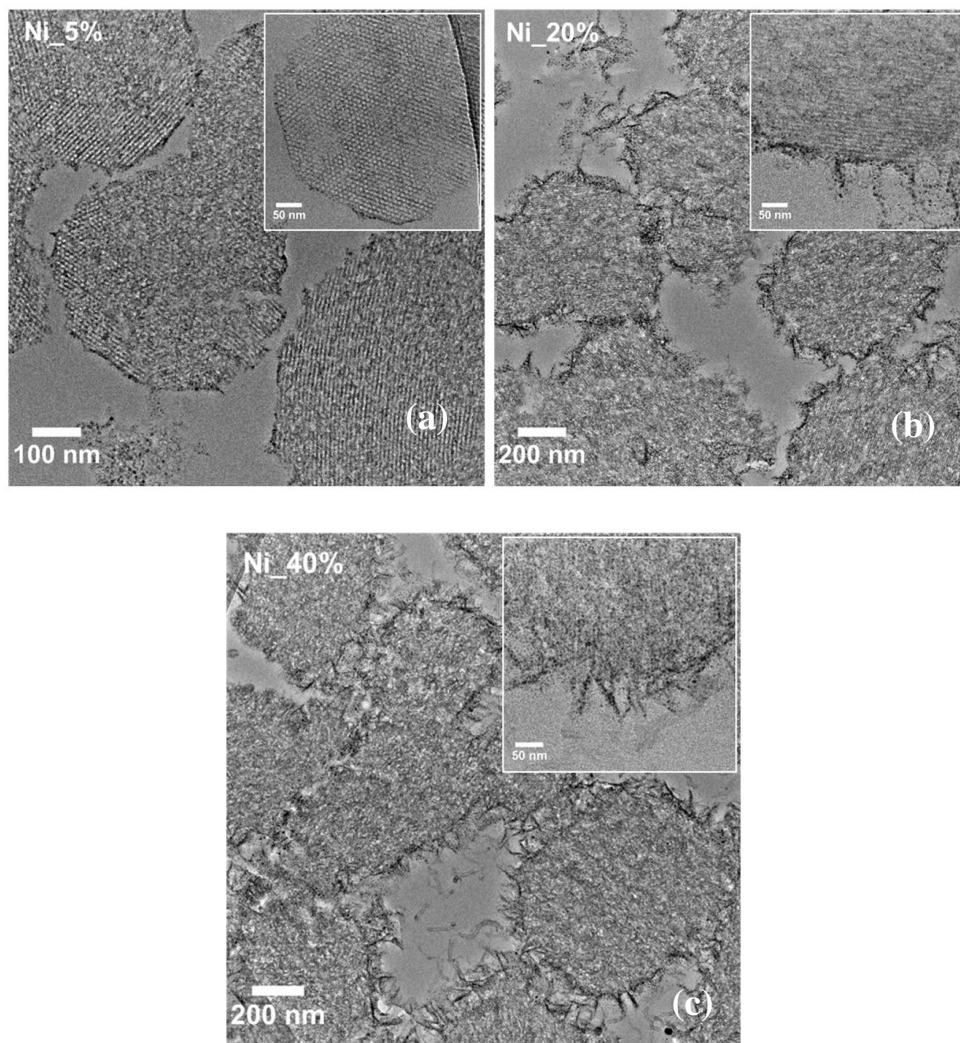


**Fig. 3-43** TEM images collected after catalytic test at 700 °C without pretreatment. CH<sub>4</sub>:CO<sub>2</sub> = 20%:20%. a) Ni\_5%/SBA-15, a) Ni\_20%/SBA-15, a) Ni\_40%/SBA-15.

In order to get higher value to compare with literature, higher mass of Ni<sub>20</sub>/SBA-15 catalyst of 50 mg is employed in DRM reaction. The initial and final CO<sub>2</sub> and CH<sub>4</sub> conversions, as well as the corresponding H<sub>2</sub>/CO ratios after the test at 600 °C and 700 °C are shown in **Fig. 3-44**. The catalyst with

higher mass of 50 mg shows unstable performance. Concretely, the initial conversions of CH<sub>4</sub> and CO<sub>2</sub> are about 46% and 50%, respectively. However, it gradually declines with time, 8% of the activity is lost during the 5h of experiments. The H<sub>2</sub>/CO ratio at 600 °C is not stable at the beginning. Afterward, it is maintained at 0.7 after 5h of stabilization. It seems that increasing the mass of catalyst leads to a deactivation of activity caused by some side reactions which are directly reflected in the obtained higher and unstable values of H<sub>2</sub>/CO ratios. This could be due to the formation of carbon deposited on the surface of catalyst.

At the higher temperature of 700 °C, CH<sub>4</sub> and CO<sub>2</sub> conversions are 69% and 78%, respectively. Only a slight decrease (4%) in the activity is observed during the 5 h of reaction time. This fact can be linked to the particular ability of this catalyst to avoid the direct methane decomposition reaction. The H<sub>2</sub>/CO ratio is about 0.78. 55.3 mg of carbon is formed after 10h of the test, so carbon formation rate is 0.11 g g<sub>cat</sub><sup>-1</sup> h<sup>-1</sup>. The results obtained are competitive with literature on SBA-15 supported catalyst. For example, compared with a recent study of dry reforming in a condition of GHSV = 24 000mL/g<sub>cat</sub> h<sup>-1</sup>, over 150mg of catalyst (10% of Ni supported on SBA-15) conducted by Omoregbe et al. [92], in which the conversions obtained at 650 °C are 48% and 60% for CH<sub>4</sub> and CO<sub>2</sub>, respectively.

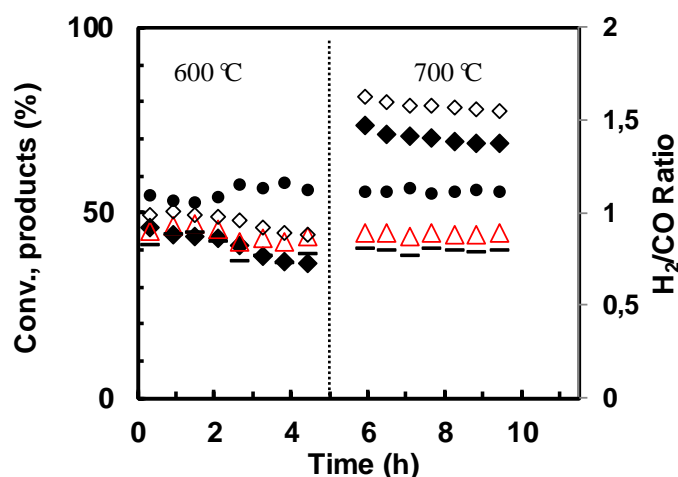
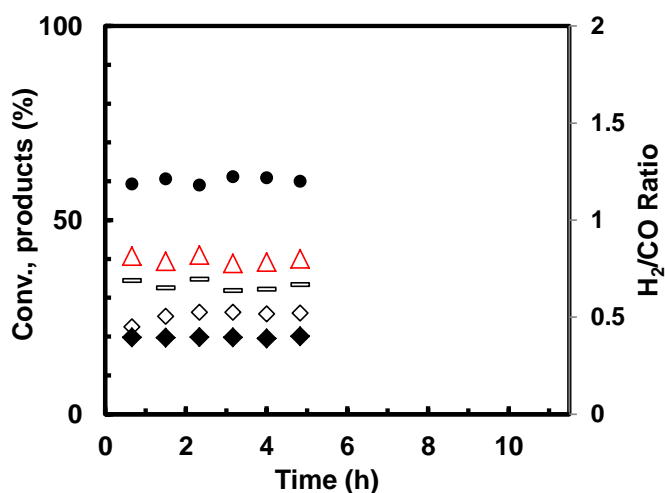


Fig. 3-44 CH<sub>4</sub> (◆), CO<sub>2</sub> (◇) conversions, H<sub>2</sub> (△), CO (●), in mol % and the H<sub>2</sub>/CO ratio (≡) obtained at 600 °C and 700 °C over the Ni<sub>20</sub>/SBA-15 catalyst (50 mg) without pretreatment. CH<sub>4</sub>:CO<sub>2</sub> = 20%:20%.

### 3.4.3 Catalytic performance in harsh condition

The best catalyst in this series Ni<sub>20</sub>/SBA-15 is tested at 600 °C in DRM with pure feed gas compositions 50%:50%. 10 mg of catalyst is pretreated in H<sub>2</sub> at 600 °C prior to reaction. The result of

this test is summarized in **Fig. 3-45**. The catalyst shows stable level of CH<sub>4</sub> and CO<sub>2</sub> conversions equal to 21 and 26%, respectively, and H<sub>2</sub>/CO ratios is around 0.66. In harsh condition, the conversion values are lower than that in 20% reactant concentration condition and a carbon formation rate of 0.08 g g<sub>cat</sub><sup>-1</sup> h<sup>-1</sup> can be calculated by weighing the spent catalyst. On another hand, the catalyst is notably active towards DRM and did not exhibit any significant evidence of deactivation.



**Fig. 3-45** CH<sub>4</sub> (◆), CO<sub>2</sub> (◇) conversions, H<sub>2</sub> (△), CO (●), in mol % and the H<sub>2</sub>/CO ratio (□) obtained versus Ni loading at 600 °C over the Ni<sub>20%</sub>/SBA-15 catalyst (10mg) with pretreatment at 600 °C. CH<sub>4</sub>:CO<sub>2</sub> =50%:50%.

### 3.4.4 Conclusion for Ni<sub>x</sub>/SBA-15 in DRM

Ni<sub>x</sub>/SBA-15 catalysts with wide range of Ni loading ( $x = 5, 10, 20$  and  $40$ ) have been tested in DRM. The influence of different parameters was studied, such as reduction temperature, Ni loading and reaction temperature. Moreover, the catalysts were characterized before and after test to find correlations between catalytic activity and physicochemical properties.

The conversions measured during DRM at relatively low temperatures between 600 °C and 700 °C did not depend strongly on Ni- loading. Increasing the pretreatment temperature leads to a slightly raised performance of Ni<sub>20%</sub>/SBA-15, but a decrease for Ni<sub>40%</sub>/SBA-15, however, the influence is not noticeable. The catalyst without pretreatment leads to higher potential of carbon formation. The Ni<sub>40%</sub>/SBA-15 with highest Ni loading is the most active one for CH<sub>4</sub> and CO<sub>2</sub> since 27% and 37% of CH<sub>4</sub> and CO<sub>2</sub> conversions are reached at 600 °C, while 57% and 68% of conversions are obtained at 700 °C. Conversions of 27% of CH<sub>4</sub> and 36% of CO<sub>2</sub> are obtained over Ni<sub>20%</sub>/SBA-15 at the low temperature of 600 °C. The results are very promising as an optimization without carbon formation due

to the well-dispersed Ni species. Increasing the mass of Ni<sub>20</sub>/SBA-15 catalyst to 50 mg (without pretreatment) leads to a comparable result with a CH<sub>4</sub> conversion of 68.7% and CO<sub>2</sub> conversion of 77.7 % and a H<sub>2</sub>/CO ratio of about 0.8 at 700 °C. Besides, good activity is also obtained in harsh conditions.

### 3.5 Conclusion for this chapter

Dry reforming of CH<sub>4</sub> (DRM) has been studied over CeNi<sub>x</sub>(Al<sub>0.5</sub>)O<sub>y</sub> catalysts. The influence of different parameters was examined, such as the reaction temperature, pretreatment in H<sub>2</sub>, Ni loading, reactants concentrations and the mass of catalyst. Reaction temperature pronouncedly influences conversions and products distribution. Conversions of CH<sub>4</sub> and CO<sub>2</sub> and H<sub>2</sub>/CO ratio increase with reaction temperature and it allows obtaining high conversions of methane (85%), carbon dioxide (93%) and a high selectivity (H<sub>2</sub>/CO = 0.93) at the temperature of 800 °C under 20% initial concentration of the reactants. Conversions globally increase with Ni content while H<sub>2</sub>/CO ratio maintained around 0.7-0.8, which seems not influenced by Ni content. Moreover, solid carbon is formed and it also increases with Ni content. Absence of pretreatment does not decrease the activity, but leads to higher potential of carbon formation. More carbon formation accompanied by a loss of activity is found in conditions of pretreatment in H<sub>2</sub> at higher temperature of 600 °C. The optimum treatment temperature can be proposed at 250 °C, taking into account conversions, products distribution, and carbon formation, which also corresponds to the first TPR peak. It is attributed to the reduction of Ni species being able to be reduced and reoxidized readily and reversibly in CeNi<sub>x</sub>O<sub>y</sub> compounds leading to partially reduced solids. The catalyst allows obtaining a good activity even in the severe condition (CH<sub>4</sub>/CO<sub>2</sub> = 50/50). For low Ni content catalyst CeNi<sub>0.3</sub>O<sub>y</sub>, conversions are quite constant and carbon formation is well suppressed. Mass of the catalyst has a significant effect on the catalytic performance, **high conversions could be reached** by increasing the mass. On the other hand, on high Ni content catalysts, CeNi<sub>1</sub>O<sub>y</sub> and CeNi<sub>2</sub>O<sub>y</sub> high activity in 50%:50% concentration conditions can be obtained, although carbon formation leads to a decrease of activity at the initial period of time. The long term stability test of DRM was studied on CeNi<sub>0.5</sub>O<sub>y</sub> and CeNi<sub>0.3</sub>O<sub>y</sub> under different conditions. The CH<sub>4</sub> and CO<sub>2</sub> conversions reach 60% and 72% after 50 h of reaction on CeNi<sub>0.5</sub>O<sub>y</sub>, showing good stability towards carbon

deposition. In the stability test under harsh conditions, the catalytic activity of  $\text{CeNi}_{0.3}\text{O}_Y$  towards  $\text{CH}_4$  and  $\text{CO}_2$  reach conversions of 41 and 49%, respectively. Moreover, the  $\text{H}_2/\text{CO}$  molar ratio obtained is about 0.76. All these results show that  $\text{CeNi}_{0.3}\text{O}_Y$  is highly active for DRM reaction and does not suffer from activity loss after 72 h of reaction under severe conditions. Moreover, the higher amount of  $\text{CeNi}_{0.5}\text{Al}_{0.5}\text{O}_Y$  catalyst with low Ni content provides a more stable result, it is highly active for DRM reaction and does not suffer from activity loss after 60 h of reaction under severe conditions.  $\text{CeNi}_{0.5}\text{O}_Y$  and  $\text{CeNi}_2\text{Al}_{0.5}\text{O}_Y$  could be considered as the best catalyst in the binary and ternary series due to the high activity, selectivity and stability with carbon resistance (presence). The addition of Al into the Ce-Ni system decreases the conversions for both  $\text{CH}_4$  and  $\text{CO}_2$  in low Ni content condition, but maintains high activity in catalysts with high Ni content. Anyway, it is more resistant to the carbon formation.

The well dispersed  $\text{Ni}_x\text{Mg}_2\text{AlO}_Y$  catalysts demonstrate high efficiency toward DRM between  $600^\circ\text{C}$  and  $700^\circ\text{C}$ , the influences of pretreatment temperature and reactant concentrations have been studied. Treatment temperature has slight influence on activity results in stabilized state. However, there is a different evolution of conversions and  $\text{H}_2/\text{CO}$  ratio at first period of time on stream. Moreover, higher treatment temperature leads to an increase of carbon formation.  $\text{Ni}_1\text{Mg}_2\text{AlO}_Y$  allows the best catalytic results for the dry reforming of methane at the low temperature of  $600^\circ\text{C}$  with 10mg of catalyst, 33% and 39% conversions of  $\text{CH}_4$  and  $\text{CO}_2$  are obtained with a high selectivity with a  $\text{H}_2/\text{CO}$  ratio of 0.9. The carbon formation rate is  $0.2 \text{ g}_{\text{cat}}^{-1} \text{ h}^{-1}$ . In harsh conditions, the catalysts still have best performance with low carbon formation as 30% of  $\text{CH}_4$  conversion and 41% of  $\text{CO}_2$  conversion are obtained. However, the  $\text{H}_2/\text{CO}$  ratio value of 0.76 is lower than that in diluted condition (0.90). In addition,  $\text{Ni}_1\text{Mg}_2\text{AlO}_Y$  allows the 50h test at  $700^\circ\text{C}$  working with using pure  $\text{CH}_4$  and  $\text{CO}_2$  showing a remarkable stability along the whole experiment. The  $\text{Ni}_{12}\text{Mg}_2\text{AlO}_Y$  catalyst allows higher catalytic activity at initial period, but strong carbon formation leads to a deactivation and a blockage in only 2h of test.  $\text{Ni}_x/\text{SBA-15}$  catalysts have been tested in DRM. The influence of different parameters was studied, such as reduction temperature, Ni content and reaction temperature. The conversions measured during DRM at relatively low temperatures between  $600^\circ\text{C}$  and  $700^\circ\text{C}$  did not depend strongly on Ni loading. Increasing the pretreatment temperature leads to a slightly raised performance of  $\text{Ni}_{20\%}/\text{SBA-15}$ , but a decrease for  $\text{Ni}_{20\%}/\text{SBA-15}$ , however, the influence is not noticeable. Furthermore, very interesting

results are obtained in catalysts without pretreatment. The Ni<sub>40%</sub>/SBA-15 with highest Ni loading is the most active one for CH<sub>4</sub> and CO<sub>2</sub> since 27% and 37% of CH<sub>4</sub> and CO<sub>2</sub> conversions are reached at 600 °C, while 57% and 68% of conversions are obtained at 700 °C. Conversions of 27% of CH<sub>4</sub> and 36% of CO<sub>2</sub> are obtained over Ni<sub>20%</sub>/SBA-15 at the low temperature of 600 °C. The results are very promising as an optimization without carbon formation due to the well-dispersed Ni species is obtained. Increasing the mass of Ni<sub>20%</sub>/SBA-15 catalyst to 50 mg (without pretreatment) leads to a comparable result with a CH<sub>4</sub> conversion of about 68.7% and CO<sub>2</sub> conversion of about 77.7 % and a H<sub>2</sub>/CO ratio of about 0.8 at 700 °C. Besides, good activity is also obtained in harsh condition.

# Chapter 4

## Oxidative dry reforming of methane over $\text{CeNi}_x(\text{Al}_z)\text{O}_y$



## 4 Oxidative dry reforming of methane over CeNi<sub>x</sub>(Al<sub>z</sub>)O<sub>y</sub>

In partial oxidation (POM) (Eq.4-1), methane is oxidized to CO and H<sub>2</sub> (synthesis gas), at atmospheric pressure (H<sub>2</sub>/CO ratio close to 2). It is a potential method to produce H<sub>2</sub> with low energy costs [144] due to moderate exothermicity. However, there is a rising hazard from the high-temperature hot-spots which could lead to catalyst deactivation from sintering. In our laboratory, cerium and nickel-based binary mixed oxides [144], and cerium nickel-zirconium-based ternary oxyhydrides [146] were prepared and exhibited good performance in POM. It has also been shown in **Chapter 3** that the CeNi<sub>x</sub>O<sub>y</sub> and CeNi<sub>x</sub>Al<sub>0.5</sub>O<sub>y</sub> catalysts enable to equally activate methane in DRM. It is still important to avoid carbon formation even when it does not deactivate the catalyst, as it can block and damage the reactor or be carried downstream by the gas flow to cause process issues like fouling. Under this scenario, although the high Ni content catalyst remains active despite substantial carbon deposition, it is better for such a catalyst to be used in a high activity process avoiding carbon formation.

Based on these observations, a comprehensive strategy to evade the defects above and improve the conversion at a lower temperature is combining the DRM (Eq.4-2) and POM in a single reactor, seen as (Eq.4-3). Co-feeding O<sub>2</sub> with CH<sub>4</sub> and CO<sub>2</sub> provides additional advantages such as: reducing the global energy requirement, enhancing catalyst stability, increasing deactivation resistance [4] and inhibiting the carbon deposition rate by gasifying carbon species, as demonstrated by Lucrecio et al. [58]. Furthermore, the H<sub>2</sub>/CO ratio could be manipulable for downstream.



Herein we report CeNi<sub>x</sub>(Al<sub>z</sub>)O<sub>y</sub> mixed oxides with different Ni contents in the oxidative reforming of methane (ODRM) at low temperatures. Various parameters are studied, such as reaction temperature, Ni content, and concentration of oxygen and their influences on catalytic stability are investigated. Besides, to be closer to the possibility of application, the reactants concentrations are chosen to correspond to a simulated biogas, and it is also compared with classic DRM test (in similar reactants

concentration).

## 4.1 Oxidative dry reforming over $\text{CeNi}_x\text{O}_y$ mixed oxides

### 4.1.1 Catalytic tests at low-temperature range

As described in **Chapter 1**, an ideal ODRM process desires to develop catalysts working at low temperatures. After an *in situ* treatment in  $\text{H}_2$  at 250 °C, the  $\text{CeNi}_x\text{O}_y$  catalysts are studied in a temperature increasing test from 500-700 °C. The reactants diluted in  $\text{N}_2$  with a molar composition of  $\text{CH}_4/\text{CO}_2/\text{O}_2 = 1:0.7:0.3$  ( $\text{CH}_4=20\%$ ,  $\text{CO}_2 / \text{CH}_4 = 0.7$  as a simulated biogas) are introduced into the reactor in a specific order.

As shown in **Fig. 4-1**,  $\text{CH}_4$  and  $\text{CO}_2$  conversions increase with temperature, due to the endothermicity of ODRM reaction in these conditions. The conversions of  $\text{CH}_4$  and  $\text{CO}_2$  increase from 43.0% and 14.2% at 500 °C to 88.9% and 78.6% at 700 °C, respectively. Noting that the  $\text{CH}_4$  conversion is much higher than  $\text{CO}_2$  conversion in all temperature ranges, the conversion of  $\text{O}_2$  is always complete in all the tests.

The  $\text{H}_2/\text{CO}$  ratio decreases with temperature, the value of 1.70 at 500 °C declines to 1.35 at 600 °C, then it continually decreases to about 1.0 at 700 °C. The variation of selectivity indicates the different reactions occurrences in the system. For example, at high temperature ( $\geq 700^\circ\text{C}$ ) the reverse water-gas shifting and dry reforming reactions become dominant reactions, leading to a ratio close to 1.1. This trend is contrary to the  $\text{H}_2/\text{CO}$  ratio evolution in DRM, which increases with reaction temperature.

The drop in  $\text{H}_2/\text{CO}$  ratio with increasing temperature is in agreement with partial oxidation becoming less significant. It seems that the benefit of  $\text{O}_2$  addition is more significant at lower temperature range. It can be remarked that negative values for  $\text{CO}_2$  conversion at 400 °C and higher fraction of water is observed in the products (but not shown in the **Figs**). The influence of reaction temperature is also studied on  $\text{CeNi}_x\text{O}_y$  catalysts with different Ni contents. Globally the same evolution of catalytic behaviors is obtained over the other catalysts with different Ni contents. Moreover, differences in conversions and products distribution due to the influence of Ni content is studied and discussed later on.

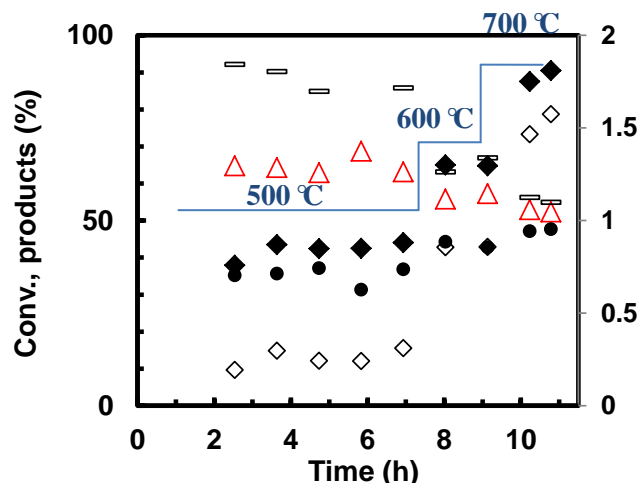


**Fig. 4-1**  $\text{CH}_4$  conversion ( $\blacklozenge$ ),  $\text{CO}_2$  conversion ( $\diamond$ ) and gas-phase products distribution at 500-700 °C on  $\text{CeNi}_{0.5}\text{O}_y$  catalyst (50 mg) pretreated in  $\text{H}_2$  at 250 °C.  $\text{H}_2$  ( $\triangle$ ),  $\text{CO}$  ( $\bullet$ ), in mol % and  $\text{H}_2/\text{CO}$  ratio ( $\square$ ),  $\text{CH}_4:\text{CO}_2:\text{O}_2 = 1:0.7:0.3$ . ( $\text{CH}_4 = 20\%$ )

#### 4.1.2 The effect of nickel content on $\text{CeNi}_x\text{O}_y$ catalysts

**Fig. 4-2** depicts the  $\text{CH}_4$ ,  $\text{CO}_2$  conversions and  $\text{H}_2/\text{CO}$  ratio measured during the ODRM experiments performed at 600 °C and 700 °C on different Ni content catalysts, and the results are reported at the steady state versus Ni content in **Fig. 4-3** (a) and (b). It can be observed that the  $\text{CH}_4$  and  $\text{CO}_2$  conversions increase with the increasing nickel content. Surprisingly, the  $\text{CeNi}_{0.5}\text{O}_y$  sample, with 12 wt.% of Ni, shows comparable performance to catalysts with much higher nickel contents ( $\text{CeNi}_1\text{O}_y$  and  $\text{CeNi}_2\text{O}_y$ ). The  $\text{CeNi}_2\text{O}_y$  catalyst shows the highest performance at 700 °C regarding  $\text{CH}_4$  and  $\text{CO}_2$  conversions. However, a decrease is observed. The conversions of  $\text{CH}_4$  and  $\text{CO}_2$  over  $\text{CeNi}_2\text{O}_y$  decrease by 8% in 2h probably due to carbon deposition. Although slight decreases in catalytic activity towards  $\text{CH}_4$  conversion is observed during all the reactions, the stability of  $\text{CeNi}_x\text{O}_y$  catalysts still get improved compared with DRM reforming under similar conditions.

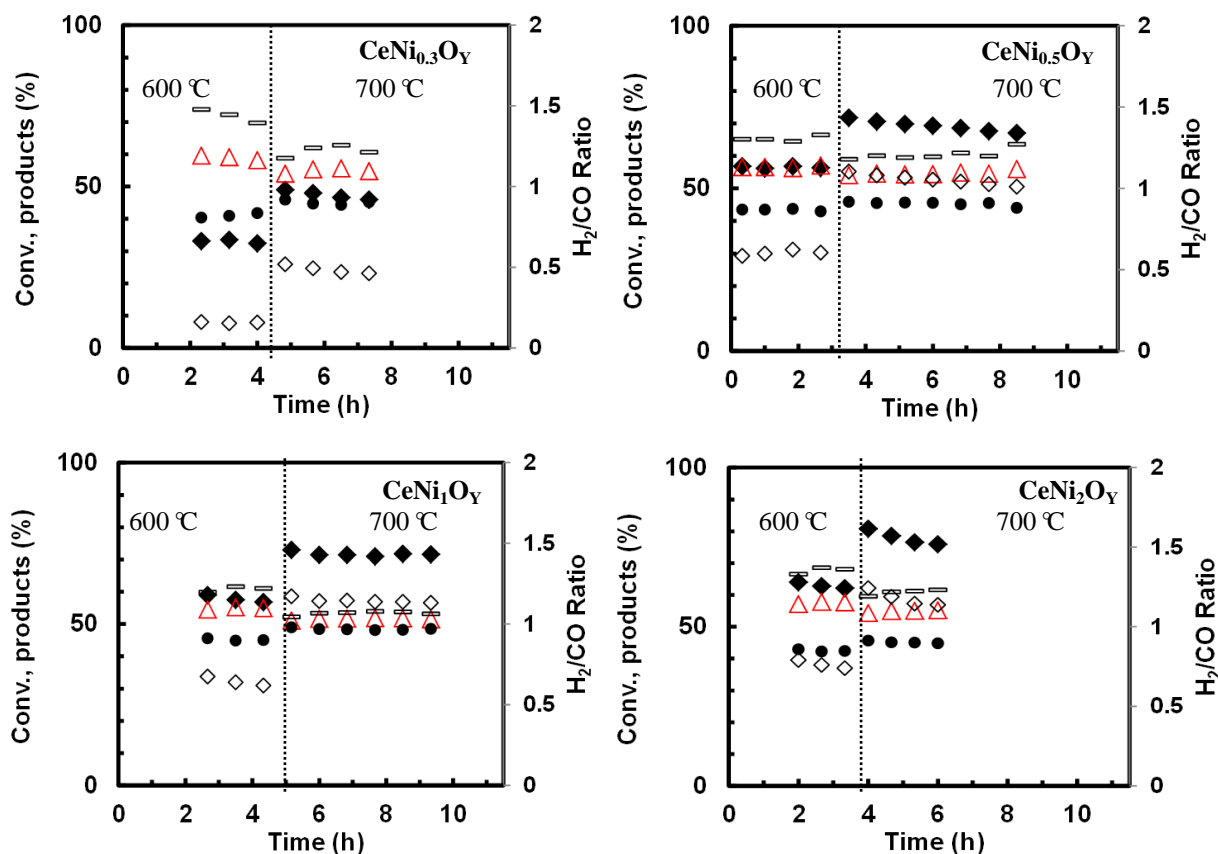


**Fig. 4-2**  $\text{CH}_4$  conversion ( $\blacklozenge$ ),  $\text{CO}_2$  conversion ( $\diamond$ ) and distribution of gas-phase products on  $\text{CeNi}_x\text{O}_y$  catalysts (10 mg) without pretreatment.  $\text{H}_2$  ( $\triangle$ ),  $\text{CO}$  ( $\bullet$ ), in mol % and  $\text{H}_2/\text{CO}$  ratio ( $\square$ ),  $\text{CH}_4:\text{CO}_2:\text{O}_2 = 1:0.7:0.3$ . (with  $\text{CH}_4 = 20\%$ )

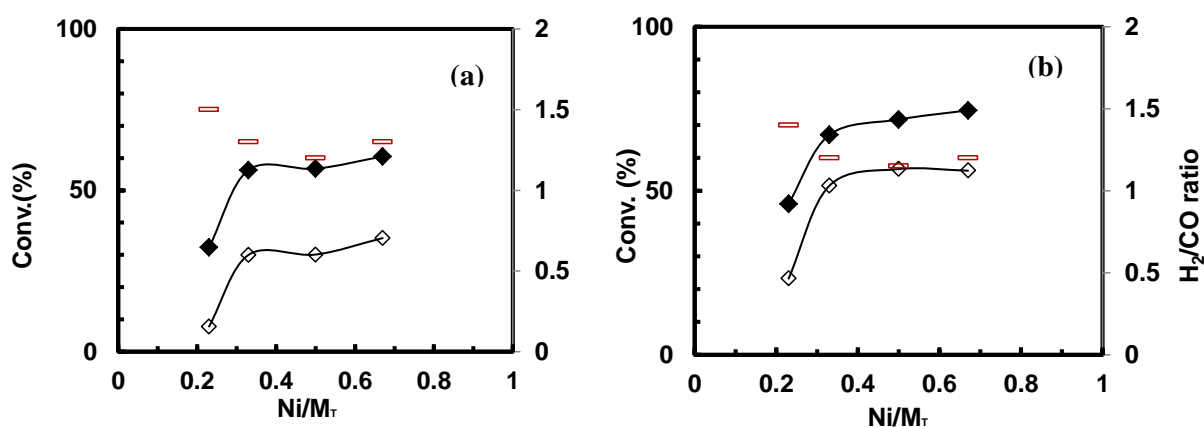


**Fig. 4-3**  $\text{CH}_4$  ( $\blacklozenge$ ),  $\text{CO}_2$  ( $\diamond$ ) conversions and the  $\text{H}_2/\text{CO}$  ratio ( $\square$ ) obtained at (a) 600 °C and (b) 700 °C on the  $\text{CeNi}_x\text{O}_y$  catalysts (10 mg) without pretreatment versus  $\text{Ni}/M_r$  ratio.  $\text{CH}_4:\text{CO}_2:\text{O}_2 = 1:0.7:0.3$ . (with  $\text{CH}_4 = 20\%$ )

However, for  $\text{CeNi}_2\text{O}_y$ ,  $\text{CH}_4$  and  $\text{CO}_2$  conversions are relatively close to thermodynamic equilibrium estimation (68% and 35% for  $\text{CH}_4$  and  $\text{CO}_2$  conversions, respectively. seen in **Annex 3**) at

the beginning which suggests the participation of other reactions such as methane oxidation or steam reforming of methane. The occurrence of reverse water-gas-shift reaction (RWGS) can be also responsible for the decrease of  $\text{H}_2/\text{CO}$  ratios. Higher  $\text{CO}_2$  concentration in the reaction could probably help to shift the RWGS reaction towards its equilibrium composition. It can be recalled that simulated biogas is used in this study with a  $\text{CH}_4/\text{CO}_2$  molar ratio of 1:0.7 used as feedstock. The  $\text{H}_2/\text{CO}$  ratio is always above 1 in the present study. Moreover, the  $\text{H}_2/\text{CO}$  ratio is affected by the nickel content, and the excess of  $\text{H}_2$  in the obtained products is found in low nickel content catalyst. The  $\text{H}_2/\text{CO}$  ratio decrease from 1.5 on  $\text{CeNi}_{0.3}\text{O}_y$  to around 1.3 on  $\text{CeNi}_1\text{O}_y$  and  $\text{CeNi}_2\text{O}_y$  at 600 °C. Such high differences in the distribution of the obtained products strongly suggest the occurrence of side reactions, as the process of ODRM is quite complicated.

#### 4.1.3 Stability test

The  $\text{CeNi}_{0.5}\text{O}_y$  catalyst is selected for 24h stability test at 700 °C. As shown in **Fig. 4-4**, quite stable performance is obtained over time on stream. A slight but steady decrease in both  $\text{CH}_4$  and  $\text{CO}_2$  conversions can be observed. The initial conversion of  $\text{CH}_4$  of 81.4% declines to a value around 77.4% after 24h of reaction. Similar trend is found for  $\text{CO}_2$  conversion which decreases from 67.0% to 62.2%. However, the  $\text{H}_2/\text{CO}$  ratio remains relatively stable at values around 1.15 throughout the reaction. Compared to the DRM stability study on  $\text{CeNi}_{0.5}\text{O}_y$  reported in **Section 3.1.5**, this result shows that the presence of  $\text{O}_2$  helps enhancing the catalytic stability, maintaining the conversions at a high and stable level. This stable evolution over time of reaction could be explained by the addition of oxygen allowing rapid oxidation of carbon species on the catalyst surface, which leads to better performances both regarding activity for  $\text{CH}_4$  and stability over time.

The results are interesting to compare with literature [191], in which Kathiraser et al. studied the 5%Ce -promoted Ni/SiO<sub>2</sub> catalysts for oxidative reforming of model biogas. 15 mg of catalyst was applied and the reaction was performed at 750 °C at a ratio of  $\text{CH}_4:\text{CO}_2:\text{O}_2$  of 1.5:1.0:0.25. 60% of  $\text{CH}_4$  conversion and 65% of  $\text{CO}_2$  conversion were obtained after 25h of test. The  $\text{H}_2/\text{CO}$  ratio was 1.13. These values are close to our catalytic results. However, lower catalyst mass and reaction temperature are used in the present study, noting that even higher  $\text{CH}_4$  conversion is obtained on  $\text{CeNi}_{0.5}\text{O}_y$  in harsher conditions. Moreover, in the recent literature [112], a LaMFeNiO<sub>3</sub> catalyst was tested at 700 °C

in a gases feed of  $\text{CH}_4:\text{CO}_2:\text{O}_2$  (1:0.7:0.3) with GHSV of 36,000 mL/h/g.cat. The  $\text{CH}_4$  conversion was 82% which is close to the value obtained in this study. However, our conditions are severer, with the value of 96,000 mL/h/g.cat. Another example [108] of ODRM reaction performed on  $\text{Ni}/5\text{ZrO}_2\text{-SiO}_2$  catalyst was conducted in the conditions of  $\text{CH}_4/\text{CO}_2/\text{O}_2 = 1:0.4:0.3$ , at 700 °C,  $\text{GHSV} = 90,000\text{h}^{-1}$ . The result after 8 h was obtained as  $\text{CH}_4$  Conv.  $\approx 68\%$  and  $\text{CO}_2$  Conv.  $\approx 52\%$ . Mohcin Akri [109] investigated oxidative reforming of methane at 800 °C using a  $\text{GHSV} = 60,000$  mL/g/h in  $\text{CH}_4/\text{CO}_2/\text{O}_2 = 1:0.8:0.2$ . Their best result over 10Ni15Ce/illite catalyst after 5h are as follow:  $\text{CH}_4$  Conv.  $\approx 84\%$ ,  $\text{CO}_2$  Conv.  $\approx 78\%$ ,  $\text{H}_2/\text{CO}$  ratio  $\approx 0.9$ .

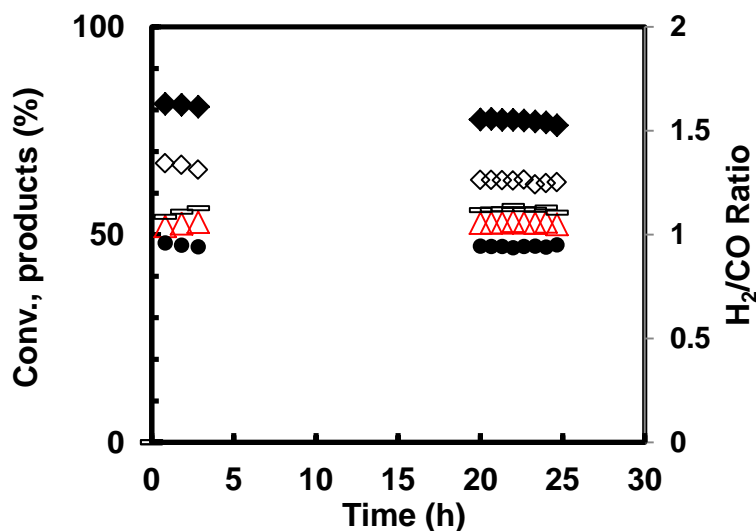


**Fig. 4-4** Catalytic stability in ODRM at 700 °C on  $\text{CeNi}_{0.5}\text{O}_y$  catalyst (50 mg) pretreated in  $\text{H}_2$  at 250 °C.  $\text{CH}_4$  (◆),  $\text{CO}_2$  (◇) conversions,  $\text{H}_2$  (△),  $\text{CO}$  (●), in mol % and the  $\text{H}_2/\text{CO}$  ratio (□).  $\text{CH}_4:\text{CO}_2:\text{O}_2 = 1:0.7:0.3$  (with  $\text{CH}_4 = 20\%$ ).

## 4.2 Oxidative dry reforming over $\text{CeNi}_x\text{Al}_{0.5}\text{O}_y$ mixed oxides

DRM Studies showed that the  $\text{CeNi}_x\text{Al}_{0.5}\text{O}_y$  mixed oxides are highly active and resistant to carbon formation probably due to the high metallic dispersion. The further potential of  $\text{CeNi}_x\text{Al}_{0.5}\text{O}_y$  compounds is studied in the oxidative reforming of methane (ODRM) at low temperatures. Different parameters are studied, such as reaction temperature, Ni content, and concentration of oxygen and their influences on catalytic stability are discussed. Carbonaceous species formed are also characterized.

### 4.2.1 Temperature influence

Fig. 4-5 presents the results of the ODRM catalytic experiments carried out at the temperature range of 500-800 °C on the  $\text{CeNi}_2\text{Al}_{0.5}\text{O}_y$  catalyst. The results are reported under steady-state conditions (after 5h). Both conversions of  $\text{CH}_4$  and  $\text{CO}_2$  become more efficient as the temperature increases. The conversions of  $\text{CH}_4$  and  $\text{CO}_2$  increase from 41% and 23% at 500 °C to 90% and 74% at 800 °C. However, the decline of  $\text{H}_2/\text{CO}$  ratio is found with the increase of reaction temperature (from a value of 1.6 at 500 °C to about 1.0 at 800 °C). As previously discussed in **Chapter 3**, when the reaction temperature is higher than 650 °C, the occurrence of reverse water-gas shift leads to a decrease of the  $\text{H}_2/\text{CO}$  ratio. This is in agreement with reported results at high-temperature range where  $\text{O}_2$  had little effect on  $\text{H}_2$  production as dry reforming of methane remains the dominant reforming reaction [64]. As already reported, partial oxidation of methane mainly occurs at lower temperature while higher temperature favors the  $\text{CO}_2$  reforming of methane [63]. Moreover, compared to dry reforming, the higher  $\text{H}_2/\text{CO}$  ratio can be adjusted by varying the reaction temperature.

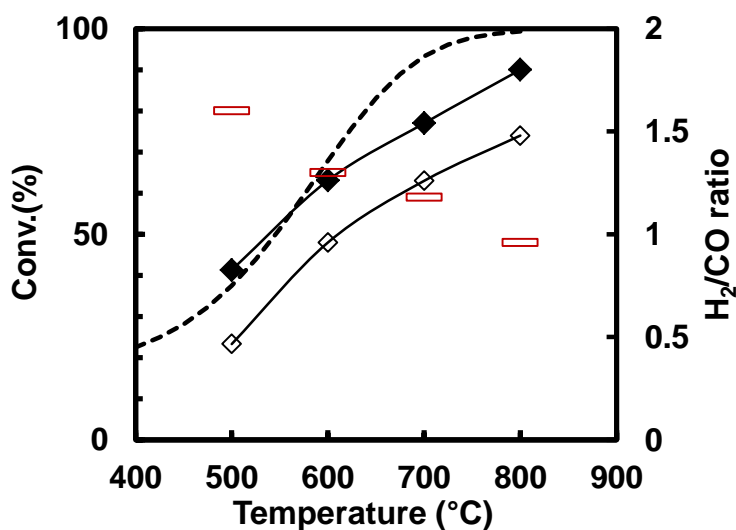


**Fig. 4-5** Catalytic activity in ODRM vs. reaction temperature on  $\text{CeNi}_2\text{Al}_{0.5}\text{O}_y$  catalyst (50 mg) pretreated in  $\text{H}_2$  at 250 °C).  $\text{CH}_4$  (◆),  $\text{CO}_2$  (◇) conversions and  $\text{H}_2/\text{CO}$  ratio (□).  $\text{CH}_4$  conversion thermodynamic limit (----)  $\text{CH}_4$ :  $\text{CO}_2$ :  $\text{O}_2$  = 1:0.7:0.3 (with  $\text{CH}_4$  = 20%).

### 4.2.2 Influence of Ni content

The  $\text{CeNi}_x\text{Al}_{0.5}\text{O}_y$  catalysts are studied at 600 °C in the same conditions as binary catalysts (10 mg

of catalyst without pretreatment). The conversions of  $\text{CH}_4$  and  $\text{CO}_2$  and  $\text{H}_2/\text{CO}$  molar ratio versus  $\text{Ni}/\text{M}_T$  are illustrated in **Fig. 4-6**. Clearly, conversions globally increase with Ni content. The conversion of  $\text{CH}_4$  is always higher than the conversion of  $\text{CO}_2$ . For  $\text{CeNi}_5\text{Al}_{0.5}\text{O}_Y$ , the methane conversion reaches 57% and the  $\text{CO}_2$  conversion is of 32%, while the  $\text{H}_2/\text{CO}$  ratio is around 1.3. The carbon formation rate is reported in **Fig. 4-7**. It drastically increases when the  $\text{Ni}/\text{M}_T$  ratio is higher than 0.4. Comparison and discussion between binary and ternary catalysts will be done in **section 4.2.5**.

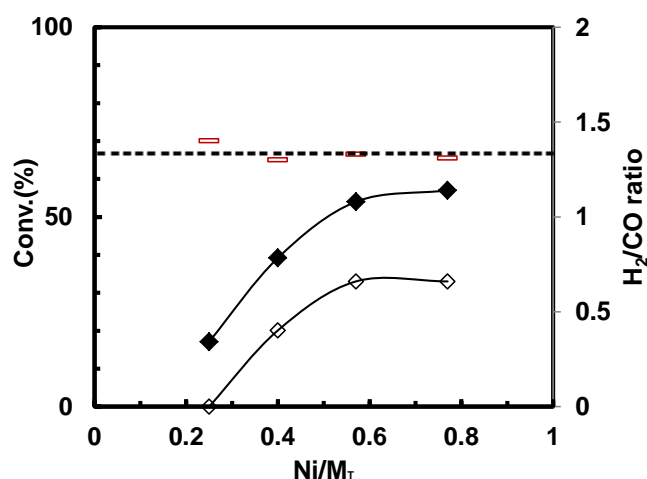


**Fig. 4-6**  $\text{CH}_4$  (◆) and  $\text{CO}_2$  (◇) conversions and  $\text{H}_2/\text{CO}$  ratio (□) at 600 °C versus Ni content on  $\text{CeNi}_x\text{Al}_{0.5}\text{O}_Y$  catalysts (10 mg), without pretreatment, ( $\text{CH}_4$  conversion thermodynamic limit ---).  $\text{CH}_4$ :  $\text{CO}_2$ :  $\text{O}_2 = 1:0.7:0.3$  (with  $\text{CH}_4 = 20\%$ ).

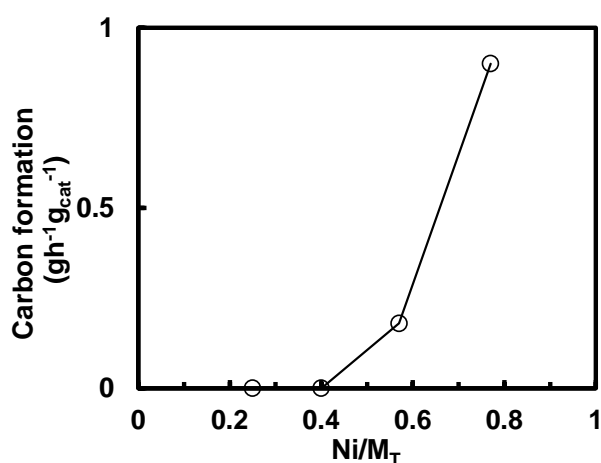


**Fig. 4-7** Carbon formation rate over  $\text{CeNi}_x\text{Al}_{0.5}\text{O}_Y$  (○) catalysts (10 mg) without pretreatment.  $\text{CH}_4$ :  $\text{CO}_2$ :  $\text{O}_2 = 1:0.7:0.3$  (with  $\text{CH}_4 = 20\%$ ).

Previously, it has been found that using higher mass of catalyst provides benefit to both conversion

and ability of resistance to carbon deposition. In dry reforming, the pretreatment in H<sub>2</sub> also leads to a better performance on elimination of carbon over Ce-Ni based catalysts. Under this scenario, higher conversions for both CH<sub>4</sub> and CO<sub>2</sub> could be expected by using higher mass of catalysts with pretreatment, even lower temperature of 500 °C could be interesting. Therefore, an ODRM study on the influence of the metal content in the CeNi<sub>x</sub>Al<sub>0.5</sub>O<sub>Y</sub> catalysts is carried out at 500 °C and 600 °C with 50mg of catalyst. The conversions of CH<sub>4</sub> and CO<sub>2</sub> and H<sub>2</sub>/CO molar ratio versus Ni/M<sub>T</sub> are illustrated in Fig. 4-8. As expected, it is clearly shown that conversions globally increase with Ni content, except for the CeNi<sub>5</sub>Al<sub>0.5</sub>O<sub>Y</sub> catalyst which leads to a lower CO<sub>2</sub> conversion at 500 °C, maybe due to the occurrence of some side reactions which form CO<sub>2</sub> in the products, like WGS reaction (CO + H<sub>2</sub>O → CO<sub>2</sub> + H<sub>2</sub>) or total methane oxidation (CH<sub>4</sub> + O<sub>2</sub> → CO<sub>2</sub> + H<sub>2</sub>O). The conversion of CH<sub>4</sub> is always higher than the conversion of CO<sub>2</sub>. On catalysts with high Ni content, the methane conversion is close to the thermodynamic equilibrium. For CeNi<sub>2</sub>Al<sub>0.5</sub>O<sub>Y</sub>, the methane conversion reaches 42% and the CO<sub>2</sub> conversion is of 21% at 500 °C, and the H<sub>2</sub>/CO ratio is at around 1.4. While at 600 °C, the CeNi<sub>5</sub>Al<sub>0.5</sub>O<sub>Y</sub> catalysts provides best performance as CH<sub>4</sub> and CO<sub>2</sub> conversions are of 68% and 43%, respectively. The H<sub>2</sub>/CO ratio is maintained at 1.4. The catalytic activity of CeNi<sub>2</sub>Al<sub>0.5</sub>O<sub>Y</sub> is slightly lower than that of CeNi<sub>5</sub>Al<sub>0.5</sub>O<sub>Y</sub> catalyst. However, the former is the optimal one due when considering the low carbon formation rate (Fig. 4-9).

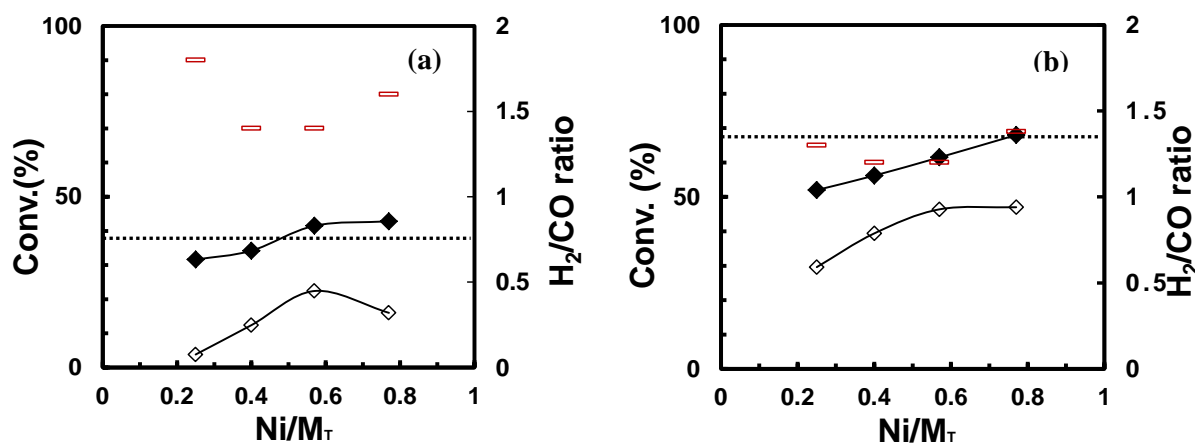
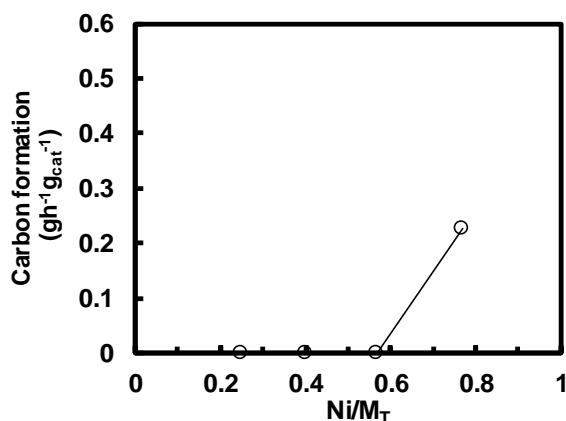


Fig. 4-8 CH<sub>4</sub> (◆) and CO<sub>2</sub> (◇) conversions and the H<sub>2</sub>/CO ratio (□) versus Ni content over CeNi<sub>x</sub>Al<sub>0.5</sub>O<sub>Y</sub> catalysts (50 mg) with pretreatment at 250 °C. (a) at 500 °C, (b) at 600 °C, (CH<sub>4</sub> conversion thermodynamic limit ---). CH<sub>4</sub>: CO<sub>2</sub>: O<sub>2</sub> = 1:0.7:0.3. (CH<sub>4</sub> = 20%)

As shown in Fig. 4-9, the carbon deposition is negligible for the tested catalysts with low Ni

contents ( $x = 0.5\sim 2$ ), only few visible darkening on the surface of the catalyst could be seen, and no carbon formation is measured by mass variation. However, it becomes effective that as the Ni content is increased up to 49.2% ( $\text{CeNi}_5\text{Al}_{0.5}\text{O}_y$ ), the carbon formation rate is increased and calculated at  $0.24 \text{ g g}_{\text{cat}}^{-1} \text{ h}^{-1}$ .



**Fig. 4-9** Carbon formation rate over  $\text{CeNi}_x\text{Al}_{0.5}\text{O}_y$  (○) catalysts (50 mg) pretreated in  $\text{H}_2$  at  $250^\circ\text{C}$ .  $\text{CH}_4$ :  $\text{CO}_2$ :  $\text{O}_2 = 1:0.7:0.3$  (with  $\text{CH}_4 = 20\%$ ).

The removal of carbon deposit may be assisted by the addition of oxygen, which helps to maintain the activity and stability of the tested catalysts. Besides, the ceria property with high oxygen mobility can play also a role. Moreover, the oxygen vacancies formation is increased in the Ni-Ce-Al-O solid solution. Furthermore, the addition of aluminum strongly modifies the structure of cerium nickel based mixed oxides by disorganizing the structure which leads to well dispersed Ni species with favored interactions between  $\text{Ni}^{2+}$ ,  $\text{Ce}^{4+}$  and  $\text{Al}^{3+}$  cations [87]. By the way, higher mass of catalysts and pretreatment in  $\text{H}_2$  at  $250^\circ\text{C}$  reduce the carbon formation compared with the result obtained for 10mg of catalyst without pretreatment (seen in **Fig. 4-7**).

#### 4.2.3 Influence of $\text{O}_2$ concentration

Herein, four different  $\text{O}_2/\text{CH}_4$  ratios (0, 0.1, 0.3 and 0.5) are selected to understand the influence of adding  $\text{O}_2$  in ODRM. Where an experiment with  $\text{O}_2/\text{CH}_4 = 0$  is employed as a comparison (dry reforming with  $\text{CH}_4:\text{CO}_2=1:0.7$ ). Throughout all the test conditions,  $\text{O}_2$  is totally converted. **Fig. 4-10** shows the effect of the different amount of oxygen addition over  $\text{CeNi}_2\text{Al}_{0.5}\text{O}_y$  catalyst. A slightly raise of the temperature is observed at the beginning of the reaction when adding  $\text{O}_2$ . This temperature

increase of about 5-12 °C depends on the  $\text{O}_2$  concentration, which is associated with the exothermic partial oxidation reaction of  $\text{CH}_4$ .  $\text{O}_2/\text{CH}_4$  ratio = 0.3 allows to maintain methane conversion at a high level ranging from 66% to 62% (4% of decrease), showing that an enhanced catalyst stability can be achieved by adding the appropriate amount of  $\text{O}_2$ . This seems to be the optimized  $\text{O}_2/\text{CH}_4$  ratio in the ODRM because it achieves a relatively high rate of conversion (seen in **Fig. 4-10**) and a relatively scarce carbon formation (a darken on the catalyst surface can be observed but no carbon formation can be deduced by weight variation, as shown in **Table 4-1**). In addition, a moderate increase in the  $\text{H}_2/\text{CO}$  ratio is obtained compared to the results obtained in dry reforming conditions. Clearly  $\text{O}_2$  addition has a largely beneficial effect. Higher fraction of  $\text{O}_2$  in reactants ( $\text{O}_2/\text{CH}_4 = 0.5$ ) results in severe decrease in  $\text{CO}_2$  conversion and higher formation of  $\text{H}_2\text{O}$ .

In all cases, the conversion of  $\text{CH}_4$  increases with the increasing of  $\text{O}_2/\text{CH}_4$  ratio while the conversion of  $\text{CO}_2$  decreases a lot due to high reactivity of  $\text{O}_2$  compared to the difficulty to activate  $\text{CO}_2$ . The DRM experiment ( $\text{CH}_4: \text{CO}_2=1:0.7$ ) shows an initial methane conversion of 63% that decreases to approximately 52% after 5 hours of reaction. Moreover, the  $\text{H}_2/\text{CO}$  molar ratio is around 1. Adding  $\text{O}_2$  resulted in better stability and higher  $\text{H}_2/\text{CO}$  ratios in all cases.  $\text{H}_2$  formation slightly increases in presence of  $\text{O}_2$  while  $\text{CO}$  formation decreases. Complementary to the classic dry reforming, different reactions could be involved when adding  $\text{O}_2$  into the system.

According to the literature [27], the main effect of the addition of oxygen observed in methane reforming process is increasing the conversion of  $\text{CH}_4$  and reducing the conversion of  $\text{CO}_2$ . Moreover, in agreement with several studies [13][14][192][193], the conversion of  $\text{CO}_2$  could be suppressed in excess of  $\text{O}_2$  or air in oxidative dry reforming process. Increasing  $\text{O}_2/\text{CH}_4$  ratio favored an increase in available  $\text{O}_2$  for partial oxidation or combustion to occur. As a matter of fact, when the formation of  $\text{CO}_2$  occurs, the  $\text{CO}_2$  conversion appears negative. Moreover, as depicted below, the partial **Eq. (4-6)** to total oxidation of methane mainly involves three reactions. In contrast to DRM and SRM, the reactions involving  $\text{CH}_4$  and  $\text{O}_2$  are exothermic (with enough  $\text{O}_2$  concentration). Chen et al. [194] studied the effect of  $\text{O}_2$  content from 0 to 15% on  $\text{Ni}/\text{SiO}_2$  in biogas reforming, they suggested that the presence of  $\text{O}_2$  in reactants greatly helped inhibiting the catalyst sintering. However, higher  $\text{O}_2$  concentrations ( $\geq 10\%$ ) resulted in a severe decrease in  $\text{CO}_2$  conversion and greater  $\text{H}_2\text{O}$  productivity. In Lee's work

[195], the O<sub>2</sub>/CH<sub>4</sub> ratio around 0.57 was employed to favor Eq.(4-2), but they still found that Eq. (4-4) and Eq. (4-5) occurred simultaneously.

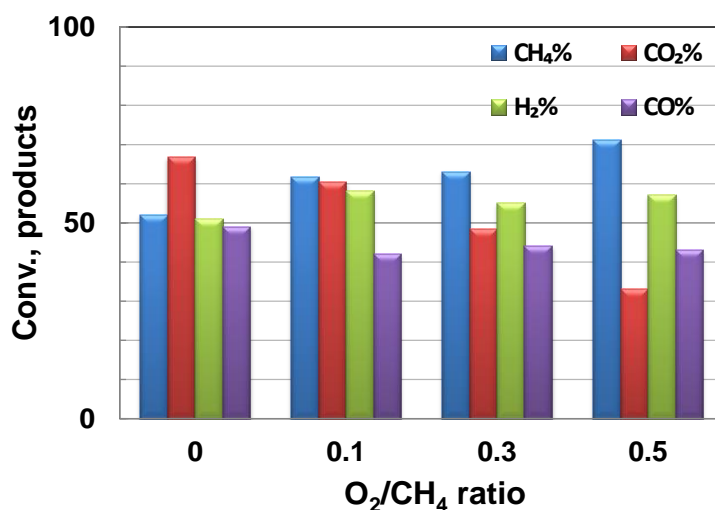


**Fig. 4-10** CH<sub>4</sub> and CO<sub>2</sub> conversions and products distribution (H<sub>2</sub>, CO in mol %) at 600 °C versus O<sub>2</sub> concentration over CeNi<sub>2</sub>Al<sub>0.5</sub>O<sub>y</sub> catalyst (50mg) pretreated in H<sub>2</sub> at 250 °C. (CH<sub>4</sub> = 20%)

**Table 4-1** H<sub>2</sub>/CO ratio and carbon formation rate in different condition of O<sub>2</sub>/CH<sub>4</sub>

O <sub>2</sub> /CH <sub>4</sub> ratio	0	0.1	0.3	0.5
H <sub>2</sub> /CO ratio	1.0	1.4	1.3	1.3
Carbon formation rate (g g <sub>cat</sub> <sup>-1</sup> h <sup>-1</sup> )	0.60	0.24	0	0

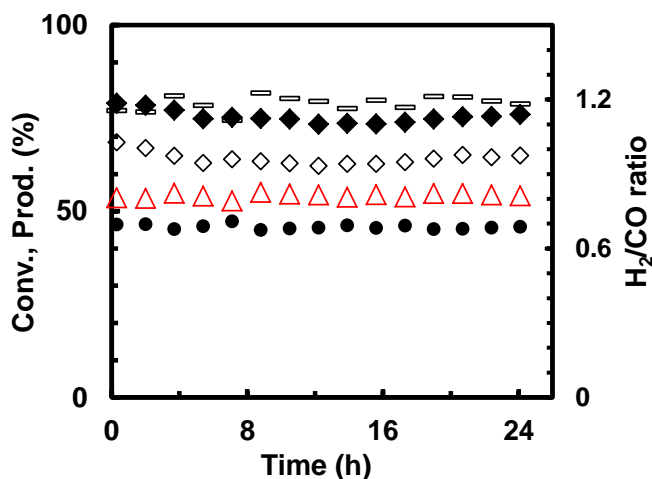
#### 4.2.4 Stability test

The CeNi<sub>2</sub>Al<sub>0.5</sub>O<sub>y</sub> catalyst is selected for stability test in the ODRM with O<sub>2</sub>/CH<sub>4</sub> ratio equal to 0.3. As presented in **Fig. 4-11** the conversions and gas phase products distribution are reported in the 24h of reaction at 700 °C. In the first 5h, the detected conversions of both CH<sub>4</sub> and CO<sub>2</sub> decrease slightly from 81% to 77%, and from 68% to 63%, respectively, then they remain constant in the following 20h. The H<sub>2</sub>/CO ratio obtained is close to 1.2 with negligible fluctuations. When comparing to dry reforming in the stoichiometric ratio (CH<sub>4</sub>:CO<sub>2</sub>=1:1), higher H<sub>2</sub>/CO ratio can be obtained. The catalyst shows an

excellent durability during at least 24h of the reaction. Visible darkening of the catalyst could be seen that could be assigned to a spot of carbon formed on the surface of the catalyst. However, no carbon formation could be measured due to negligible mass variation. Finally, the comparable catalytic result is obtained with this catalyst in ODRM process.

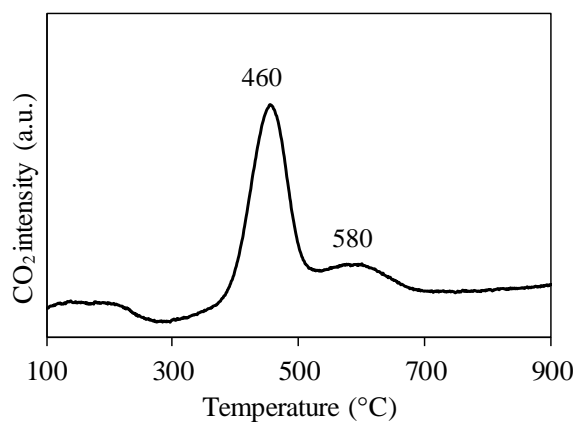
Asencios et al. [27] studied the catalysts composed of  $\text{NiO}/\text{Y}_2\text{O}_3/\text{ZrO}_2$  mixtures (100 mg) in the oxidative reforming of a model biogas ( $1.5\text{CH}_4:1\text{CO}_2$ ) in similar conditions. The performance of conversion of  $\text{CH}_4$  and  $\text{CO}_2$  were 65% and 70%, respectively in presence of oxygen ( $1.5\text{CH}_4 + 1\text{CO}_2 + 0.25\text{O}_2$ ) at  $750^\circ\text{C}$ , with the  $\text{H}_2/\text{CO}$  ratio was around 1. In another study [108] Jing Gao et al. prepared  $\text{Ni}/5\text{ZrO}_2\text{-SiO}_2$  catalyst with larger  $\text{Ni-ZrO}_2$  boundary and tested it in the conditions of  $\text{CH}_4/\text{CO}_2/\text{O}_2 = 1:0.4:0.3$  at  $700^\circ\text{C}$ . with a  $\text{GHSV} = 90,000\text{h}^{-1}$ , the result after 8 h was reported as  $\text{CH}_4$  and  $\text{CO}_2$  conversions are 68% and 52%, respectively. Mohcin Akri and co-workers [109] investigated oxidative reforming of methane over  $10\text{Ni}15\text{Ce}/\text{illite}$  at  $800^\circ\text{C}$  using a  $\text{GHSV} = 60,000\text{ mL/g/h}$  in  $\text{CH}_4/\text{CO}_2/\text{O}_2 = 1:0.8:0.2$ . The best result obtained was as follow:  $\text{CH}_4$  conversion was around 84% and the conversion for  $\text{O}_2$  was 78%, and  $\text{H}_2/\text{CO}$  ratio obtained was 0.9. In Xuejing's study [107] the effects of various  $\text{O}_2$  concentrations in biogas on initial conversions and stability at various temperatures on a  $\text{Ni}/\text{SiO}_2$  catalyst were investigated. They used  $\text{O}_2$  co-feeding with model biogas mixture ( $\text{CH}_4/\text{CO}_2/\text{N}_2 = 0.4:0.4:0.2$ ) over 100 mg of catalysts with  $\text{GHSV}$  of  $30,000\text{ mL/h/g}_{\text{cat}}$ . In the  $\text{CH}_4/\text{CO}_2/\text{O}_2 = 1:1:0.3$  condition, the catalyst provided 73% of  $\text{CH}_4$  conversion and 45% of  $\text{CO}_2$  conversion, the  $\text{H}_2/\text{CO}$  ratio was 1.0. It has been shown that an appropriate percentage of  $\text{O}_2$  in reactants improved the activity and stability of the catalysts which was attributed to the inhibited sintering.

It appears that the catalyst in the present study shows similar activity but at lower temperature of  $700^\circ\text{C}$  (with  $96,000\text{ mL/g/h}$ ), evidencing highly interesting results.



**Fig. 4-11** Stability test of ODRM at 700 °C over  $\text{CeNi}_2\text{Al}_{0.5}\text{O}_\gamma$  catalyst (50 mg) pretreated in  $\text{H}_2$  at 250 °C.  $\text{CH}_4$  conversion (◆),  $\text{CO}_2$  conversion (◇) and  $\text{H}_2$  (△),  $\text{CO}$  (●), in mol % and  $\text{H}_2/\text{CO}$  ratio (□) distribution of gas-phase products.  $\text{CH}_4 : \text{CO}_2 : \text{O}_2 = 1:0.7:0.3$ . ( $\text{CH}_4 = 20\%$ )

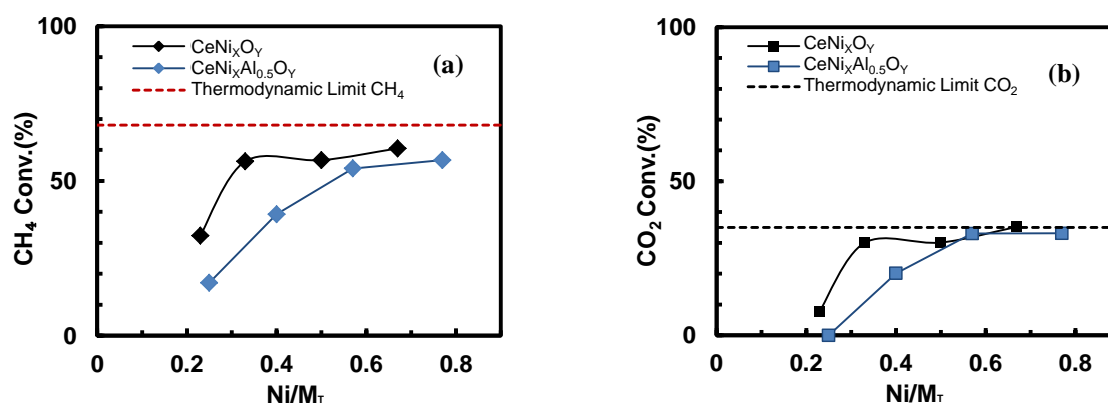
Although no carbon is measured after test by weighting, the catalyst is further analyzed after test by TPO analysis. As shown in **Fig. 4-12**, the TPO profile presents 2 peaks one at 460 °C and a very small broad one at 580 °C. As mentioned in above sections, different types of carbon can be formed, such as amorphous carbon or mixture of CNFs and CNTs, which leading to high stability without noticeable decrease in ODRM for 24 h time on stream. In the literature, a peak at  $450 \pm 20$  °C was interpreted by migration of carbon atoms from the metal to the support [196]. Due to the ODRM test is performed at 700 °C in presence of  $\text{O}_2$ , the carbon formed could be easily oxidized in this condition. Therefore, further analysis should be done to identify the carbon.



**Fig. 4-12** TPO profile of used  $\text{CeNi}_2\text{Al}_{0.5}\text{O}_\gamma$  catalysts after ODRM for 24h

#### 4.2.5 The influence of Al in the catalysts

Fig. 4-13 illustrates the comparison between binary and ternary  $\text{CeNi}_x(\text{Al}_z)\text{O}_y$  catalysts in ODRM reaction. Both binary and ternary catalysts present high activity close to the thermodynamic limits. With  $\text{Ni}/\text{M}_T$  ratios higher than 0.5,  $\text{CeNi}_x\text{O}_y$  catalysts show similar activity to  $\text{CeNi}_x\text{Al}_{0.5}\text{O}_y$  compounds. On the other hand, when the  $\text{Ni}/\text{M}_T$  ratio is lower than 0.5, binary catalysts provide higher  $\text{CH}_4$  and  $\text{CO}_2$  conversions than the ternary compounds. Moreover, the  $\text{H}_2/\text{CO}$  ratio slightly declines with the  $\text{Ni}/\text{M}_T$  increasing. Carbon formation rate increases exponentially with Ni content. Clearly, catalysts with Al have a distinct advantage over the binary catalyst in the aspect of mitigating carbon deposition. In fact, the evolution of conversions and carbon formation rates are similar with that in dry reforming. It is important to recall that the strong interactions between Ni and Ce and/or Al species are strengthened in  $\text{CeNi}_x\text{Al}_{0.5}\text{O}_y$  compounds. It is also known that the Ce-Ni-Al-O solid solution formed has good thermal stability and better oxygen storage capacity than  $\text{CeO}_2$  alone [179]. XRD results reveal that the average NiO crystallite size is also minimized to 7 nm by the presence of Al. Smaller size of NiO crystallites has been proposed as a main factor for mitigating carbon deposition and offering high and stable activity, and this is also observed in the present study. As a matter of fact, with the similar results in high Ni content compounds, the addition of aluminum is also beneficial for replacing more cerium by nickel in the catalyst, as we know, nickel is much cheaper than cerium, therefore, low cost could be achieved by alternating the formulation of the catalyst.



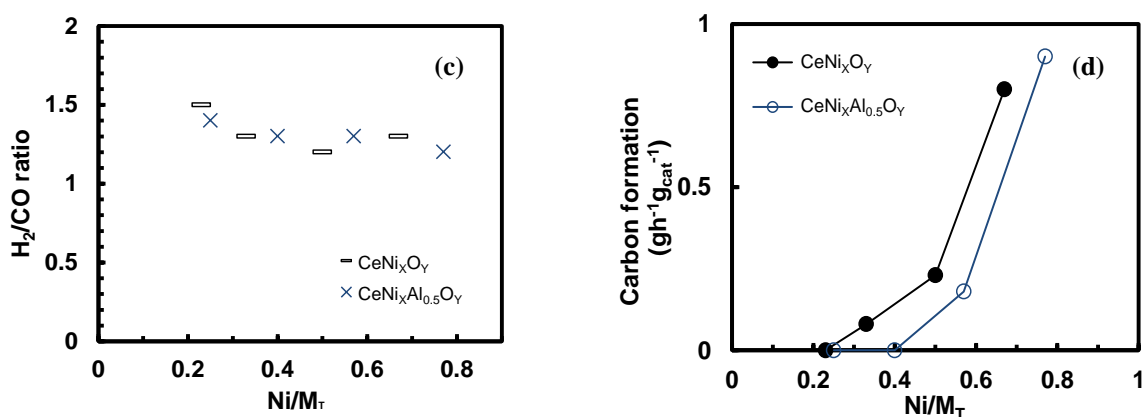


**Fig. 4-13** ODRM reaction at 600 °C ( $\text{CH}_4:\text{CO}_2:\text{O}_2=1:0.7:0.3$ ) on  $\text{CeNi}_x(\text{Al}_z)\text{O}_y$  catalysts (10 mg) without pretreatment. (a)  $\text{CH}_4$  conversion, (b)  $\text{CO}_2$  conversion, (c)  $\text{H}_2/\text{CO}$  molar ratio, and (d) carbon formation rate. Thermodynamic limit ( ---)

## Conclusions

In this chapter, the binary ( $\text{CeNi}_x\text{O}_y$ ) and ternary ( $\text{CeNi}_x\text{Al}_{0.5}\text{O}_y$ ) mixed oxides were tested in oxidative dry reforming of methane (ODRM) and the results were compared with the classical dry reforming. The effect of temperature, nickel content, and  $\text{O}_2$  addition were investigated.

The addition of  $\text{O}_2$  increases  $\text{CH}_4$  conversion but decreases  $\text{CO}_2$  conversion. As expected, the addition of oxygen reduces carbon formation greatly, which helps to maintain the activity and stability. Moreover,  $\text{O}_2/\text{CH}_4=0.3$  could be the optimized condition due to high activity, selectivity and low carbon formation.

It can be concluded that, Ni content strongly affects conversions and carbon formation. All of the experiments evidence an increase of methane conversion with the increasing Ni content. However, the carbon deposition trend also follows the raise of Ni content. With the presence of Al, carbon formation rate over ternary catalysts is lower than on binary catalysts with similar Ni content. Moreover, the  $\text{CeNi}_2\text{Al}_{0.5}\text{O}_y$  catalyst operates at 700 °C showing no sign of deactivation during 24 h with a ratio of  $\text{O}_2/\text{CH}_4=0.3$  in the feed mixture. Conversions of  $\text{CH}_4$  at 77% and of  $\text{CO}_2$  at 63% are still obtained after 24h of reaction. A relatively high and stable rate of conversion and a relatively low carbon deposition are obtained. The ODRM exhibits high conversion rates and selectivity on the  $\text{CeNi}_x\text{O}_y$  and  $\text{CeNi}_x\text{Al}_{0.5}\text{O}_y$  catalysts, demonstrating that this coupled reaction can be performed efficiently and stably.

# **Chapter 5**

## **General discussion**



## 5 General discussion

### 5.1 Comparison and discussion

In the present study, several series of Ni-based catalysts are studied,  $\text{CeNi}_x(\text{Al}_z)\text{O}_y$  ( $z=0$  or  $0.5$ ) and  $\text{Ni}_x\text{Mg}_2\text{AlO}_y$  mixed oxides, prepared by co-precipitation method, and SBA-15 supported Ni catalysts ( $\text{Ni}_x/\text{SBA-15}$ ), prepared by deposition-precipitation method.

The surface areas for  $\text{CeNi}_x\text{O}_y$  ( $x=0.1, 0.3, 0.5, 1$ ) compounds are ranging between  $95\text{-}127\text{ m}^2\text{ g}^{-1}$ . Whereas ternary  $\text{CeNi}_x\text{Al}_{0.5}\text{O}_y$  ( $x=0.5, 1, 2, 5$ ) compounds have larger surface areas ranging from  $73$  to  $141\text{ m}^2\text{ g}^{-1}$ . In  $\text{CeNi}_x(\text{Al}_z)\text{O}_y$  based catalysts, only a ceria like phase is clearly apparent in each sample, while the NiO crystalline phase can be detected in high Ni content compounds;  $x \geq 0.5$  for binary and  $x > 0.5$  for ternary compounds. No crystallographic structure involving aluminum has ever been detected in these catalysts. Adding Al into Ce-Ni system leads to a delay of the appearance of NiO crystalline phase with Ni content. For  $\text{CeNi}_x\text{O}_y$  catalysts, the average crystallites size is found at about  $4\text{-}5\text{ nm}$  for  $\text{CeO}_2$  and  $8\text{-}10\text{ nm}$  for NiO while for  $\text{CeNi}_x\text{Al}_{0.5}\text{O}_y$  catalysts, the average crystallites size of NiO is at  $5\text{-}7\text{ nm}$ . Raman and XPS results evidence the existence of strong interactions between nickel and cerium (and aluminum) species in agreement with the presence of a solid solution. Therefore, the  $\text{CeNi}_x(\text{Al}_z)\text{O}_y$  compounds can be described as a mixture of NiO and  $\text{CeO}_2$  nanoparticles, coexisting with a cerium-nickel-(aluminum) solid solution.

The reduction of  $\text{Ni}^{2+}$  species in different environments can be observed in  $\text{CeNi}_x(\text{Al}_z)\text{O}_y$  compounds.  $\text{CeNi}_x\text{O}_y$  solids possess Ni species presenting a reduction peak at about  $250\text{ }^\circ\text{C}$ , able to be reduced and reoxidized easily and reversibly allowed by their close interaction with Ce species, in complement to Ni species related to the presence of NiO presenting a reduction peak at higher temperature. On the other hand, the  $\text{CeNi}_x\text{Al}_{0.5}\text{O}_y$  mixed oxides show peaks at low temperature (around  $250\text{ }^\circ\text{C}$ ) and higher temperatures ( $450\text{-}500\text{ }^\circ\text{C}$ ) regardless of the Ni content. This phenomenon is assigned to the reduction of  $\text{Ni}^{2+}$  in different environments: 1) in small NiO nanoparticles and/or in solid solution at low temperature; and 2) in larger NiO nanoparticles (visible by XRD) at higher temperature. The addition of Al influences the reducibility of the catalysts.

$\text{Ni}_x\text{Mg}_2\text{AlO}_y$  catalysts ( $x= 1, 3$  and  $12$ ) with different Ni contents are also studied. They are assigned to a mixture of nanoparticles of NiO, MgO and/or solid solution of Ni-Mg-(Al)-O. Very small and uniform nano-crystallites ranging between 3-6 nm are obtained depending on the Ni content. The surface areas of these compounds are ranging between 100 and 200  $\text{m}^2 \text{g}^{-1}$ . The XPS, XRD and TPR results show the existence of strong interactions between Ni species and Mg and/or Al species in agreement with the formation of Ni-Mg-O and/or Ni-Mg-Al-O solid solution.

$\text{Ni}_x\text{Mg}_2\text{AlO}_y$  mixed oxides show a single broad TPR peak between 560 and 844 °C which is assigned to the reduction of Ni species. For low Ni content the strong interactions between nickel species and other cations either in Ni-Mg-(Al)-O solid solution and/or at the interfaces between small nanoparticles of NiO, MgO and/or Ni-Mg-(Al)-O make the solid difficult to reduce. Then, the increase of Ni content makes the solid becoming closer to that of bulk NiO, which is easier to be reduced. However, there are still strong interactions existing between Ni cations and some other cations.

$\text{Ni}_x/\text{SBA-15}$  catalysts, with 4 different Ni loadings (wt% = 5%, 10%, 20% and 40%), remain after calcination with quite high surface areas between 306-363  $\text{m}^2\text{g}^{-1}$ . High thermal stability of  $\text{Ni}_x/\text{SBA-15}$  catalysts is revealed by *in situ* XRD and confirmed by TEM. For low Ni loading, the Ni species are well dispersed on the surface of SBA-15. For higher Ni loadings, more Ni species are loaded and extended surround the edges instead of inside the silica grains. The alteration of the ordered structure is confirmed by TEM, which also reveals that filaments are formed preferentially outside the silica grain. Moreover, with increasing metal loading, both the number and length of phyllosilicates are growing, regardless of out and inside the silica grain.

The catalyst with highest Ni loading presents a higher reduction temperature than low Ni content samples. Thus, for higher reduction temperature, partial reduction of Ni phyllosilicate leads to very well dispersed Ni metal particles and the non-rigorous phyllosilicate filaments. The remained unsupported phyllosilicates are located both inside the support and on the external surface. For all the samples, to observe Ni species in the only  $\text{Ni}^0$  state, a total reduction at 800 °C is required. Besides, the nanoparticles are not sintering even for high metal loading.

Table 5-1 summarizes the average crystallites/particles size of each type of catalysts. It is clear that for all the catalysts, nano-particles are obtained (with sizes lower than 10 nm).

Small particles size is a main factor for methane reforming reaction, not only for the activity, but also for selectivity. Literature [180] reveals that the ensemble size necessary for carbon formation is larger than that for methane reforming. Duprez et al. [34] studied the particles size effect over the catalytic activity and carbon deposition in the cyclopentane hydrogenolysis and they observed that the nucleation of carbon starts on particles with a diameter larger than 6 nm.

Table 5-1 Average crystallites/particles size of the catalysts

Catalyst	Mean crystallites/particles size (nm)	
	Oxide containing Ni	CeO <sub>2</sub>
CeNi <sub>x</sub> O <sub>y</sub>	8-10	4-5
CeNi <sub>x</sub> Al <sub>0.5</sub> O <sub>y</sub>	5-7	4
Ni <sub>x</sub> Mg <sub>2</sub> AlO <sub>y</sub>	3-6	/
Ni <sub>x</sub> /SBA-15	3-7	/

All the catalysts are studied in dry reforming of CH<sub>4</sub> (DRM). The influence of different parameters is examined, such as the reaction temperature, pretreatment in H<sub>2</sub>, Ni content, reactants concentration and the mass of catalyst.

For CeNi<sub>x</sub>(Al<sub>z</sub>)O<sub>y</sub> (z = 0 or 0.5) catalysts, reaction temperature, Ni content and the presence of Al pronouncedly influence conversions and products distribution. In DRM performed in diluted conditions (CH<sub>4</sub> = 20%), the influence of the pretreatment temperature in H<sub>2</sub> has been studied on some compounds. On CeNi<sub>0.5</sub>O<sub>y</sub> catalyst, similar CH<sub>4</sub> and CO<sub>2</sub> conversions (31% for CH<sub>4</sub> and 45% for CO<sub>2</sub>) are obtained under the condition of without pretreatment and pretreatment in H<sub>2</sub> at 250 °C. However, the absence of pretreatment leads to a higher carbon formation rate (0.28 g g<sub>cat</sub><sup>-1</sup> h<sup>-1</sup>) compared to with a pretreatment in H<sub>2</sub> at 250 °C (0.19 g g<sub>cat</sub><sup>-1</sup> h<sup>-1</sup>). Increasing pretreatment temperature in H<sub>2</sub> up to 600 °C leads to lower conversions (20 % for CH<sub>4</sub> and 29 % for CO<sub>2</sub>) and higher carbon formation rate (0.32 g g<sub>cat</sub><sup>-1</sup> h<sup>-1</sup>), which indicates that changing pretreatment temperature has different effects on conversion evolutions and carbon formation rate. For CeNi<sub>2</sub>Al<sub>0.5</sub>O<sub>y</sub> catalyst, pretreatment at 600 °C also leads to an increase of the carbon formation rate to 2.42 g g<sub>cat</sub><sup>-1</sup> h<sup>-1</sup>. The optimum treatment temperature in H<sub>2</sub> can be proposed at 250 °C taking into account conversions, products distribution, and carbon formation. It could be related to the reduction of Ni species being able to be reduced and reoxidized readily and

reversibly in  $\text{CeNi}_x(\text{Al}_z)\text{O}_y$  compounds at this temperature. Conversions globally increase with Ni content while  $\text{H}_2/\text{CO}$  ratio maintains between 0.7-0.8, which is close to the thermodynamic limit of 0.84. Moreover, solid carbon is formed and it also increases with Ni content.  $\text{CeNi}_2\text{Al}_{0.5}\text{O}_y$  is evidenced to be the best catalyst in the ternary series analyzed due to the high activity: 37.2% of  $\text{CH}_4$  conversion and 48.5% of  $\text{CO}_2$  conversion at 600 °C.

The  $\text{CeNi}_x\text{O}_y$  catalyst allows obtaining a good activity even in the severe conditions of DRM ( $\text{CH}_4/\text{CO}_2 = 50/50\%$ ). For low Ni content  $\text{CeNi}_{0.3}\text{O}_y$  catalyst, conversions are quite constant, and carbon formation is well suppressed. On the other hand, high Ni content catalysts,  $\text{CeNi}_1\text{O}_y$  and  $\text{CeNi}_2\text{O}_y$  show higher activity with a decrease of conversions at the initial period of time certainly due to a higher carbon formation.

The long-term DRM stability test is studied on  $\text{CeNi}_{0.5}\text{O}_y$  and  $\text{CeNi}_{0.3}\text{O}_y$  catalysts under different conditions. In 20%  $\text{CH}_4$  condition at 700 °C, the  $\text{CH}_4$  and  $\text{CO}_2$  conversions reach 60% and 72%, respectively, after 50 h of reaction on 50mg of  $\text{CeNi}_{0.5}\text{O}_y$ , showing good stability towards carbon deposition. In stability test at 600 °C under harsh conditions, the catalytic activity of  $\text{CeNi}_{0.3}\text{O}_y$  towards  $\text{CH}_4$  and  $\text{CO}_2$  reach conversions of 41 and 49%, respectively. And the  $\text{H}_2/\text{CO}$  molar ratio obtained is about 0.76. Similarly, stable results are also obtained on  $\text{CeNi}_{0.5}\text{Al}_{0.5}\text{O}_y$  catalyst in DRM reaction at 600 °C without suffering from activity loss after 60 h of reaction under harsh conditions. Finally, the addition of Al into the Ce-Ni system decreases the conversions for both  $\text{CH}_4$  and  $\text{CO}_2$  for low Ni content, but maintains high activity in catalysts with high Ni contents. Anyway, the carbon resistance ability is always enhanced.

The well dispersed  $\text{Ni}_x\text{Mg}_2\text{AlO}_y$  catalysts demonstrate high efficiency toward DRM between 600°C and 700 °C. Treatment temperature in  $\text{H}_2$  of the catalyst has slight influence on activity in stabilized state. However, there is a different evolution of conversions and  $\text{H}_2/\text{CO}$  ratio at first period of time on stream. Without pretreatment the  $\text{Ni}_1\text{Mg}_2\text{AlO}_y$  catalyst shows an increase of conversions of  $\text{CH}_4$  and  $\text{CO}_2$  in the first 3 h of test. Moreover, higher pretreatment temperature in  $\text{H}_2$  at 550 °C or without pretreatment leads to an increase of the carbon deposition. The  $\text{Ni}_1\text{Mg}_2\text{AlO}_y$  catalyst allows the best results for the dry reforming of methane (20%  $\text{CH}_4$ -20%  $\text{CO}_2$ ) at the low temperature of 600 °C with 10mg of catalyst, 33% and 39% conversions of  $\text{CH}_4$  and  $\text{CO}_2$  are obtained with a high selectivity with a

$H_2/CO$  ratio of 0.9. The carbon formation rate is  $0.2 \text{ g g}_{\text{cat}}^{-1} \text{ h}^{-1}$ . In addition,  $Ni_1Mg_2AlO_Y$  catalyst in the 50h test at  $700 \text{ }^\circ\text{C}$  in pure  $CH_4$  and  $CO_2$  reactants shows a remarkable stability along the whole experiment.

The  $Ni_x/SBA-15$  catalysts show similar conversions during DRM ( $CH_4 = 20\%$ ) that do not depend strongly on Ni-loading. Pretreatment in  $H_2$  at  $600 \text{ }^\circ\text{C}$  has a different effect on the catalysts with different Ni loading. The promoted result is only obtained on  $Ni_{20\%}/SBA-15$  catalyst. For  $Ni_{40\%}/SBA-15$ , increasing the pretreatment temperature has negative effect on conversions and selectivity for catalysts in the test at  $600 \text{ }^\circ\text{C}$ . The  $Ni_{40\%}/SBA-15$  with highest Ni loading is the most active one since 27% and 37% of  $CH_4$  and  $CO_2$  conversions are reached, respectively, at  $600 \text{ }^\circ\text{C}$ , while 57% of  $CH_4$  and 68% of  $CO_2$  conversions are obtained at  $700 \text{ }^\circ\text{C}$ .

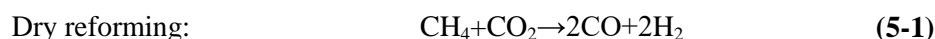
As a summary, pretreatments in  $H_2$  of the catalysts have different influence on conversions evolution and products distribution in all the catalysts tested. It seems that the samples reach a similar activity for  $CH_4$  and  $CO_2$  at stabilized state without pretreatment or pretreated at proper temperature. Anyway, for all the studied catalysts, without pretreatment or pretreated at high temperatures (over reduced) lead to more carbon formed, meaning that reduced in reaction conditions or in  $H_2$  at too high temperature promotes a structure of the nickel particles that increases the carbon deposition. These results indicate that the best catalytic activity and selectivity are obtained with partially reduced catalysts at appropriate temperatures.

Furthermore, the hydrogen production from oxidative dry reforming of methane (**Eq. 5-2**), is also analyzed on binary ( $CeNi_xO_Y$ ) and ternary ( $CeNi_xAl_{0.5}O_Y$ ) mixed oxides and compared to the classical dry reforming. The addition of  $O_2$  increases  $CH_4$  conversion but decreases  $CO_2$  conversion. As expected, the addition of oxygen reduces carbon formation greatly, which helps to maintain the activity and stability. Moreover,  $O_2/CH_4 = 0.3$  could be the optimized condition due to high activity, selectivity and low carbon formation. Clearly, Ni content strongly affects conversions and carbon formation, as increasing methane conversion and carbon deposition is observed with the increasing of Ni content. With the presence of Al, carbon formation rate over ternary catalysts is lower than that on binary catalysts with similar Ni content. The  $CeNi_2Al_{0.5}O_Y$  catalyst shows no sign of deactivation during 24 h of reaction with a ratio of  $O_2/CH_4=0.3$  in the feed mixture. A relatively high and stable rate of

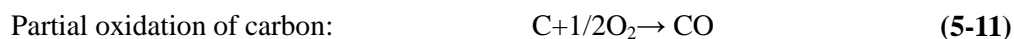
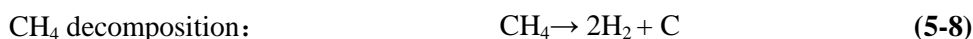
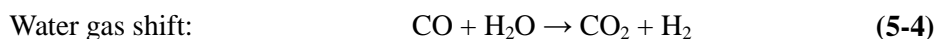
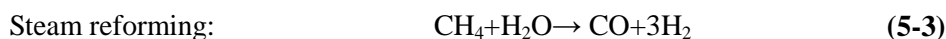
conversions of CH<sub>4</sub> (77%) and CO<sub>2</sub> (63%) and a relatively low carbon deposition are obtained after 24h of the test at 700 °C with CeNi<sub>2</sub>Al<sub>0.5</sub>O<sub>Y</sub> catalysts. The ODRM exhibits high conversion rates and selectivity on the CeNi<sub>X</sub>O<sub>Y</sub> and CeNi<sub>X</sub>Al<sub>0.5</sub>O<sub>Y</sub> catalysts, demonstrating that this coupled reaction can be performed efficiently and stably.

Dry reforming process is incorporating many side reactions (Eqs. 5-3 - 5-8). In presence of O<sub>2</sub>, the system is even more complicated with several reactions related to O<sub>2</sub> (Eqs. 5-9 – 5-12). With the objective to produce H<sub>2</sub> and CO, different Ni-based catalysts could have different performances based on the environment of Ni species.

#### Main reactions



#### Side reactions

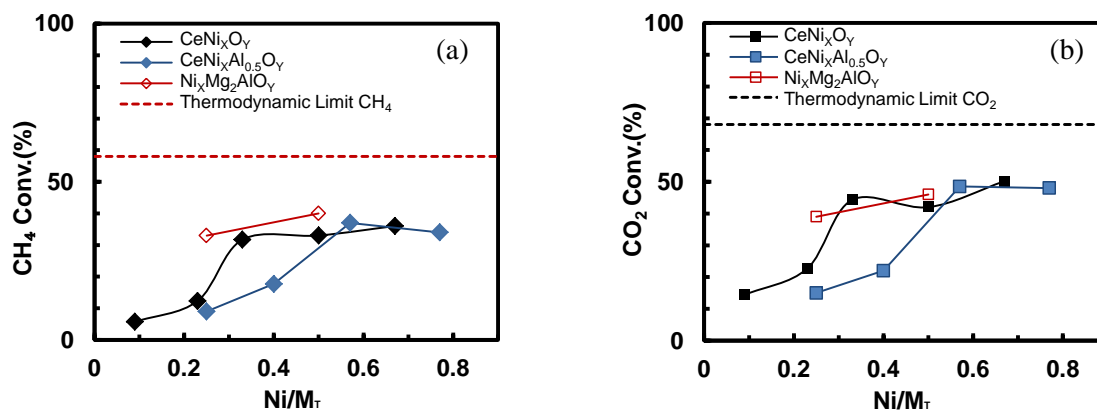


## 5.2 Proposal of active site and possible mechanism

Ni is recognized as an efficient active element and often used in the composition of catalysts for DRM, as largely reviewed [83], [69], [84], [85]. However, the exact nature of the active species is still under debate in the literature. In order to determine the active phase/active species converting methane and CO<sub>2</sub>, a comparison is illustrated in Fig. 5-1, which reports activity, selectivity and carbon

formation rate in DRM measured at 600 °C as a function of the Ni proportion in the different studied compounds.

**Fig. 5-1(a)** and (b) reports the activity at 600 °C in diluted conditions ( $\text{CH}_4:\text{CO}_2=20\%:20$ ) for  $\text{CH}_4$  and  $\text{CO}_2$  transformations with different catalysts. Catalysts activities increase with Ni content up to limited values with a kind of stabilization. This shows the important role that nickel plays in the dry reforming reaction. The different catalysts studied exhibit similar activity with high Ni content when  $\text{Ni}/\text{M}_\text{T}$  ratio higher than 0.5 with  $\text{CH}_4$  conversion of about 35-40%. The catalytic ability is reaching a limit, whatever the compound is. Main differences in conversions can be observed at low  $\text{Ni}/\text{M}_\text{T}$  ratio, where the number of active Ni species in each compound increases with Ni content in different structures and different Ni-M cation environment. For  $\text{Ni}/\text{M}_\text{T} > 0.2$  the  $\text{H}_2/\text{CO}$  ratio becomes steady for all the compounds, in particular on  $\text{CeNi}_x\text{Al}_{0.5}\text{O}_y$  catalysts. **Fig. 5-1 (d)** and (e) displays that the carbon formation rate is increased significantly with Ni content in all compounds, but with different slopes, showing that the environment of Ni species in the different compounds has a high impact on carbon formation rate. Clearly, with high Ni content, the activity is stabilized while carbon generation is increasing with Ni.



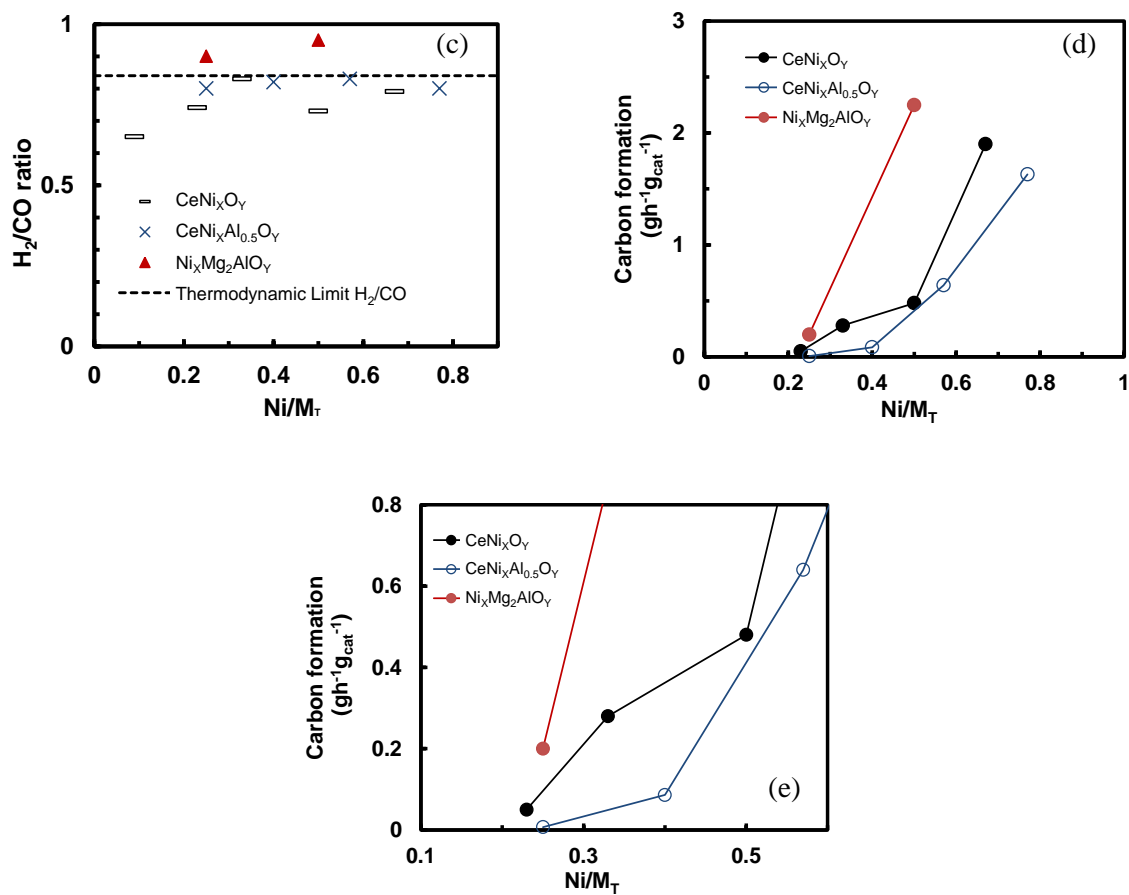


**Fig. 5-1** DRM reaction at 600 °C carried out over Ni based catalysts (10 mg) without pretreatment.  $\text{CH}_4:\text{CO}_2=20\%:20\%$ . (a)  $\text{CH}_4$  conversion, (b)  $\text{CO}_2$  conversion, (c)  $\text{H}_2/\text{CO}$  molar ratio, (d) Carbon formation rate. (e) Carbon formation rate (zoom of d)

As shown in **Fig. 5-2**, the  $\text{Ni}_x/\text{SBA-15}$  catalysts are tested in the same conditions ( $\text{CH}_4:\text{CO}_2=20\%:20\%$ ) at 600 °C. Increasing the Ni wt% from 5% to 40% just leads to very limited increase (5%) on conversions of  $\text{CH}_4$  and  $\text{CO}_2$ . Only the  $\text{H}_2/\text{CO}$  ratio increases from 0.50 to 0.60. It is clear that the catalyst with 5wt% of Ni presents a high proportion of active Ni species compared to the catalysts with higher Ni loadings. Therefore, the highest proportion of active Ni species is obtained at the low Ni loading, where the highest proportion on Ni species is found in high interaction.

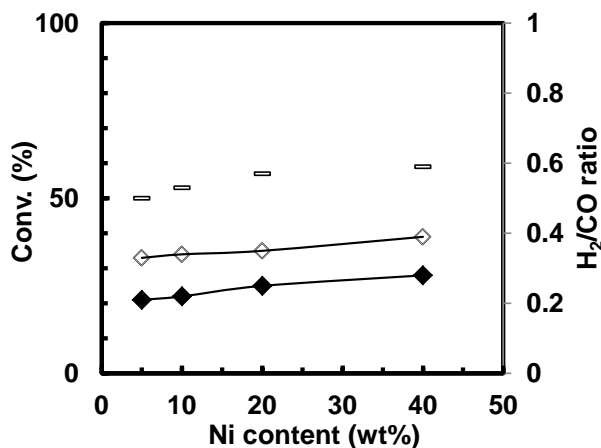


**Fig. 5-2** CH<sub>4</sub> (◆), CO<sub>2</sub> (◇) conversions, and H<sub>2</sub>/CO ratio (□) at 600 °C obtained versus Ni content over the Ni<sub>x</sub>/SBA-15 catalysts (10 mg) without pretreatment. CH<sub>4</sub>:CO<sub>2</sub> = 20%:20%.

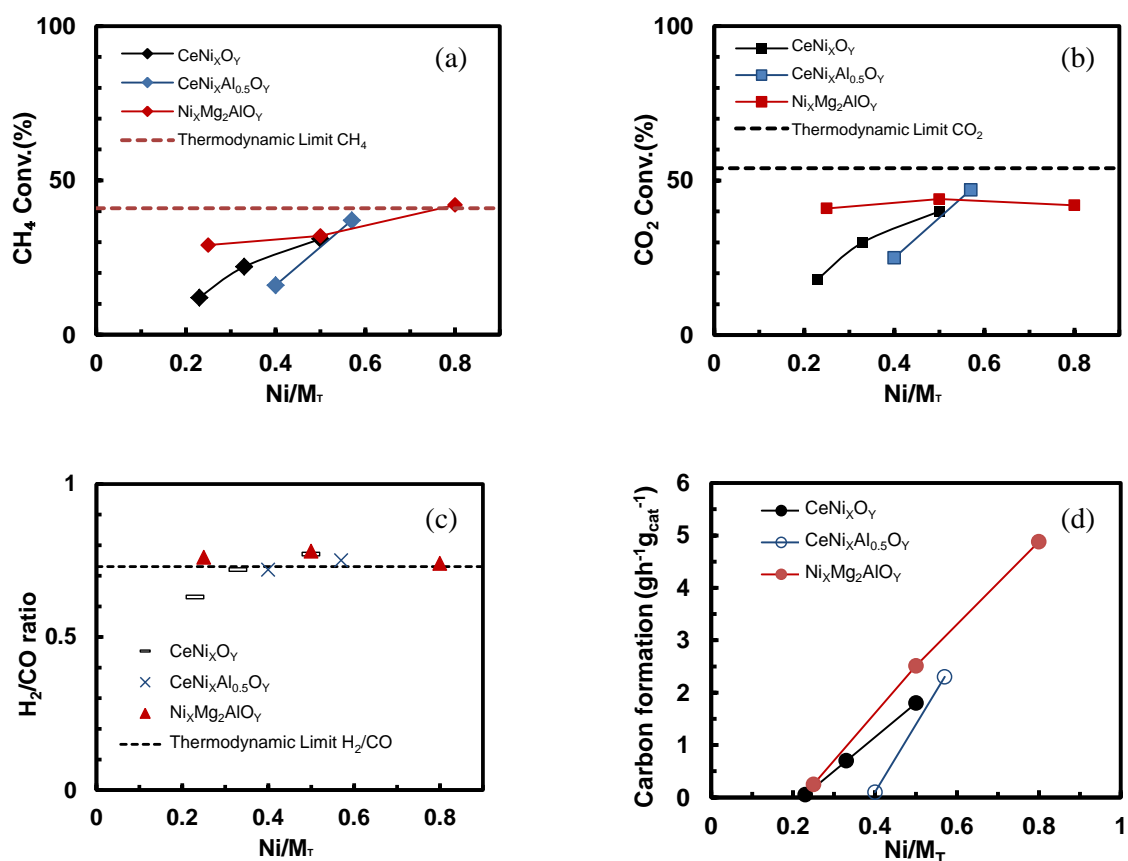
DRM reaction at 600 °C is also conducted in high concentration (harsh) conditions (CH<sub>4</sub>:CO<sub>2</sub> = 50:50%). It should be emphasized that, low reaction temperature and low mass of catalyst is always employed in this study to optimize the analysis. As shown in **Fig. 5-3**, similar trends for activity and carbon formation are obtained at 600 °C with Ni content over the different catalysts in harsh conditions. All of them follow an increase with Ni/M<sub>T</sub> ratio up to stabilization for a Ni/M<sub>T</sub> ratio of about 0.5. It is very interesting to find out that all the catalysts exhibit very good similarity in catalytic behaviors at Ni/M<sub>T</sub> ≈ 0.5, exhibiting very similar methane and CO<sub>2</sub> conversions about 30% and 40%, respectively, as well as a H<sub>2</sub>/CO ratio around 0.7. As observed in diluted conditions, the main differences in conversions can be observed at low Ni/M<sub>T</sub> ratio, where the number of active Ni species in each compound increases with Ni content, and where the Ni species are in different structures and with different Ni-M cation environment. For example, the Ni<sub>1</sub>Mg<sub>2</sub>AlO<sub>Y</sub> catalyst shows interesting performances.

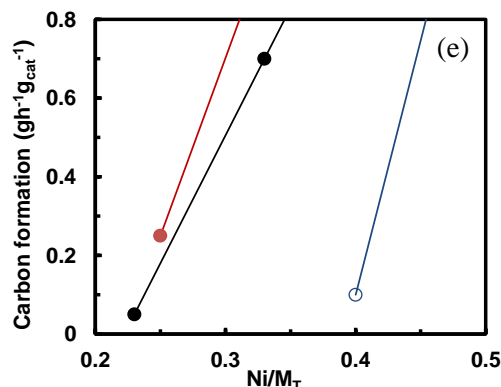
As shown in **Fig. 5-3(d)**, globally, the carbon deposition increases with Ni content, and it follows different slopes depending on the different environment of Ni species. As an example, CeNi<sub>x</sub>Al<sub>0.5</sub>O<sub>Y</sub> catalysts are more resistant to carbon formation. This could be due to the small crystallites size of ceria at 4 nm. The oxygen mobility is more rapid in smaller ceria crystallites than that in bigger ones because the smaller crystallites have shorter diffusion path of oxygen anions from the material bulk to the surface. As seen in **Table 5.2**, Ni<sub>20</sub>%/SBA-15 catalyst also provides stable results with low carbon formation.

This could be explained by the metal-support interaction and confinement effect of mesoporous silica support.

Some differences can be seen in conversions evolution and products distribution for low Ni content. It is relatively logical that the influence of the second (or third) cation is easier to be seen when it is found in higher concentration, when strong interactions are improved due to the higher concentrations of Ce and Mg or Al cations, or even with the SBA-15 support.

In literatures, the experimental and theoretical studies confirmed that smaller Ni particles have a better ability to suppress the carbon deposition or to produce only amorphous surface carbon which oxidizes at low temperature [197][177][198]. Some researches are devoted to confining the Ni particles size within the nanoscale dimension, to avoid the sintering of the Ni particles under severe reaction conditions of DRM [177].





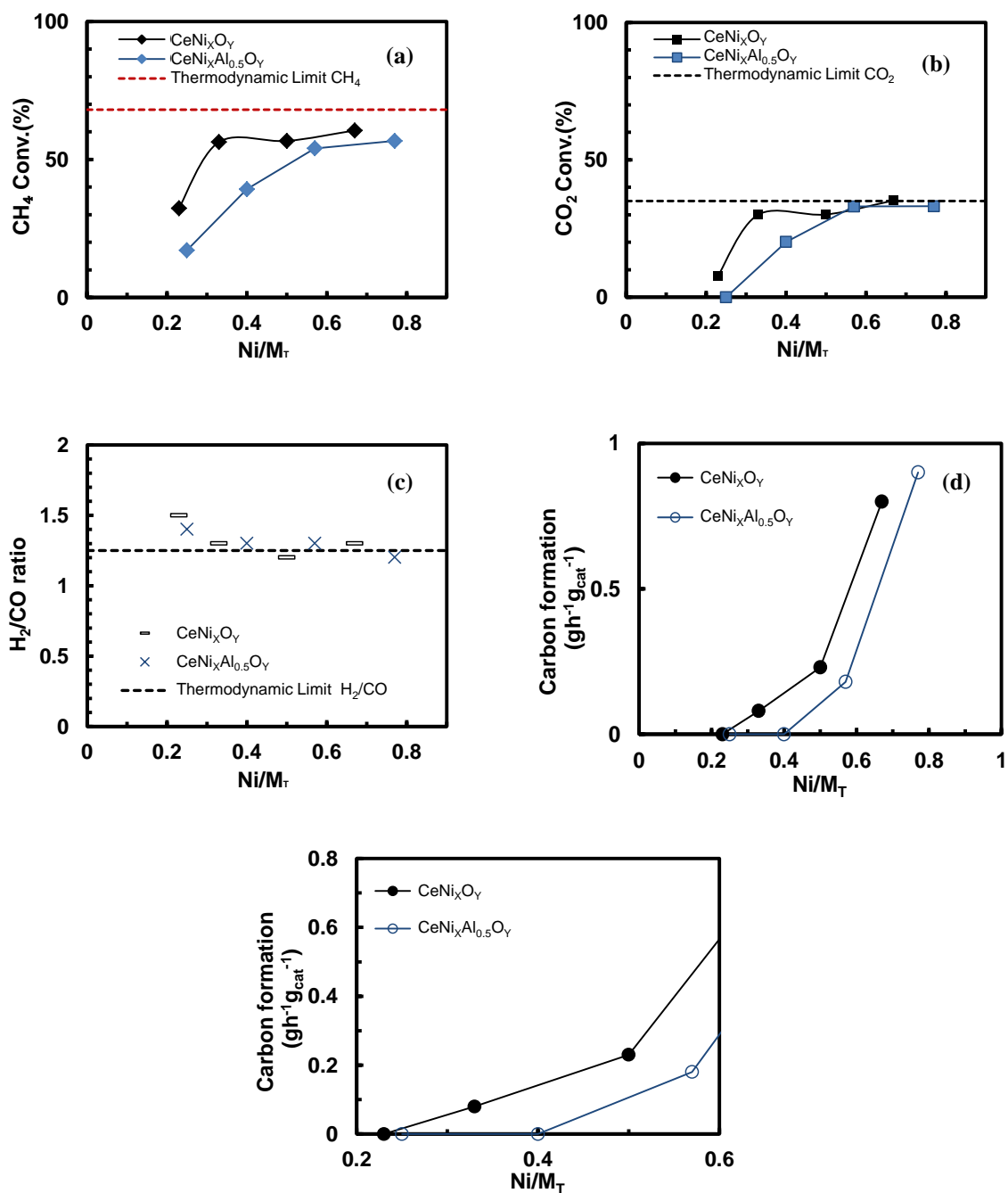
**Fig. 5-3.** DRM reaction at 600 °C carried out over Ni based catalysts (10 mg). CH<sub>4</sub>:CO<sub>2</sub>=50%:50%. (a) CH<sub>4</sub> conversion, (b) CO<sub>2</sub> conversion, (c) H<sub>2</sub>/CO molar ratio, (d) Carbon formation rate, (e) Carbon formation rate (zoom of d). CeNi<sub>x</sub>(Al<sub>z</sub>)O<sub>y</sub> catalysts pretreated in H<sub>2</sub> at 250 °C; Ni<sub>x</sub>Mg<sub>2</sub>AlO<sub>y</sub> catalysts pretreated in H<sub>2</sub> at 450 °C. All the results reported after 5h of time on stream except for Ni<sub>12</sub>Mg<sub>2</sub>AlO<sub>y</sub> (2h).

Table 5-2 DRM reaction at 600 °C on Ni<sub>20</sub>%-SBA15 (10 mg) pretreated in H<sub>2</sub> at 600 °C (CH<sub>4</sub>:CO<sub>2</sub>=50%:50%)

Catalyst	Reaction (°C)	CH <sub>4</sub> conv. (%)	CO <sub>2</sub> conv. (%)	H <sub>2</sub> /CO ratio	Carbon formation rate (g g <sub>cat</sub> <sup>-1</sup> h <sup>-1</sup> )
Ni <sub>20</sub> %-SBA15	600	16	25	0.70	0.14

As the gasification of adsorbed carbon from CH<sub>4</sub> fragments could occur on nickel surface as well as at the boundary of nickel-support, a well dispersed Ni species on the surface with strong interactions, help to mitigate carbon deposition and to gasify the carbon immediately. In a similar study, Zuo [126] suggested that the most substantial metal-support interaction (MSI) between NiO and support was formed in the dual-support Mg-Al mixed oxides and SBA-15 catalysts. Moreover, the existence of MSI decreased the probability of aggregation of Ni species, further reducing the potential of carbon formation.

Furthermore, it is interesting to analyse the activity of Ni species in presence of O<sub>2</sub>. **Fig. 5-4** compares catalytic results in ODRM at 600 °C with CH<sub>4</sub>:CO<sub>2</sub>:O<sub>2</sub>=1:0.7:0.3 conditions on CeNi<sub>x</sub>(Al<sub>0.5</sub>)O<sub>y</sub> catalysts as a function of the Ni proportion in the compounds. It is important to note that total oxygen conversion is obtained in all tests independently on any parameters. Similar as DRM, conversions are found to obey an increase curve with Ni molar ratio. CeNi<sub>x</sub>O<sub>y</sub> catalysts seem to show a steadily higher methane conversion than the value obtained on CeNi<sub>x</sub>Al<sub>0.5</sub>O<sub>y</sub> catalysts. All the conversions and H<sub>2</sub>/CO ratio reach thermodynamic values when Ni/M<sub>T</sub> at about 0.5. However, some difference in activities can be observed on CeNi<sub>x</sub>O<sub>y</sub> and CeNi<sub>x</sub>Al<sub>0.5</sub>O<sub>y</sub> catalysts at low Ni contents.



**Fig. 5-4** ODRM reaction at 600 °C carried out over  $\text{CeNi}_x(\text{Al}_{0.5})\text{O}_y$  catalysts (10 mg) without pretreatment.  $\text{CH}_4:\text{CO}_2:\text{O}_2=1:0.7:0.3$ . (a) CH<sub>4</sub> conversion, (b) CO<sub>2</sub> conversion, (c) H<sub>2</sub>/CO molar ratio, (d) Carbon formation rate, (e) Carbon formation rate (zoom of d).

**Table 5-3** shows the difference between DRM and ODRM over  $\text{CeNi}_2\text{Al}_{0.5}\text{O}_y$  catalyst, where the experiment noted at  $\text{O}_2/\text{CH}_4$  zero corresponds to dry reforming (with  $\text{CH}_4:\text{CO}_2=1:0.7$  conditions), for comparison. It can be clearly seen that the conversion of CH<sub>4</sub> increases while the conversion of CO<sub>2</sub> decreases in presence of oxygen. High rate of conversion and low carbon deposition can be achieved by

adding the appropriate amount of O<sub>2</sub>.

**Table 5-3** Comparison of DRM and ODRM on CeNi<sub>2</sub>Al<sub>0.5</sub>O<sub>Y</sub> at 600 °C (50 mg) pretreated in H<sub>2</sub> at 250 °C

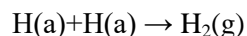
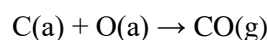
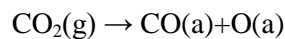
O <sub>2</sub> /CH <sub>4</sub> ratio	CH <sub>4</sub> conv. (%)	CO <sub>2</sub> conv. (%)	H <sub>2</sub> /CO ratio	Carbon formation rate (g g <sub>cat</sub> <sup>-1</sup> h <sup>-1</sup> )
0	51	67	1.0	0.6
0.3	63	49	1.3	0

After comparing all the catalysts in different conditions (DRM in diluted or pure reactants and ODRM in diluted reactants), clearly, all the different catalysts have Ni species behaving as active species. For low Ni content, there is a higher proportion of small nanoparticles and/or solid solution with the strong interactions able to dissociate methane without generating carbon. For example, strong interactions exist between nickel and cerium (and aluminum) species in cerium and nickel based compounds. Ni species can be surrounded and influenced greatly by different neighbor atoms, as Ni species are strongly interacting with Ce, Al or Mg species which is confirmed by (XRD, XPS, Raman and TPR) and also in supported SBA15 compounds. Higher Ni content catalysts with larger amount of Ni species promote the catalytic performance but limited by a certain value, while carbon formation is enhanced. Different Ni-based mixed oxides with the Ni/M<sub>T</sub> ratio higher than 0.5 demonstrate very similar catalytic performances for either DRM or ODRM. High Ni content has less and not proportional effect on conversions but product distributions, as increased carbon formation is obtained.

Metallic Ni<sup>0</sup> has been proposed to have an important role in the reaction when it is present. It is often reported that metallic nickel is beneficial to activate methane to syngas [199][132]. However, there is a debate on the exact nature of the active site on Ni based catalysts for reforming processes, in literature [200]. Some authors suggested that the nickel species with different oxidation state play a different role in surface reaction steps, and that the strong metal-oxide interaction produces active sites [201]. In a recent literature on Ir/CeO<sub>2</sub> catalyst [202], Siwei et al. confirmed that the chemical state of Ir could be finely tuned by altering the loading of the metal. They showed that the chemical state of Ir species, induced by a SMSI, has a major impact on the reaction selectivity in carbon dioxide hydrogenation reaction. They reported that the modulation of the chemical state of metal species by a strong metal–support interaction is important for regulation of the observed selectivity (metallic Ir

particles select for methane while partially oxidized Ir species select for CO production).

Besides, it has been proposed that the DRM [203] process likely involves the following series of sequential reactions:



Furthermore, in literature, it is generally accepted that the C–H bond activation is the determining (limiting) step in DRM reaction [204][161]. It has been proposed that once the first hydrogen is removed from the reactant molecule, a quick  $\text{CH}_3 \rightarrow \text{CH}_2 \rightarrow \text{CH} \rightarrow \text{C}$  transformation occurs on the surface and the deposited carbon could react with oxygen atoms to yield gaseous CO. The H atoms abstracted from the reactant could transfer to  $\text{H}_2$  or  $\text{H}_2\text{O}$ . Zongyuan et al. [99] studied DRM over Ni-CeO<sub>2</sub> catalyst, they suggested that the active phase of the catalyst consists of small nanoparticles of nickel dispersed on partially reduced ceria. Methane dissociated on Ni/CeO<sub>2</sub> at temperatures as low as 300 K, generating CH<sub>x</sub> and CO<sub>x</sub> species on the surface of the catalyst. The strong metal-support interactions activated Ni for the dissociation of methane.

It is often reported that the lattice oxygen atoms contribute to the gasification of CH<sub>x</sub>, which is helpful to the catalytic activity and the resistance to carbon deposition. It has strong influence on catalytic behavior. Literature showed that oxygen vacancies in Ce-Ni-(Al) based catalysts can be produced by the transformation between Ce<sup>3+</sup> and Ce<sup>4+</sup> [205]. The higher Ce<sup>3+</sup> percentage the more oxygen vacancies formed. On the other hand, the existence of Ni particles weakens the bond energy between Ni particles and oxygen atoms closed to Ni particles in the CeO<sub>2</sub> crystal lattice, which makes this kind of oxygen atom more easily to be reduced, so the number of oxygen vacancies can be increased [205].

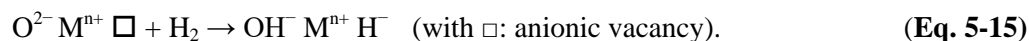
Clearly, all the results obtained in the present study cannot be explained by simply attributing the activity to Ni<sup>0</sup>. Depending on the catalytic results and characterizations, it is more probable that a high activity without carbon formation could be related to a partially reduced solid involving Ni cations.

Furthermore, the reduction process of the present CeNi<sub>x</sub>(Al<sub>z</sub>)O<sub>y</sub> catalysts can also facilitate the

formation of anionic vacancies at low temperature due to the existence of a redox process between Ni and Ce cations as (Eq. 5-13) and (Eq. 5-14) [149]. This phenomenon allows increasing the number of anionic vacancies [206].



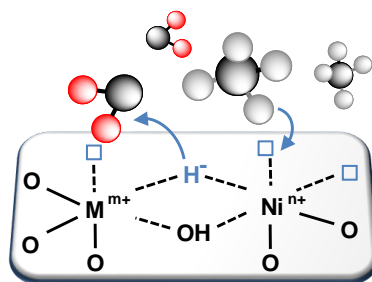
The pretreatment in  $\text{H}_2$  at 250 °C for  $\text{CeNi}_x(\text{Al}_z)\text{O}_y$  or 450 °C for  $\text{Ni}_x\text{Mg}_2\text{AlO}_y$  has significant effect on product distributions, leading to less carbon. In a previous study [207] of the relation between  $\text{H}^*$  contents and treatment temperature in this series of catalysts, it was clear that the treatment in  $\text{H}_2$  at an appropriate temperature  $T_T$  induces the creation of a large catalytic hydrogen reservoir that was related to the creation of anionic vacancies [130]. The anionic vacancies are able to receive hydrogen in a hydride form. During the activation in  $\text{H}_2$  (Eq. 5-15), the anionic vacancy is filled with hydride species by the heterolytic splitting of  $\text{H}_2$ :



Besides, it has been proposed that  $\text{CH}_4$  in presence of  $\text{O}_2$  (POM) can be also activated on an anionic vacancy on the cerium nickel based mixed oxides as reported in Eq. 5-16 [144][146]. Moreover, it is known that  $\text{CO}_2$  activation is very difficult, and the presence of strong metal support interactions, anionic vacancies and hydrogen species in the solids can help activating  $\text{CO}_2$  [202][208].

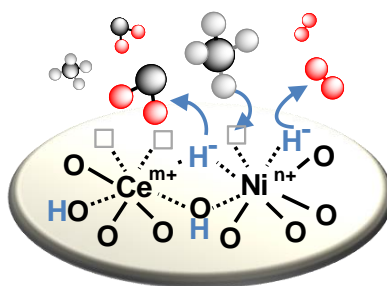


Taking into account the structure of the solids, an active site can be modeled by an ensemble of two cations in strong interaction involving anionic vacancies. Such a  $^x\text{M}-^y\text{M}'$  site is modeled by an ensemble of two cations in close interaction. Different ensembles  $^x\text{M}-^y\text{M}'$  as active sites depending on the distinct environment of nickel species can be created, x and y are the numbers of coordinative unsaturations, i.e. anionic vacancies on each cation, leading to Coordinatively Unsaturated Sites (CUS). An example is shown in Scheme 1 on the Ni-Mg-Al-O solid solution. The dehydrogenation of  $\text{CH}_4$  firstly requires the abstraction of hydrogen species from  $\text{CH}_4$ , with the rupture of C-H bond. Therefore, an active site involving an anionic vacancy and an  $\text{O}^{2-}$  species of the solid can be envisaged for the heterolytic dissociation of  $\text{CH}_4$  leading to the formation of C species. Then the C species could react with oxygen atoms of the solid to yield gaseous CO.



**Scheme 1.** Active site and proposition of mechanism on the Ni-Mg-Al-O solid solution. ( $\text{Ni}^{n+}$ :  $\text{Ni}^{2+}$  or  $\text{Ni}^{\delta+}$ ,  $\text{M}^{m+}$ :  $\text{Mg}^{2+}$  or  $\text{Al}^{3+}$  and  $\square$ : anionic vacancy (position and number arbitrary)).

In the case of ODRM reaction, highly reactive hydride species will react with  $\text{O}_2$  to generate hydroxyl groups (**Eq. 5-17**). The ability of the solid to abstract hydrogen species from  $\text{CH}_4$  is still the important step for the reaction. As an example, an active site constituted by an ensemble of two cations in close interaction in the solid solution of cerium and nickel is presented in **Scheme 2**. Therefore, by analogy to heterolytic dissociation of  $\text{H}_2$ , heterolytic dissociation of  $\text{CH}_4$  can be envisaged on a low coordination site involving an anionic vacancy as (**Eq. 5-16**). It also permits transformation of  $\text{O}_2$  into selective oxygen species  $\text{O}^{2-}$  which regenerates the active site (**Eq. 5-17** and **5-18**). The hydroxyl groups formed at the surface can lead to the formation and elimination of water (**Eq. 5-18**) [144].



**Scheme 2.** Active site and proposition of mechanism on the solid solution of cerium and nickel ( $\text{Ni}^{n+} = \text{Ni}^{2+}, \text{Ni}^{\delta+}$ ,  $\text{Ce}^{m+} = \text{Ce}^{4+}, \text{Ce}^{3+}$ ,  $\square$ : anionic vacancy (position and number arbitrary)).

# **Chapter 6**

## **General conclusion**



## 6 General conclusion

CeNi<sub>x</sub>(Al<sub>z</sub>)O<sub>y</sub>, Ni<sub>x</sub>Mg<sub>2</sub>AlO<sub>y</sub> and Ni<sub>x</sub>/SBA-15 catalysts are studied in dry reforming of methane (DRM) and the CeNi<sub>x</sub>(Al<sub>z</sub>)O<sub>y</sub> are further studied in oxidative dry reforming of methane (ODRM). All the tests are performed at low temperature between 600 -700 °C.

The CeNi<sub>x</sub>(Al<sub>z</sub>)O<sub>y</sub> (0.1 ≤ x ≤ 5 ; z=0 or 0.5) and Ni<sub>x</sub>Mg<sub>2</sub>AlO<sub>y</sub> (1 ≤ x ≤ 12) mixed oxides are prepared by the co-precipitation method, while the Ni<sub>x</sub>/SBA-15 (5% ≤ x ≤ 40%) catalysts are prepared by the deposition-precipitation method. All the catalysts are characterized by numerous physicochemical techniques. The surface areas of the CeNi<sub>x</sub>O<sub>y</sub> compounds are ranging between 95-127 m<sup>2</sup> g<sup>-1</sup>, whereas ternary CeNi<sub>x</sub>Al<sub>0.5</sub>O<sub>y</sub> compounds have larger surface areas ranging from 73 to 141 m<sup>2</sup> g<sup>-1</sup>. XRD shows that CeNi<sub>x</sub>O<sub>y</sub> compounds are constituted of nano-crystallites of CeO<sub>2</sub> (4-5 nm) and NiO (8-10 nm) depending on Ni content. While for CeNi<sub>x</sub>Al<sub>0.5</sub>O<sub>y</sub> compounds, the presence of aluminum mitigates the crystallites size of NiO to 5-7 nm (when visible by XRD). Raman and XPS results evidence the existence of strong interactions between nickel and cerium (aluminum) species. Therefore, the CeNi<sub>x</sub>(Al<sub>z</sub>)O<sub>y</sub> compounds can be ascribed as a mixture of CeO<sub>2</sub> and NiO nanoparticles, coexisting with a cerium-nickel-(aluminum) solid solution. The CeNi<sub>x</sub>(Al<sub>z</sub>)O<sub>y</sub> mixed oxides show TPR peaks at low and high temperatures regardless of the Ni content. This phenomenon is assigned to the reduction of Ni<sup>2+</sup> in different environments: 1) in solid solution and/or small NiO particles at low temperature; and 2) in larger NiO particles (visible by XRD) at higher temperature. The addition of Al influences the reducibility of the catalysts.

The surface areas of Ni<sub>x</sub>Mg<sub>2</sub>AlO<sub>y</sub> catalysts are ranging between 100 and 200 m<sup>2</sup> g<sup>-1</sup>. The nano-compounds are composed of small and uniform nanoparticles of NiO, MgO and/or the solid solution of Ni-Mg-(Al)-O with average crystallites sizes between 3-6 nm determined by XRD. The XPS, XRD and TPR results show the existence of strong interactions between Ni species and Mg and/or Al species due to the formation of Ni-Mg-O and/or Ni-Mg-Al-O solid solution. Ni<sub>x</sub>Mg<sub>2</sub>AlO<sub>y</sub> mixed oxides show a single broad TPR peak between 560 and 844 °C which is assigned to the reduction of Ni species. For low Ni content the strong interactions between nickel species and other cations either in Ni-Mg-(Al)-O solid solution and/or at the interfaces between small nanoparticles of NiO, MgO and/or

Ni-Mg-(Al)-O make the solid difficult to reduce.

Ni<sub>x</sub>/SBA-15 catalysts have quite high surface area values between 306-363 m<sup>2</sup>g<sup>-1</sup>. High thermal stability of Ni<sub>x</sub>/SBA-15 catalysts is revealed by *in situ* XRD and confirmed by TEM. For low Ni loading, the Ni species are well dispersed on the surface of SBA-15. For high Ni loading, more Ni species are loaded and extended surround the edges instead of inside the silica grains. The alteration of the ordered structure is confirmed by TEM, which also reveals that filaments are formed preferentially outside the silica grain. Moreover, with increasing metal loading, both the number and length of phyllosilicates are growing, regardless of out and inside the silica grain. The catalysts with higher Ni loading present a higher reduction temperature than lower Ni loading samples. Thus, for higher reduction temperature, the total reduction of Ni phyllosilicate leads to very well dispersed Ni metal particles and the non-rigorous phyllosilicate filaments. The remained unsupported phyllosilicates are located both inside the support and on the external surface.

Similar CH<sub>4</sub> and CO<sub>2</sub> conversions are obtained in DRM on CeNi<sub>0.5</sub>O<sub>Y</sub> catalyst, without pretreatment and after pretreated in H<sub>2</sub> at 250 °C. Without pretreatment or increasing pretreatment temperature up to 600 °C lead to higher carbon formation, indicating that changing pretreatment temperatures has different effect on carbon formation. The best candidate CeNi<sub>0.5</sub>O<sub>Y</sub> (50 mg) in DRM (CH<sub>4</sub>/CO<sub>2</sub> = 20%/20%) provides 60% of methane conversion and 72% of CO<sub>2</sub> conversion at 700 °C while the H<sub>2</sub>/CO ratio is 0.83, showing good stability towards the carbon deposition. Under hard conditions (10 mg of CeNi<sub>0.5</sub>O<sub>Y</sub> and CH<sub>4</sub>/CO<sub>2</sub> = 50%/50%) at low temperature of 600 °C, 22% conversion of CH<sub>4</sub> and 30% conversion of CO<sub>2</sub> are obtained, with a H<sub>2</sub>/CO ratio of 0.72. On CeNi<sub>2</sub>Al<sub>0.5</sub>O<sub>Y</sub> catalyst, without pretreatment and pretreatment at 600 °C also lead to higher amount of carbon formed. CeNi<sub>2</sub>Al<sub>0.5</sub>O<sub>Y</sub> catalyst, pretreated in H<sub>2</sub> at 250 °C, is evidenced to be the best catalyst in the ternary series analyzed due to the high activity at 600 °C in harsh condition (10 mg of catalyst, CH<sub>4</sub>/CO<sub>2</sub> = 50%/50%): 37% for CH<sub>4</sub> conversion and 48% for CO<sub>2</sub> conversion, and the H<sub>2</sub>/CO ratio is 0.75. Adding Al into the Ce-Ni system decreases the conversions for both CH<sub>4</sub> and CO<sub>2</sub> on low Ni content compounds, but maintains high activity in catalysts with high Ni content. Anyway, the carbon resistance ability is always enhanced.

Without or with pretreatment in H<sub>2</sub> at 450 °C has slight influence on the Ni<sub>x</sub>Mg<sub>2</sub>AlO<sub>Y</sub> catalysts

activity in stabilized state. However, higher treatment temperature in H<sub>2</sub> at 550 °C or without pretreatment leads to an increase of the carbon deposition. The Ni<sub>1</sub>Mg<sub>2</sub>AlO<sub>Y</sub> catalyst allows the best results for the dry reforming of methane (20% CH<sub>4</sub>-20% CO<sub>2</sub>) at the low temperature of 600 °C with 10 mg of catalyst, 33% and 39% conversions of CH<sub>4</sub> and CO<sub>2</sub> are obtained with a high selectivity with a H<sub>2</sub>/CO ratio of 0.9. The carbon formation rate is 0.20 g g<sub>cat</sub><sup>-1</sup> h<sup>-1</sup>. In harsh conditions (50% CH<sub>4</sub>-50% CO<sub>2</sub>), Ni<sub>1</sub>Mg<sub>2</sub>AlO<sub>Y</sub> allows a remarkable stability during at least 50h at 700 °C.

DRM on Ni<sub>x</sub>/SBA-15 catalysts do not depend strongly on Ni loading. Pretreatment in H<sub>2</sub> at 600 °C has a different effect on the catalysts with different Ni loadings. For Ni<sub>40</sub>/SBA-15, increasing the pretreatment temperature has negative effect on conversions and selectivity at 600 °C. A promoted result is only obtained on Ni<sub>20</sub>/SBA-15 catalyst. Conversions of 27% of CH<sub>4</sub> and 36% of CO<sub>2</sub> are obtained over 10 mg of Ni<sub>20</sub>/SBA-15 at low temperature of 600 °C (20% CH<sub>4</sub>-20% CO<sub>2</sub>).

Therefore, all the studied catalysts present high activities and selectivities allowing obtaining very interesting results in particular in harsh conditions i.e. at low temperature of 600 °C, in pure reactants (without dilution) and using a very low mass of catalyst (down to 10 mg). Globally, the carbon formation increases with Ni content.

The binary (CeNi<sub>X</sub>O<sub>Y</sub>) and ternary (CeNi<sub>X</sub>Al<sub>0.5</sub>O<sub>Y</sub>) mixed oxides are tested in ODRM and the results are compared with the classical dry reforming. The addition of O<sub>2</sub> increases CH<sub>4</sub> conversion but decreases CO<sub>2</sub> conversion. As expected, the addition of oxygen reduces carbon formation greatly, which helps to maintain the activity and stability. Moreover, O<sub>2</sub>/CH<sub>4</sub> = 0.3 could be the optimized condition due to high activity, selectivity and low carbon formation. For the condition of CeNi<sub>0.5</sub>O<sub>Y</sub> (10 mg) without pretreatment, 56% of CH<sub>4</sub> conversion and 30 % of CO<sub>2</sub> conversion are obtained, and the H<sub>2</sub>/CO ratio is 1.35. With the presence of Al, carbon formation rate is lower on ternary catalysts compared to binary catalysts with similar Ni content. The catalyst CeNi<sub>2</sub>Al<sub>0.5</sub>O<sub>Y</sub> operated at 700 °C shows no sign of deactivation during 24 h with a ratio of O<sub>2</sub>/CH<sub>4</sub> = 0.3 in the feed mixture with conversions of CH<sub>4</sub> at 77% and of CO<sub>2</sub> at 63%. A relatively high and stable rate of conversion and a relatively low carbon deposition are obtained.

All the catalysts show very similar evolution of CH<sub>4</sub> conversion and products distribution: increasing methane conversion with increasing Ni content (up to a limit), related to the homogeneous

distribution of the active Ni species surrounded by different neighbor atoms. However, the carbon deposition trend also follows the Ni content.

Finally, taking into account the structure and properties of the catalysts, an active site involving Ni species in close interactions with other cations is proposed, as well as a reaction mechanism. It is related to a partially reduced catalyst involving anionic vacancies,  $O^{2-}$  species, and cations, which is formed during the *in situ*  $H_2$  treatment or  $CH_4$  flow.

## References

- [1] P. Mohanty, K. K. Pant, and R. Mittal, "Hydrogen generation from biomass materials: Challenges and opportunities," *Wiley Interdiscip. Rev. Energy Environ.*, vol. 4, no. 2, pp. 139–155, 2015.
- [2] I. E. A. IEA, "World Energy Outlook 2011," *Int. Energy Agency*, p. 666, 2011.
- [3] M. Balat, "Potential importance of hydrogen as a future solution to environmental and transportation problems," *Int. J. Hydrogen Energy*, vol. 33, no. 15, pp. 4013–4029, 2008.
- [4] H. J. Alves, C. Bley Junior, R. R. Niklevicz, E. P. Frigo, M. S. Frigo, and C. H. Coimbra-Araújo, "Overview of hydrogen production technologies from biogas and the applications in fuel cells," *Int. J. Hydrogen Energy*, vol. 38, no. 13, pp. 5215–5225, 2013.
- [5] C. Italiano, A. Vita, C. Fabiano, M. Laganà, and L. Pino, "Bio-hydrogen production by oxidative steam reforming of biogas over nanocrystalline Ni/CeO<sub>2</sub> catalysts," *Int. J. Hydrogen Energy*, pp. 1–8, 2015.
- [6] C. a Haynes and R. Gonzalez, "Rethinking biological activation of methane and conversion to liquid fuels," *Nat. Chem. Biol.*, vol. 10, no. 5, pp. 331–339, 2014.
- [7] FreedomCAR & Fuel Partnership, "Hydrogen production overview of technology options," 2009.
- [8] J. a Turner, "Sustainable hydrogen production.," *Science*, vol. 305, no. 5686, pp. 972–974, 2004.
- [9] International Energy Agency, "Hydrogen Production and Storage. R&D Priorities and Gaps," *Hydrog. Implement. Agreem.*, vol. 13, pp. 392–392, 2006.
- [10] T. Rostrup-Nielsen, "Manufacture of hydrogen," *Catal. Today*, vol. 106, no. 1–4, pp. 293–296, 2005.
- [11] K. Urbaniec, A. Friedl, D. Huisingh, and P. Claassen, "Hydrogen for a sustainable global economy," *J. Clean. Prod.*, vol. 18, no. SUPPL. 1, pp. S1–S3, 2010.
- [12] European Commission, *World Energy Technology Outlook - 2050 WETO - H<sub>2</sub>*. 2006.
- [13] S. Sharma and S. K. Ghoshal, "Hydrogen the future transportation fuel: From production to applications," *Renew. Sustain. Energy Rev.*, vol. 43, pp. 1151–1158, 2015.
- [14] H. Balat and E. Kirtay, "Hydrogen from biomass - Present scenario and future prospects," *Int. J. Hydrogen Energy*, vol. 35, no. 14, pp. 7416–7426, 2010.
- [15] A. A. Iordanidis, P. N. Kechagiopoulos, S. S. Voutetakis, A. A. Lemonidou, and I. A. Vasalos, "Autothermal sorption-enhanced steam reforming of bio-oil/biogas mixture and energy generation by fuel cells: Concept analysis and process simulation," *Int. J. Hydrogen Energy*, vol. 31, no. 8, pp. 1058–1065, 2006.
- [16] M. Lo Faro, A. Vita, L. Pino, and A. S. Aricò, "Performance evaluation of a solid oxide fuel cell coupled to an external biogas tri-reforming process," *Fuel Process. Technol.*, vol. 115, pp. 238–245, 2013.
- [17] F. Manenti, R. Pelosato, P. Vallevi, A. R. Leon-Garzon, G. Dotelli, A. Vita, M. Lo Faro, G. Maggio, L. Pino, and A. S. Aricò, "Biogas-fed solid oxide fuel cell (SOFC) coupled to tri-reforming process: Modelling and simulation," *Int. J. Hydrogen Energy*, pp. 1–11, 2015.
- [18] R. Luque, "Fuels of the future," *Energy Environ. Sci.*, vol. 3, no. 3, p. 253, 2010.
- [19] S. Sato, S.-Y. Lin, Y. Suzuki, and H. Hatano, "Hydrogen production from heavy oil in the presence of calcium hydroxide," *Fuel*, vol. 82, no. 5, pp. 561–567, 2003.
- [20] B. D. Solomon and A. Banerjee, "A global survey of hydrogen energy research, development and policy," *Energy Policy*, vol. 34, no. 7, pp. 781–792, 2006.
- [21] G. W. Huber, I. Sara, and A. Corma, "Synthesis of Transportation Fuels from Biomass," *Chem Rev.*, vol. 2, no. 106, pp. 4044–4098, 2006.

- [22] U.S Energy Information Administration, *International Energy Outlook 2016*, vol. 484, no. May. 2016.
- [23] M. John Turner, George Sverdrup, y, Margaret K. Mann, Pin-Ching Maness, Ben Kroposki, “Renewable hydrogen production,” *Int. J. energy Res.*, vol. 32, no. 2008, pp. 379–407, 2008.
- [24] S. Rasi, A. Veijanen, and J. Rintala, “Trace compounds of biogas from different biogas production plants,” *Energy*, vol. 32, no. 8, pp. 1375–1380, 2007.
- [25] A. Effendi, K. Hellgardt, Z. G. Zhang, and T. Yoshida, “Optimising H<sub>2</sub> production from model biogas via combined steam reforming and CO shift reactions,” *Fuel*, vol. 84, no. 7–8, pp. 869–874, 2005.
- [26] P. Kolbitsch, C. Pfeifer, and H. Hofbauer, “Catalytic steam reforming of model biogas,” *Fuel*, vol. 87, no. 6, pp. 701–706, 2008.
- [27] Y. J. O. Asencios, C. B. Rodella, and E. M. Assaf, “Oxidative reforming of model biogas over NiO-Y<sub>2</sub>O<sub>3</sub>-ZrO<sub>2</sub> catalysts,” *Appl. Catal. B-Environmental*, vol. 132, pp. 1–12, 2013.
- [28] H. Shiga, K. Shinda, K. Hagiwara, A. Tsutsumi, M. Sakurai, K. Yoshida, and E. Bilgen, “Large-scale hydrogen production from biogas,” *Int. J. Hydrogen Energy*, vol. 23, no. 8, pp. 631–640, 1998.
- [29] E. Wikner, “Modeling Waste to Energy systems in Kumasi , Ghana,” no. September, pp. 1–70, 2009.
- [30] J. Van Herle, Y. Membrez, and O. Bucheli, “Biogas as a fuel source for SOFC co-generators,” *J. Power Sources*, vol. 127, no. 1–2, pp. 300–312, 2004.
- [31] V. P. Rathod, J. Shete, and P. V. Bhale, “Experimental investigation on biogas reforming to hydrogen rich syngas production using solar energy,” *Int. J. Hydrogen Energy*, vol. 41, no. 1, pp. 132–138, 2016.
- [32] M. H. Rafiq and J. E. Hustad, “Experimental and thermodynamic studies of the catalytic partial oxidation of model biogas using a plasma-assisted gliding arc reactor,” *Renew. Energy*, vol. 36, no. 11, pp. 2878–2887, 2011.
- [33] B. Saha, A. Khan, H. Ibrahim, and R. Idem, “Evaluating the performance of non-precious metal based catalysts for sulfur-tolerance during the dry reforming of biogas,” *Fuel*, vol. 120, pp. 202–217, 2014.
- [34] S. Appari, V. M. Janardhanan, R. Bauri, and S. Jayanti, “Deactivation and regeneration of Ni catalyst during steam reforming of model biogas: An experimental investigation,” *Int. J. Hydrogen Energy*, vol. 39, no. 1, pp. 297–304, 2014.
- [35] S. A. Chattanathan, S. Adhikari, M. McVey, and O. Fasina, “Hydrogen production from biogas reforming and the effect of H<sub>2</sub>S on CH<sub>4</sub>conversion,” *Int. J. Hydrogen Energy*, vol. 39, no. 35, pp. 19905–19911, 2014.
- [36] J.-M. Lavoie, “Review on dry reforming of methane, a potentially more environmentally-friendly approach to the increasing natural gas exploitation.,” *Front. Chem.*, vol. 2, no. November, p. 81, 2014.
- [37] Y. Zhang, X.-S. Li, Y. Wang, Z.-Y. Chen, and K.-F. Yan, “Decomposition conditions of methane hydrate in marine sediments from South China Sea,” *Fluid Phase Equilib.*, vol. 413, pp. 110–115, 2016.
- [38] J. Woo, J. Seong, M. Suk, and H. Lee, “Applied Catalysis B : Environmental Uncoupling the size and support effects of Ni catalysts for dry reforming of methane,” *Applied Catal. B, Environ.*, vol. 203, pp. 625–632, 2017.
- [39] J. H. Lunsford, “Catalytic conversion of methane to more useful chemicals and fuels: A challenge for the 21st century,” *Catal. Today*, vol. 63, no. 2–4, pp. 165–174, 2000.
- [40] S. Khajeh, Z. Arab Aboosadi, and B. Honarvar, “A comparative study between operability of fluidized-bed and fixed-bed reactors to produce synthesis gas through tri-reforming,” *J. Nat. Gas Sci. Eng.*, vol. 19, pp. 152–160, 2014.
- [41] Q. S. Jing and X. M. Zheng, “Combined catalytic partial oxidation and CO<sub>2</sub> reforming of methane over ZrO<sub>2</sub>-modified Ni/SiO<sub>2</sub> catalysts using fluidized-bed reactor,” *Energy*, vol. 31, no. 12, pp. 1848–1856, 2006.
- [42] N. D. Charisiou, G. Siakavelas, K. N. Papageridis, A. Baklavaridis, L. Tzounis, D. G. Avraam, and M. A. Goula, “Syngas production via the biogas dry reforming reaction over nickel supported on modified with CeO<sub>2</sub> and/or La<sub>2</sub>O<sub>3</sub> alumina catalysts,” *J. Nat. Gas Sci. Eng.*, vol. 31, pp. 164–183, 2016.
- [43] H. Jin, Y. Xu, R. Lin, and W. Han, “A proposal for a novel multi-functional energy system for the production of

- hydrogen and power,” *Int. J. Hydrogen Energy*, vol. 33, no. 1, pp. 9–19, 2008.
- [44] A. Antzara, E. Heracleous, L. Silvester, D. B. Bukur, and A. A. Lemonidou, “Activity study of NiO-based oxygen carriers in chemical looping steam methane reforming,” *Catal. Today*, vol. 272, pp. 32–41, 2015.
- [45] M. H. Jin, C. B. Lee, D. W. Lee, S. W. Lee, J. W. Park, D. Oh, K. R. Hwang, K. Y. Lee, and J. S. Park, “Microchannel methane steam reformers with improved heat transfer efficiency and their long-term stability,” *Fuel*, vol. 176, pp. 86–92, 2016.
- [46] K. Tomishige, M. Nurunnabi, K. Maruyama, and K. Kunimori, “Effect of oxygen addition to steam and dry reforming of methane on bed temperature profile over Pt and Ni catalysts,” *Fuel Process. Technol.*, vol. 85, no. 8–10, pp. 1103–1120, 2004.
- [47] A. P. E. York, T. Xiao, and M. L. H. G. Ã, “Brief overview of the partial oxidation of methane to synthesis gas,” *Top. Catal.*, vol. 22, no. April, pp. 345–358, 2003.
- [48] D. A. Hickman and L. D. Schmidt, “Synthesis gas formation by direct oxidation of methane over Pt monoliths,” *J. Catal.*, vol. 138, no. 1, pp. 267–282, 1992.
- [49] D. a Hickman and L. D. Schmidt, “Steps in CH<sub>4</sub> Oxidation on Pt and Rh Surfaces - High-Temperature Reactor Simulations,” *Aiche J.*, vol. 39, no. 7, pp. 1164–1177, 1993.
- [50] L. A. Schulz, L. C. S. Kahle, K. H. Delgado, S. A. Schunk, A. Jentys, O. Deutschmann, and J. A. Lercher, “On the coke deposition in dry reforming of methane at elevated pressures,” *Appl. Catal. A Gen.*, vol. 504, pp. 599–607, 2015.
- [51] D. Pakhare and J. Spivey, “A review of dry (CO<sub>2</sub>) reforming of methane over noble metal catalysts,” *Chem. Soc. Rev.*, vol. 43, p. , 2014.
- [52] L. N. Bobrova, A. S. Bobin, N. V. Mezentseva, V. A. Sadykov, J. W. Thybaut, and G. B. Marin, “Kinetic assessment of dry reforming of methane on Pt+Ni containing composite of fluorite-like structure,” *Appl. Catal. B Environ.*, vol. 182, pp. 513–524, 2016.
- [53] S. Y. Foo, C. K. Cheng, T.-H. Nguyen, and A. a. Adesina, “Syngas production from CH<sub>4</sub> dry reforming over Co–Ni/Al<sub>2</sub>O<sub>3</sub> catalyst: Coupled reaction-deactivation kinetic analysis and the effect of O<sub>2</sub> co-feeding on H<sub>2</sub>:CO ratio,” *Int. J. Hydrogen Energy*, vol. 37, no. 22, pp. 17019–17026, 2012.
- [54] H. Ay and D. Üner, “Dry reforming of methane over CeO<sub>2</sub> supported Ni, Co and Ni–Co catalysts,” *Appl. Catal. B Environ.*, vol. 179, pp. 128–138, 2015.
- [55] W. Zhang, Y. Zhang, M. Zhang, C. Tian, and W. Zhao, “The characteristic of CH<sub>4</sub> -CO<sub>2</sub> reforming catalyzed by carbonaceous catalyst.”
- [56] a. I. Paksoy, B. S. Caglayan, and a. E. Aksoylu, “A study on characterization and methane dry reforming performance of Co–Ce/ZrO<sub>2</sub> catalyst,” *Appl. Catal. B Environ.*, vol. 168–169, pp. 164–174, 2015.
- [57] R. Benrabaa, H. Boukhlof, A. Löffberg, A. Rubbens, R. N. Vannier, E. Bordes-Richard, and A. Barama, “Nickel ferrite spinel as catalyst precursor in the dry reforming of methane: Synthesis, characterization and catalytic properties,” *J. Nat. Gas Chem.*, vol. 21, no. 5, pp. 595–604, 2012.
- [58] A. F. Lucrédio, J. M. Assaf, and E. M. Assaf, “Methane conversion reactions on Ni catalysts promoted with Rh: Influence of support,” *Appl. Catal. A Gen.*, vol. 400, no. 1–2, pp. 156–165, 2011.
- [59] B. Li, K. Maruyama, M. Nurunnabi, K. Kunimori, and K. Tomishige, “Temperature profiles of alumina-supported noble metal catalysts in autothermal reforming of methane,” *Appl. Catal. A Gen.*, vol. 275, no. 1–2, pp. 157–172, 2004.
- [60] V. R. Choudhary, K. C. Mondal, and A. S. Mamman, “High-temperature stable and highly active/selective supported NiCoMgCeO<sub>x</sub> catalyst suitable for autothermal reforming of methane to syngas,” *J. Catal.*, vol. 233, no. 1, pp. 36–40, 2005.
- [61] M. P. Kohn, M. J. Castaldi, and R. J. Farrauto, “Auto-thermal and dry reforming of landfill gas over a Rh/Al<sub>2</sub>O<sub>3</sub>

- monolith catalyst,” *Appl. Catal. B Environ.*, vol. 94, no. 1–2, pp. 125–133, 2010.
- [62] S. Authayanun, D. Saebea, Y. Patcharavorachot, and A. Arpornwichanop, “Evaluation of an integrated methane autothermal reforming and high-temperature proton exchange membrane fuel cell system,” *Energy*, vol. 80, pp. 331–339, 2015.
- [63] J. Guo, Z. Hou, J. Gao, and X. Zheng, “Syngas production via combined oxy-CO<sub>2</sub> reforming of methane over Gd<sub>2</sub>O<sub>3</sub>-modified Ni/SiO<sub>2</sub> catalysts in a fluidized-bed reactor,” *Fuel*, vol. 87, no. 7, pp. 1348–1354, 2008.
- [64] C. S. Lau, A. Tsolakis, and M. L. Wyszynski, “Biogas upgrade to syn-gas (H<sub>2</sub>-CO) via dry and oxidative reforming,” *Int. J. Hydrogen Energy*, vol. 36, no. 1, pp. 397–404, 2011.
- [65] M. Akri, T. Chafik, P. Granger, P. Ayrault, and C. Batiot-Dupeyrat, “Novel nickel promoted illite clay based catalyst for autothermal dry reforming of methane,” *Fuel*, vol. 178, no. March, pp. 139–147, 2016.
- [66] N. Kumar, M. Shojaee, and J. J. Spivey, “Catalytic bi-reforming of methane : from greenhouse gases to syngas,” *Curr. Opin. Chem. Eng.*, vol. 9, pp. 8–15.
- [67] G. Olah, A. Goepfert, M. Czaun, T. Mathew, R. B. May, and G. K. S. Prakash, “Single Step Bi-reforming and Oxidative Bi-reforming of Methane (Natural Gas) with Steam and Carbon Dioxide to Metgas (CO-2H<sub>2</sub>) for Methanol Synthesis: Self-Sufficient Effective and Exclusive Oxygenation of Methane to Methanol with Oxygen,” *J. Am. Chem. Soc.*, vol. 137, no. 27, pp. 8720–8729, 2015.
- [68] L. Pino, A. Vita, M. Laganà, and V. Recupero, “Hydrogen from biogas: Catalytic tri-reforming process with Ni/LaCeO mixed oxides,” *Appl. Catal. B Environ.*, vol. 148–149, pp. 91–105, 2014.
- [69] J.-M. Lavoie, “Review on dry reforming of methane, a potentially more environmentally-friendly approach to the increasing natural gas exploitation.,” *Front. Chem.*, vol. 2, no. November, p. 81, 2014.
- [70] A. J. Majewski and J. Wood, “Tri-reforming of methane over Ni@SiO<sub>2</sub> catalyst,” *Int. J. Hydrogen Energy*, vol. 39, no. 24, pp. 12578–12585, 2014.
- [71] Solov’ev, Y. V. Gubareni, Y. P. Kurilets, and Orlik, “Tri-reforming of methane on structured Ni-containing catalysts,” *Theor. Exp. Chem.*, vol. 48, no. 3, pp. 199–205, 2012.
- [72] D. Sun, X. Li, S. Ji, and L. Cao, “Effect of O<sub>2</sub> and H<sub>2</sub>O on the tri-reforming of the simulated biogas to syngas over Ni-based SBA-15 catalysts,” *J. Nat. Gas Chem.*, vol. 19, no. 4, pp. 369–374, 2010.
- [73] S. Velu, K. Suzuki, and C. S. Gopinath, “Photoemission and in situ XRD investigations on CuCoZnAl-mixed metal oxide catalysts for the oxidative steam reforming of methanol,” *J. Phys. Chem. B*, vol. 106, no. 49, pp. 12737–12746, 2002.
- [74] U. Oemar, K. Hidajat, and S. Kawi, “Pd–Ni catalyst over spherical nanostructured Y<sub>2</sub>O<sub>3</sub> support for oxy-CO<sub>2</sub> reforming of methane: Role of surface oxygen mobility,” *Int. J. Hydrogen Energy*, vol. 40, no. 36, pp. 12227–12238, 2015.
- [75] L. Marra, P. F. Wolbers, F. Gallucci, and M. V. S. Annaland, “Development of a RhZrO<sub>2</sub> catalyst for low temperature autothermal reforming of methane in membrane reactors,” *Catal. Today*, vol. 236, pp. 23–33, 2014.
- [76] Y. J. O. Asencios and E. M. Assaf, “Combination of dry reforming and partial oxidation of methane on NiO-MgO-ZrO<sub>2</sub> catalyst: Effect of nickel content,” *Fuel Process. Technol.*, vol. 106, pp. 247–252, 2013.
- [77] B. Koubaissy, A. Pietraszek, A. C. Roger, and A. Kiennemann, “CO<sub>2</sub> reforming of methane over Ce-Zr-Ni-Me mixed catalysts,” *Catal. Today*, vol. 157, no. 1–4, pp. 436–439, 2010.
- [78] B. Li, K. Maruyama, M. Nurunnabi, K. Kunitomi, and K. Tomishige, “Effect of Ni Loading on Catalyst Bed Temperature in Oxidative Steam Reforming of Methane over r-Al<sub>2</sub>O<sub>3</sub> -Supported Ni Catalysts,” *Scanning*, pp. 485–494, 2005.
- [79] J. Zhu, X. Peng, L. Yao, D. Tong, and C. Hu, “CO<sub>2</sub> reforming of methane over Mg-promoted Ni/SiO<sub>2</sub> catalysts: the influence of Mg precursors and impregnation sequences,” *Catal. Sci. Technol.*, vol. 2, no. 3, p. 529, 2012.

- [80] L. Pino, C. Italiano, A. Vita, M. Laganà, and V. Recupero, "Ce<sub>0.70</sub>La<sub>0.20</sub>Ni<sub>0.10</sub>O<sub>2-δ</sub> catalyst for methane dry reforming: Influence of reduction temperature on the catalytic activity and stability," *Appl. Catal. B Environ.*, pp. 0–47, 2017.
- [81] M. A. Vasiliades, M. M. Makri, P. Djinović, B. Erjavec, A. Pintar, and A. M. Efstathiou, "Dry reforming of methane over 5 wt% Ni/Ce<sub>1-x</sub>Pr<sub>x</sub>O<sub>2-δ</sub> catalysts: Performance and characterisation of active and inactive carbon by transient isotopic techniques," *Appl. Catal. B Environ.*, vol. 197, pp. 168–183, 2016.
- [82] A. Löffberg, J. Guerrero-Caballero, T. Kane, A. Rubbens, and L. Jalowiecki-Duhamel, "Ni/CeO<sub>2</sub> based catalysts as oxygen vectors for the chemical looping dry reforming of methane for syngas production," *Appl. Catal. B Environ.*, vol. 212, pp. 159–174, 2017.
- [83] S. Li and J. Gong, "Strategies for improving the performance and stability of Ni-based catalysts for reforming reactions," *Chem. Soc. Rev.*, vol. 43, no. 21, pp. 7245–7256, 2014.
- [84] M. Usman, W. M. a. Wan Daud, and H. F. Abbas, "Dry reforming of methane: Influence of process parameters—A review," *Renew. Sustain. Energy Rev.*, vol. 45, pp. 710–744, 2015.
- [85] B. Abdullah, N. A. Abd Ghani, and D.-V. N. Vo, "Recent Advances in Dry Reforming of Methane over Ni-based Catalysts," *J. Clean. Prod.*, 2017.
- [86] J. W. Han, C. Kim, J. S. Park, and H. Lee, "Highly coke-resistant Ni nanoparticle catalysts with minimal sintering in dry reforming of methane," *ChemSusChem*, vol. 7, no. 2, pp. 451–456, 2014.
- [87] A. Ponchel, A. D'huysser, C. Lamonier, and L. Jalowiecki-duhamel, "CeNiO and CeAlNiO solids studied by electron microscopy," *Phys Chem Chem Phys*, vol. 2, pp. 303–312, 2000.
- [88] J. Han, Y. Zhan, J. Street, F. To, and F. Yu, "Natural gas reforming of carbon dioxide for syngas over Ni–Ce–Al catalysts," *Int. J. Hydrogen Energy*, vol. 42, no. 29, pp. 18364–18374, 2017.
- [89] T. Odedairo, J. Chen, and Z. Zhu, "Metal-support interface of a novel Ni-CeO<sub>2</sub> catalyst for dry reforming of methane," *Catal. Commun.*, vol. 31, pp. 25–31, 2013.
- [90] D. E. Resasco and G. L. Haller, "A model of metal-oxide support interaction for Rh on TiO<sub>2</sub>," *J. Catal.*, vol. 82, no. 2, pp. 279–288, 1983.
- [91] X. Li, D. Li, H. Tian, L. Zeng, Z. Zhao, and J. Gong, "Dry reforming of methane over Ni/La<sub>2</sub>O<sub>3</sub> nanorod catalysts with stabilized Ni nanoparticles," *Appl. Catal. B Environ.*, vol. 202, p. , 2016.
- [92] O. Omoregbe, H. T. Danh, C. Nguyen-huy, H. D. Setiabudi, S. Z. Abidin, Q. Duc, and D. N. Vo, "Syngas production from methane dry reforming over Ni / SBA-15 catalyst : Effect of operating parameters," *Int. J. Hydrogen Energy*, pp. 1–12, 2017.
- [93] R. Dębek, M. Motak, D. Duraczyska, F. Launay, M. E. Galvez, T. Grzybek, and P. Da Costa, "Methane dry reforming over hydrotalcite-derived Ni–Mg–Al mixed oxides: the influence of Ni content on catalytic activity, selectivity and stability," *Catal. Sci. Technol.*, vol. 1, pp. 192–208, 2016.
- [94] H. Liu, D. Wierzbicki, R. Debek, M. Motak, T. Grzybek, P. Da Costa, and M. E. Gálvez, "La-promoted Ni-hydrotalcite-derived catalysts for dry reforming of methane at low temperatures," *Fuel*, vol. 182, pp. 8–16, 2016.
- [95] X. Yu, N. Wang, W. Chu, and M. Liu, "Carbon dioxide reforming of methane for syngas production over La-promoted NiMgAl catalysts derived from hydrotalcites," *Chem. Eng. J.*, vol. 209, pp. 623–632, 2012.
- [96] N. Miletić, U. Izquierdo, I. Obregón, K. Bizkarra, I. Agirrezabal-Telleria, L. V. Barrio, and P. L. Arias, "Oxidative steam reforming of methane over nickel catalysts supported on Al<sub>2</sub>O<sub>3</sub>–CeO<sub>2</sub>–La<sub>2</sub>O<sub>3</sub>," *Catal. Sci. Technol.*, vol. 5, no. 3, pp. 1704–1715, 2015.
- [97] X. Huang, C. Ji, C. Wang, F. Xiao, N. Zhao, N. Sun, W. Wei, and Y. Sun, "Ordered mesoporous CoO–NiO–Al<sub>2</sub>O<sub>3</sub> bimetallic catalysts with dual confinement effects for CO<sub>2</sub> reforming of CH<sub>4</sub>," *Catal. Today*, 2015.
- [98] H. Xiao, Z. Liu, X. Zhou, and K. Zhu, "A unique method to fabricate Ni<sub>x</sub>Mg<sub>1-x</sub>O (111) nano-platelet solid solution catalyst for CH<sub>4</sub>–CO<sub>2</sub> dry reforming," *Catal. Commun.*, vol. 34, pp. 11–15, 2013.

- [99] Z. Liu, D. C. Grinter, P. G. Lustemberg, et al. "Dry Reforming of Methane on a Highly-Active Ni-CeO<sub>2</sub> Catalyst: Effects of Metal-Support Interactions on C-H Bond Breaking," *Angew. Chemie Int. Ed.*, vol. 55, pp. 7455–7459, 2016.
- [100] Y. H. Hu, "Solid-solution catalysts for CO<sub>2</sub> reforming of methane," *Catal. Today*, vol. 148, no. 3–4, pp. 206–211, 2009.
- [101] Q. Li, Z. Huang, P. Guan, R. Su, Q. Cao, Y. Chao, W. Shen, J. Guo, H. Xu, and R. Che, "Simultaneous Ni Doping at Atom Scale in Ceria and Assembling into Well-Defined Lotuslike Structure for Enhanced Catalytic Performance," *ACS Appl. Mater. Interfaces*, vol. 9, no. 19, pp. 16243–16251, 2017.
- [102] H. Wu, G. Pantaleo, V. La Parola, A. M. Venezia, X. Collard, C. Aprile, and L. F. Liotta, "Bi- and trimetallic Ni catalysts over Al<sub>2</sub>O<sub>3</sub> and Al<sub>2</sub>O<sub>3</sub>-MO<sub>x</sub> (M=Ce or Mg) oxides for methane dry reforming: Au and Pt additive effects," *Appl. Catal. B Environ.*, vol. 156–157, pp. 350–361, 2014.
- [103] C. E. Daza, J. Gallego, F. Mondragón, S. Moreno, and R. Molina, "High stability of Ce-promoted Ni/Mg-Al catalysts derived from hydrotalcites in dry reforming of methane," *Fuel*, vol. 89, no. 3, pp. 592–603, 2010.
- [104] H.-W. Chen, C.-Y. Wang, C.-H. Yu, L.-T. Tseng, and P.-H. Liao, "Carbon dioxide reforming of methane reaction catalyzed by stable nickel copper catalysts," *Catal. Today*, vol. 97, no. 2–3, pp. 173–180, 2004.
- [105] A. Moral, I. Reyero, C. Alfaro, F. Bimbela, and L. M. Gandía, "Syngas production by means of biogas catalytic partial oxidation and dry reforming using Rh-based catalysts," *Catal. Today*, no. March, pp. 0–1, 2017.
- [106] a F. Lucrecio, J. M. Assaf, and E. M. Assaf, "Reforming of a model biogas on Ni and Rh-Ni catalysts: Effect of adding La," *Fuel Process. Technol.*, vol. 102, pp. 124–131, 2012.
- [107] X. Chen, J. Jiang, K. Li, S. Tian, and F. Yan, "Energy-efficient biogas reforming process to produce syngas: The enhanced methane conversion by O<sub>2</sub>," *Appl. Energy*, vol. 185, pp. 687–697, 2017.
- [108] J. Gao, Z. Hou, X. Liu, Y. Zeng, M. Luo, and X. Zheng, "Methane autothermal reforming with CO<sub>2</sub> and O<sub>2</sub> to synthesis gas at the boundary between Ni and ZrO<sub>2</sub>," *Int. J. Hydrogen Energy*, vol. 34, no. 9, pp. 3734–3742, 2009.
- [109] M. Akri, T. Chafik, P. Granger, P. Ayrault, and C. Batiot-Dupeyrat, "Novel nickel promoted illite clay based catalyst for autothermal dry reforming of methane," *Fuel*, vol. 178, pp. 139–147, 2016.
- [110] F. Meshkani, M. Rezaei, and M. Andache, "Investigation of the catalytic performance of Ni/MgO catalysts in partial oxidation, dry reforming and combined reforming of methane," *J. Ind. Eng. Chem.*, vol. 20, no. 4, pp. 1251–1260, 2014.
- [111] Z. Hou, J. Gao, J. Guo, D. Liang, H. Lou, and X. Zheng, "Deactivation of Ni catalysts during methane autothermal reforming with CO<sub>2</sub> and O<sub>2</sub> in a fluidized-bed reactor," *J. Catal.*, vol. 250, no. 2, pp. 331–341, 2007.
- [112] J. Deng, M. Cai, W. Sun, X. Liao, W. Chu, and X. S. Zhao, "Oxidative methane reforming with an intelligent catalyst: Sintering-tolerant supported nickel nanoparticles," *ChemSusChem*, vol. 6, no. 11, pp. 2061–2065, 2013.
- [113] B. Abdullah, N. A. Abd Ghani, and D. V. N. Vo, "Recent advances in dry reforming of methane over Ni-based catalysts," *J. Clean. Prod.*, vol. 162, pp. 170–185, 2017.
- [114] J. R. Rostrup-Nielsen, "Production of synthesis gas," *Catal. Today*, vol. 18, no. 4, pp. 305–324, 1993.
- [115] M. K. Nikoo and N. A. S. Amin, "Thermodynamic analysis of carbon dioxide reforming of methane in view of solid carbon formation," *Fuel Process. Technol.*, vol. 92, no. 3, pp. 678–691, 2011.
- [116] A. Shamsi and C. D. Johnson, "Effect of pressure on the carbon deposition route in CO<sub>2</sub> reforming of CH<sub>4</sub>," *Catal. Today*, vol. 84, no. 1–2, pp. 17–25, 2003.
- [117] R. D??bek, M. Radlik, M. Motak, M. E. Galvez, W. Turek, P. Da Costa, and T. Grzybek, "Ni-containing Ce-promoted hydrotalcite derived materials as catalysts for methane reforming with carbon dioxide at low temperature - On the effect of basicity," *Catal. Today*, vol. 257, no. P1, pp. 59–65, 2015.
- [118] N. Laosiripojana, W. Sutthisripok, and S. Assabumrungrat, "Synthesis gas production from dry reforming of methane

- over CeO<sub>2</sub> doped Ni/Al<sub>2</sub>O<sub>3</sub>: Influence of the doping ceria on the resistance toward carbon formation,” *Chem. Eng. J.*, vol. 112, no. 1–3, pp. 13–22, 2005.
- [119] S. Zhang, S. Muratsugu, N. Ishiguro, and M. Tada, “Ceria-doped Ni/SBA-16 catalysts for dry reforming of methane,” *ACS Catal.*, vol. 3, no. 8, pp. 1855–1864, 2013.
- [120] B. Djebbari, V. M. Gonzalez-Delacruz, D. Halliche, K. Bachari, A. Saadi, A. Caballero, J. P. Holgado, and O. Cherifi, “Promoting effect of Ce and Mg cations in Ni/Al catalysts prepared from hydrotalcites for the dry reforming of methane,” *React. Kinet. Mech. Catal.*, vol. 111, no. 1, pp. 259–275, 2014.
- [121] A. Albarazi, P. Beaunier, and P. Da Costa, “Hydrogen and syngas production by methane dry reforming on SBA-15 supported nickel catalysts: On the effect of promotion by Ce<sub>0.75</sub>Zr<sub>0.25</sub>O<sub>2</sub> mixed oxide,” *Int. J. Hydrogen Energy*, vol. 38, no. 1, pp. 127–139, 2013.
- [122] S. M. Lima, J. M. Assaf, M. A. Pea, and J. L. G. Fierro, “Structural features of La<sub>1-x</sub>Ce<sub>x</sub>NiO<sub>3</sub> mixed oxides and performance for the dry reforming of methane,” *Appl. Catal. A Gen.*, vol. 311, no. 1–2, pp. 94–104, 2006.
- [123] F. Huang, R. Wang, C. Yang, H. Driss, W. Chu, and H. Zhang, “Catalytic performances of Ni/mesoporous SiO<sub>2</sub> catalysts for dry reforming of methane to hydrogen,” *J. Energy Chem.*, vol. 25, no. 4, pp. 709–719, 2016.
- [124] J. Karuppiah, E. Linga Reddy, and Y. Mok, “Anodized Aluminum Oxide Supported NiO-CeO<sub>2</sub> Catalyst for Dry Reforming of Propane,” *Catalysts*, vol. 6, no. 10, p. 154, 2016.
- [125] Q. Zhang, T. Zhang, Y. Shi, B. Zhao, M. Wang, Q. Liu, J. Wang, K. Long, Y. Duan, and P. Ning, “A sintering and carbon-resistant Ni-SBA-15 catalyst prepared by solid-state grinding method for dry reforming of methane,” *J. CO<sub>2</sub> Util.*, vol. 17, pp. 10–19, 2017.
- [126] Z. J. Zuo, C. F. Shen, P. J. Tan, and W. Huang, “Ni based on dual-support Mg-Al mixed oxides and SBA-15 catalysts for dry reforming of methane,” *Catal. Commun.*, vol. 41, pp. 132–135, 2013.
- [127] A. Albarazi, M. E. Glvez, and P. Da Costa, “Synthesis strategies of ceria-zirconia doped Ni/SBA-15 catalysts for methane dry reforming,” *Catal. Commun.*, vol. 59, pp. 108–112, 2015.
- [128] L. Jalowiecki-Duhamel, “Hydrogen storage and induced properties in non-metallic catalytic materials,” *Int. J. Hydrogen Energy*, vol. 31, no. 2, pp. 191–195, 2006.
- [129] L. Jalowiecki-Duhamel, A. Ponchel, and C. Lamonier, “Storage of reactive hydrogen species in CeM<sub>x</sub>O<sub>y</sub> (M = Cu, Ni; 0 ≤ x ≤ 1) mixed oxides,” *Int. J. Hydrogen Energy*, vol. 24, no. 11, pp. 1083–1092, 1999.
- [130] C. Lamonier, A. Ponchel, A. D’Huysser, and L. Jalowiecki-Duhamel, “Studies of the cerium-metal-oxygen-hydrogen system (metal=Cu, Ni),” *Catal. Today*, vol. 50, no. 2, pp. 247–259, 1999.
- [131] L. Jalowiecki-Duhamel, J. Carpentier, and A. Ponchel, “Catalytic hydrogen storage in cerium nickel and zirconium (or aluminium) mixed oxides,” *Int. J. Hydrogen Energy*, vol. 32, no. 13, pp. 2439–2444, 2007.
- [132] A. Vita, L. Pino, F. Cipiti, M. Laganà, and V. Recupero, “Biogas as renewable raw material for syngas production by tri-reforming process over NiCeO<sub>2</sub> catalysts: Optimal operative condition and effect of nickel content,” *Fuel Process. Technol.*, vol. 127, pp. 47–58, 2014.
- [133] G. Li, J. Smith R.L., and H. Inomata, “Synthesis of nanoscale Ce<sub>1-x</sub>Fe<sub>x</sub>O<sub>2</sub> solid solutions via a low-temperature approach [14],” *J. Am. Chem. Soc.*, vol. 123, no. 44, pp. 11091–11092, 2001.
- [134] S. Zhong, L. Zhang, L. Wang, W. Huang, C. Fan, and A. Xu, “Uniform and Porous Ce<sub>1-x</sub>Zn<sub>x</sub>O<sub>2-δ</sub> Solid Solution Nanodisks: Preparation and Their CO Oxidation Activity,” *J. Phys. Chem. C*, no. 116, pp. 13127–13132, 2012.
- [135] L. Barrio, A. Kubacka, G. Zhou, M. Estrella, A. Martínez-Arias, J. C. Hanson, M. Fernández-García, and J. a. Rodriguez, “Unusual Physical and Chemical Properties of Ni in Ce<sub>1-x</sub>Ni<sub>x</sub>O<sub>2-y</sub> Oxides: Structural Characterization and Catalytic Activity for the Water Gas Shift Reaction,” *J. Phys. Chem. C*, vol. 114, no. 29, pp. 12689–12697, 2010.
- [136] W. Fang, C. Pirez, S. Paul, M. Capron, H. Jobic, F. Dumeignil, and L. Jalowiecki-Duhamel, “Room Temperature Hydrogen Production from Ethanol over CeNi<sub>x</sub>H<sub>2</sub>O<sub>y</sub> Nano-Oxyhydride Catalysts,” *ChemCatChem*, vol. 5, no. 8, pp.

- 2207–2216, 2013.
- [137] A. Mineshige, “Oxygen chemical potential variation in ceria-based solid oxide fuel cells determined by Raman spectroscopy,” *Solid State Ionics*, vol. 135, no. 1–4, pp. 481–485, 2000.
- [138] N. Dharmaraj, P. Prabu, S. Nagarajan, C. H. Kim, J. H. Park, and H. Y. Kim, “Synthesis of nickel oxide nanoparticles using nickel acetate and poly(vinyl acetate) precursor,” *Mater. Sci. Eng. B Solid-State Mater. Adv. Technol.*, vol. 128, no. 1–3, pp. 111–114, 2006.
- [139] M. Palard, J. Balencie, A. Maguer, and J.-F. Hochepeid, “Effect of hydrothermal ripening on the photoluminescence properties of pure and doped cerium oxide nanoparticles,” *Mater. Chem. Phys.*, vol. 120, pp. 79–88, 2010.
- [140] N. Paunović, Z. Dohčević-Mitrović, R. Scurtu, S. Aškračić, M. Prekajski, B. Matović, and Z. V. Popović, “Suppression of inherent ferromagnetism in Pr-doped CeO<sub>2</sub> nanocrystals,” *Nanoscale*, vol. 4, no. 17, p. 5469, 2012.
- [141] L. Jalowiecki-Duhamel, C. Pirez, M. Capron, F. Dumeignil, and E. Payen, “Hydrogen production from ethanol in presence of water over cerium and nickel mixed oxides,” *Catal. Today*, vol. 157, no. 1–4, pp. 456–461, 2010.
- [142] M. Akri, S. Pronier, T. Chafik, O. Achak, P. Granger, P. Simon, M. Trentesaux, and C. Batiot-Dupeyrat, “Development of nickel supported La and Ce-natural illite clay for autothermal dry reforming of methane: Toward a better resistance to deactivation,” *Appl. Catal. B Environ.*, vol. 205, pp. 519–531, 2017.
- [143] W. Fang, S. Paul, M. Capron, A. V. Biradar, S. B. Umbarkar, M. K. Dongare, F. Dumeignil, and L. Jalowiecki-Duhamel, “Highly loaded well dispersed stable Ni species in Ni<sub>x</sub>Mg<sub>2</sub>AlO<sub>y</sub> nanocomposites: Application to hydrogen production from bioethanol,” *Appl. Catal. B Environ.*, vol. 166–167, pp. 485–496, 2015.
- [144] L. Jalowiecki-Duhamel, H. Zarrou, and a. D’Huysser, “Hydrogen production at low temperature from methane on cerium and nickel based mixed oxides,” *Int. J. Hydrogen Energy*, vol. 33, no. 20, pp. 5527–5534, 2008.
- [145] L. Jalowiecki-Duhamel, S. Debeusscher, H. Zarrou, D’Huysser, H. Jobic, and E. Payen, “Hydrogen storage in CeNi<sub>x</sub>O<sub>y</sub> and CeM<sub>0.5</sub>Ni<sub>x</sub>O<sub>y</sub> (M = Zr or Al) mixed oxides,” *Catal. Today*, vol. 138, no. 3–4, pp. 266–271, 2008.
- [146] L. Jalowiecki-Duhamel, H. Zarrou, and a. D’Huysser, “Low temperature hydrogen production from methane on cerium nickel- and zirconium-based oxyhydrides,” *Catal. Today*, vol. 138, no. 3–4, pp. 124–129, 2008.
- [147] R. Debek, M. E. Galvez, F. Launay, M. Motak, T. Grzybek, and P. Da Costa, “Low temperature dry methane reforming over Ce, Zr and CeZr promoted Ni-Mg-Al hydrotalcite-derived catalysts,” *Int. J. Hydrogen Energy*, vol. 1, pp. 0–7, 2015.
- [148] A. P. Grosvenor, M. C. Biesinger, R. S. C. Smart, and N. S. McIntyre, “New interpretations of XPS spectra of nickel metal and oxides,” *Surf. Sci.*, vol. 600, no. 9, pp. 1771–1779, 2006.
- [149] W. Fang, S. Paul, M. Capron, F. Dumeignil, and L. Jalowiecki-Duhamel, “Hydrogen production from bioethanol catalyzed by Ni<sub>x</sub>Mg<sub>2</sub>AlO<sub>y</sub> ex-hydrotalcite catalysts,” *Appl. Catal. B Environ.*, vol. 152–153, no. 1, pp. 370–382, 2014.
- [150] A. F. Lucrédio, J. D. A. Bellido, and E. M. Assaf, “Effects of adding la and Ce to hydrotalcite-type Ni/Mg/Al catalyst precursors on ethanol steam reforming reactions,” *Appl. Catal. A Gen.*, vol. 388, no. 1–2, pp. 77–85, 2010.
- [151] E. Dahdah, J. A. Rached, S. Aouad, C. Gennequin, and E. A. Aad, “CO<sub>2</sub> reforming of methane over Ni<sub>x</sub>Mg<sub>6-x</sub>Al<sub>2</sub> catalysts: Effect of lanthanum doping on catalytic activity and stability,” *Int. J. Hydrogen Energy*, vol.42, pp. 12808-12817, 2017.
- [152] A. J. Marchi, J. L. G. Fierro, J. Santamaría, and A. Monzón, “Dehydrogenation of isopropyl alcohol on a Cu/SiO<sub>2</sub> catalyst: A study of the activity evolution and reactivation of the catalyst,” *Appl. Catal. A Gen.*, vol. 142, no. 2, pp. 375–386, 1996.
- [153] W. Yang, H. Liu, Y. Li, H. Wu, and D. He, “CO<sub>2</sub> reforming of methane to syngas over highly-stable Ni/SBA-15 catalysts prepared by P123-assisted method,” *Int. J. Hydrogen Energy*, pp. 1–11, 2015.
- [154] P. Burattin, M. Che, and C. Louis, “Characterization of the Ni(II) Phase Formed on Silica Upon Deposition–

- Precipitation,” *J. Phys. Chem. B*, vol. 101, no. 36, pp. 7060–7074, 1997.
- [155] J. Park, H. Lee, J. Bang, K. Park, and H. Song, “Chemical transformation and morphology change of nickel-silica hybrid nanostructures via nickel phyllosilicates,” *Chem. Commun. (Camb.)*, no. 47, pp. 7345–7, 2009.
- [156] T. Lehmann, T. Wolff, C. Hamel, P. Veit, B. Garke, and A. Seidel-Morgenstern, “Physico-chemical characterization of Ni/MCM-41 synthesized by a template ion exchange approach,” *Microporous Mesoporous Mater.*, vol. 151, pp. 113–125, 2012.
- [157] P. Burattin, M. Che, and C. Louis, “Molecular Approach to the Mechanism of Deposition–Precipitation of the Ni(II) Phase on Silica,” *J. Phys. Chem. B*, vol. 102, no. 15, pp. 2722–2732, 1998.
- [158] M. V. Sivaiah, S. Petit, J. Barrault, C. Batiot-Dupeyrat, and S. Valange, “CO<sub>2</sub> reforming of CH<sub>4</sub> over Ni-containing phyllosilicates as catalyst precursors,” *Catal. Today*, vol. 157, no. 1–4, pp. 397–403, 2010.
- [159] O. a. Bereketidou and M. a. Goula, “Biogas reforming for syngas production over nickel supported on ceria-alumina catalysts,” *Catal. Today*, vol. 195, no. 1, pp. 93–100, 2012.
- [160] M. M. Barroso-Quiroga and A. E. Castro-Luna, “Catalytic activity and effect of modifiers on Ni-based catalysts for the dry reforming of methane,” *Int. J. Hydrogen Energy*, vol. 35, no. 11, pp. 6052–6056, 2010.
- [161] L. Yao, J. Shi, H. Xu, W. Shen, and C. Hu, “Low-temperature CO<sub>2</sub> reforming of methane on Zr-promoted Ni/SiO<sub>2</sub> catalyst,” *Fuel Process. Technol.*, vol. 144, pp. 1–7, 2016.
- [162] A. Serrano-Lotina and L. Daza, “Influence of the operating parameters over dry reforming of methane to syngas,” *Int. J. Hydrogen Energy*, vol. 39, no. 8, pp. 4089–4094, 2014.
- [163] C. Batiot-Dupeyrat, G. A. S. Gallego, F. Mondragon, J. Barrault, and J. M. Tatibouët, “CO<sub>2</sub> reforming of methane over LaNiO<sub>3</sub> as precursor material,” *Catal. Today*, vol. 107–108, pp. 474–480, 2005.
- [164] J. Juan-Juan, M. C. Román-Martínez, and M. J. Illán-Gómez, “Nickel catalyst activation in the carbon dioxide reforming of methane. Effect of pretreatments,” *Appl. Catal. A Gen.*, vol. 355, no. 1–2, pp. 27–32, 2009.
- [165] E. C. Lovell, A. Fuller, J. Scott, and R. Amal, “Enhancing Ni-SiO<sub>2</sub> catalysts for the carbon dioxide reforming of methane: Reduction-oxidation-reduction pre-treatment,” *Appl. Catal. B Environ.*, vol. 199, pp. 155–165, 2016.
- [166] R. Debek, M. Motak, M. E. Galvez, T. Grzybek, and P. Da Costa, “Promotion effect of zirconia on Mg(Ni,Al)O mixed oxides derived from hydrotalcites in CO<sub>2</sub> methane reforming,” *Appl. Catal. B Environ.*, 2016.
- [167] C. Gennequin, M. Safariamin, S. Siffert, A. Aboukaïs, and E. Abi-Aad, “CO<sub>2</sub> reforming of CH<sub>4</sub> over Co-Mg-Al mixed oxides prepared via hydrotalcite like precursors,” *Catal. Today*, vol. 176, no. 1, pp. 139–143, 2011.
- [168] J. Z. Luo, Z. L. Yu, C. F. Ng, and C. T. Au, “CO<sub>2</sub>/CH<sub>4</sub> Reforming over Ni – La<sub>2</sub>O<sub>3</sub>/5A : An Investigation on Carbon Deposition and Reaction Steps,” vol. 210, pp. 198–210, 2000.
- [169] W. Fang, C. Pirez, M. Capron, S. Paul, T. Raja, P. L. Dhepe, F. Dumeignil, and L. Jalowiecki-Duhamel, “Ce–Ni mixed oxide as efficient catalyst for H<sub>2</sub> production and nanofibrous carbon material from ethanol in the presence of water,” *RSC Adv.*, vol. 2, no. 25, p. 9626, 2012.
- [170] M. C. J. Bradford and M. A. Vannice, “Catalytic reforming of methane with carbon dioxide over nickel catalysts II. Reaction kinetics,” *Appl. Catal. A Gen.*, vol. 142, no. 1, pp. 97–122, 1996.
- [171] A. W. Musumeci, G. G. Silva, W. N. Martens, E. R. Waclawik, and R. L. Frost, “Thermal decomposition and electron microscopy studies of single-walled carbon nanotubes,” *J. Therm. Anal. Calorim.*, vol. 88, no. 3, pp. 885–891, 2007.
- [172] Horváth, K. Baán, E. Varga, A. Oszkó, Vágó, M. Tőro, and A. Erdohelyi, “Dry reforming of CH<sub>4</sub> on Co/Al<sub>2</sub>O<sub>3</sub> catalysts reduced at different temperatures,” *Catal. Today*, 2015.
- [173] N. Wang, K. Shen, L. Huang, X. Yu, W. Qian, and W. Chu, “Facile route for synthesizing ordered mesoporous Ni-Ce-Al oxide materials and their catalytic performance for methane dry reforming to hydrogen and syngas,” *ACS Catal.*, vol. 3, no. 7, pp. 1638–1651, 2013.
- [174] I. Luisetto, S. Tuti, C. Battocchio, S. Lo Mastro, and A. Sodo, “Ni/CeO<sub>2</sub>-Al<sub>2</sub>O<sub>3</sub> catalysts for the dry reforming of

- methane: The effect of CeAlO<sub>3</sub> content and nickel crystallite size on catalytic activity and coke resistance,” *Appl. Catal. A Gen.*, vol. 500, pp. 12–22, 2015.
- [175] S. Lee and E. J. Huang, “Author ’ s Accepted Manuscript,” *Brain Res.*, 2015.
- [176] K. Jabbour, P. Massiani, A. Davidson, S. Casale, and N. El Hassan, “Ordered mesoporous ‘one-pot’ synthesized Ni-Mg(Ca)-Al<sub>2</sub>O<sub>3</sub> as effective and remarkably stable catalysts for combined steam and dry reforming of methane (CSDRM),” *Appl. Catal. B Environ.*, vol. 201, pp. 527–542, 2017.
- [177] W. Cai, L. Ye, L. Zhang, Y. Ren, B. Yue, X. Chen, and H. He, “Highly Dispersed Nickel-Containing Mesoporous Silica with Superior Stability in Carbon Dioxide Reforming of Methane: The Effect of Anchoring,” *Materials (Basel)*, vol. 7, no. 3, pp. 2340–2355, 2014.
- [178] L. Jalowiecki-Duhamel and Ponchel, “Relationship between Structure of CeNi<sub>x</sub>O<sub>y</sub> Mixed Oxides and Catalytic Properties in Oxidative Dehydrogenation of Propane,” *Langmuir*, no. 16, pp. 1511–1517, 2001.
- [179] H.-S. Roh, H. S. Potdar, K.-W. Jun, J.-W. Kim, and Y.-S. Oh, “Carbon dioxide reforming of methane over Ni incorporated into Ce-ZrO<sub>2</sub> catalysts,” *Appl. Catal. A Gen.*, vol. 276, no. 1–2, pp. 231–239, 2004.
- [180] S. C. Dantas, K. A. Resende, R. L. Rossi, A. J. Assis, and C. E. Hori, “Hydrogen production from oxidative reforming of methane on supported nickel catalysts: An experimental and modeling study,” *Chem. Eng. J.*, vol. 197, pp. 407–413, 2012.
- [181] W. Chen, G. Zhao, Q. Xue, L. Chen, and Y. Lu, “High carbon-resistance Ni/CeAlO<sub>3</sub>-Al<sub>2</sub>O<sub>3</sub> catalyst for CH<sub>4</sub>/CO<sub>2</sub> reforming” *Applied Catal. B, Environ.*, vol. 136–137, pp. 260–268, 2013.
- [182] N. Hadian and M. Rezaei, “Combination of dry reforming and partial oxidation of methane over Ni catalysts supported on nanocrystalline MgAl<sub>2</sub>O<sub>4</sub>,” *Fuel*, vol. 113, pp. 571–579, 2013.
- [183] D. M. Walker, S. L. Pettit, J. T. Wolan, and J. N. Kuhn, “Synthesis gas production to desired hydrogen to carbon monoxide ratios by tri-reforming of methane using Ni-MgO-(Ce,Zr)O<sub>2</sub> catalysts,” *Appl. Catal. A Gen.*, vol. 445–446, pp. 61–68, 2012.
- [184] K. Jabbour, P. Massiani, A. Davidson, S. Casale, and N. El Hassan, “Ordered mesoporous ‘one-pot’ synthesized Ni-Mg(Ca)-Al<sub>2</sub>O<sub>3</sub> as effective and remarkably stable catalysts for combined steam and dry reforming of methane (CSDRM),” *Appl. Catal. B Environ.*, vol. 201, pp. 527–542, 2017.
- [185] R. Dębek, M. E. Galvez, F. Launay, M. Motak, T. Grzybek, and P. Da Costa, “Low temperature dry methane reforming over Ce, Zr and CeZr promoted Ni-Mg-Al hydrotalcite-derived catalysts,” *Int. J. Hydrogen Energy*, vol. 41, no. 27, pp. 11616–11623, 2016.
- [186] X. Lin, R. Li, M. Lu, C. Chen, D. Li, Y. Zhan, and L. Jiang, “Carbon dioxide reforming of methane over Ni catalysts prepared from Ni-Mg-Al layered double hydroxides: Influence of Ni loadings,” *Fuel*, vol. 162, pp. 271–280, 2015.
- [187] D. Zhao, D. Zhao, J. Feng, Q. Huo, N. Melosh, G. H. Fredrickson, B. F. Chmelka, and G. D. Stucky, “Triblock Copolymer Syntheses of Mesoporous Silica with Periodic 50 to 300 Angstrom Pores Triblock Copolymer Syntheses of Mesoporous Silica with Periodic 50 to 300 Angstrom Pores,” vol. 548, no. 1998, 2012.
- [188] N. Wang, X. Yu, Y. Wang, W. Chu, and M. Liu, “A comparison study on methane dry reforming with carbon dioxide over LaNiO<sub>3</sub> perovskite catalysts supported on mesoporous SBA-15, MCM-41 and silica carrier,” *Catal. Today*, vol. 212, pp. 98–107, 2013.
- [189] L. Qian, Z. Ma, Y. Ren, H. Shi, B. Yue, S. Feng, and J. Shen, “Investigation of La promotion mechanism on Ni / SBA-15 catalysts in CH<sub>4</sub> reforming with CO<sub>2</sub>,” *FUEL*, vol. 122, pp. 47–53, 2014.
- [190] V. Arcotumapathy, D.-V. N. Vo, D. Chesterfield, C. T. Tin, A. Siahvashi, F. P. Lucien, and A. A. Adesina, “Catalyst design for methane steam reforming,” *Appl. Catal. A Gen.*, vol. 479, pp. 87–102, 2014.
- [191] Y. Kathiraser, Z. Wang, M. L. Ang, L. Mo, Z. Li, U. Oemar, and S. Kawi, “Highly active and coke resistant Ni/SiO<sub>2</sub> catalysts for oxidative reforming of model biogas : Effect of low ceria loading,” vol. 19, pp. 284–295, 2017.

- [192] M. P. Lai, W. H. Laia, R. F. Horng, C. Y. Chen, W. C. Chiu, S. S. Su, and Y. M. Chang, "Experimental study on the performance of oxidative dry reforming from simulated biogas," *Energy Procedia*, vol. 29, pp. 225–233, 2012.
- [193] B. Zhu, X. S. Li, J. L. Liu, and A. M. Zhu, "Optimized mixed reforming of biogas with O<sub>2</sub> addition in spark-discharge plasma," *Int. J. Hydrogen Energy*, vol. 37, no. 22, pp. 16916–16924, 2012.
- [194] X. Chen, J. Jiang, K. Li, S. Tian, and F. Yan, "Energy-efficient biogas reforming process to produce syngas : The enhanced methane conversion by O<sub>2</sub>," *Appl. Energy*, 2016.
- [195] S. Lee, D. Applegate, S. Ahmed, S. Calderone, and T. Harvey, "Hydrogen from natural gas: part I—autothermal reforming in an integrated fuel processor," *Int. J. Hydrogen Energy*, vol. 30, no. 8, pp. 829–842, 2005.
- [196] D. Duprez, M. C. DeMicheli, P. Marecot, J. Barbier, O. A. Ferretti, and E. N. Ponzi, "Deactivation of steam-reforming model catalysts by coke formation. I. Kinetics of the Formation of Filamentous Carbon in the Hydrogenolysis of cyclopentane on Ni/Al<sub>2</sub>O<sub>3</sub> Catalysts," *J. Catal.*, vol. 124, no. 2, pp. 324–335, 1990.
- [197] N. Wang, W. Chu, T. Zhang, and X. S. Zhao, "Synthesis, characterization and catalytic performances of Ce-SBA-15 supported nickel catalysts for methane dry reforming to hydrogen and syngas," *Int. J. Hydrogen Energy*, vol. 37, no. 1, pp. 19–30, 2012.
- [198] L. Smoláková, M. Kout, L. Čapek, A. Rodriguez-Gomez, V. M. Gonzalez-Delacruz, L. Hromáčko, and A. Caballero, "Nickel catalyst with outstanding activity in the DRM reaction prepared by high temperature calcination treatment," *Int. J. Hydrogen Energy*, vol. 41, no. 20, pp. 8459–8469, 2016.
- [199] D. Li, X. Li, and J. Gong, "Catalytic Reforming of Oxygenates: State of the Art and Future Prospects," *Chem. Rev.*, vol. 116, no. 19, pp. 11529–11653, 2016.
- [200] Z. Liu, S. D. Senanayake, and J. A. Rodriguez, "Elucidating the interaction between Ni and CeO<sub>x</sub> in ethanol steam reforming catalysts: A perspective of recent studies over model and powder systems," *Appl. Catal. B Environ.*, vol. 197, pp. 184–197, 2016.
- [201] J. Xu, W. Zhou, Z. Li, J. Wang, and J. Ma, "Biogas reforming for hydrogen production over nickel and cobalt bimetallic catalysts," *Int. J. Hydrogen Energy*, vol. 34, no. 16, pp. 6646–6654, 2009.
- [202] S. Li, Y. Xu, Y. Chen, W. Li, L. Lin, M. Li, Y. Deng, X. Wang, B. Ge, C. Yang, S. Yao, J. Xie, Y. Li, X. Liu, and D. Ma, "Tuning the Selectivity of Catalytic Carbon Dioxide Hydrogenation over Iridium/Cerium Oxide Catalysts with a Strong Metal–Support Interaction," *Angew. Chemie - Int. Ed.*, vol. 56, no. 36, pp. 10761–10765, 2017.
- [203] Y. T. Shah and T. H. Gardner, "Dry Reforming of Hydrocarbon Feedstocks," *Catal. Rev.*, vol. 56, no. 4, pp. 476–536, 2014.
- [204] T. M. Gür, "Comprehensive review of methane conversion in solid oxide fuel cells: Prospects for efficient electricity generation from natural gas," *Prog. Energy Combust. Sci.*, vol. 54, pp. 1–64, 2016.
- [205] X. Du, D. Zhang, L. Shi, R. Gao, and J. Zhang, "Morphology dependence of catalytic properties of Ni/CeO<sub>2</sub> nanostructures for carbon dioxide reforming of methane," *J. Phys. Chem. C*, vol. 116, no. 18, pp. 10009–10016, 2012.
- [206] L. Jalowiecki-Duhamel, S. Debeusscher, H. Zarrou, A. D'Huysser, H. Jobic, and E. Payen, "Hydrogen storage in CeNi<sub>x</sub>O<sub>y</sub> and CeM<sub>0.5</sub>Ni<sub>x</sub>O<sub>y</sub> (M = Zr or Al) mixed oxides," *Catal. Today*, vol. 138, no. 3–4, pp. 266–271, 2008.
- [207] S. Debeusscher and A. Einstein, "mixed oxides ' catalytic hydrogen reservoirs," vol. 2, no. 2, pp. 148–158, 2009.
- [208] I. Dincer, A. Midilli, A. Hepbasli, and T. H. Karakoc, "Global warming: Engineering solutions," *Green Energy Technol.*, vol. 31, 2010.
- [209] J. Gao, Z. Hou, H. Lou, and X. Zheng, *Dry (CO<sub>2</sub>) Reforming*. pp. *Fuel Cells: Technologies for Fuel Processing*, pp.191-221, 2011.
- [210] C. Karakaya and R. J. Kee, "Progress in the direct catalytic conversion of methane to fuels and chemicals," *Prog. Energy Combust. Sci.*, vol. 55, pp. 60–97, 2016.



# Annex

# Annex

## Annex 1

### Characterization method for Ni based mixed oxides

#### Elemental analysis:

For all the catalysts prepared by co-precipitation method, the metal loading of Ni, Ce, Mg and Al were analyzed by the ICP technique (Agilent 720-ES ICP-OES). The Ni/M<sub>T</sub> molar ratio reported corresponding to the nickel molar proportion in all the metals. For Ce-Ni catalyst, M<sub>T</sub> = x + 1, Ni/M<sub>T</sub> = x/(x + 1) ; For Ce-Ni-Al catalyst, M<sub>T</sub> = x + 1.5, Ni/M<sub>T</sub> = x/(x + 1.5) ; For Ni-Mg-Al catalyst, M<sub>T</sub> = x + 3, Ni/M<sub>T</sub> = x/(x + 3).

#### Surface area measurements:

The specific surface area (BET) was estimated from the N<sub>2</sub> adsorption by using (TriStar II 3020) analyzer. The samples were degassed for 40 min at 150 °C prior to each measurement.

#### X Ray diffraction (XRD) analysis:

X-ray powder diffraction measurements were performed with a Bruker D8 Advance x-ray diffractometer equipped using a fast detector type LynxEye with a copper anticathode. The XRD patterns were registered in the 2θ domain (10-90 °) with a measured step of 0.02 ° and the time integration of 0.3 s. The particle size was calculated based on the width of the main diffraction peak as assessed with the MDI Jade 6.5 software using the Scherrer equation. From the most intense reflections observed for the NiO and CeO<sub>2</sub> crystallographic structures: (1 1 1), (2 0 0), and (2 2 0). Crystallites sizes were calculated using the Scherrer equation:  $D_{hkl} = K \lambda / B \cos\theta$ , where K is a structure constant (0.9 for spherical crystals); λ is the incident ray wavelength; B is the peak width at half height after correction for instrumental broadening; and θ is the Bragg angle. The lattice parameter 'a' was calculated using the most prominent peak (200) according to the following formulas:

$$a = d\sqrt{h^2 + k^2 + l^2} \quad (1)$$

$$d = \lambda / 2\sin\theta \quad (2)$$

Where d represents the inter-planar spacing and θ represents the diffraction angle of the (111)

plane.

**Raman:**

Raman spectra were acquired on a Labram Infinity HORIBA JOBIN YVON Raman spectrometer using a visible laser with an output laser power of  $\lambda = 532$  nm at room temperature.

**XPS:**

The X-ray photoelectron spectroscopy (XPS) of the sample was obtained on a KRATOS Axis Ultra spectrometer under ultrahigh vacuum condition, using a twin Al x-ray source (1486.6 eV) at a pass energy of 40 eV. The solids in the form of pellets were fixed on a copper holder with copper tape. For calibration of the binding energy (BE) scale of photoemission features, the charge effect was adjusted by taking the C 1s peak at 284.5 eV as a reference for all the samples before the reaction. While for the catalysts after the reaction, a reference to Al 2p peak at 74.7eV was taken into account.

**H<sub>2</sub>-TPR:**

Temperature programmed reduction (TPR) analyses of the catalysts were conducted on a Micromeritics Autochem II Chemisorption analyzer, and the hydrogen consumption was measured by a thermal conductivity detector (TCD). Treatment were performed by heating 50mg of catalyst sample from room temperature to 1000 °C in the 5% H<sub>2</sub>-95% Ar (v/v) gas mixture with a slope of 10 °C min<sup>-1</sup>.

**O<sub>2</sub>-TPO:**

The TPO measurements were performed on a Micromeritics Autochem 2920 analyzer. The sample was treated in the 5 vol% O<sub>2</sub>-95 vol% He mixture with a flow rate of 50 mL min<sup>-1</sup>. The temperature was increased to 900 °C at a heating rate of 5 °C min<sup>-1</sup>.

**Characterization method of Ni<sub>x</sub>/SBA-15**

The samples were systematically characterized in oxidized state using XRD at high angles, nitrogen physisorption, TEM-EDXS, TPR. Characterization was also performed after reduction in order to evaluate the benefit of the phyllosilicate stabilization on the dispersion of the metallic phase in the final material, also some characterization were made after the catalytic test in order to prove the performances of the DP mediated catalyst.

**Nitrogen physisorption:**

$N_2$ -physisorption isotherms were recorded at  $-196\text{ }^\circ\text{C}$  on a Micromeritics Tristar II automated gas sorption system. Before analysis, the samples were outgassed under dynamic vacuum at  $350\text{ }^\circ\text{C}$  for 3 h. Textural properties were determined from the adsorption/desorption isotherms. BET surface area was determined using the multipoint BET algorithm in the  $P/P_0$  range from 0.1 to 0.25. The t-plot method was applied to quantitatively determine the micropore volumes and to assess to the micropore surface areas (de Boer statistical thickness  $L$  3.8–6.5 Å). The mesopore size distribution was determined by NLDFT equilibrium algorithm for cylindrical pores.

#### **Transmission electron microscopy (TEM):**

Micrographs were recorded on a JEOL 2100 UHR instrument (operated at 200 kV with a LaB6 source and equipped with a Gatan Ultra scan camera), with a resolution of 0.19 nm, and equipped with an Energy Dispersive X-ray Spectroscopy EDXS detector. All the samples were embedded in a polymeric resin (spurr) and cut into section as small as 50 nm using an ultramicrotome equipped with a diamond knife. Cuts were then deposited on a carbon grid. TEM analysis was used for characterize pore structure and TM distribution in the materials.

#### **Powder XRD:**

Patterns were recorded on a PanAnalytical Empyrean X-ray diffractometer, Bragg Bentano configuration, with  $\text{CuK}_\alpha$  radiation at  $\lambda = 1.54184\text{ \AA}$  as X-ray source. For small angle analysis, the data were collected in the  $2\theta$  range from  $0.5^\circ$  to  $5^\circ$  with a step of  $0.01^\circ$  (step time of 280 s). For wide angle analysis, the data were collected in the  $2\theta$  range from  $10^\circ$  to  $80^\circ$  with a step of  $0.05^\circ$  (step time of 120 s). Phase identification was made by comparison with the JCPDS database.

#### **In situ powder XRD:**

Patterns were recorded on a Bruker D8 ADVANCE X-ray diffractometer equipped with a VANTEC-1 detector, using a  $\text{CuK}_\alpha$  radiation ( $\lambda = 1.54184\text{ \AA}$ ) as X-ray source. The calcined samples were placed on a kanthal filament (FeCrAl) cavity, and then subjected to thermo-programmed reduction under a flow of 3.0 vol.%  $\text{H}_2$  in He ( $30\text{ mL min}^{-1}$ ) from  $30\text{ }^\circ\text{C}$  to  $500\text{ }^\circ\text{C}$  (heating ramp of  $5\text{ }^\circ\text{C min}^{-1}$ ). The *in situ* diffractograms were recorded at definite temperatures in the  $2\theta$  range from  $15$  to  $70^\circ$  with a step of  $0.05^\circ$  (step time of 2 s). Crystal phase identification was made by comparison with ICDD database.

#### **$\text{H}_2$ -TPR**

TPR was conducted on an Autochem chemisorption analyzer (Micromeritics), equipped with a

TCD and coupled with a mass spectrometer (Omnistar, Pfeiffer) to follow possible desorption of O<sub>2</sub>, and CO<sub>2</sub> during the experiments. Consumed H<sub>2</sub> was driven from the TCD signal after calibration. Before H<sub>2</sub>-TPR run, the solid was activated up to its calcination temperature (from room temperature to 500 °C, heating ramp of 5 °C min<sup>-1</sup>, and isothermal time of 1 h) under simulated air at a total flow rate of 30 mL min<sup>-1</sup>. After cooling down to 50 °C, the H<sub>2</sub> containing flow was stabilized (50 mL min<sup>-1</sup>, 5.0 vol.% H<sub>2</sub> in Ar) and the temperature-programmed reduction was performed (from 50 °C to 900 °C, with a temperature ramp of 5 °C min<sup>-1</sup>).

## Annex 2

### Experimental

In dry reforming test, the catalytic test was conducted under atmospheric pressure in a fixed-bed quartz reactor (i.d. = 4 mm). The reactor was mounted into a tubular electric furnace and the temperature was controlled by a temperature controller. Prior to experiment with pretreatment, the sample was reduced depending on different type of catalysts, then the catalyst bed was washed for 30 minutes with a flow of pure He, followed by the sample was brought to the reaction temperature by 10 °C/min. Finally the reactant mixture was fed in. The stoichiometric molar ratio  $\text{CH}_4/\text{CO}_2$  in reactants was maintained at 1 while varying the reactant concentration by adding  $\text{N}_2$  as carry gas. When doing a test without pretreatment, the reactants directly introduced into the reactor after the oven is headed to a target temperature in He. Gas flow was controlled by calibrated MFCs (Bronkhorst High-Tech BV, various models). The result reported in the thesis is the value after 5h of TOS if no special instructions. The time of stability test is more than 24 h depending on different operation. The reaction conditions are as follow:

#### Experiment condition:

- Total starting flow rate:** 80 mL/min; ( $\text{CH}_4$ ,  $\text{CO}_2$ ,  $\text{N}_2$  and  $\text{O}_2$ ).
- Mass of catalyst:** 10 mg – 300 mg;
- Pretreatment:** in *situ* reduced in 30mL of pure  $\text{H}_2$  for 12h at different operating temperature.

Oxidative dry reforming reactions were conducted in the same conditions. No matter how the ratio of  $\text{O}_2/\text{CH}_4$  altering in the reactants, the total flow rate was fixed at 80 ml/min by the  $\text{N}_2$  balance. In each test, after the sample heated to reaction temperate,  $\text{N}_2$  was firstly introduced into the reactor, then a mixture of a simulated biogas ( $\text{CH}_4/\text{CO}_2 = 1: 0.7$ , 20%  $\text{CH}_4$ ) was fed in,  $\text{O}_2$  was introduced at last. It should precisely adjust the temperature after the catalyst bed was over heated by adding  $\text{O}_2$ , then stabilized for a while until there is no temperature fluctuation. All the products were analyzed on-line by gas chromatography (TRACE GC ULTRA) equipped with a thermal-conductivity detector (TCD) and a flame ionization detector (FID). **Fig. 1** illustrated the scheme of experimental apparatus.

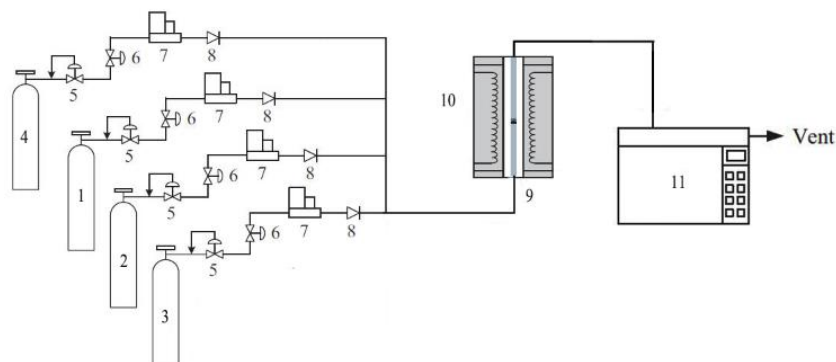


**Fig. 1** Schematic diagram of experimental apparatus. 1-CH<sub>4</sub>; 2-CO<sub>2</sub>; 3-O<sub>2</sub>; 4-N<sub>2</sub>; 5-pressure regulator; 6-ball valve; 7-mass flow controller; 8-check valve; 9-heater and thermal insulator; 10-reactor; 11-gas chromatography.

The catalytic performance was assessed using reactant conversion (CH<sub>4</sub>, CO<sub>2</sub>), and distribution of the products, given as H<sub>2</sub>/CO molar ratio during dry reforming and Oxidative dry reforming reaction as given in **Eqs. (3, 4 and 5)**. H<sub>2</sub>O are also formed but the quantity was not analyzed.

$$X_{CH_4} = \frac{(CH_4^{in} - CH_4^{out})}{CH_4} \times 100\% \quad (3)$$

$$X_{CO_2} = \frac{(CO_2^{in} - CO_2^{out})}{CO_2} \times 100\% \quad (4)$$

$$H_2 / CO \text{ ratio} = F_{H_2}^{out} / F_{CO}^{out} \quad (5)$$

Where  $F_{H_2}^{out}$  and  $F_{CO}^{out}$  corresponds to the flow rate of each component in the feed or effluent.

The thermodynamic equilibrium values were calculated by using HSC chemistry 6 for providing a basis for comparison. Appropriate blank runs show that under our experimental test conditions contribution of gas phase reaction is negligible.

## Annex 3

### Thermodynamic study

Theoretically, the DRM reaction is highly endothermic ( $247 \text{ kJ mol}^{-1}$ ) and requires an external energy source. It is accompanied by several simultaneous side-reactions. As an example, The RWGS reaction reduces the selectivity of DRM with respect to  $\text{H}_2$ , producing  $\text{H}_2\text{O}$  byproduct and lowering the yield of  $\text{H}_2$ .

Before DRM testing, different gaseous composition used for conducting the reaction was checked from thermodynamic simulations. Equilibrium values for  $\text{CH}_4$  conversion,  $\text{CO}_2$  conversion and  $\text{H}_2/\text{CO}$  ratio were calculated at atmospheric pressure (as used in the experiments), solid carbon phase is not taking into account due to various possible tend of carbon formation for different catalysts in this work. Since the equilibrium calculation does not take into account the removal of material into a second phase, it is inadequate for strongly carbon-forming catalysts.

**Fig.2** illustrates of main and side-reactions [176] possibly occurring during dry reforming of methane and probability of occurrence (Favorable or Not Favorable) as evaluated from thermodynamic calculations of the Gibbs free energy change ( $\Delta G$ ) using the HSC 6.0 Chemistry software.

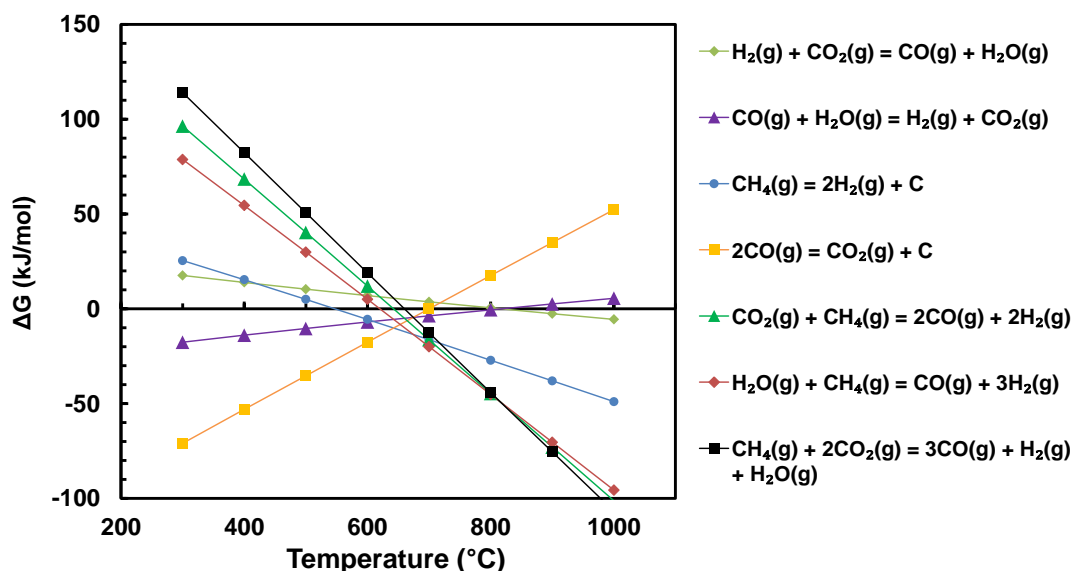


**Fig. 2** Gibbs free energy for DRM and main side reactions

Moreover, simulations were performed using the HSC 6 Chemistry software (where H, S and C stand for the enthalpy, entropy and heat capacity, respectively) which principle is to calculate, based

on the Gibbs free energy minimization's principle [209], the equilibrium gas composition depending on the applied conditions (initial molar gas mixture, temperature, pressure, etc.). The chosen initial gaseous  $\text{CH}_4(\text{g})/\text{CO}_2(\text{g})/\text{N}_2(\text{g})$  composition was 20/20/60 ( $\text{N}_2$  is used as inert diluent) or  $\text{CH}_4(\text{g})/\text{CO}_2(\text{g})$  was 50:50 without dilution. Equilibrium compositions (unconverted reactants and expected  $\text{H}_2(\text{g})$ ,  $\text{CO}(\text{g})$  and  $\text{H}_2\text{O}(\text{g})$  products) were determined in the temperature range of 200-900 °C.

Taking only stable species, and neglecting the catalytic phase (on which only a small fraction of the material should be adsorbed), it is possible to calculate a good theoretical approximation of the thermodynamic limits of a real process. **Fig. 3** illustrates the effect of temperature on a stoichiometric mixture of  $\text{CH}_4$  and  $\text{CO}_2$  at a ratio of 20%: 20% at a constant pressure (0.1 MPa). It is quite clear that methane is the most stable molecular structure during the dry reforming reaction. The conversions of methane and  $\text{CO}_2$  below 500 °C are not significant, and the calculated equilibrium conversion of methane is 95.4% at 800 °C. The final  $\text{H}_2/\text{CO}$  ratio in product gas reaches 0.99 in dry reforming of methane at 900 °C. Higher conversion and higher selectivity to  $\text{H}_2$  and  $\text{CO}$  are obtained with increasing temperatures.

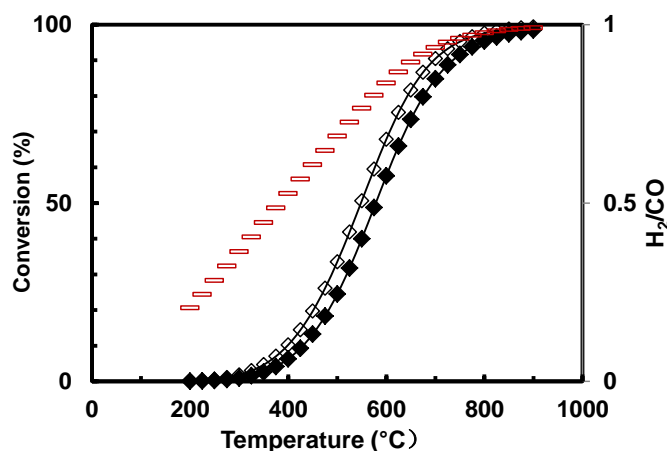


**Fig. 3** Effect of temperature on dry reforming of methane, equilibrium values of  $\text{CH}_4$  ( $\blacklozenge$ ),  $\text{CO}_2$  ( $\diamond$ ) conversions and  $\text{H}_2/\text{CO}$  ratio ( $\blacksquare$ )  $\text{CH}_4:\text{CO}_2=20\%:20\%$ . (0.1 MPa).

**Fig. 4** shows the equilibrium values for the condition without dilution with a mixture of  $\text{CH}_4$  and  $\text{CO}_2$  at a ratio of 50% : 50%. Very similar evolution for each value is obtained compared with the condition diluted to 20%. However, lower value of 90.3% of methane conversion is obtained at final state at 800 °C due to the high concentration of reactants. Generally, dry methane reforming predominantly takes place above 600 °C but with co-existence of some side reactions until 750 °C (particularly methane decomposition, WGS and RWGS, seen in.  $\text{CH}_4$  decomposition remains one

possible reaction route at high temperatures. This can ultimately cause severe catalytic deactivation in case of graphitic carbon deposition (even in low amount) as often observed with Ni-based methane reforming catalysts [184].

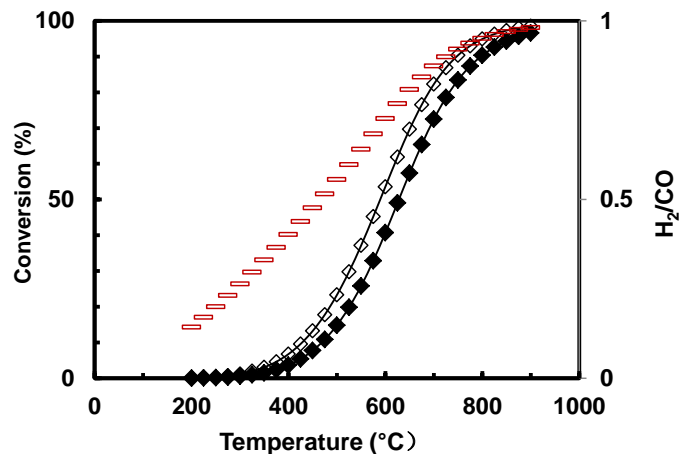


**Fig. 4** Effect of temperature on dry reforming of methane, equilibrium values of  $\text{CH}_4$  ( $\blacklozenge$ ),  $\text{CO}_2$  ( $\diamond$ ) conversions and the  $\text{H}_2/\text{CO}$  ratio ( $\Rightarrow$ ) (50%  $\text{CH}_4$ : $\text{CO}_2$ =50%: 50%. (0.1 MPa).

In **Table 1** and **Table 2**, the equilibrium values are calculated in the same condition with the experimental test in this thesis. It is easy to directly compare these thermodynamic limit values with experiment values and to have references when planning a new test.

**Table 1** The thermodynamic limits of  $\text{CH}_4$  and  $\text{CO}_2$  conversions and  $\text{H}_2/\text{CO}$  molar ratio for selected temperatures  $\text{CH}_4/\text{CO}_2=20\%:20\%$ .

Thermodynamic limit	500 °C	600 °C	700 °C	800 °C
$\text{CH}_4$ conversion (%)	14.8	57.6	84.8	95.4
$\text{CO}_2$ conversion (%)	23.3	67.9	90.5	97.6
$\text{H}_2/\text{CO}$ molar ratio (-)	0.69	0.84	0.94	0.98

**Table 2** The thermodynamic limits of  $\text{CH}_4$  and  $\text{CO}_2$  conversions and  $\text{H}_2/\text{CO}$  molar ratio for selected temperatures  $\text{CH}_4/\text{CO}_2=50\%:50\%$ .

Thermodynamic limit	500 °C	600 °C	700 °C	800 °C
$\text{CH}_4$ conversion(%)	24.5	40.7	72.5	90.3
$\text{CO}_2$ conversion (%)	33.5	53.6	82.3	94.9
$\text{H}_2/\text{CO}$ molar ratio (-)	0.56	0.73	0.87	0.95

It is well known that the methane reforming processes requires high temperatures and favors low pressure due to Le Chatelier's principle.[210] In this part, as an important way to understand how the  $\text{O}_2$  influence the reforming process of methane, the predicted calculation of different  $\text{O}_2/\text{CH}_4$  ratio

condition was carried out at a constant pressure of 1 atm. Theoretical equilibrium calculations for temperature range of 200-900 were performed and the results are shown in **Fig. 5** and **Table 3**.

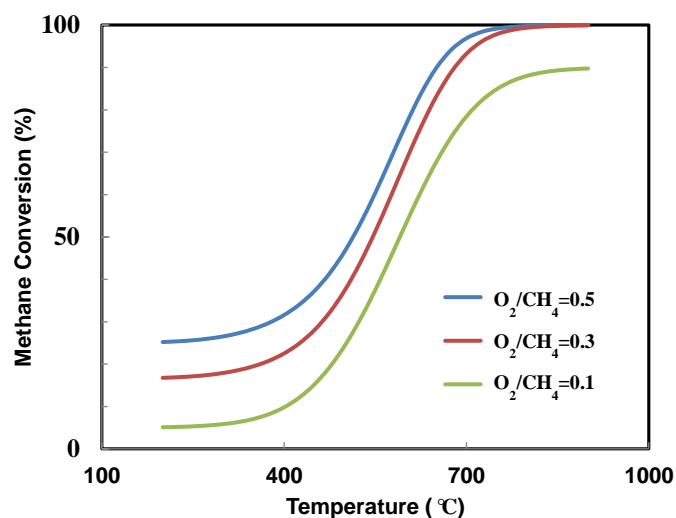


**Fig. 5** Equilibrium results of methane conversion v.s temperature in oxidative dry reforming of methane  $\text{CH}_4:\text{CO}_2:\text{O}_2=1:0.7/x$  ( $x = 0.1, 0.3$  and  $0.5$ )

**Table 3** The thermodynamic limits of  $\text{CH}_4$  and  $\text{CO}_2$  conversions and  $\text{H}_2/\text{CO}$  molar ratio for selected temperatures ( $\text{CH}_4= 20\%$ )  $\text{CH}_4:\text{CO}_2:\text{O}_2=1:0.7/0.3$

Thermodynamic limit	500 °C	600 °C	700 °C	800 °C
$\text{CH}_4$ conversion (%)	37.5	67.9	93.3	95.4
$\text{CO}_2$ conversion (%)	-6.0	34.8	66.1	75.8
$\text{H}_2/\text{CO}$ molar ratio (-)	1.6	1.25	1.22	1.19

# RESUME

## CHAPITRE 1 - Introduction générale

L'hydrogène est proposé comme un vecteur d'énergie propre d'avenir. Cependant, la production d'hydrogène à partir de ressources fossiles est aujourd'hui la plus répandue, et elle ne peut pas constituer une solution à long terme au vu de la quantité limitée de ces ressources, et des problèmes environnementaux qu'elle génère. Elle ne peut constituer qu'une solution à court et moyen terme car l'hydrogène est produit actuellement majoritairement à partir de gaz naturel (ressource fossile, constitué principalement de méthane,  $\text{CH}_4$ ). Afin de développer une économie basée sur l'hydrogène, il est souhaitable de pouvoir le produire à partir de ressources renouvelables, telles que la biomasse ou le biogaz constitué essentiellement d'un mélange de  $\text{CH}_4$  et  $\text{CO}_2$  et par transformation de ces molécules ( $\text{CH}_4$  et  $\text{CO}_2$ ) qui sont, de plus, des gaz à effet de serre (GES). Le reformage à sec (DRM) et le reformage oxydant du méthane (ODRM) sont des voies prometteuses pour produire  $\text{H}_2$  et CO à partir des GES et suscitent une grande attention en raison des préoccupations environnementales actuelles.

Ce chapitre présente l'état de l'art, de la littérature, sur la production d'hydrogène par reformage du méthane, en reportant les différents procédés de production (reformage à l'eau, oxydation partielle, reformage à sec et reformage oxydant), les catalyseurs étudiés permettant d'effectuer ces réactions, ainsi que les problèmes rencontrés telles que la désactivation des catalyseurs par formation de carbone ou frittage. Les catalyseurs à base de Ni sont largement étudiés dans la littérature du fait de leur très grande activité cependant ils subissent souvent une désactivation due à la formation de carbone et/ou à cause du frittage.

Dans ce contexte, l'objectif de la thèse est de développer des catalyseurs à base de Ni, actifs et sélectifs en limitant la formation de carbone et en évitant le frittage. Il s'agit de développer des catalyseurs performants pour la production d'hydrogène par transformation catalytique du méthane en présence de  $\text{CO}_2$  (reformage à sec) et également en présence d'oxygène (reformage oxydant). De plus, afin d'analyser au mieux les performances des catalyseurs, ces réactions sont étudiées à basse température (600-700°C), conditions permettant d'utiliser moins d'énergie, mais favorisant la formation de carbone.

## CHAPITRE 2 - Préparation et caractérisation des catalyseurs

Les catalyseurs étudiés sont des oxydes mixtes  $CeNi_x(Al_z)O_y$ ,  $Ni_xMg_2AlO_y$ , et des catalyseurs supportés Ni/SBA-15 comportant des teneurs variables en Ni. Dans ce chapitre sont reportés leurs préparations et caractérisations physico-chimiques.

Les oxydes mixtes  $CeNi_x(Al_z)O_y$  (avec  $x$  le rapport molaire Ni/Ce,  $0,1 \leq x \leq 5$  ;  $z = 0$  ou  $0,5$ ) et  $Ni_xMg_2AlO_y$  ( $1 \leq x \leq 12$ ) sont préparés par co-précipitation, tandis que les catalyseurs supportés Ni\_x/SBA-15 (avec  $x$  le pourcentage massique en Ni variant de 5% à 40%) sont préparés par dépôt-précipitation. Diverses techniques physico-chimiques ont été utilisées pour caractériser les catalyseurs, tels que ICP, BET, DRX, XPS, TPR et Raman.

Les catalyseurs ont une surface spécifique variant de 95 à 127  $m^2/g$  pour les catalyseurs binaires  $CeNi_xO_y$  et de 73 à 141  $m^2/g$  pour les composés ternaires  $CeNi_xAl_{0,5}O_y$  suivant la teneur en Ni. Quel que soit le catalyseur, binaire ou ternaire, la phase cérique est présente. Pour les catalyseurs  $CeNi_xAl_{0,5}O_y$ , quand le rapport molaire Ni/Ce est supérieur à 0,5 la phase NiO apparaît. Enfin, dans le cas des catalyseurs ternaires, aucune phase associée à l'aluminium n'est observée par DRX. La taille moyenne des cristallites de NiO varie entre 8 et 10 nm et celle de  $CeO_2$  entre 4 et 5 nm, en fonction de la nature du catalyseur et de la teneur en Ni.

Les différentes techniques de caractérisations physico-chimiques montrent que les composés  $CeNi_x(Al_z)O_y$  sont constitués d'un mélange de nanoparticules de  $CeO_2$  et de NiO, coexistant avec une solution solide de cérium-nickel (et aluminium) suivant la teneur en Ni. Ces composés comportent des espèces Ni en interaction forte avec d'autres cations, en particulier à faible teneur en Ni. Les oxydes mixtes de  $CeNi_x(Al_z)O_y$  présentent des pics en TPR à basse et haute température. Ce phénomène est attribué à la réduction des espèces  $Ni^{2+}$  dans différents environnements : en solution solide et/ou dans de petites particules de NiO à basse température et dans des nanoparticules de NiO plus grandes (visibles par DRX) à température plus élevée. L'addition d'aluminium influence la réductibilité des catalyseurs.

Les surfaces spécifiques des catalyseurs  $Ni_xMg_2AlO_y$  sont comprises entre 100 et 200  $m^2.g^{-1}$  suivant la teneur en Ni. Les composés sont constitués de petites nanoparticules de NiO, MgO et/ou de solution solide de Ni-Mg-(Al)-O avec une taille moyenne de cristallites de la phase oxyde à 4-6 nm suivant la teneur en Ni. Les résultats des analyses XPS, DRX et TPR montrent l'existence d'interactions fortes entre les espèces Ni et Mg et/ou Al en accord avec la formation d'une solution solide Ni-Mg-O et/ou Ni-Mg-Al-O. Les oxydes mixtes  $Ni_xMg_2AlO_y$  présentent un pic large en TPR,

situé entre 560 et 844 °C et attribué à la réduction des espèces Ni. Pour les faibles teneurs en Ni, les interactions fortes entre les espèces nickel et les autres cations peuvent exister en solution solide Ni-Mg-(Al)-O et/ou aux interfaces entre de petites nanoparticules de NiO, MgO et/ou Ni-Mg-(Al)-O rendant le solide plus difficile à réduire.

La stabilité thermique élevée des catalyseurs Ni<sub>x</sub>/SBA-15 est révélée par DRX in situ et confirmée par TEM. Pour une faible teneur en Ni, les espèces Ni sont réparties de manière homogène dans la silice alors que pour une charge de Ni élevée, des espèces Ni entourent les bords de la silice. L'altération de la structure ordonnée est confirmée par TEM et la physisorption de N<sub>2</sub> qui révèle la dissolution de la silice nécessaire à la formation des structures de type phyllosilicates. De plus, avec l'augmentation de la charge en métal, le nombre et la longueur des phyllosilicates augmentent, indépendamment du grain de silice et à l'extérieur. Les catalyseurs à charge en Ni élevée présentent une température de réduction plus élevée que les échantillons à teneur en Ni inférieure. Une température de réduction élevée de 800 °C conduit à la réduction totale des phyllosilicates en particules métalliques Ni<sup>0</sup> très bien dispersées sur le support de silice. Une température de réduction inférieure permet l'obtention d'une réduction partielle du composé.

### CHAPITRE 3 - Reformage à sec du méthane sur des catalyseurs à base de Ni

Les catalyseurs oxydes mixtes CeNi<sub>x</sub>(Al<sub>z</sub>)O<sub>y</sub>, Ni<sub>x</sub>Mg<sub>2</sub>AlO<sub>y</sub>, et les catalyseurs supportés Ni/SBA-15 sont étudiés en reformage à sec (DRM : CH<sub>4</sub>+CO<sub>2</sub>→ 2CO+2H<sub>2</sub>). L'influence de différents paramètres a été examinée, telles que la température de réaction, le prétraitement sous H<sub>2</sub>, la teneur en Ni, la masse de catalyseur et les concentrations en réactifs.

Des conversions similaires de CH<sub>4</sub> et de CO<sub>2</sub> sont obtenues en DRM sur le meilleur candidat CeNi<sub>0,5</sub>O<sub>y</sub>, avec prétraitement sous H<sub>2</sub> à 250 °C ou sans prétraitement du catalyseur. Sans prétraitement ou avec une augmentation de la température de prétraitement sous H<sub>2</sub> jusqu'à 600 °C conduisent à une formation plus élevée de carbone, montrant l'importance de l'effet du prétraitement sous H<sub>2</sub> sur la formation de carbone. En DRM et à 700 °C, le catalyseur CeNi<sub>0,5</sub>O<sub>y</sub> (50 mg) (CH<sub>4</sub>/CO<sub>2</sub> = 20%/20% dilué en N<sub>2</sub>) permet des conversions de 60% du méthane et de 72% du CO<sub>2</sub> et formation de H<sub>2</sub> et CO (produits formés) avec un rapport H<sub>2</sub>/CO égal à 0,83, et montrant une bonne stabilité. Dans des conditions riches en réactifs (sans dilution) et en utilisant une faible masse de catalyseur, c'est-à-dire des conditions dures (10 mg et CH<sub>4</sub>/CO<sub>2</sub> = 50%/50%), 22% de conversion du CH<sub>4</sub> et 30 % de conversion du CO<sub>2</sub> sont obtenues,

avec une formation d'un mélange de produits H<sub>2</sub> et CO présentant un rapport H<sub>2</sub>/CO de 0,72.

Le catalyseur CeNi<sub>2</sub>Al<sub>0,5</sub>O<sub>Y</sub>, prétraité sous H<sub>2</sub> à 250 °C, est le meilleur catalyseur de la série CeNi<sub>X</sub>Al<sub>0,5</sub>O<sub>Y</sub>, en raison de l'activité élevée à 600 °C dans des conditions dures (10 mg de catalyseur, CH<sub>4</sub>/CO<sub>2</sub> = 50%/50%). En effet, 37% de conversion du CH<sub>4</sub> et 48% de conversion du CO<sub>2</sub> sont obtenues avec formation d'un mélange de produits H<sub>2</sub> et CO avec un rapport H<sub>2</sub>/CO égal à 0,83. L'ajout d'Al dans le système Ce-Ni diminue les conversions de CH<sub>4</sub> et CO<sub>2</sub> sur des composés à faible teneur en Ni, mais maintient une activité élevée sur les catalyseurs à haute teneur en Ni. Quoiqu'il en soit, la capacité de résistance au carbone est toujours améliorée comparativement aux catalyseurs binaires (sans Al). Le catalyseur CeNi<sub>2</sub>Al<sub>0,5</sub>O<sub>Y</sub>, non prétraité ou prétraité à 600 °C sous H<sub>2</sub>, conduit également à une formation de carbone plus élevée comparativement au catalyseur prétraité sous H<sub>2</sub> à 250 °C, comme observé précédemment sur le catalyseur binaire.

Un prétraitement sous H<sub>2</sub> à 450°C ou l'absence de prétraitement, a une légère influence sur l'activité des catalyseurs Ni<sub>X</sub>Mg<sub>2</sub>AlO<sub>Y</sub> à l'état stabilisé. Cependant, une température de traitement plus élevée sous H<sub>2</sub> de 550 °C ainsi que l'absence de prétraitement conduisent à une augmentation du dépôt de carbone. Le catalyseur Ni<sub>1</sub>Mg<sub>2</sub>AlO<sub>Y</sub> (10mg) permet d'obtenir de meilleurs résultats catalytiques en DRM (CH<sub>4</sub>/CO<sub>2</sub> = 20%/20%), avec des conversions de 33% pour CH<sub>4</sub> et de 39% pour CO<sub>2</sub> à une température basse de 600 °C. Dans des conditions riches en réactifs (CH<sub>4</sub>/CO<sub>2</sub> = 50%/50%), Ni<sub>1</sub>Mg<sub>2</sub>AlO<sub>Y</sub> (50 mg) montre une stabilité remarquable pendant au moins 50h à 700 °C. 67% de conversion du CH<sub>4</sub> et 76% de conversion du CO<sub>2</sub> sont obtenues avec formation d'un mélange de produits H<sub>2</sub> et CO avec un rapport H<sub>2</sub>/CO égal à 0,84.

Les catalyseurs Ni<sub>X</sub>/SBA-15 montrent des conversions assez similaires en DRM (CH<sub>4</sub> = 20%) ne dépendant pas fortement de la charge en Ni. Le prétraitement sous H<sub>2</sub> à 600 °C a un effet différent sur les catalyseurs avec des teneurs variables en Ni. Un résultat bénéfique n'est obtenu que sur un catalyseur Ni<sub>20</sub>%/SBA-15. Pour Ni<sub>40</sub>%/SBA-15, l'augmentation de la température de prétraitement sous H<sub>2</sub> a un effet négatif. Dans des conditions CH<sub>4</sub>/CO<sub>2</sub> = 20%/20% (dilué dans N<sub>2</sub>), le catalyseur Ni<sub>40</sub>%/SBA-15 (10 mg) avec la charge en Ni la plus élevée est le plus actif pour la transformation de CH<sub>4</sub> et de CO<sub>2</sub> puisque des conversions de CH<sub>4</sub> et de CO<sub>2</sub> égales à 27 et 37%, respectivement, sont atteintes à 600 °C. Des conversions très proches de 27% pour CH<sub>4</sub> et 36% pour CO<sub>2</sub> sont obtenues sur Ni<sub>20</sub>%/SBA-15 dans les mêmes conditions opératoires. Avec les mêmes concentrations en réactifs (20% CH<sub>4</sub>-20% CO<sub>2</sub>), l'augmentation de la masse du catalyseur Ni<sub>20</sub>%/SBA-15 jusqu'à 50 mg, pour un test effectué sans

prétraitement du catalyseur sous  $H_2$ , conduit à une conversion de  $CH_4$  de 68% et une conversion de  $CO_2$  de 77%, avec un rapport  $H_2/CO$  d'environ 0,8 à 700 °C.

Ainsi tous les catalyseurs étudiés présentent des activités et sélectivités élevées, et permettent d'obtenir des résultats très intéressants, en particulier dans des conditions de réaction dures, c'est-à-dire à basse température de réaction (600 °C), pour de fortes concentrations en réactifs (non dilués) et en utilisant une faible masse de catalyseur (jusqu'à 10 mg). De manière globale, la formation de carbone augmente avec la teneur en Ni.

#### CHAPITRE 4 – Reformage oxydant du méthane sur des catalyseurs à base de Ni

Les catalyseurs à base de cérium et nickel binaires et ternaires sont étudiés en reformage oxydant. Différents paramètres sont étudiés comme le rapport  $O_2/CH_4$ .

L'ajout d'oxygène augmente la conversion du  $CH_4$ , diminue la conversion du  $CO_2$ , et diminue fortement la formation de carbone. Sur le catalyseur  $CeNi_{0,5}O_Y$  (10 mg) sans prétraitement sous  $H_2$ , 56% de conversion du  $CH_4$  et 30 % de conversion du  $CO_2$  sont obtenus, avec une formation de  $H_2$  et  $CO$  présentant un rapport  $H_2/CO$  de 1,35. Avec la présence de Al, la vitesse de formation de carbone sur les catalyseurs ternaires est plus faible que sur les catalyseurs binaires pour une teneur en Ni similaire. Le rapport  $O_2/CH_4$  égal à 0,3 semble être la condition opératoire optimale en raison de l'activité élevée et de la sélectivité avec l'absence de formation de carbone. Le catalyseur  $CeNi_2Al_{0,5}O_Y$  (50 mg) testé à 700 °C avec un rapport  $O_2/CH_4$  égal à 0,3 dans le mélange réactionnel ne montre aucun signe de désactivation pendant 24 h. Des conversions égales à 77% pour  $CH_4$  et à 63% pour  $CO_2$  sont obtenues, mettant en évidence un taux de conversion élevé et stable.

#### CHAPITRE 5 – Discussion générale

Dans ce chapitre une étude approfondie est menée sur les relations pouvant exister entre les propriétés des catalyseurs et leurs performances catalytiques, faisant une synthèse de l'ensemble des résultats obtenus. L'objectif est de déterminer les espèces actives et sélectives pour l'activation et la transformation des molécules de  $CH_4$  et  $CO_2$  et de proposer un site actif et sélectif qui permettrait d'éviter la formation de carbone ainsi qu'un mécanisme réactionnel.

Tous les catalyseurs montrent une évolution de la conversion du  $CH_4$  et de la distribution des produits : augmentation de la conversion du méthane avec une teneur en Ni croissante (jusqu'à une limite)

lié à la distribution homogène des espèces Ni actives présentes dans différents environnements (entourées par différents atomes voisins), ainsi qu'une formation de carbone qui augmente également avec la teneur en Ni. De plus, les meilleures activités catalytiques et sélectivités sont obtenues sur des catalyseurs partiellement réduits à température appropriée.

L'addition d'O<sub>2</sub> présente un effet bénéfique, avec une augmentation de la conversion de CH<sub>4</sub> mais conduisant aussi à une diminution de la conversion de CO<sub>2</sub>. Ainsi le rapport O<sub>2</sub>/CH<sub>4</sub> égal à 0,3 apparaît comme le rapport optimal, en raison des activités et sélectivités élevées permettant de supprimer la formation de carbone.

Finalement, prenant en compte l'ensemble des résultats obtenus, diverses discussions présentées dans la littérature, ainsi que la structure des solides, un site actif impliquant des espèces Ni en interaction forte avec d'autres cations est proposé. Il est obtenu sur un catalyseur partiellement réduit formé pendant le traitement in situ sous H<sub>2</sub> ou sous flux de CH<sub>4</sub>, il implique des lacunes anioniques, des espèces O<sup>2-</sup> et des cations.



## **Production d'hydrogène à basse température par reformage à sec et reformage oxydant du méthane sur divers catalyseurs à base de nickel**

Afin de développer une économie basée sur l'hydrogène, il est souhaitable de pouvoir le produire à partir de ressources renouvelables comme le biogaz, constitué essentiellement de CH<sub>4</sub> et CO<sub>2</sub> gaz à effet de serre (GES). Le reformage à sec (DRM) et le reformage oxydant du méthane (ODRM) sont des voies prometteuses pour produire H<sub>2</sub> et CO à partir des GES et suscitent une grande attention en raison de préoccupations environnementales. Ces réactions ont été étudiées à basse température (600-700 °C) sur des oxydes mixtes CeNi<sub>x</sub>(Al<sub>z</sub>)O<sub>y</sub>, Ni<sub>x</sub>Mg<sub>2</sub>AlO<sub>y</sub>, et sur des catalyseurs supportés Ni/SBA-15. Diverses techniques physico-chimiques ont été utilisées pour caractériser les catalyseurs, telles que DRX, XPS, TPR et Raman. L'influence de différents paramètres a été examinée, comme la température de réaction, le prétraitement sous H<sub>2</sub>, la teneur en Ni, la masse de catalyseur et les concentrations en réactifs. En particulier, les réactions ont été étudiées à 600 °C, sans dilution des réactifs et sur 10 mg de catalyseur. Les meilleures activités catalytiques et sélectivités sont obtenues sur des catalyseurs partiellement réduits à température appropriée. L'addition d'O<sub>2</sub> augmente la conversion du CH<sub>4</sub> mais diminue la conversion du CO<sub>2</sub>, et O<sub>2</sub>/CH<sub>4</sub> = 0,3 apparaît comme la condition optimisée en raison des activités et sélectivités élevées. Enfin, un site actif impliquant des espèces Ni en interaction forte avec d'autres cations est proposé. Celui-ci est obtenu sur un catalyseur partiellement réduit, il implique des lacunes anioniques, des espèces O<sup>2-</sup> et des cations et est formé pendant le traitement *in situ* sous H<sub>2</sub> ou sous flux de CH<sub>4</sub>.

**Mots-clés:** Catalyse hétérogène, Reformage à sec, Reformage oxydant, Méthane, Production d'hydrogène, Oxyde mixte, Nickel, Cérium.

## **Hydrogen production at low temperature by dry reforming and oxidative dry reforming of methane on various Ni-based catalysts**

In order to develop a sustainable hydrogen economy, it is desirable to produce hydrogen from renewable resources such as biogas constituted mainly of CH<sub>4</sub> and CO<sub>2</sub>, greenhouse gases (GHG). Dry reforming (DRM) and oxidative dry reforming of methane (ODRM) are promising routes to produce H<sub>2</sub> and CO from GHG and have received much attention due environment concerns. Herein, these reactions were studied at low temperatures (600-700 °C) over CeNi<sub>x</sub>(Al<sub>z</sub>)O<sub>y</sub>, Ni<sub>x</sub>Mg<sub>2</sub>AlO<sub>y</sub> mixed oxides and Ni/SBA-15 supported catalysts. Various physico-chemical techniques were employed to characterize the catalysts, such as XRD, XPS, H<sub>2</sub>-TPR and Raman. The influences of different parameters were examined, such as reaction temperature, pretreatment in H<sub>2</sub>, Ni content, mass of catalyst and reactants concentration, in particular, at 600 °C in harsh conditions (feed gases without dilution) on low mass of catalyst (10 mg). The best catalytic activity and selectivity are obtained on partially reduced catalysts at appropriate temperature. The addition of O<sub>2</sub> increases CH<sub>4</sub> conversion but decreases CO<sub>2</sub> conversion, and O<sub>2</sub>/CH<sub>4</sub> = 0.3 could be the optimized condition due to high activity and selectivity. Finally, an active site involving Ni species in close interactions with other cations is proposed. It is related to a partially reduced catalyst involving anionic vacancies, O<sup>2-</sup> species, and cations, which is formed during the *in situ* H<sub>2</sub> treatment or CH<sub>4</sub> flow.

**Keywords:** Heterogeneous catalysis, Dry reforming, Oxidative dry reforming, Methane, Hydrogen production, Mixed oxide, Nickel, Cerium.